



**HAL**  
open science

# Chromatin mark interplays in the mammalian oocyte

Lorraine Bonneville

► **To cite this version:**

Lorraine Bonneville. Chromatin mark interplays in the mammalian oocyte. Human health and pathology. Université Paris Cité, 2022. English. NNT : 2022UNIP7090 . tel-04227849

**HAL Id: tel-04227849**

**<https://theses.hal.science/tel-04227849>**

Submitted on 4 Oct 2023

**HAL** is a multi-disciplinary open access archive for the deposit and dissemination of scientific research documents, whether they are published or not. The documents may come from teaching and research institutions in France or abroad, or from public or private research centers.

L'archive ouverte pluridisciplinaire **HAL**, est destinée au dépôt et à la diffusion de documents scientifiques de niveau recherche, publiés ou non, émanant des établissements d'enseignement et de recherche français ou étrangers, des laboratoires publics ou privés.

**Université Paris Cité**

ED 474 - Frontières de l'Innovation en  
Recherche et Education

**Institut Curie**

Génétique et Biologie du Développement  
CNRS U934 – INSERM U3215  
*Décisions épigénétiques et reproduction*

# Chromatin mark interplays in the mammalian oocyte

Thèse de doctorat de biologie cellulaire et biologie du développement

Par **Lorraine BONNEVILLE**

Dirigée par Deborah Bourc'his

Présentée et soutenue publiquement le **13 septembre 2022**

Devant un jury composé de :

Dr. **Kikue Tachibana**, directrice de recherche, Max-Planck Institute of Biochemistry,  
Munich - *Rapportrice*

Dr. **Robert Feil**, directeur de recherche, Université de Montpellier - *Rapporteur*

Dr. **Marie-Emilie Terret**, directrice de recherche, Sorbonne Université - *Examinatrice*

Pr. **Patricia Fauque**, PU-PH, Université Bourgogne-Franche Comté - *Examinatrice*

Dr. **Pierre-Antoine Defossez**, directeur de recherche, Université Paris Cité - *Examineur*

Dr. **Deborah Bourc'his**, directrice de recherche, Sorbonne Université - *Directrice de thèse*



**Université Paris Cité**

ED 474 - Frontières de l'Innovation en  
Recherche et Education

**Institut Curie**

Génétique et Biologie du Développement  
CNRS U934 – INSERM U3215  
*Décisions épigénétiques et reproduction*

# Chromatin mark interplays in the mammalian oocyte

Thèse de doctorat de biologie cellulaire et biologie du développement

Par **Lorraine BONNEVILLE**

Dirigée par Deborah Bourc'his

Présentée et soutenue publiquement le **13 septembre 2022**

Devant un jury composé de :

Dr. **Kikue Tachibana**, directrice de recherche, Max-Planck Institute of Biochemistry,  
Munich - *Rapportrice*

Dr. **Robert Feil**, directeur de recherche, Université de Montpellier - *Rapporteur*

Dr. **Marie-Emilie Terret**, directrice de recherche, Sorbonne Université - *Examinatrice*

Pr. **Patricia Fauque**, PU-PH, Université Bourgogne-Franche Comté - *Examinatrice*

Dr. **Pierre-Antoine Defossez**, directeur de recherche, Université Paris Cité - *Examinateur*

Dr. **Deborah Bourc'his**, directrice de recherche, Sorbonne Université - *Directrice de thèse*



# ACKNOWLEDGMENTS

I first would like to thank the members of my jury who agreed to review my work : Dr. Kikue Tachibana, Dr. Robert Feil, *rapporteurs*; Dr. Marie-Emilie Terret, Dr. Pierre-Antoine Defossez and Dr. Patricia Fauque, *examineurs*. Being evaluated by such inspiring scientists is a rare privilege, I am grateful for their time and their help.

I joined the lab of Deborah Bourc'his almost 4 years ago. When I arrived, I barely knew academic research but Deborah trusted me and supported my first steps into this path. She encouraged me to work alongside an amazing post-doc, Raquel Perez-Palacios and this is how I started to work on maternal epigenetic inheritance, a fast-evolving research area that passionated me. I want to thank Deborah for always having been supportive of my ideas and for the freedom and trust she gave me to pursue my project. She gave me benevolent opportunities to discuss science and gain in self-confidence to express my ideas. Deborah's way of managing always ensured a trustful and warm atmosphere in the lab, that enabled me to greatly enjoy these years of PhD. I feel very grateful to have had the chance to evolve in such a stimulating environment.

As I mentioned, when I arrived in the lab, I started working with Raquel Perez-Palacios. I couldn't be more grateful to have had such an amazing mentor ! Raquel taught me everything: from how to mouth-pipet, to handle a mouse or to not get discouraged after long weeks of CUT&RUN optimization. Raquel left the lab 3 years ago but she always remained available to discuss science and to provide me great advices and ideas.

I want to thank Aurélie Teissandier, our amazing bioinformatician. Aurélie, I could seriously not have done anything without you ! Thank you for being so patient with me, for cheering me up when I was drowning in the ocean of data and for being so welcoming when I was coming to your office with a thousandth idea of re-analysis or just to discuss our last weekend around a croissant. I learned so much by working with you.

I also want to sincerely thank Germaine Karam, a master student that I mentored during the last year of my PhD. I was able to focus on writing this thesis thanks to her precious help for the experiments and analysis.

More generally, I want to thank all the members of the Bourc'his lab that I got to meet during my time here. Juliane, Joan and Max for inspiring me and having been my models as PhD students or post-docs; Mélanie and Julian for your help with the mice; Fatima for all your kind advices and interest in my project; Maud for your help with PGCs collection; Charlotte P. for all the nice discussions and for the energy you brought to the lab; Tomek for all the laughs, our complicity and all our amazing discussions; Charlotte D. for your great scientific advices and for the really nice time we had in the lab when you were here; Nico for your encouragements and all the nice scientific discussions. I also want to give a special thanks to Nicolas Fayaubost, our zootechnician. It has been a real pleasure to work with you, thank you for your kindness, your reliability and your patience.

I want to especially thank our little team of PhD students : Mathilde, Mathieu, Emeline and Elena. Leaving half my life with you during the last 4 years has been one the best thing of my PhD ! You gave me so much strength and support in all possible ways. I have been so lucky to have you in the lab. Mathieu, thank you for your support, for being understanding, reliable and so passionate about science and all the rest. Emeline, sharing this desk with you for three years has been amazing : thank for being so benevolent and understanding, for being able to put things in perspective, for never losing motivation. Elena, thank you for adding your laughs and your energy to the team ! I loved seeing you evolve in the lab, always motivated and sincere. Finally, Mathilde, thank you for everything, for your daily support even after leaving the lab, for all the laughs and for your incredible strength that inspires me so much ! Thank you for our "lock-down phone-calls", during which I had the best scientific discussions of my entire PhD. Thank you for being such an amazing friend.

I also would like to thank the MD-PhD program of l'Ecole de l'INSERM – Liliane Bettencourt, it is thanks to them that I decided to discover academic research in the first place. Their spirit of emulation, their vision of medical research and their continuous support have been the driving force of my whole path. I also want to especially thank Dr. Cédric Menard, who was one of my

teacher during my medical studies. He greatly encouraged me at every step of my studies and of my PhD.

Finally, I cannot end this PhD manuscript without thanking all my friends that were not in the lab but without which these last three years would not have been the same ! Besides being the three most scientifically challenging years, this PhD has also been the most intense and amazing time thanks to all of you !

Etienne and Christophe, thank you for being the best possible roommates, for having been so supportive during the stressful periods and for knowing so well how to cheer me up ! Thank you Pauline for your continuous support and for all the times we discussed my PhD (even though she doesn't know much about biology ! You can count on me to do the same during yours.) I want to thank Sylvain and Laure for sharing together the good and hard times of our PhDs. Simon, for having been such an amazing holiday and lock-down companion. The whole Kohantasty team for your energy, your sweet madness and for becoming awesome friends. A very special thanks also to my little team of "doctor friends", Thibaut, Eva, Léna, Antoine, Julie, Claire : not only are you the most faithful (across seas and ECN) and crazy of my friends but you also truly are an inspiration. I am looking forward to go back to medicine thanks to your example !

Thank you all, even the one that I could not mention here, for being such incredible and inspiring friends. You guys, have given me so much strength and support at every step of my PhD. You always have known how to be there for me, in your own very different ways.

I want to thank my parents, Blandine, Jean-Baptiste and Agnès for their unconditional love and support.



# **ABSTRACT / RESUME**



## ABSTRACT

Germ cells have the unique ability to transmit not only the genetic material but also epigenetic information to the progeny. During oogenesis, the epigenome of future female gametes is extensively reprogrammed: somatic patterns are erased and an oocyte-specific chromatin landscape is acquired. After fertilization, the oocyte epigenetic information can persist at least during the first days of preimplantation development. Whether maternally-inherited chromatin patterns can influence the transcriptional program and the phenotype of the progeny is an intense area of research.

The oocyte is known to be the theater of unusual chromatin interplays: the sum of attractive and repulsive feedbacks between chromatin marks seems to rule their precise targeting, their role in regulating gene expression and their transmission to the embryo. In particular, two repressive chromatin marks –DNA methylation and trimethylation of histone H3 lysine 27 (H3K27me3)– show mirror distribution patterns, which are transmitted to the preimplantation embryo. However, while known for their functional antagonism in somatic cells, the nature of their relationship and their mutual impact on oocyte and preimplantation development remained unknown. In particular, while maternal DNA methylation inheritance has been extensively studied in the context of maternal imprinting and post-implantation development, its role, prior to reprogramming, in zygotic genome activation (ZGA) and pre-implantation development had never been studied. During my PhD, I therefore investigated the determinants and functions of DNA methylation and H3K27me3 in shaping the maternal epigenetic heritage.

First, by analysing the chromatin features of wild-type and mutant oocytes for either DNA methylation (using the *Dnmt3L* mutant model) or H3K27me3 (using the *Eed*<sup>ckO</sup> model) by both cytological and molecular means, I discovered novel interplays in the oocyte epigenome. I showed that the classical compensation mechanisms observed in somatic cells between H3K27me3 and DNA methylation do not apply to oocytes. In contrast, DNA methylation-free oocytes displayed genome-wide reduction in Polycomb marks, both H3K27me3 and H2Aub. This unveils an unsuspected positive link between DNMT3L-dependent DNA methylation and Polycomb dynamics, whose origin and significance require further study. In parallel, I found H3K4me3 to accumulate at normally hypermethylated regions in *Dnmt3L*<sup>KO</sup> oocytes, demonstrating a role for DNA methylation in protecting CG-rich regions against ectopic H3K4me3 invasion.

While these multiple chromatin changes seem to have little impact on the oocyte developmental program itself, I showed that it impacts ZGA fine-tuning after fertilization. I observed an excessive transcriptional activity during the minor wave of ZGA in *Dnmt3L*<sup>matKO</sup> zygotes. This increase in RNA production was associated with a developmental delay and a decrease in embryo implantation rate.

As a whole, my work demonstrated a novel function of DNA methylation as a master regulator of the maternal chromatin landscape, with consequences on preimplantation development. It allowed to gain insights into the complexity and importance of maternal epigenetic heritage in the control of zygotic genome activation.

**Keywords :** DNA methylation, polycomb, H3K4me3, oocyte, preimplantation development, maternal epigenetic inheritance, zygotic genome activation, CUT&RUN



## INTERACTIONS EPIGENETIQUES DANS L'OVOCYTE MURIN

**Résumé :** Les cellules germinales ont la capacité unique de transmettre à la descendance non seulement le matériel génétique mais aussi une information dite épigénétique. Au cours de l'ovogenèse, l'épigénome des futurs gamètes femelles est extensivement reprogrammé : les marques somatiques sont effacées et un profil chromatinien spécifique à l'ovocyte est établi. Après fécondation, les marques chromatiniennes portées par l'ovocyte peuvent perdurer au moins pendant les premiers jours du développement préimplantatoire. Comment ces profils chromatiniens maternels influencent le programme transcriptionnel embryonnaire et les phénotypes est un intense domaine de recherche.

L'ovocyte est connu pour être le théâtre d'interactions inhabituelles entre marques chromatiniennes : de leur relations complexes émerge un paysage chromatinien unique, dont l'assemblage influence l'expression des gènes et la capacité d'être transmis à l'embryon. En particulier, deux marques chromatiniennes répressives -la méthylation de l'ADN et la triméthylation de la lysine 27 de l'histone H3 (H3K27me3)- montrent une distribution en miroir qui est transmise à l'embryon. Cependant, alors que leur antagonisme fonctionnel est bien documenté dans les cellules somatiques, la nature de leurs interactions et leur impact mutuel sur le développement de l'ovocyte et de l'embryon précoce étaient inconnus. Au cours de mon doctorat, j'ai étudié les déterminants et les fonctions de la méthylation de l'ADN et de H3K27me3 dans l'héritage épigénétique maternel.

Tout d'abord, en analysant les caractéristiques chromatiniennes d'ovocytes dépourvus de méthylation de l'ADN (en utilisant le modèle mutant *Dnmt3L*) ou H3K27me3 (en utilisant le modèle *Eed<sup>CKO</sup>*) par des méthodes cytologiques et moléculaires, j'ai révélé de nouvelles interactions spécifiques de l'épigénome ovocytaire. J'ai montré que les mécanismes classiques de compensation, observés dans les cellules somatiques entre H3K27me3 et la méthylation de l'ADN, ne s'appliquent pas à l'ovocyte. Les ovocytes *Dnmt3L<sup>KO</sup>* présentent en effet une perte générale de l'enrichissement en marques Polycomb, H3K27me3 et H2Aub. Ceci dévoile un mode d'interaction positif entre la méthylation de l'ADN dépendante de DNMT3L et la dynamique des marques Polycomb dans l'ovocyte. A l'inverse, une accumulation en marques H3K4me3 est observée dans les ovocytes *Dnmt3L<sup>KO</sup>*, résultant de l'envahissement des régions normalement méthylées, démontrant un rôle de la méthylation de l'ADN dans la protection des régions riches en CG contre la déposition ectopique de H3K4me3.

Alors que le remodelage du patrimoine chromatinien maternel résultant de l'absence de méthylation de l'ADN semble avoir peu de conséquences sur le développement ovocytaire, nous avons montré qu'il a un impact sur l'activation du génome zygotique après fécondation. En effet, une activité transcriptionnelle excessive est observée dans les zygotes *Dnmt3L<sup>matKO</sup>*. Cette augmentation de la production d'ARN est associée à un retard de développement et à une capacité diminuée de l'embryon à s'implanter.

Dans l'ensemble, mon travail a démontré une nouvelle fonction de la méthylation de l'ADN comme régulateur général du paysage chromatinien maternel, avec des conséquences sur le développement préimplantatoire. Ils ont permis de mieux comprendre la complexité et l'importance du patrimoine épigénétique maternel dans le contrôle de l'activation du génome zygotique.

**Mots-clés :** Méthylation de l'ADN, polycomb, H3K4me3, ovogénèse, développement pré-implantatoire, transmission épigénétique maternelle, activation génome embryonnaire, CUT&RUN



# RESUME SUBSTANTIEL

- INTERACTIONS EPIGENETIQUES DANS L'OVOCYTE MURIN -

La fécondation correspond à l'union d'un spermatozoïde, d'origine paternelle, avec un ovocyte, d'origine maternelle, pour former le noyau primaire d'un embryon. Les ovocytes et les spermatozoïdes ont la capacité unique de transmettre des informations à la descendance: ils transmettent le matériel génétique, mais aussi une autre forme d'information, dite épigénétique, qui n'est pas codée dans l'ADN mais qui influence son expression. Les marques épigénétiques ovocytaires peuvent être transmises à l'embryon et persister au moins pendant les premiers jours du développement. L'étude du rôle de cet héritage épigénétique maternel dans le contrôle du programme embryonnaire est un intense domaine de recherche.

L'ovocyte est connu pour être le théâtre de relations particulièrement dynamiques entre marques chromatinienne : la somme des interactions attractives et répulsives entre les différentes marques semble régir leur ciblage précis, leur transmission à l'embryon et leur impact sur l'expression des gènes. En particulier, deux marques chromatinienne répressives présentent une distribution en miroir et sont transmises, au moins transitoirement, de l'ovocyte à l'embryon : la méthylation de l'ADN et la tri-méthylation de la lysine 27 de l'histone H3 (H3K27me3). Si ces deux marques sont connues pour leur interactions fonctionnelles complexes impliquant antagonismes et mécanismes de compensation dans les cellules somatiques, l'importance de leur relations fonctionnelles au cours l'ovogénèse et leur rôle dans la régulation du développement des ovocytes et des embryons préimplantatoires demeuraient cependant inconnus. En particulier, alors que la méthylation de l'ADN héritée maternellement a été largement étudié dans le contexte de l'empreinte génomique maternelle et du développement post-implantatoire, son rôle précoce dans l'activation du génome embryonnaire et le développement préimplantatoire n'avait jamais été étudié.

Au cours de ma thèse, j'ai étudié les déterminants et les fonctions de la méthylation de l'ADN et des marques H3K27me3 au cours de l'ovogénèse et du développement embryonnaire précoce, sur le modèle murin. Mes travaux ont apporté des résultats nouveaux et importants dans le domaine de la transmission épigénétique maternel, en adressant trois points majeurs : 1) le rôle de la méthylation de l'ADN et d'H3K27me3 au cours de l'ovogénèse 2) les interactions entre marques chromatinienne ovocytaires, en particulier dans le contexte

d'une déficience en méthylation de l'ADN ou en H3K27me3 et 3) l'impact des remaniements de l'héritage chromatinien maternel associés à l'absence de la méthylation de l'ADN ovocytaire sur l'activation du génome embryonnaire.

### **1. Analyse du rôle de la méthylation de l'ADN et de H3K27me3 dans le contrôle du programme de développement ovocytaire**

Des profils non-canoniques de méthylation de l'ADN et d'H3K27me3 sont établis au cours de l'ovogénèse. S'il était connu que la perte de méthylation de l'ADN ou d'H3K27me3 n'empêche pas la production d'ovocytes fonctionnels, l'analyse plus précise de leur rôle dans le contrôle du programme développemental ovocytaire n'avait jamais été réalisée. Au travers d'une caractérisation développementale et transcriptomique, j'ai donc étudié l'impact de la perte de méthylation de l'ADN (dans des ovocytes *Dnmt3L*<sup>KO</sup>) ou de H3K27me3 (dans des ovocytes conditionnellement déplétés en *Eed*, qui code pour un composant essentiel de PRC2, via le modèle *Gdf9*-CRE ; *Eed*<sup>CKO</sup>). Bien que la méthylation de l'ADN et H3K27me3 soient deux marques habituellement associées à la répression transcriptionnelle, j'ai montré par marquage de la transcription native qu'elles ne sont pas nécessaires à la compaction chromatinienne et à l'arrêt de l'activité transcriptionnelle qui a normalement lieu au cours de la maturation ovocytaire. Le transcriptome de l'ovocyte, analysé par séquençage d'ARN en cellules uniques (scRNA-seq), est également peu impacté par la perte de la méthylation de l'ADN. Cette analyse suggère que la méthylation de l'ADN et d'H3K27me3 ne sont pas essentielles au contrôle de l'activité transcriptionnelle ovocytaire ou alternativement, que des mécanismes compensatoires sont mis en place en absence de l'une de ces deux marques.

### **2. Nouvelles perspectives sur les relations fonctionnelles entre méthylation de l'ADN et marques d'histones au cours de l'ovogénèse**

L'établissement simultané de profils chromatinien non-canoniques dans une cellule mitotiquement quiescente fait de l'ovocyte le théâtre d'importantes interactions entre marques épigénétiques et un modèle unique d'étude. L'observation d'une importante résilience transcriptionnelle ovocytaire face à l'absence de méthylation de l'ADN ou d'H3K27me3 nous a poussé à analyser les relations fonctionnelles entre ces marques chromatinien au cours de l'ovogénèse.

L'utilisation de la technique de CUT&RUN, que j'ai adaptée à de petites quantités de cellules, m'a permis de générer une cartographie précise des marques H3K4me3 et H3K27me3

au cours de l'ovogénèse. J'ai ainsi pu analyser la dynamique et les corrélations entre méthylation de l'ADN et marques d'histones. Forte de ces observations en conditions physiologiques, je me suis tournée vers l'analyse des remaniements chromatinien qui pourraient résulter de l'absence de méthylation de l'ADN ou de H3K27me3. J'ai pu ainsi identifier de nouvelles interactions entre marques chromatinien dans l'épigénome de l'ovocyte.

Alors qu'il avait été montré dans de nombreux modèles cellulaires qu'H3K27me3 a tendance à envahir les régions ayant perdu la méthylation de l'ADN et vice versa, j'ai révélé que cette relation fonctionnelle ne s'applique pas à l'ovocyte : la perte de l'une de ces marques n'est pas remplacée par l'autre marque.

En combinant des approches quantitatives par immunofluorescence et de nouvelles stratégies de normalisation de CUT&RUN, j'ai pu montrer que la perte de la méthylation de l'ADN dans l'ovocyte est associée à une accumulation d'H3K4me3 au niveau des régions normalement méthylées et à une diminution générale de l'enrichissement en marques Polycomb, à la fois H3K27me3 et H2Aub. Ceci révèle un rôle de protection de la méthylation de l'ADN contre l'acquisition aberrante de H3K4me3 dans l'ovocyte, en particulier au niveau de régions riches CG. La perte de H3K27me3 et H2Aub dans les ovocytes *Dnmt3L*<sup>KO</sup> dévoile une relation positive insoupçonné entre méthylation de l'ADN et marques Polycomb, ouvrant de nouvelles perspectives pour la compréhension des interactions moléculaires entre ces deux voies chromatinien.

L'identification des remaniements chromatinien de l'ovocyte *Dnmt3L*<sup>KO</sup> témoigne d'un rôle clé de la méthylation de l'ADN pour la structuration correcte de l'héritage chromatinien maternel.

### **3. La transmission des remaniements chromatinien, associés à la perte de méthylation ovocytaire, perturbe le développement pré-implantatoire et le programme d'activation du génome zygotique**

Si les effets post-implantatoires de la perte d'empreinte maternelle ont été largement décrits, le rôle immédiat de la méthylation de l'ADN maternel lors de sa transmission à l'embryon était inconnu. En effet, les profils de méthylation de l'ADN maternels sont globalement transmis à l'embryon au moment de la fécondation, et persistent avant d'être progressivement effacés au cours des divisions cellulaires. Cette transmission transitoire de la

méthylation maternelle pourraient affecter la mise en place du programme de développement embryonnaire. Nous avons montré pour la première fois que la perturbation de la méthylation de l'ADN maternel et les remodelages chromatinien associés peuvent affecter le développement pré-implantatoire. La génération d'embryons *Dnmt3L*<sup>matKO</sup> à partir d'ovocytes *Dnmt3L*<sup>KO</sup> dépourvus de méthylation de l'ADN et fécondés par des spermatozoïdes WT m'a permis d'analyser les effets de la transmission d'un héritage épigénétique maternel perturbé sur le développement embryonnaire précoce.

Les embryons *Dnmt3L*<sup>matKO</sup> héritent en effet, comme j'ai pu l'identifier dans l'ovocyte et le confirmer par immunofluorescence dans le zygote, de profils chromatinien maternels dépourvus de méthylation de l'ADN et présentant une accumulation de H3K4me3 et une diminution de l'enrichissement en marques Polycomb, H3K27me3 et H2Aub. Ceci est associé à une augmentation aberrante de l'activité transcriptionnelle au moment de la première vague d'activation du génome embryonnaire dans le zygote *Dnmt3L*<sup>matKO</sup>. A ce stade, j'ai en effet observé une augmentation de la quantité de transcrits natifs et une plus grande accessibilité ou décompaction du génome embryonnaire pour la transcription. Ceci s'accompagne d'une augmentation anormale de la quantité totale d'ARN messagers présents au stade 2-cellules, que nous avons pu mesurer par normalisation du nombre de reads en scRNA-seq.

La modification des profils épigénétiques présents sur tout le génome maternel, en particulier la perte de marques répressives comme la méthylation de l'ADN/Polycomb et le gain de la marque active H3K4me3, pourraient rendre la chromatine plus permissive à l'activation transcriptionnelle. De plus, *Dux*, un important activateur de la transcription embryonnaire, et ses effecteurs en aval connus pour favoriser une décompaction de la chromatine, sont surexprimés dans le zygote *Dnmt3L*<sup>matKO</sup>. Cette surexpression est associée à la perte de la marque H3K27me3 au niveau du locus *Dux* dans l'ovocyte *Dnmt3L*<sup>KO</sup>, qui pourrait expliquer l'augmentation de l'activation de *Dux* sur l'allèle maternel de l'embryon, en absence de marques répressives Polycomb normalement héritées de l'ovocyte. La perturbation de l'héritage chromatinien maternel est donc responsable d'une augmentation aberrante de l'activité transcriptionnelle.

Le suivi du développement préimplantatoire des embryons *Dnmt3L*<sup>KO</sup> par imagerie nous a permis d'identifier un retard de développement apparaissant de manière concomitante à l'activation excessive du génome embryonnaire, à la transition de 2 à 4 cellules. Ce retard de développement d'environ 6h entraîne la formation de blastocystes *Dnmt3L*<sup>KO</sup> contenant un

plus petit nombre de cellules et aux capacités diminuées d'implantation dans l'utérus maternel. Le remodelage de l'héritage épigénétique maternel semble donc responsable d'une perturbation du programme de développement embryonnaire et d'une diminution du fitness des embryons pré-implantatoires.

En conclusion, j'ai révélé au cours de ma thèse de nouveaux modes d'interaction entre la méthylation de l'ADN, H3K4me3 et H3K27me3 au cours de l'ovogénèse grâce à l'optimisation de la technique de CUT&RUN dans l'ovocyte. J'ai démontré l'impact que ces relations fonctionnelles peuvent avoir dans des ovocytes dépourvus de méthylation de l'ADN. L'absence de méthylation de l'ADN y est en effet associée à de multiples remaniements majeurs du paysage chromatinien : une accumulation d'H3K4me3 dans les régions normalement méthylées et une diminution généralisée de l'enrichissement en marques Polycomb. Alors que cette réorganisation de l'épigénome maternel n'a pas de conséquences notoires sur le programme ovocytaire, elle perturbe l'activation du génome embryonnaire lors de sa transmission, après fécondation. Les zygotes dépourvus de méthylation de l'ADN maternelle présentent ainsi un réveil transcriptionnel excessif, associé à un retard de développement et à une diminution du taux d'implantation.

J'ai ainsi identifié un rôle majeur de la méthylation de l'ADN dans la structuration du patrimoine chromatinien de l'ovocyte, avec des conséquences pour la mise en place du programme de développement préimplantatoire. Ceci met en lumière l'importance de l'héritage épigénétique maternel et ouvre de nouvelles perspectives en matière de médecine reproductive, notamment pour l'identification de nouvelles causes de subfertilité féminine liée à des troubles du développement pré-implantatoire. Cette voie de recherche pourrait également permettre de cerner l'influence de facteurs externes, comme les procédures médicales d'aide à la procréation (PMA), sur l'héritage épigénétique maternel et les grossesses associées.



# TABLE OF CONTENTS



<b>INTRODUCTION</b> .....	<b>27</b>
<b>I – PREFACE</b> .....	<b>29</b>
<b>II – FEMALE GERM CELL DEVELOPMENT</b> .....	<b>30</b>
<b>1 – An overview of female germ cell development, from specification to sex determination</b> .....	<b>30</b>
1.1 Primordial germ cell specification.....	30
1.2 Primordial germ cell migration and formation of “germ cell cysts” .....	31
1.3 Sex specification.....	32
<b>2 – Meiosis entry</b> .....	<b>33</b>
<b>3 – Folliculogenesis</b> .....	<b>35</b>
3.1 Follicular assembly .....	35
3.2 Follicle maturation .....	36
- Granulosa cells proliferation.....	38
- Theca cells .....	38
3.3 Oocyte maturation.....	39
- Growing phase of oogenesis.....	39
- Chromatin remodeling : the surrounded nucleoli transition .....	40
- Zona pellucida secretion.....	41
- Meiotic maturation .....	41
<b>4 – Ovulation and meiotic resumption</b> .....	<b>42</b>
4.1 Ovulation process .....	42
4.2 Germinal vesicle breakdown and meiosis resumption.....	43
<b>5 – Overview of embryonic preimplantation development</b> .....	<b>45</b>
5.1 Early cleavages and zygotic genome activation process .....	45
- Parental genome fusion and early cleavages.....	45
- Zygotic genome activation.....	46
5.2 Compaction and blastocyst formation .....	48
- Compaction.....	48
- Blastocoel formation.....	49
<b>III – EPIGENETIC MARKS AND THEIR INTERPLAYS</b> .....	<b>50</b>
<b>1 – DNA methylation</b> .....	<b>50</b>
1.1 DNA methylation generalities.....	50
1.2 DNA methylation distribution and functions.....	52
1.3 DNA methylation in development .....	53
1.4 The <i>de novo</i> DNA methylation machinery : focus on DNMT3A-DNMT3L.....	56
<b>2 – Polycomb marks (H3K27me3 and H2Aub)</b> .....	<b>58</b>
2.1 Polycomb repressive complex 2 (PRC2) and H3K27me3 .....	59
2.2 Polycomb repressive complex 1 (PRC1) and H2Aub.....	61

2.3 Polycomb-mediated transcriptional silencing .....	62
<b>3 – Histone H3 Lysine-4 Trimethylation (H3K4me3) .....</b>	<b>64</b>
3.1 H3K4me3 distribution and functions .....	64
3.2 H3K4 methyltransferases .....	66
<b>4 – Other post-translational histone modifications .....</b>	<b>68</b>
4.1 Histone H3 Lysine-36 trimethylation (H3K36me3).....	68
4.2 Histone H3 Lysine-9 trimethylation (H3K9me3) .....	68
<b>5 – Interplays between chromatin marks .....</b>	<b>69</b>
5.1 H3K4me3 and DNA methylation antagonism .....	70
5.2 H3K36me2/me3 promotes <i>de novo</i> DNA methylation.....	72
5.3 Antagonism between H3K27me3 and the DNA methylation-H3K36me3 duo.....	73
- Negative crosstalks between H3K27me3 and DNA methylation .....	73
- The complex case of H3K36me3, DNA methylation and H3K27me3 crosstalks.....	74
5.4 H3K27me3 and H3K4me3.....	76
<b>IV – EPIGENETIC INTERPLAYS DURING OOGENESIS.....</b>	<b>78</b>
<b>1 – Epigenetic reprogramming in primordial germ cells .....</b>	<b>78</b>
1.1 DNA methylation erasure.....	79
1.2 Remodeling of somatic histone modifications patterns.....	81
1.3 Prolonged phase of hypomethylation until puberty.....	83
<b>2 – Acquisition of oocyte-specific chromatin patterns with maternal heritable properties .....</b>	<b>84</b>
2.1 Maternal DNA methylation establishment and functions.....	85
- DNMT3A-DNMT3L-dependent DNA methylation deposition .....	86
- DNA methylation patterns deposition through precise DNMT3 targeting to chromatin .....	87
- The functional role of DNA methylation in the oocyte.....	90
- Maternal DNA methylation inheritance .....	90
2.2 Oocyte-specific H3K4me3 non-canonical landscape and functions.....	92
- Canonical promoter H3K4me3 enrichment in oocytes .....	93
- Non-canonical broad H3K4me3 domains acquisition.....	93
- Repressive function of broad ncH3K4me3 domains in the oocyte .....	94
- Maternal ncH3K4me3 inheritance .....	95
2.3 Polycomb marks in maternal epigenetic inheritance.....	97
- Broad H3K27me3 domains in the oocyte epigenome .....	97
- The actors of ncH3K27me3 domain establishment.....	99
- H3K27me3 and H2Aub co-enrichment in the oocyte epigenome.....	99
- Maternal inheritance of H3K27me3.....	100
- H2Aub guides maternal H3K27me3 inheritance .....	101
- Polycomb-mediated non-canonical imprinting.....	102
- Maternal H2Aub function in ZGA.....	104

- Polycomb-associated domains (PADs).....	104
2.4 H3K36me3 in maternal epigenome and embryonic development .....	106
2.5 H3K9 methylation dynamics in oocytes and embryos.....	107
<b>3 – Interplays between chromatin marks in the oocyte epigenome .....</b>	<b>109</b>
3.1 Active histone marks regulate <i>de novo</i> DNA methylation in oocytes .....	109
- H3K36me3 is essential for DNA methylation patterns establishment .....	109
- Promoter H3K4me3 dynamics dictates DNA methylation deposition.....	110
3.2 DNA methylation anti-correlates with ncH3K4me3 and H3K27me3.....	111
- H3K4me3 and DNA methylation antagonism .....	112
- H3K27me3 and DNA methylation mutual exclusivity.....	113
3.3 Perturbations in absence of DNA methylation-H3K36me3 enriched compartments .....	113
3.4 ncH3K27me3 and ncH3K4me3 equilibrium .....	115
<b>4 – Relevance for the field of reproductive medicine .....</b>	<b>118</b>
<b>MATERIAL &amp; METHODS.....</b>	<b>123</b>
<b>RESULTS .....</b>	<b>137</b>
Dynamics of oocyte epigenome establishment.....	140
Oocyte development and transcriptome are minimally disrupted in absence of H3K27me3.....	144
Chromatin remodeling in <i>Eed<sup>CKO</sup></i> oocytes : lack of DNA methylation spreading.....	146
Oocyte development and transcriptome are minimally disrupted upon loss of DNA methylation.....	147
Global H3K27me3 decrease in <i>Dnmt3L<sup>KO</sup></i> oocytes.....	150
H3K4me3 accumulates at regions that have lost DNA methylation in <i>Dnmt3L<sup>KO</sup></i> oocytes.....	153
Towards the mechanisms behind H3K4me3 and H3K27me3 remodeling in absence of DNMT3L.....	156
Significance of the observed chromatin remodeling for transcriptional control in <i>Dnmt3L<sup>KO</sup></i> oocytes	160
The remodeled oocyte chromatin mark patterns are transmitted to the <i>Dnmt3L<sup>matKO</sup></i> embryos .....	160
<i>Dnmt3L<sup>matKO</sup></i> embryos exhibit enhanced zygotic genome activation.....	161
Developmental delay and fitness decrease in <i>Dnmt3L<sup>matKO</sup></i> preimplantation embryos .....	165
<b>DISCUSSION .....</b>	<b>167</b>
<b>1 – General conclusion and personal impression .....</b>	<b>169</b>
<b>2 – Transcriptional regulation in the oocyte .....</b>	<b>170</b>
2.1 The role of DNA methylation and H3K27me3 in oocyte transcriptional regulation.....	170
2.2 Oocyte transcriptional shutdown is not affected by the loss of H3K27me3 or DNA methylation .....	171
2.3 The puzzling case of transposable element regulation in the oocyte epigenome .....	172
2.4 The challenges of studying transcription in oocytes and early embryos.....	174
<b>3 – New insights into DNA methylation, H3K27me3 and H3K4me3 functional relationships .....</b>	<b>174</b>
3.1 The overlooked fact : the importance of <i>spike-in</i> in chromatin profiling technics.....	174
3.2 H3K4me3 accumulation in absence of DNA methylation at the NSN-to-SN transition.....	176

3.3 DNA methylation – Polycomb marks : unusual relationships in the oocyte context .....	178
- Molecular mechanisms behind the Polycomb mark reduction in <i>Dnmt3L</i> <sup>KO</sup> oocytes .....	179
<b>4 – Maternal epigenetic heritage and zygotic genome activation .....</b>	<b>181</b>
4.1 Developmental role for maternal DNA methylation in preimplantation embryos .....	181
4.2 What could cause increased transcription at minor ZGA in <i>Dnmt3L</i> <sup>matKO</sup> embryos ? .....	182
- Remodeling of maternal chromatin patterns could affect ZGA in <i>Dnmt3L</i> <sup>matKO</sup> embryos .....	182
- Transcriptional kindling of ZGA through Dux overexpression in <i>Dnmt3L</i> <sup>matKO</sup> embryos .....	184
4.3 Increased RNA production and developmental delay .....	185
4.4 Significance for the field of reproductive medicine .....	186
<b>REFERENCES .....</b>	<b>189</b>

# INTRODUCTION



## I - Preface

Fertilization corresponds to the union of a spermatozoon nucleus, of paternal origin, with an oocyte nucleus, of maternal origin, to form the primary nucleus of an embryo. Oocytes and spermatozoa are differentiated cells, highly specialized to perform the multi-step fertilization process. They also have the unique ability to transmit information to the progeny : they transmit genetic material, but also another form of information that is not encoded in the DNA but influences its expression, and that is broadly defined as “epigenetic”. Oocyte epigenetic patterns are known to exhibit maternal heritability and to persist at least during the first days of preimplantation development in the embryo. The oocyte is known to be the theater of intense chromatin marks interplays : the sum of attractive and repulsive feedbacks between chromatin marks seems to rule their precise targeting, their transmission to the embryo and their role in regulating gene expression. In my PhD, I investigated the determinants and functions of maternal DNA methylation and H3K27me3 in maternal epigenetic heritage. My project was organized in two aims : 1) investigating the chromatin marks interplays in the oocyte genome, in particular in the context of DNA methylation or H3K27me3 deficiency and 2) identifying the role of maternal H3K27me3 and DNA methylation in regulating the developmental program of oocytes and early embryos.

In this introduction chapter, I will first provide an overview of oogenesis and the different steps of this unique developmental program. In particular, I will focus on the growing phase of oogenesis, which coincides with the establishment of oocyte-specific epigenetic patterns. I will then briefly describe the key steps of embryonic preimplantation development. In a second part, I will describe the main chromatin mark systems, their establishment and associated-players, with a particular emphasis on the known interplays between chromatin states. Contrary to somatic cells, epigenetic patterns are highly dynamic during germ cells development. I will therefore detail in the third part of this introduction how chromatin patterns are established during oogenesis and transmitted to the preimplantation embryo. I will provide an overview of the current state of the research on the interplays and functions of maternal epigenetic marks.

## II - Female germ cell development

### 1 - An overview of female germ cell development, from specification to sex determination

#### 1.1 - Primordial germ cell specification:

Primordial germ cells (PGCs) are the primary undifferentiated cell types that will give rise to the whole male or female germline and ultimately, will differentiate towards mature gametes, spermatozoa or oocytes. In mammals, the origin of PGCs has remained long unclear. In invertebrates and some lower vertebrates like *Drosophila melanogaster* or *Xenopus laevis*, PGC specification is ensured by the presence of a preformed germ cell determinant in the egg, called the germplasm. The germplasm corresponds to a localized specialized cytoplasm that contains RNAs and proteins needed for PGC formation. In this mode of germ cell specification, called 'preformation', the germline continuity is ensured by the germ cells directly. However, in mammals, such mechanism does not exist: the germline is formed through the 'epigenesis' mode (Nikolic et al., 2016), whereby PGCs are specified from somatic cells during embryogenesis, and have to undergo profound identity reprogramming.

Mammalian PGCs were first identified in the mouse by Duncan Chiquoine in 1954 (Chiquoine, 1954). In embryos at around embryonic day 7.25 of development (E7.25), he reported a small cluster of cells capable of generating both oocytes and spermatozoa, present at the basis of the incipient allantois, in the endoderm of the yolk sac. In mice, PGC specification indeed occurs in response to complex signaling cross-talks just before gastrulation. The simultaneous signal in Bone morphogenetic protein 4 (BMP4) secreted from the extra-embryonic ectoderm (ExE) and BMP2 from the posterior visceral endoderm, induces the formation around E6.5 of a cluster of PGC cells in the posterior epiblast, at the site with the highest levels of BMP signals. In contrast, the anterior visceral endoderm secretes antagonists of BMPs (like CER1 or WNT), which prevent PGC induction. The PGC population is characterized by the expression of the transcription factor PR domain zinc-finger protein1 (PRDM1, also called BLIMP1) that simultaneously represses the somatic mesodermal differentiation program and activates germline-specific genes (Saitou & Yamaji, 2012).

An interesting notion is that contrary to the unique egg cylinder structure of peri-gastrulation development that mice present, humans and non-rodent mammals develop as a

planar disc. PGCs arise around day 12 post-fertilization in humans in this time of developmental 3D divergence (Chen et al., 2019). Although BMP signaling seems conserved between humans and mice, the spread of these secreted factors and the gene regulatory networks of PGC specification differ (W. W. C. Tang et al., 2016). The study of PGCs in humans is difficult due to the technical and ethical restrictions in obtaining such cells from early post-implantation human embryos. Nevertheless, the timing and dynamic of PGC specification seems conserved among mammals.

## 1.2 - Primordial germ cell migration and formation of 'germ cells cysts' in the genital ridges

Soon after their specification, PGCs start displaying cytoplasmic protrusions and polarized structures. They then migrate to the developing hindgut endoderm, through the mesentery, and colonize the genital ridges at E10.5 in the mouse (Saitou & Yamaji, 2012). During this migration process, PGCs are highly proliferative, going from a small population of 40 cells to several thousands in the genital ridges at E13.5. During migration, PGCs also undergo extensive epigenome reprogramming, which leads to the erasure of the somatic patterns of chromatin marks and subsequent establishment of oocyte- or sperm- specific patterns during the next phases of germline development. The details of these epigenetic processes will be discussed in Chapter IV of this Introduction.

In females, after colonization of the genital ridges, PGCs continue their mitotic proliferation but this time with incomplete cytokinesis, leaving the sister cells joined by intercellular bridges (**Figure 1**). This leads to the formation of 'germ cell cysts' that divide synchronously, forming chains of  $2^n$  interconnected cells (Pepling, 2006). At this stage, germ cells are termed oogonia. Their cytoplasmic bridges are the source of inter-cellular exchanges of RNAs, proteins and organelles. However, the biological significance of such connection is still poorly understood.

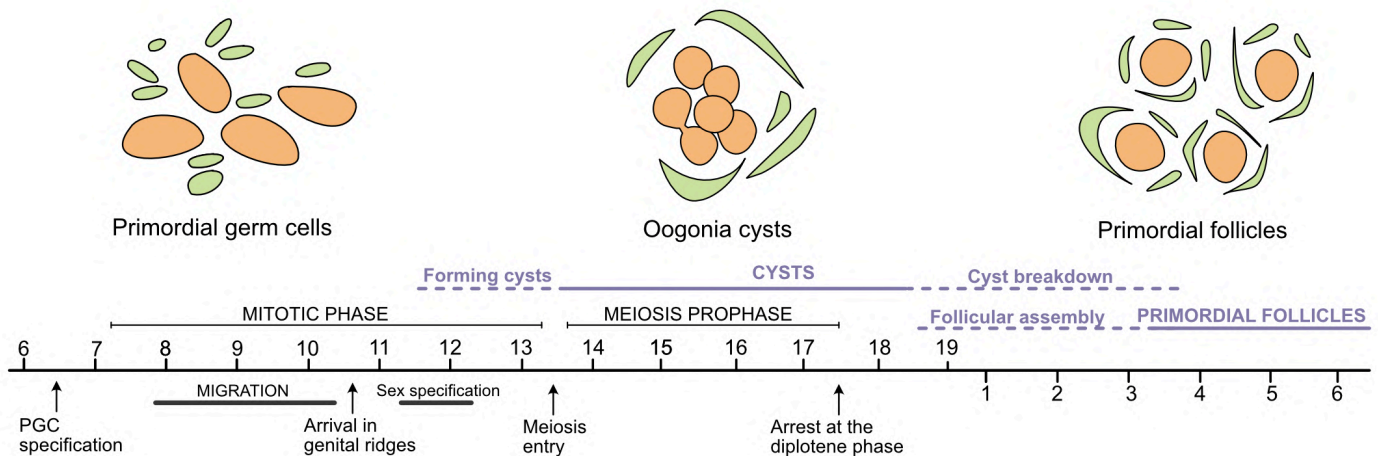


**Figure 1: Timeline of early female germ cell development in the mouse.** Primordial germ cells (PGCs) are specified around E6.5 and migrate towards the genital ridges. Incomplete cytokinesis during their phase of intense mitotic proliferation leads to formation of oogonia cysts. Following sex specification, germ cells within cysts enter meiosis and progress through meiotic prophase until they arrest at the diplotene stage around E17.5. After birth, germ line cysts break and granulosa cells enclose individual oocytes to form primordial follicles. The primordial follicles formed around birth constitute the entire pool of oocytes available during the female reproductive life. *Orange: germ cells; green: somatic cells.*

### 1.3 - Sex specification

Male and female germ cells are indistinguishable during genital ridge colonization and until E12.5. They must however differentiate to generate the type of gametes specific of each sex. Oogonia sex specification is not dependent on their own sexual chromosomes but relies on the sexual phenotype of their somatic environment. It was shown indeed by chimeric gonad experiments that a XX germ cell, when residing in XY testicular environment, will differentiate into male spermatogonia (and vice versa for a XY germ cell in a XX environment) (Mclaren & Mammalian, 1981). The sex-determining region on the Y chromosome *Sry*, expressed in Sertoli cells in the testis, has been shown to be responsible for the male fate acquisition and the masculinization of the reproductive tract (Koopman et al., 1991).

Retinoic acid (RA) synthesized from E10.5 in the gonads of both sexes favors meiosis entry (Ewen & Koopman, 2010). The male-specific expression of the cytochrome CYP26B1, a potent antagonist of RA, leads to mitotic arrest in the male and delayed entry into meiosis, which will occur after birth only. Conversely, in absence of this antagonist, RA signaling leads in the female germ cells to expression of early meiosis markers like STRA8 (stimulated by retinoic acid 8, the earliest marker of female germ cell sexual differentiation that is essential for pre-meiotic DNA replication). Female germ cells progressively enter meiosis prophase I from E13.5 on. The hallmark of sex differentiation is thus the entry into meiosis for the female germline

and the beginning of a mitotically quiescent phase for male germ cells. The latter will resume proliferation only after birth to form spermatogonial stem cells, which sustain continuous waves of spermatozoa production during the whole life of the male individual. In direct relevance with my PhD project, the rest of this chapter will be exclusively focused on the development of the female germline.

## 2 - Meiosis entry

Following 'germ cell cysts' formation, mitotic proliferation stops and the oogonia initiate meiosis, thereby becoming primary oocytes, which correspond to the first female-specific stage of germ cell development (**Figure 1**). Meiosis is characterized by one round of DNA replication followed by two consecutive rounds of chromosome segregation. It enables the formation of haploid cells, necessary for fertilization.

Meiosis entry proceeds in a wave from the anterior to posterior part of the ovary, which correlates with a rostro-caudal gradient in retinoic acid (RA) concentration. Particularly high levels of RA are found in the mesonephric tubules that are in contact with the anterior part of the ovary. It induces a cranio-caudal wave of meiotic markers activation that correlates with the dynamic of meiosis entry from E13.5 to E15.5 ([Menke et al., 2003](#)). Meiosis entry is characterized first by the expression of STRA8, which is responsible for pre-meiotic DNA replication, followed by SYCP3 (synaptonemal complex protein 3) and DMC1 (DNA meiotic recombinase 1). SYCP3 is a component of the synaptonemal complex, a meiosis-specific structure responsible for homologous chromosome pairing during prophase I. DMC1 is required for double-strand break repair during recombination.

Meiosis initiates with prophase I, a crucial and extended stage during which the oocytes transit through four cytological sub-stages ([Kar & Hochwagen, 2021](#)) (**Figure 2**):

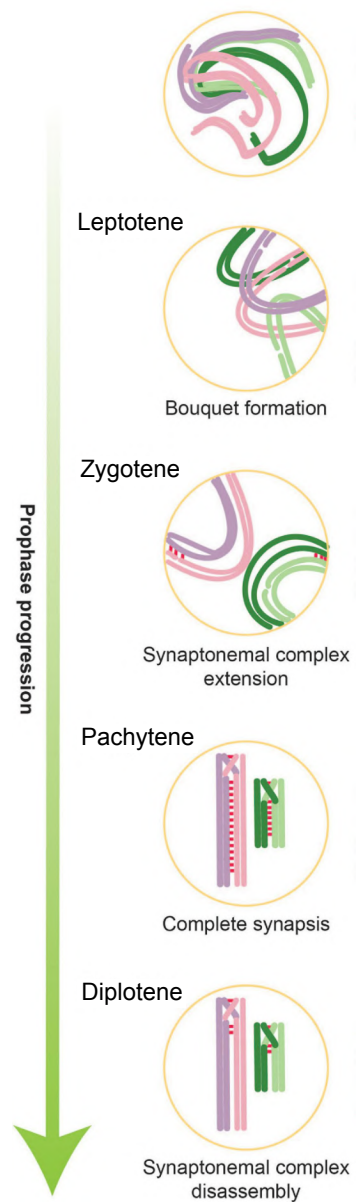
**Leptotene:** Directly after DNA replication, chromatin starts to condensate and individual chromosomes become identifiable. At the same time, programmed double strand breaks (DSB) are created by the topoisomerase-like protein SPO11 ([Baudat et al., 2000](#)). These DSBs are essential for initiating homologous recombination between chromosomes of the same pair.

**Zygotene:** At this stage, chromatin is condensed and homologous chromosomes undergo synapsis, a process by which synaptonemal complexes pair matching regions of homologous chromosomes. It corresponds to a protein structure composed of SYCP1, SYCP2, SYCP3 and TEX12 that hold the aligned chromosomes together (Page & Hawley, 2004).

**Pachytene:** Synapsis is now complete and recombination sites appear at some foci of previously generated DSBs. This leads to formation of crossing-overs between homologous chromosomes with exchange of genetic material.

**Diplotene:** De-synapsis is initiated by partial dissociation of the two homologous chromosomes. Indeed, synaptonemal complexes dissolve and homologous chromosomes remain attached through chiasmata, at locations where recombination occurred.

Figure 2: Overview of stages of the prophase of meiosis I. Adapted from Kar & Hochwagen, 2021. See in the text for the description of the different sub-stages.



Around E17.5, oocytes reach the final stage of the first meiotic prophase and arrest at the diplotene stage. The high levels of cAMP (cyclic adenosine 3',5'-monophosphate) present in the oocytes are responsible for this arrest. Indeed, in order to pursue meiosis and enter metaphase, phosphorylation of the cell cycle regulator protein complex cyclin B-CDK1 (cyclin-dependent kinase 1) is needed. However, high levels of intracellular cAMP lead to activation of an inhibitory pathway for CDK1 phosphorylation (Pan & Li, 2019). The oocyte will thus stay arrested in diplotene phase until meiotic resumption at the final stages of oogenesis.

## 3 - Folliculogenesis

### 3.1 - Follicular assembly:

From E17.5 to P5, oocytes become enclosed in primordial follicles (**Figure 1**), consisting of one diplotene-arrested oocyte and several somatic cells, called granulosa cells. Follicles correspond to the functional units of the ovary. To enable follicular assembly, oocytes first need to separate through a process called 'cyst breakdown' (Pepling, 2012). During this process, two third of the oocytes in each cyst will die through apoptosis. One cell dies in the middle of a cyst, leading to scission of the large cyst into two smaller cysts. This programmed cell death is repeated until only individualized oocytes remain. As the oocytes separate, they become enclosed in a layer of granulosa cells. Some cytoplasmic processes extending from somatic cells have been observed between oocytes and seem to be playing a role in physically separating the oocytes to form individual follicles.

One pathway has also been shown as particularly important for follicle formation: in absence of the growth differentiation factor 9 (GDF9), ovaries display altered gene expression in granulosa cells and significant number of multiple oocyte follicles (MOFs) (Elvin et al., 2000). MOFs correspond to the presence of more than one oocyte per follicles and would be a consequence of incomplete cyst breakdown. GDF9 is secreted by the oocyte, suggesting that the signals between oocyte and granulosa cells are important for ensuring follicle formation.

Another example of the importance of the oocyte-somatic communication within a follicle is the role of granulosa cells in the maintenance of meiotic arrest. High intracellular levels of cAMP, which ensures meiotic arrest, are maintained in the oocyte thanks to metabolites secreted by the surrounding granulosa cells (Adhikari & Liu, 2013). These metabolites will be recognized by oocyte-specific receptors and will lead to activation of cAMP production pathway. Upon oocyte dissection and follicular cell removal, the oocyte will therefore have a tendency to spontaneously resume meiosis. Gap junctions are also formed between granulosa cells and the oocytes, forming another crucial communication way. In ovaries deficient for connexin 43 (CX43), a protein necessary for maintaining oocyte-granulosa gap junctions, an early arrest in folliculogenesis is observed (Simon et al., 1997). It has also been hypothesized that cAMP generated in follicular cells can be transported through gap junctions to maintain meiotic arrest (Dekel, 1988).

The primordial follicles formed around birth constitute the entire pool of oocytes available during the female's reproductive life. Although the notion that new oocytes could be formed post-birth has been recently proposed ([Johnson et al., 2004](#)), the actual model is still that females display a finite and pre-formed pool of primordial follicles, precursors of mature oocytes. Primordial follicles stay arrested in development until sexual maturity, when pools of follicles are recruited by hormonal follicle activation. They will thus resume development, going through oocyte growth phase and follicle maturation. Some activated follicles will eventually die by follicular atresia, while oocytes in surviving follicles will undergo ovulation.

### 3.2 – Follicle maturation

Continuously during the female's reproductive life, cohorts of dormant primordial follicles are activated: they are recruited to initiate folliculogenesis, a very dynamic process that lasts two weeks in mice and around six months in human ovaries. The dormant primordial follicles display three possible fates: 1.) remain quiescent, 2.) be activated, enter the pool of growing follicles but degrade through atresia or 3.) complete their maturation process until ovulation. At each stage of folliculogenesis, some follicles will indeed go through atresia. Folliculogenesis is characterized by an intense growth phase of the oocyte itself, associated with proliferation and differentiation of the surrounding follicular cells ([Rimon-Dahari et al., 2016](#)).

Folliculogenesis is often described in two parts: the pre-antral stage, and as the follicle continues to develop, a liquid cavity called antrum appears and the follicle reaches the antral stage (**Figure 3**). The pre-antral follicle is still independent from extraovarian factors and is rather regulated by paracrine signals between the oocyte and the surrounding somatic cells. At the opposite, antral follicles rely on pituitary hormones for their development: the Follicle-stimulating hormone (FSH) and luteinizing hormone (LH) are the gonadotropins that coordinate antral folliculogenesis and ovulation.

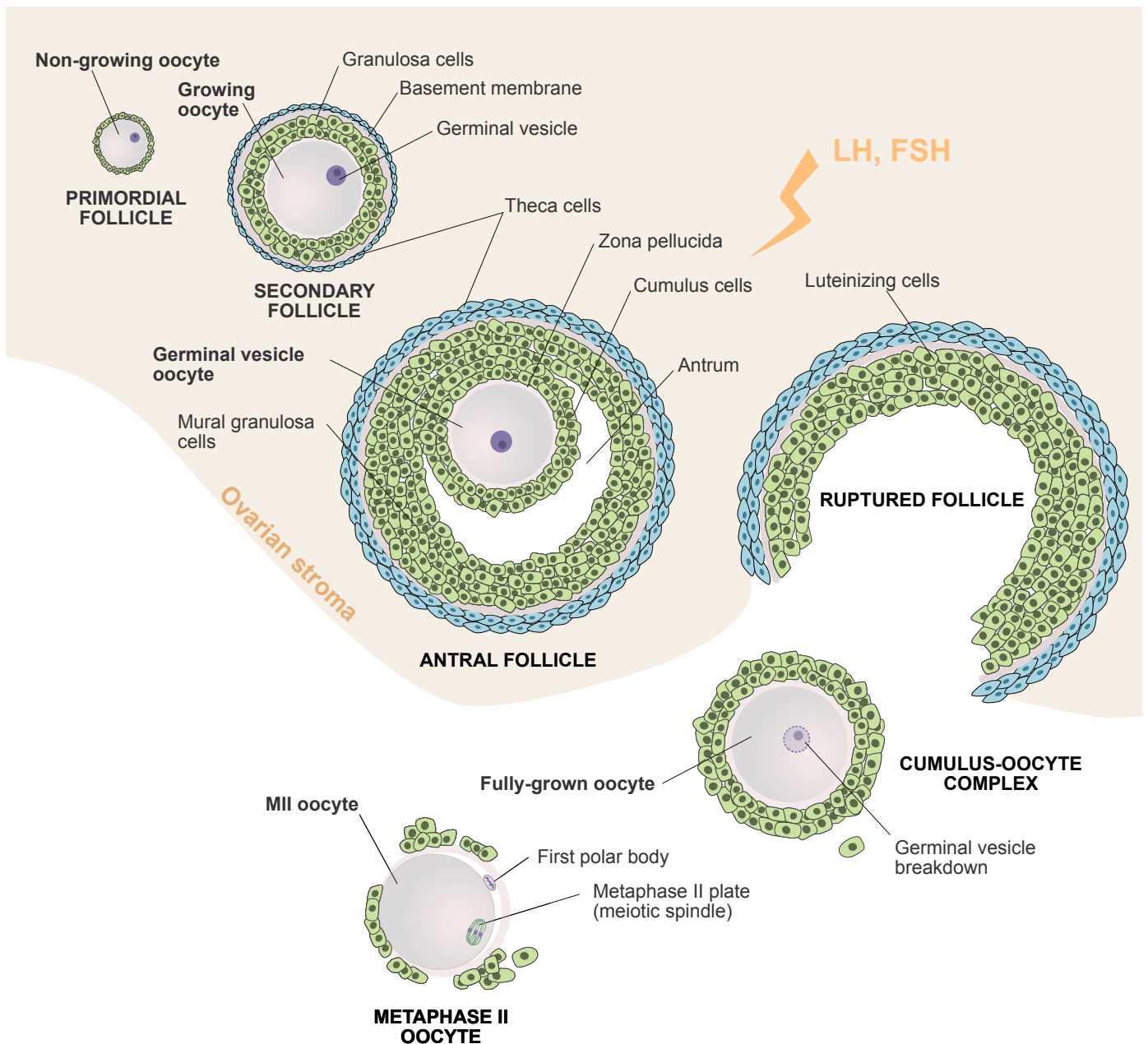


**Figure 3: Schematic presentation of the main stages in ovarian folliculogenesis.** Primordial follicles present at birth form the functional units in ovary and the entire pool of oocytes available during the female's reproductive life. Each follicle corresponds to a diplotene-arrested oocyte surrounded by one layer of granulosa cells. They stay arrested in development until sexual maturity, when pools of follicles are recruited by hormonal follicle activation (paracrine signals or LH/FSH). During folliculogenesis, granulosa cells proliferate and differentiate in two distinct cell types upon antrum formation: the cumulus cells and mural granulosa cells. Theca cells differentiate from the ovarian stroma to surround the developing follicle. In parallel, the oocyte enters its growing phase, characterized by drastic size increase, intense RNA/proteins production and secretion of a glycoprotein layer, the zona pellucida. Upon hormonal stimulation, ovulation will occur with release of the cumulus-oocyte complex in the infundibulum. The remaining granulosa and theca cells will differentiate in luteinizing cells to form the corpus luteum. In the hours following ovulation, germinal vesicle breakdown marks the resumption of meiosis I. Almost immediately after the first meiotic chromosome segregation and the extrusion of the first polar body, the oocyte enters meiosis-II. It stays arrested at the metaphase II state until fertilization.

I will review below the dynamic changes that affect the architecture of the follicles and the organization of surrounding somatic cells during the different steps of folliculogenesis.

- Granulosa cells proliferation:

The activation of primordial follicles and the transition to a primary follicle state is characterized by a change in granulosa cell morphology, from squamous to cuboidal, and the beginning of oocyte growth. During the formation of secondary follicles, granulosa cells further proliferate and constitute two or more layers around the growing oocyte. A basement membrane appears around the outer part of the granulosa cell layers, forming the limit of the follicle.

Progressively, multiple small fluid-filled spaces accumulate in the follicle and merge to form an antral cavity that separates the granulosa cells in two distinct populations, depending on their position relative to the oocyte and the antrum: the mural granulosa cells on the outer part of the follicle, and the cumulus cells that are adjacent to the oocyte and will expand on a hyaluoronan-rich extracellular matrix to form the cumulus-oocyte complex (**Figure 3**) (Edson et al., 2009).

- Theca cells:

Somatic cells from the ovarian stroma will differentiate to form theca cells that surround

this basement membrane and encapsulate the whole follicle. Theca cells display the particular feature of having mitochondria with tubular cristae needed for steroid hormone production. Indeed, the principal function of theca cells is to produce androgen (**Figure 4**). Indeed, the luteinizing hormone (LH) stimulates the expression of key steroidogenic enzymes in theca cells that enable converting androgens from cholesterol (Magoffin, 2005). Androstenedione will then diffuse through the basement membrane, before being converted in estradiol by mural

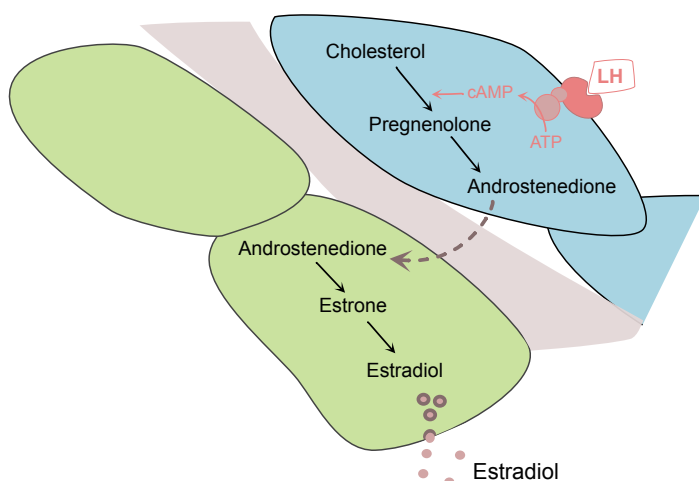


**Figure 4: Theca-granulosa cells coupling for androgen production.** LH stimulates the expression of steroidogenic enzymes in theca cells (blue on the scheme), which are responsible for conversion of cholesterol into androstenedione. It will diffuse through the basement membrane and will be converted in estradiol by granulosa cells (green). Estradiol is then secreted by the ovary and regulate ovulation and endometrial growth.

granulosa cells. Experiments with isolated theca or granulosa cells showed that none of them is able to recapitulate the whole process of estradiol production without the other, the two-cell coupling of the process is necessary (Magoffin, 2005). Estradiol is thus produced during the pre-ovulatory phase of the cycle in the granulosa cells. It stimulates endometrial growth and has a positive feedback on LH production in the hypothalamus, leading to LH surge at mid-cycle that triggers ovulation. The peri-ovulation surge in LH and FSH also leads to downregulation of a key actor of androgen production, the CYP17 enzyme, in the theca cells. CYP17 downregulation will lead to androgen production decrease : steroidogenesis is redirected towards progesterone production after ovulation.

### 3.3 – Oocyte maturation:

#### - Growing phase of oogenesis:

During folliculogenesis, meiosis-arrested oocytes enter a phase of dramatic growth: their volume is increased around a 100 fold, to reach a diameter of 80um (**Figure 3**). Oocyte growth is associated with a period of intense transcription and accumulation of RNAs and proteins in the oocyte cytoplasm. Fully-grown oocytes have been estimated to contain around 0.6ng of RNA, which is around 200 times more than in a somatic cell. Such accumulation is vital for oocyte maturation and preimplantation development: indeed a so-called “maternal pool” of transcripts and proteins will be transmitted upon fertilization to the embryo and help sustaining the embryonic program of development until the embryo activates its own genome, which occurs around the 2-cell stage in the mouse.

A remarkable feature of RNA synthesis during oocyte maturation is the establishment of a peculiar oocyte-specific transcriptome. Indeed, Long terminal repeat (LTR) retrotransposons (also known as endogenous retroviruses), whose expression is usually repressed in somatic cells, are especially active in germ cells and early embryos. In the oocyte, MT (mouse transcript) elements, members of the MaLR family of LTR, are the most transcribed and hundreds of them have been co-opted as oocyte-specific gene promoters. Their derepression leads to the formation of LTR-driven chimeric transcript. Genes are thus transcribed from LTR-associated alternative promoter, located for most of them upstream from their canonical transcription start site (TSS) (Peaston et al., 2004; Veselovska et al., 2015; Brind’Amour et al., 2018). It was estimated that over 15% of all mouse oocyte transcripts initiate in an LTR, leading to alternative transcriptional regulation and splicing. As LTR insertions are highly variable

across species, hundreds of species-specific transcripts, mainly initiating in solo LTRs private to a single species were identified between mouse, rats and humans (Brind'Amour et al., 2018). This LTR polymorphism therefore drives species-specific and heritable changes in oocyte transcription. It is also during the growing phase that oocyte-specific patterns of DNA methylation and histones post-translational modifications will be progressively re-established. The oocyte epigenome establishment and functions will be described in the chapter IV of this introduction.

- Chromatin remodeling: the surrounded nucleoli transition

Meiotically-arrested oocytes are characterized by the presence of a large nucleus known as “germinal vesicle” (GV). The intense synthesis of transcripts that happens in the GV contrasts with the genome-wide transcriptional silencing that takes place afterwards, at the end of oocyte growth. Indeed, antrum formation coincides with a drastic chromatin condensation process that is associated with transcriptional shut-down (Zuccotti et al., 1995; Zuccotti et al., 1998; Christians et al., 1999). More specifically, the oocyte transitions from the ‘non-surrounded nucleolus’ (NSN) stage, in which chromatin is dispersed throughout the nucleolus and actively transcribed, to the ‘surrounded-nucleolus’ (SN) configuration, in which a ring of extremely condensed chromatin appears around the nucleolus (**Figure 5**) (Bouniol-Baly et al., 1999). The SN configuration is associated with the arrest of RNA polymerase I and polymerase II-dependent transcription: the use of specific inhibitors of RNAPI or RNAPII showed that both transcriptional activities are present in NSN oocytes and are arrested as soon as the chromatin begins to condense around the nucleolus (Bouniol-Baly et al., 1999). Consistent with these observations, immunostaining showed reduced chromatin-bound RNAPII in SN compared to NSN oocytes. RNAPII was even completely undetectable on chromatin in metaphase II oocytes, suggesting an unloading of RNAPII from chromatin or even their complete degradation.

The fact that higher chromatin condensation level and transcriptional inactivity are always associated at the SN stage in mouse, but also in human oocytes (Parfenov et al., 1989), suggests a biochemical link between the two. Whether transcriptional silencing really is a consequence of the concomitant chromatin remodeling remains however unknown.

SN oocytes also display a better developmental competence: NSN oocytes can be fertilized but will face developmental arrest at the 2-cell stage. However, it was shown by metaphase II plates transfer in enucleated NSN/SN oocytes that rather than the chromatin configuration itself, the cytoplasmic material within SN-type oocytes is essential for full developmental potential (Inoue et al., 2008).

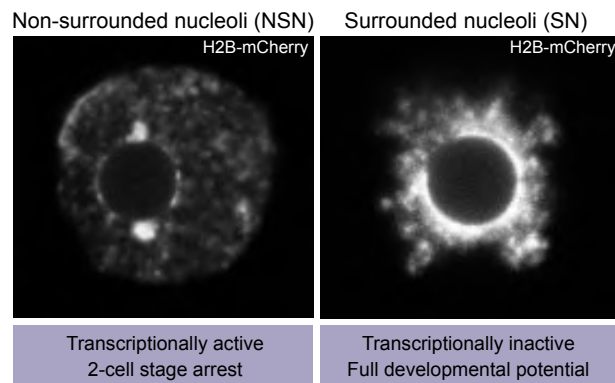


**Figure 5: Representative images and characteristics of non-surrounded nucleolus and surrounded nucleolus oocytes.** Chromatin is stained through *H2B-mCherry* transgene.

- Zona pellucida secretion:

As the oocyte starts to grow, its plasma membrane becomes surrounded by a thin extracellular coat called the zona pellucida (ZP) (Figure 3) (Wassarman et al., 2004). It will progressively increase in thickness up to around 6.5um large. The mouse ZP consists of three glycoproteins, termed ZP1, ZP2, ZP3 that are secreted by the oocyte: nascent polypeptides are targeted to the endoplasmic reticulum and the Golgi apparatus where oligosaccharides are added to each ZP protein. This glycoprotein synthesis is so intense that it is considered to represent 15% of total egg protein synthesis. The increased biosynthesis activity of the Golgi is reflected by changes in its structure with a transition from flattened stacks to swollen lamellae with large vacuoles in mature stage of oogenesis. The zona pellucida is playing a fundamental role for oocyte and early embryo protection but also during fertilization (Wassarman, 2001). A species-specific binding of sperm to ZP3 enables acrosome reaction, a cellular exocytosis process needed for zona pellucida entry and plasma membrane fusion with the oocyte. *Zp3*-null mice thus display sterility due to decreased number of ovulated oocytes and fertilization failure (Lui et al., 1996).

- Meiotic maturation:

Acquisition of meiotic competence is characterized by the oocyte's ability to resume meiosis upon release from the follicles through ovulation, or by mechanical dissociation in

culture: these meiotically-mature oocytes are referred to as competent. Meiotic maturation therefore corresponds to the process that prepares oocytes for meiotic resumption. It involves a cascade of events, initiated by the pre-ovulatory LH surge around the time of antrum formation. Microinjections of CDK1 into incompetent oocytes is not sufficient for them to resume meiosis ([De Vantéry et al., 1997](#)), showing that meiotic competence involves a broader process of both nuclear and cytoplasmic maturation.

By preventing CDK1 activation, cAMP is known as a key regulator of meiotic arrest, allowing meiotic resumption (for more information, see previous section on meiosis). Gap junctions between granulosa cells and meiotically-arrested oocytes play an important role for supplying to the oocyte with somatically produced cAMP. In rat ovarian follicle, LH stimulation—starting at antrum formation—was shown to downregulate Connexin 43 (Cx43) expression, the main component of gap junctions ([Granot & Dekel, 1994](#)). The resulting disruption of gap junction communication seems to be one of the major triggers of meiotic maturation. The transport of cAMP and cGMP, an inhibitor of cAMP hydrolysis, into oocytes is thus blocked, leading to cAMP concentration decrease and CDK1 activation ([Adhikari & Liu, 2013](#)).

Regulation of oocyte transcripts is another key process for meiotic maturation, mainly composed of a massive wave of transcript degradation ([Sánchez & Smits, 2012](#)), estimated to be roughly responsible for degradation of 30% of the RNA pool. Because oocytes are transcriptionally silent at this stage, the regulation of RNA and protein abundance relies on post-transcriptional modifications. Notably, transcripts and proteins that are linked to meiotic arrest and oocyte growth are degraded. For example, the translation of CDH1, which represses the CDK1 cofactor cyclin B1, is reduced by 70%. In contrast, signaling factors for MII transition and maternal-effect transcripts are retained.

## 4 – Ovulation and meiotic resumption

### 4.1 - Ovulation process

Follicles that have completed folliculogenesis—meaning that they possess the most granulosa cells and a competent oocyte—will be selected as “dominant follicles” for ovulation. All the other subordinate follicles will enter apoptosis and undergo degradation.

Ovulation is a multistep process that occurs in response to the preovulatory surge in LH. FSH induces antral follicle growth: theca and granulosa cells thus proliferate and start producing increasing levels of estradiol. These high levels of estradiol trigger the LH surge, specific to ovulation. Upon LH stimulation, a sequence of three events that characterize ovulation will occur: the expansion/mucification of the cumulus, the rupture of the follicle and the release of a cumulus-oocyte complex (COC) that contain the fertilizable oocyte. Cumulus expansion corresponds to the intense secretion of hyaluronan in the extracellular matrix of the cumulus cells, the granulosa cells adjacent to the oocyte. This hyaluronan-rich matrix forms the structural backbone of the COC. The part of the follicle that protrude out from the ovary stroma will then break and the COC will be released from the follicle to the infundibulum (**Figure 3**). The remaining mural granulosa cells and theca cells from the ruptured follicle will undergo rapid differentiation to luteinizing cells and form the corpus luteum. Steroidogenesis will be redirected towards progesterone production in luteinizing cells, the hormone essential for establishing and maintaining pregnancy. In absence of implantation and pregnancy, the corpus luteum will degenerate.

#### 4.2 - Germinal vesicle breakdown and meiosis resumption

In the hours following the release of the COC in the fallopian tube, the oocytes that have acquired meiotic competence (as previously described) will start resuming meiosis. Perioovulatory LH surge and mechanical release of the oocyte from the mature follicle are necessary to trigger meiosis. The very first sign of exit from prophase I and of meiosis resumption is the germinal vesicle breakdown ([Mihajlović & FitzHarris, 2018](#)). It corresponds to nuclear envelope breakdown of the germinal vesicle, associated with meiosis-I spindle formation. The spindle, a dynamic and transient microtubule-based structure, is at the heart of chromosome segregation and sorting (**Figure 6**). In somatic cells, the spindle is formed by microtubules that are nucleated from centrosomes. Mammalian oocytes adopt a non-canonical centrosome-free strategy to assemble the spindle ([Bennabi et al., 2016](#)): microtubules gradually organize during oocyte growth and form large acentriolar microtubule organization centers (MTOCs) that will fragment to generate smaller MTOCs at the time of germinal vesicle breakdown. Microtubules are nucleated from these MTOCs and will elongate to form a dense structure onto the surface of which the kinetochores of the individualized chromosomes get anchored. Under the control of this spindle, chromosomes align and

become bioriented to form a metaphase plate, while MTOCs distribute towards two opposing poles. The meiosis-I spindle will then migrate prior to the first meiotic chromosome segregation, from the center to the periphery of the oocyte.

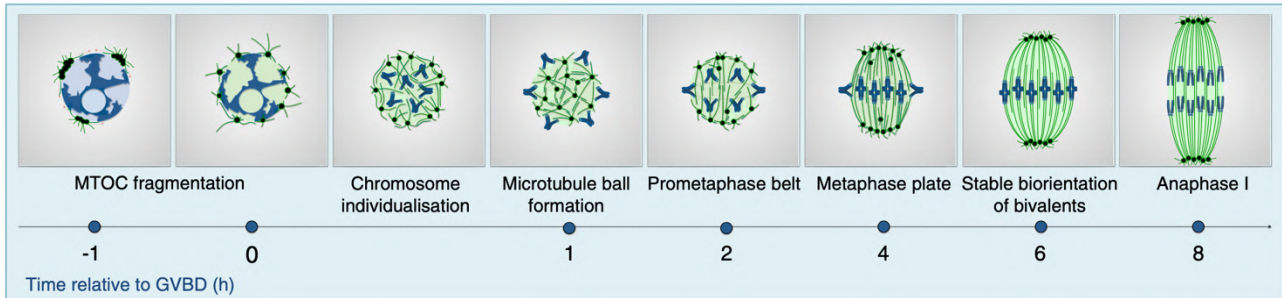


**Figure 6: Acentrosomal spindle formation during meiosis-I in the oocyte.** Adapted from [Mihajlović & FitzHarris, 2018](#). At the time of germinal vesicle breakdown, MTOCs (black dots) stretch along the nuclear envelope and fragment. Chromosomes (blue) individualize and the microtubules (green) become nucleated. MTOCs transit to the spindle assembly site and chromosomes occupy the surface position on the newly formed microtubule ball. Chromosomes then invade the center of the prometaphase belt and become bioriented to form the metaphase plate. Meanwhile, the MTOCs gradually become distributed towards the two opposing poles of the microtubule ball. Finally, once all of the chromosomes bivalents achieve a stable biorientation at the metaphase plate anaphase takes place and homologous chromosomes are separated.

The positioning of the spindle at the oocyte cortex at anaphase gives rise to highly asymmetric cell divisions at meiosis I and II, responsible for the production of only one fertilizable egg ([Brunet & Verlhac, 2011](#)). The end products of each meiotic division consist in a large cell, the oocyte, and a tiny cell termed the “polar body”, each of them receiving half of the chromosomal material. Indeed, meiosis-I separates homologous chromosomes while meiosis-II separates sister chromatids, thus leaving in the egg a haploid set of chromosomes as the maternal genetic contribution to the developing embryo. This highly specialized and complex chromosome choreography leads to increased challenges in terms of cohesin pairing and more frequent segregation errors, in particular in older females where meiotic errors leading to aneuploidy become more frequent ([Chiang et al., 2010](#); [Tachibana-Konwalski et al., 2010](#)). Aged oocytes were indeed associated with defects in Rec8-cohesin, responsible for maintaining sister chromatid cohesion in meiosis ([Chatzidaki et al., 2021](#)). This could contribute to explain the increased production of aneuploid eggs upon ageing. Interestingly, long-term ovulation suppression (like hormonal contraception) seems to protect against Rec8 loss, suggesting that maternal age effect could be reduced in mice through ovulation inhibition ([Chatzidaki et al., 2021](#)).

Almost immediately after completion of the first meiotic chromosome segregation and the extrusion of the first polar body, oocytes enters meiosis-II. They complete prophase II, the meiosis-II spindle is formed and chromosomes align in a metaphase-II plate . But once again, the cell cycle stops and metaphase-II oocytes stay in the infundibulum until fertilization (**Figure 3**). Fertilization triggers the resumption of meiosis-II, sister chromatids segregation and formation of the second polar body. The maternal genome then enters interphase during which it will fuse with the paternal pronucleus, marking the beginning of embryonic development.

## 5 - Overview of embryonic preimplantation development

Mouse preimplantation development is the period extending from fertilization (E0.5) to implantation (E4.5) (**Figure 7**). Preimplantation development is characterized by a series of cell divisions. These cells proliferate, compact and undergo cavitation to finally form a blastocyst with three distinct cell lineages, at the origin of the different embryonic and extra-embryonic tissues. Finally, the blastocyst will hatch out of the zona pellucida and implant to the uterine wall.

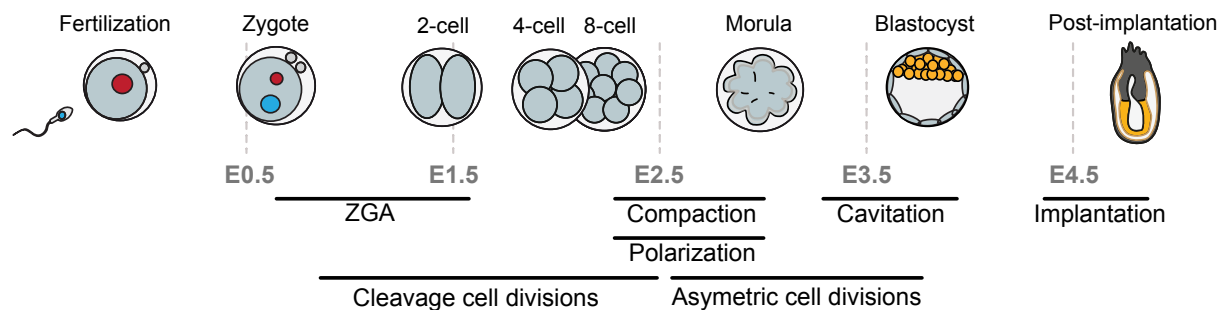


**Figure 7: Overview of embryonic preimplantation development.** Stages, timing and important events of preimplantation development are displayed.

### 5.1 – Early cleavages and zygotic genome activation

- Parental genome fusion at the zygotic stage and early cleavages:

Fertilization marks the beginning of preimplantation development and implicates sperm-oocyte binding and fusion. The sperm first binds to the zona pellucida, which triggers acrosomal exocytosis, meaning rupture and secretion of the content of the acrosome present of the head of the spermatozoa. The inner acrosomal membrane of the sperm becomes exposed following acrosomal exocytosis and fuse with the oocyte membrane (Inoue et al.,

2011). The sperm nucleus and organelles are incorporated into the oocyte cytoplasm, forming a zygote. The sperm nucleus undergoes a series of changes, including chromatin decondensation and the formation of a new nuclear envelope, to form the male pronucleus. While the paternal pronucleus is formed, the oocyte genome completes the second division of meiosis and eliminates the second polar body. Both pronuclei migrate towards each other and are directed towards the center of the cytoplasm (Clift & Schuh, 2013; Chaigne et al., 2017). The membrane of the two pronuclei then fuse and genetic material mixes, resulting in formation of the diploid nucleus of the zygote. The stages of zygotic development can be classified in PN1 to PN5 stages, depending on the relative position of the two pronuclei (J. Lan et al., 2017): PN1 stage displays the most distant pronuclei, PN4 stage corresponds to adjacent pronuclei, while pronuclei fuse at PN5.

The zygote then begins to divide mitotically ; the resulting cells are called blastomeres. As long as cleavage progresses, the cells proliferate and become progressively smaller as the whole size and shape of the embryo remain the same. The first two cell divisions, which lead to the formation of a two-cell and then four-cell embryo consecutively, occur approximately every 24 hours (Artus & Cohen-Tannoudji, 2008). The mitotic proliferation then accelerates and the embryo reaches around E2.25-2.5 the eight-cell stage, when compaction will start (Figure 7).

- Zygotic genome activation:

A fundamental transition during preimplantation development is the transfer of developmental control from the mother to the zygote. After an intense phase of mRNA and protein synthesis in the oocyte, the maternal genome becomes transcriptionally silent at the SN stage, similarly to the paternal one at mature stages of spermatogenesis. Once fused in a diploid nucleus, the zygotic genome remains transcriptionally quiescent during the first hours of preimplantation development. Protein synthesis in the mammalian zygote initially relies on maternally loaded mRNAs. The maternal-to-zygotic transition involves two coordinated processes (Figure 8): the clearance of maternal products and the gradual onset of embryo-specific transcriptional program during zygotic genome activation (ZGA) (Wu & Vastenhouw, 2020). ZGA takes place quite early in the mouse embryo: a first burst of transcription is observed at the late zygote stage, followed by a second activation phase at the two-cell stage (Figure 8). These two bursts are respectively referred to as “minor wave of ZGA” and “major

wave of ZGA”, even though recent studies seem to indicate that ZGA would rather be a continuum of genes that become gradually and continuously activated (Abe et al., 2018; Wu & Vastenhouw, 2020). Widespread transcriptional activation of zygotic genes coincides with lengthening of the cell cycle. However, the exact relationship between transcriptional activity and cell cycle control in the embryo remains poorly understood (Edgar & Schubiger, 1986; Blythe & Wieschaus, 2015).

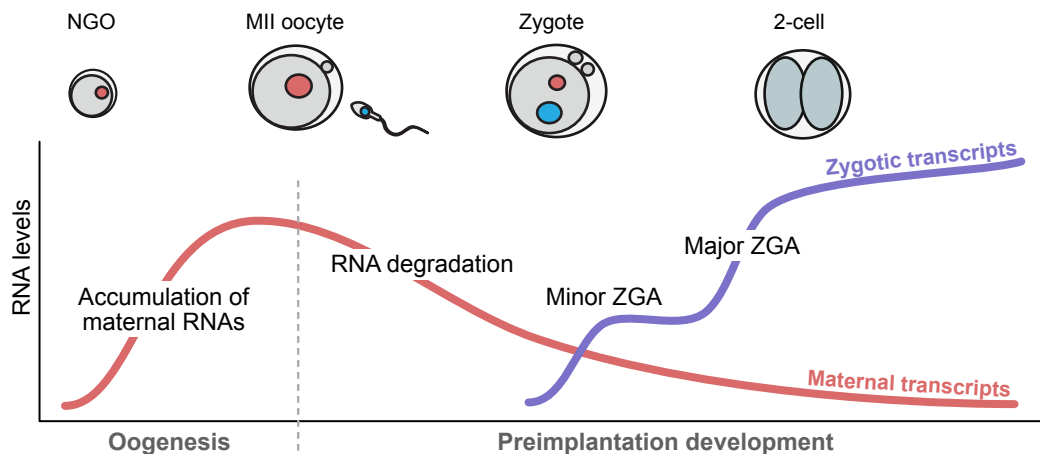


**Figure 8: Maternal-to-zygotic transition in early embryos.** The maternal-to-zygotic transition involves two coordinated processes: the degradation of maternal products and the gradual onset of embryo-specific transcriptional program during zygotic genome activation. ZGA is composed of a minor wave (in late zygotes) and a major wave (in 2-cell embryos).

Among genes transcribed at ZGA, genes involved in basic cellular function, protein synthesis, RNA metabolism and transcription are over-represented. In particular, transcriptional activation of endogenous retroviruses occurs during ZGA, where they are thought to act as gene expression regulators or alternative promoters (Peaston et al., 2004; Fu et al., 2019). Because of their high prevalence in the mammalian genome, they might help to uncompact and broadly activate transcription. Interestingly, the LTR expressed in the early embryos differs from the ones driving transcription in the oocyte : in oocytes, MaLR elements are mainly expressed, while younger LTR, of the MERVL class are expressed at ZGA. A large percentage of ZGA-associated genes are located in proximity to MERVL elements. LTR promoters of MERVL elements are known to contain a binding motif for DUX, which is a pioneer transcription factor of ZGA.

Recent studies have indeed reported the DUX transcription factor family as one of the major activators of ZGA (De Iaco et al., 2017; Hendrickson et al., 2017). *Dux* is expressed before

ZGA and has been shown to bind the promoters of ZGA-associated genes to activate their transcription. Additionally, induced expression of *Dux* in embryonic stem cells (ESCs) is enough to provoke transcriptional activation of genes and transposable elements normally expressed at ZGA in two-cell stage embryos (De Iaco et al., 2017). Although some *Dux*<sup>KO</sup> embryos give rise to viable pups, the zygotic depletion of *Dux* leads to defective ZGA and impaired pre- and post-embryonic development, leading to high embryonic mortality rates (De Iaco et al., 2020; Bosnakovski et al., 2021). This indicates that *Dux* is an important but not strictly essential activator of ZGA. It also appears that *Dux* itself is activated by upstream factors like *Dppa2*, *Dppa4* and *p53* (Eckersley-Maslin et al., 2019; Grow et al., 2021).

ZGA is also concomitant in mice to extensive chromatin reprogramming happening in both maternal and paternal genomes. The biological significance of parentally-transmitted epigenetic marks for ZGA control, only begins to be understood (see chapter IV of this introduction).

## 5.2 – Compaction and blastocyst formation

### - Compaction:

The early cleavage divisions produce an eight-cell embryo that progressively display increased intercellular adhesion, causing all cells to adopt a more flattened morphology. This process, called compaction, is essential to initiate cell differentiation and proper segregation of the three embryonic lineages (Mihajlović & Bruce, 2017). Compaction is associated with the formation of adherens and tight junctions between cells. E-cadherin, a major component of adheren junction is indeed expressed from the eight-cell stage onward, and disruption of E-cadherin-mediated cell adhesion inhibits compaction (Hyafil et al., 1980).

Blastomeres do not carry signs of intracellular polarity until compaction. Concomitant with increased adhesion, cells polarize and define an apical region distinct from the basolateral region (Johnson & Ziomek, 1981). The cytoplasm also becomes reorganized according to this newly established polarity: the nucleus moves basolaterally and microvilli accumulate at the apical pole, together with endosomes.

Once the eight-cell embryo has compacted and polarized, it undergoes further rounds of cell divisions, transitioning to the 16- and 32-cell stages and reaching the so-called morula stage. During these divisions, inheritance of the polarized state is influenced by the orientation

of the cleavage plane: a dividing blastomere can produce a polarized outside daughter cell and an apolar cell, located on the inside of the morula (Balakier & Pedersen, 1982; Fleming, 1987). These two cell populations will progressively acquire distinct developmental fates from the 32-cell stage onwards: cells on the outside of the embryo will contribute to extraembryonic trophoderm (TE) lineages, while inside cells will contribute to the inner cell mass (ICM), the group of cells that will, among others, give rise the future embryonic lineages.

- Blastocoel formation:

Starting at the morula stage, when the outside cells of the embryo are becoming fully committed to the TE lineage, fluid-filled cavities begins to form between inner cells (Wiley, 1984). This process of water accumulation in the embryo is due to aquaporins, present in TE, and osmotic gradient, that enable water movements towards the inside of the embryo (Barcroft et al., 2003). Progressively these cavities will fuse to form a single large fluid-filled blastocoel. Once it is formed, maintenance of the blastocoel depends on the epithelial character of the outer TE cells. The blastocoel grows between the enveloping layer of TE cells and the inner cell mass. With the formation of the blastocoel around E3.5, the mouse embryo has transitioned to the blastocyst stage. During blastocyst development, further differentiation of the ICM produces a thin layer of cells, called embryonic endoderm, that separates the blastocoel from the rest of the ICM, now termed epiblast (Rossant & Tam, 2009). The epiblast will give rise to embryonic tissues, while both TE and endoderm will serve to establish extraembryonic and placental tissues. Upon blastocyst hatching from the zona pellucida at E4.5, TE cells will adhere and implant into the uterine wall. Embryonic development will then proceed with morphogenesis and post-implantation development.

## III - Epigenetic marks and their interplays

### 1 - DNA methylation

#### 1.1 – DNA methylation generalities

DNA methylation corresponds to the epigenetic modification by which a methyl group (-CH<sub>3</sub>) is covalently linked to the fifth carbon of cytosines (5mC) (**Figure 9A**). Cytosine methylation is highly conserved across vertebrates, plants and bacteria and one of the most well-characterized epigenetic mark. In mammals, DNA methylation is present primarily in the context of cytosine-guanine dinucleotides, referred to as CpGs (“p” implying the phosphodiester bond), which provide a symmetric template on the two DNA strands ([Greenberg & Bourc’his, 2019](#)). Only 5% of cytosines are methylated in somatic cells, but these represent 70-80% of all CpGs ([Ehrlich et al., 1982](#); [Lister et al., 2009](#)). Most CpG dinucleotides are thus methylated in the genome: it includes intergenic, intragenic regions and importantly, repetitive sequences.

Deposition of DNA methylation includes two different processes (**Figure 9A**). First, *de novo* establishment is under the control of the DNA methyltransferase 3 (DNMT3) family that is competent to methylate previously unmethylated cytosines. The DNMT3 family comprises four members in mice, the DNMT3A, DNMT3B, and DNMT3C enzymes and their catalytically inactive cofactor DNMT3L. Maintenance of DNA methylation through cell divisions is ensured by DNMT1, which has the ability to copy DNA methylation patterns on the newly synthesized strand of DNA produced through replication ([Chen & Zhang, 2020](#)). During S phase, DNMT1 is indeed tethered to chromatin by its direct interaction with UHRF1, which contains a methyl DNA binding domain with preference for hemi-methylated CpGs ([Bostick et al., 2007](#)). DNMT1 and UHRF1 enable faithful maintenance of DNA methylation, making it the chromatin mark considered as most stable.

DNA demethylation can be achieved either by passive dilution through cell divisions in absence of DNMT1 or by active removal by the Ten-Eleven Translocation (TET) family of enzymes ([Rasmussen & Helin, 2016](#)) (**Figure 9A**). The TET enzymes catalyze oxidation of 5-methylcytosine to 5-hydroxymethylcytosine (5hmC). 5hmC can be further oxidized and then either passively lost through dilution or recognized by DNA repair pathways and replaced by unmethylated cytosines.

DNA methylation comes with an evolutionary cost: while spontaneous deamination can be rescued by the base-excision repair machinery at unmethylated cytosines, methylated cytosines that have lost an amine group will not be recognized, resulting in a C to T transition. As a result, the genome is globally depleted of CpGs compared to the expected frequency (Bird, 1980). However, CpG dinucleotides can be found at high frequency at some places in the genome: these are named “CpG islands” (CGI) (Ehrlich et al., 1982; Lister et al., 2009). They correspond to regions of more than 200bp with a CG content over 50% and they act as major regulatory regions of the mammalian genome. About 50% of CGIs are within gene promoters and 25% lie in gene bodies, where they may serve as alternative, intragenic promoters. While most CG dinucleotides are methylated genome-wide, CGIs are globally unmethylated, and in particular in the male germline, allowing them to resist to evolutionary erosion by deamination (Weber et al., 2007).

DNA methylation can also be sporadically found in non-CpG sequence context (CpG, CpA, CpC and CpT) but only symmetrical CpG methylation is maintained through cell divisions. As a result, while almost only CpG methylation is found in dividing cells, DNA methylation can also be found in a CpA or CpG context in quiescent cells and in tissues with high expression of *de novo* DNMT3s, such as oocytes, prospermatogonia, embryonic stem cells or in the brain (Greenberg & Bourc’his, 2019).

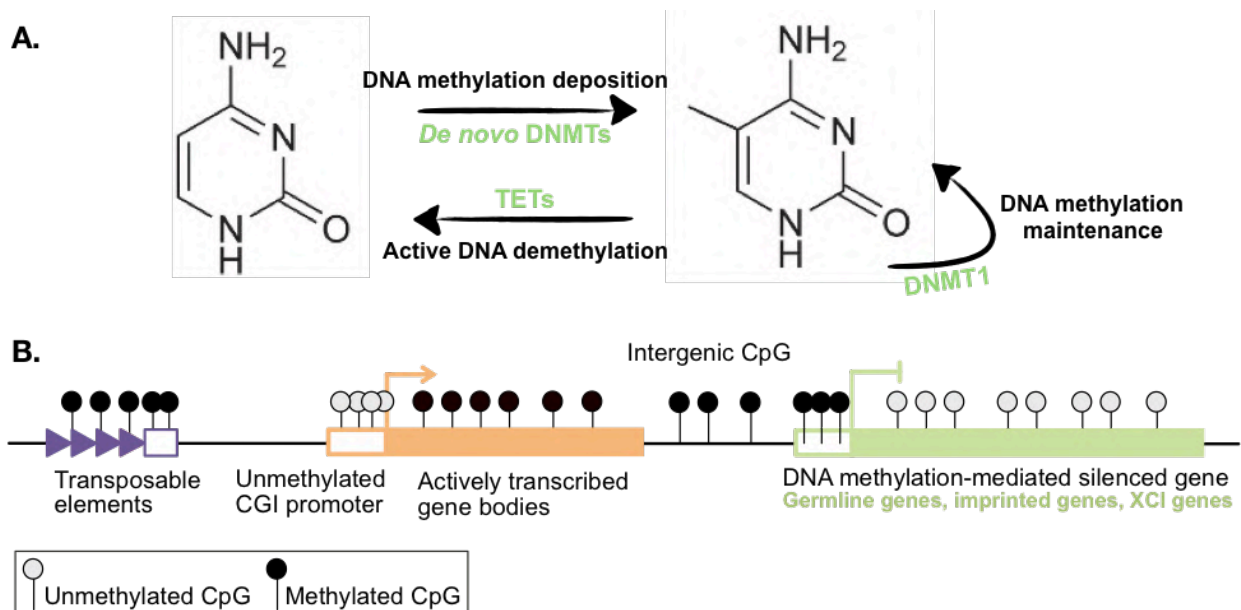


**Figure 9: DNA methylation in mammals.** A. Topological formula of unmethylated and methylated cytosines. Addition of the methyl group is catalyzed by *de novo* DNMTs, its maintenance through cell divisions is ensured by DNMT1. TETs can remove the methyl group. B. Typical mammalian DNA methylation landscape in somatic cells. Transposable elements, actively transcribed gene bodies, intergenic CpG and promoters of germline genes or imprinted genes are usually methylated.

## 1.2 – DNA methylation distribution and functions

DNA methylation is involved in many cellular processes in mammals including X chromosome inactivation, genomic imprinting and silencing of transposable elements (Goll & Bestor, 2005). Its function varies according to the genomic location of the mark (Figure 9B).

In 1975, two key studies proposed a role of DNA methylation in regulating the expression of genes and in cellular memory processes (Holliday & Pugh, 1975; Riggs, 1975). In the next years, a strong correlation between hypermethylated promoters and gene repression was demonstrated in various contexts and cell types (Sager & Kitchin, 1975; McGhee & Ginder, 1979; Mattei et al., 2022;). It is now widely accepted that the presence of DNA methylation at promoter regions is associated with gene silencing (Figure 9B). As two-thirds of mammalian promoters contain a CGI, which are generally hypomethylated (as previously explained), the repressive function of DNA methylation at promoters is mostly limited to three major classes of genes, in which lifelong DNA methylation-based silencing in somatic tissues is very important: germline-specific genes, imprinted genes, genes located on the inactive X chromosome (Chen & Zhang, 2020). How DNA methylation confers transcriptional repression is, however, still not fully understood. It has been proposed that DNA methylation enrichment at promoters leads to impossibility for DNA methylation-sensitive transcription factors to bind and promote RNA polymerase-dependent transcription (Yin et al., 2017). DNA methylation could also contribute to heterochromatin formation by recruiting DNMT-associated or methyl-binding proteins and chromatin modifiers. DNMTs are for example known to function in complex with H3K9 methyltransferases and histone deacetylases (Deplus et al., 2002; Estève et al., 2006).

Beside the promoters of the specific classes of genes named above, DNA methylation is actually the most prominent on repetitive sequences and in particular transposable elements (TEs) (Figure 9B). The evolutionarily youngest classes of TE are controlled by CpG-rich promoters that are heavily methylated, and methylation matters for their transcriptional silencing. In *Dnmt1* knockout embryos, intracisternal A particle (IAP) retrotransposons—a class of endogenous retroviruses that can still get actively mobilized in rodent genomes—lose promoter methylation and become massively derepressed (Walsh et al., 1998). Similarly, in the male mouse germline, lack of *Dnmt3C* or *Dnmt3L* result in a failure to

remethylate different classes of young TEs, and their transcriptional reactivation at meiosis (Bourc'his & Bestor, 2004; Barau et al., 2016).

DNA methylation is also enriched in the body of highly transcribed genes (Figure 9B). There, it is not associated with gene silencing but is thought to be a secondary consequence of transcriptional elongation activity (Jones, 2012). Its precise function is still unclear but it may play a role in preventing cryptic transcription and in facilitating transcriptional elongation and/or co-transcriptional splicing (Gelfman & Ast, 2013; Neri et al., 2017; Shayevitch et al., 2018).

None of the *de novo* DNMT3s have been shown to have sequence specificity, beside cytosine recognition, leading to questions regarding how they are recruited to specific genomic regions to establish DNA methylation patterns. Strong positive and negative correlations exist between the genome-wide distribution of DNA methylation and patterns of post-translational histone modifications (H3K4me3, H3K36me2/3, H3K9me3, H3K27me3) suggesting important interplays between chromatin marks. This will be discussed in more details in the chapter III. 5. of this introduction.

### 1.3 – DNA methylation in development

Although DNA methylation patterns are very stable and faithfully propagated by DNMT1 in differentiated somatic cells, they are, at the opposite, very dynamic during development (Figure 10). Indeed, twice during mouse embryonic development, DNA methylation patterns are erased at a global scale before being reestablished with a different paradigm (Chen & Zhang, 2020). This process called “epigenetic reprogramming” not only affects DNA methylation but also histone modifications, and to a certain extent, tridimensional genome architecture.

The first reprogramming event occurs during preimplantation development. DNA methylation levels drop from an average level of 70% in the zygote at fertilization (E0.5) to 20% at the blastocyst stage (E3.5-E4.5) (Smith et al., 2012). It is important to note that the paternal and maternal genomes are not reprogrammed with the exact same dynamic: the heavily-methylated sperm genome (around 90% CpG methylation) is mainly actively reprogrammed right after fertilization before the first cell division through TET activity (Oswald et al., 2000). At the opposite, the maternal genome is only covered at 40% by DNA

methylation domains. They will be progressively erased until the eight-cell stage, mainly by passive loss across cell divisions, as the maintenance DNMT1 is excluded from the nucleus at these stages (Cardoso & Leonhardt, 1999). Only imprinted genes, characterized by a parent-specific monoallelic methylation, will escape this wave of DNA methylation erasure; their maternally or paternally inherited patterns being protected from erosion by KRAB-containing Zinc-Finger Proteins (ZFP57 and ZFP445) (Li et al., 2008; Takahashi et al., 2019). Embryonic patterns will be established *de novo* after implantation from E4.5 on, reaching 80% by E8.5. At this stage, local changes in DNA methylation are associated with cell lineage differentiation, and *de novo* events rely on DNMT3A.

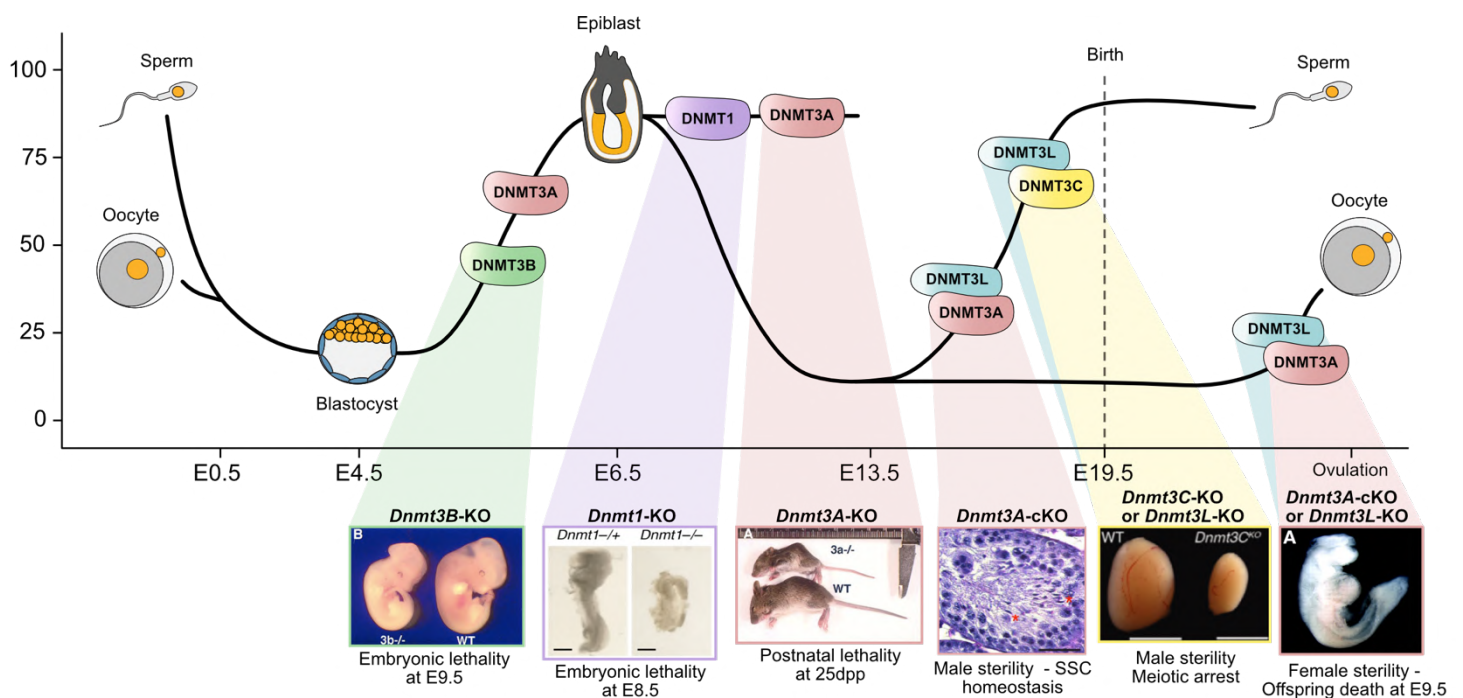


**Figure 10: DNA methylation dynamics during mouse development.** Two phases of epigenetic reprogramming occur during mouse development: DNA methylation patterns are erased and reestablished during both early embryonic development and germline development. Maternal and paternal genomes have different kinetics. DNMT3 proteins that are expressed and playing an essential role at a given stage are represented, together with the associated phenotype.

Genetic studies in the mouse have highlighted the specific roles of DNMT1, DNMT3A, and DNMT3B in embryonic DNA methylation. Deletion of *Dnmt3B* leads to embryonic lethality just after E9.5, due to growth retardation and neural tube defects (Figure 10) (Okano et al., 1999). Deletion of *Dnmt3A* results in postnatal lethality at 25dpp, linked to reduced growth and multiple organ failure (Okano et al., 1999). This indicates that the wave of DNA methylation establishment after implantation is prominently dependent on DNMT3B, while DNMT3A is

rather essential for postnatal development. It was shown to have important functions in hematopoiesis, for example (Challen et al., 2011). By comparing DNA methylation maps from embryos lacking DNMT3A or DNMT3B activity, Auclair et al. identified that DNMT3A and DNMT3B act redundantly to methylate bulk genome and repetitive elements, while DNMT3B has a predominant role in CGI methylation at this stage (Auclair et al., 2014). Interestingly, while DNMT3L is highly expressed along with DNMT3A and DNMT3B in the early embryo, it is dispensable for *de novo* embryonic DNA methylation (Bourc'his et al.; 2001, Guenatri et al 2013).

The second reprogramming event coincides with germline specification. It occurs in developing germ cells and will be further discussed in the section IV. 1. of this introduction. Briefly, somatic DNA methylation patterns are erased in primordial germ cells (PGCs) (Seisenberger et al., 2012; Zeng & Chen, 2019). The remethylation phase shows a striking sexual dimorphism. In males, DNA methylation is reestablished in prospermatogonia during fetal development (from E14.5 to E20.5) prior to meiosis, while in females this process occurs in the growing oocytes at puberty, after meiosis. In mice, constitutive deletion of *Dnmt3L* or germline-specific deletion of *Dnmt3A* leads to complete sterility in both males and females (**Figure 10**) (Bourc'his et al., 2001; Kaneda et al., 2004). *Dnmt3A* conditional deletion in the male germline impacts the homeostasis of spermatogonia stem-cell, which lose their ability to ensure continuous production of spermatozoa (Dura et al., 2022). Loss of DNMT3L or DNMT3A activity in the female germline results in embryonic lethality of the progeny due to impaired imprinted genes regulation and placental development (Bourc'his et al., 2001). While *Dnmt3B* is highly expressed in developing germ cells, it does not seem to be playing a role for germ cell development and fertility (Kaneda et al., 2004). In addition to the active DNMT3A-DNMT3L complex, DNMT3C is also active in the germline of male mice, to selectively methylate the promoters of evolutionarily young TEs, hence only 1% of the whole genome (Barau et al., 2016). DNMT3C does not exist outside of Muroidea rodents, and it has been suggested that DNMT3A may methylate TEs in the human male germline (Molaro et al., 2020). Both DNMT3L and DNMT3C have no function outside of the germline, highlighting the selective pressure imposed by reproduction for the evolution of the DNA methylation machinery.

Mouse models of total or conditional loss of function of DNA methyltransferase genes have highlighted the key role of DNA methylation in embryonic development (Greenberg & Bourc'his, 2019).

#### 1.4 – The *de novo* methylation machinery: focus on DNMT3A-DNMT3L

As my work relates to DNA methylation targeting during oogenesis, I will focus here on the *de novo* DNA methylation machinery and in particular on DNMT3A and DNMT3L that are the principal actors of DNA methylation deposition in the oocyte. The structure of DNMT1, DNMT3B or DNMT3C is comprehensively detailed in the following review (Chen & Zhang, 2020). Biochemical studies of DNMT3 domain organizations and functions are critical for improving our comprehension of their activity and interactions with DNA, histone modifications or chromatin proteins. It allows us to understand how DNMTs can be targeted to specific chromatin contexts (Figure 11).

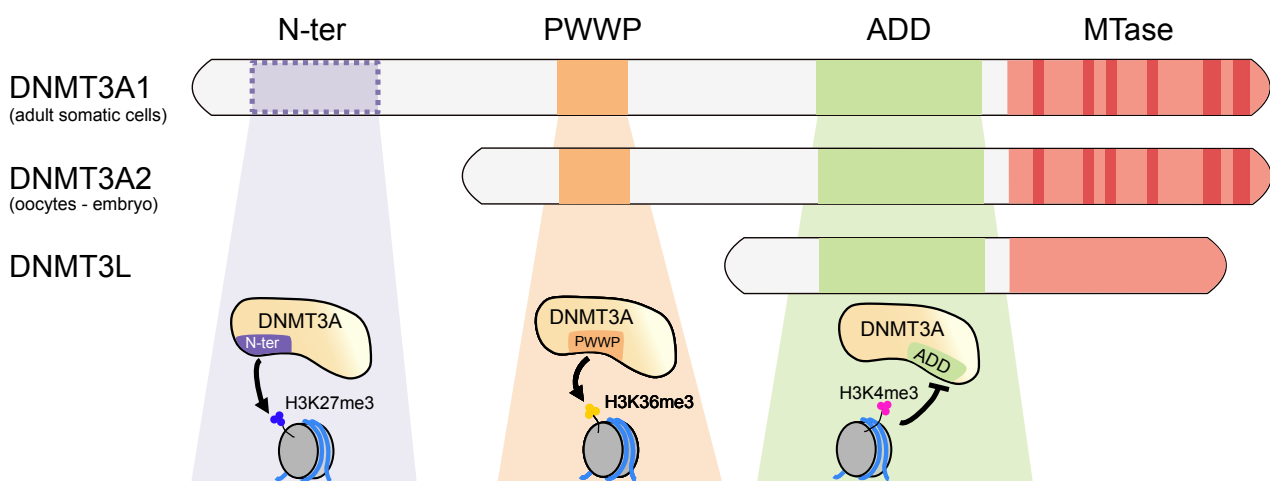


**Figure 11: Domain structure of mouse DNMT3A and DNMT3L, and their predicted interactors.** The disorganized N-terminal domain of DNMT3A1 is required for localization at the shores of H3K27me3 domains in somatic cells. DNMT3A is recruited to H3K36me2/3-marked chromatin through the PWWP domain. The ADD domain maintains DNMT3A in an inactive allosteric conformation, which can only be released through the binding to unmethylated H3K4 residues; this leads to mutual exclusivity between DNA methylation and H3K4me3. DNMT3L has no catalytic activity per se, due to poor conservation of the MTase domain.

All catalytically active DNMTs (DNMT3A, DNMT3B, DNMT3C and DNMT1) share the same C-terminal catalytic methyltransferase (MTase) domains that are responsible for the methylation reaction (Figure 11). The DNMT3L MTase domain is poorly conserved, which makes it a catalytically inactive cofactor that is nonetheless essential for *de novo* DNA methylation in both male and female germ cells. It has been shown to stimulate DNMT3

enzymes through the formation of a tetrameric complex (Jia et al., 2007): DNMT3L can directly binds DNMT3 through its carboxyl-terminal half (Suetake et al., 2004).

- ADD domain and H3K4me3

DNMT3A and DNMT3L also possess a ATRX-DNMT3L-DNMT3A (ADD) domain (**Figure 11**). The ADD domain plays an inhibitory role on DNMT3A enzymatic activity by masking the DNA binding site of the MTase domain (X. Guo et al., 2015). However, the ADD domain is able to recognize unmethylated lysine 4 of histone 3 (H3K4), in presence of which, ADD-mediated inhibition will be released, so that DNMT3A will be able to methylate chromatinized DNA. In presence of H3K4 methylation—a mark of promoter activity—ADD can no longer recognize the H3K4 tail, DNMT3A stays in its inhibited state and is repulsed from chromatin (Ooi et al., 2007). This structural characteristic results in a strong anti-correlation between DNA methylation and H3K4me3 distribution throughout the genome, and in particular, at promoters.

- PWWP domain and H3K36me2/3

The PWWP domain (Pro-Trp-Trp-Pro motif) is a member of the Tudor domain family and mostly found in chromatin-interacting proteins. This domain present in DNMT3A, DNMT3B but not DNMT3L and DNMT3C (**Figure 11**), can recognize di- and tri- methylation of lysine 36 of histone H3 (H3K36me2/3) (Dhayalan et al., 2010). Depletion of the H3K36me3 methyltransferase SETD2 in mouse embryonic stem cells (mESCs) has been shown to lead to reduced DNMT3 binding and decreased DNA methylation levels in H3K36me3-enriched regions (Baubec et al., 2015). DNMT3B seems to have the most affinity for H3K36me3, which is characteristically enriched at gene bodies of actively transcribed genes, while DNMT3A is co-enriched with H3K36me2 that has a more diffuse distribution encompassing both genic and intergenic regions (Weinberg et al., 2019). However, in absence of H3K36me2, a marked redistribution of DNMT3A to H3K36me3-enriched gene bodies is observed (Weinberg et al., 2019). DNMT3A<sub>PWWP</sub> thus seems to recognize both H3K36 di- and trimethylation but with greater affinity for H3K36me2.

Recent studies also showed that mutations in the PWWP domain of DNMT3A lead to DNA methylation gain at Polycomb-associated regions, thus demonstrating a previously unknown role of the PWWP domain in restricting DNA methylation deposition (Heyn et al., 2019; Kibe et al., 2021). PWWP-mediated anchoring of DNMT3s to H3K36me3-enriched domains thus

seems important to avoid off-target methylation by excess of mis-localized available DNMT3 proteins.

- N-terminal domain and H3K27me3:

DNMT3A has two isoforms: DNMT3A1, the longer isoform present in adult somatic tissues and DNMT3A2, a shorter isoform that is expressed in oocytes and embryonic stem cells. They diverge only by the truncation of the N-terminal domain in DNMT3A2 (**Figure 11**).

DNMT3A1 is known to localize preferentially to the shores of Polycomb-enriched chromatin domains or bivalent domains (both H3K4me3 and H3K27me3 enriched) ([Manzo et al., 2017](#)). Long isoform DNMT3A1, but not DNMT3A2, was identified to be essential for post-natal development by regulating methylation deposition around bivalent neurodevelopmental genes in the brain ([Gu et al., 2022](#)). Indeed, PWWP mutations were recently shown to promote localization of DNMT3A1 to Polycomb regions containing PRC1-mediated monoubiquitylation of Lysine 119 on histone H2A (H2AK119ub or H2Aub), irrespective of the H3K27me3 status. Ablation of PRC1 abrogated this mislocalization. This DNMT3A binding to H2Aub would be dependent on a putative ubiquitin-interacting motif embedded in the N-terminal domain, as DNMT3A2 does not display the same behavior ([Gu et al., 2022](#)). The N-terminal domain would thus provide an additional form of DNMT3A genomic targeting that is augmented by the loss of PWWP ([Weinberg et al., 2021](#)).

## 2. Polycomb marks (H3K27me3 and H2Aub)

Polycomb group (PcG) proteins are a well-studied group of chromatin modifiers. The term Polycomb originates from a *Drosophila* mutant with improper body segmentation because of perturbed PcG-mediated homeotic (*Hox*) gene repression ([Lewis, 1978](#)). Polycomb proteins were thus first identified as gene repressors in *Drosophila* and have been since shown to be conserved in other animals, including mammals. The concept of what is named a PcG protein has evolved over time from the original mutant characterization in flies to the current biochemical definition based on complex formation. Nowadays, Polycomb proteins are defined by their belonging to one or the two multi-protein complexes that compose this family: Polycomb repressive complex 1 (PRC1) and PRC2 ([Margueron & Reinberg, 2011](#)). These complexes are associated with gene repression, especially of developmental regulators and *Hox* genes, as the original discovery of these proteins suggested. Deletion of core PcG proteins

results in early embryonic lethality, highlighting their key role in development (O'Carroll et al., 2001).

PRC1 and PRC2 complexes and functions are conserved in *Drosophila* and mammals: the main function of PRC1 is to compact chromatin (Shao et al., 1999) and catalyze H2A mono-ubiquitination of lysine 119 (Wng et al., 2004), while PRC2 deposits various levels of H3 methylation on lysine 27 (H3K27me1, 2 and 3) (Cao et al., 2002).

## 2.1 – Polycomb repressive complex 2 (PRC2) and H3K27me3

PRC2 is a methyltransferase responsible for mono-, di- and tri-methylation of H3K27 (H3K27me1, H3K27me2, H3K27me3). The catalytical activity of PRC2 is dependent on enhancer of zeste homologue 1 or 2 (EZH1 or EZH2) that bear the catalytically active SET domain (Czermin et al., 2002). Two other subunits are essential for EZH1/2 function: these are embryonic ectoderm development (EED) and suppressor of zeste 12 (SUZ12), in absence of which EZH1/2 histone methyltransferase activity is abolished (Cao et al., 2002; Cao & Zhang, 2004). Together with RB binding proteins (RBBP4 or RBBP7), these proteins are considered as the core components of PRC2 (**Figure 12**) and can associate with a lot of other subunits to form the complex variants of PRC2. The accessory PcG subunits are not essential for the catalytic activity of the core unit but can modulate its activity and recruitment to chromatin. AE binding protein 2 (AEBP2), for example, further stabilizes the complex and enhances its activity. JARID2 (Jumonji And AT-Rich Interaction Domain Containing 2) and Polycomb-like (PCL) proteins are also implicated in modulating its activity and recruitment (Margueron & Reinberg, 2010).

H3K27 methylation is very abundant, as around 80% of H3K27 are methylated, mostly dimethylated (50%) or sometimes trimethylated (15-20%) (Peters et al., 2003). How H3K27me2 versus -me3 deposition is specifically achieved is not well understood: it may rely on PRC2 abundance at the locus or on slightly different PRC2 variants such as PCLs, which are required for H3K27me3 but not -me2 deposition (Sarma et al., 2008). H3K27me2 does not seem to be associated with transcriptional repression, but could represent an important intermediate state.

Despite being considered as more dynamic and less stable than DNA methylation, H3K27me3 can be maintained through cell divisions thanks to an EED-mediated positive-feedback loop. EED binds specifically to H3K27me3 through its C-terminal WD40 domain and

therefore recruits PRC2 in previously H3K27 methylated regions to ensure its maintenance upon DNA replication (**Figure 12**) (Margueron et al., 2009). The molecular structure of PRC2 also suggests that EED binding to one nucleosome places EZH2 catalytic domain above the H3 tail of the next nucleosome: this feedback loop would therefore also allow spreading of H3K27me3 along chromatin fibers (Ciferri et al., 2012).

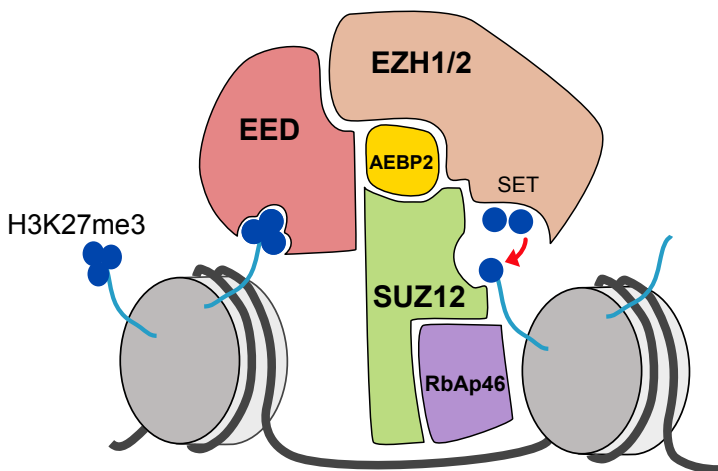


**Figure 12: Protein structure and model for PRC2 complex binding to nucleosomes.** SUZ12 and RbAp46 serve as docking modules for chromatin binding. EED binding to one nucleosome places EZH2 SET domain in proximity with the H3 tail of the adjacent nucleosome.

H3K27me3 usually harbors two distinct types of patterns in mammalian cells: it can be found in very large domains of more than 100kb, like at the *Hox* locus and on the inactive X chromosome, or in smaller domains of a few kilobases. These latter mostly overlap with promoters of developmentally important genes that are known to be Polycomb targets. In ESC cells for example, 60% of H3K27me3 peaks coincide with promoter regions, marking around 10% of all genes, especially developmental genes that are not required in the pluripotent state (Boyer et al., 2006). At the exception of the very large domains, H3K27me3 distribution almost perfectly overlaps with CpG islands: it was shown indeed that PRC2 is attracted to CpG islands, at the condition that they are not DNA methylated and not enriched in activating transcription factors (Jermann et al., 2014). Indeed, PCL proteins that are accessory subunits of the PRC2 complex, specifically bind to unmethylated CpG motifs and have been shown to be crucial for proper H3K27me3 establishment at promoters (Li et al., 2017). It also appears that PRC2 can be recruited by long non-coding RNAs (lncRNAs) to form large H3K27me3 domains: PRC2 is recruited in *cis* by the *Xist* lncRNA at the inactive X chromosome in mammalian female cells (Plath et al., 2003) or in *trans* at the *HoxD* locus by the *HOTAIR* lncRNA (Rinn et al., 2007). The JARID2 accessory subunit of PRC2 seems to have RNA binding properties and could be involved

in *Xist*-mediated PRC2 recruitment (da Rocha et al., 2014). It remains however unclear whether lncRNA-mediated repression really requires PRC2 or whether PRC2 recruitment is a consequence of the already established gene silencing (Portoso et al., 2017).

Interestingly, some of the H3K27me3-enriched promoters are also targeted by H3K4me3, a mark associated with active transcription (Bernstein et al., 2006). These domains are termed “bivalent” and are particularly frequent in ES cells. Bivalency is hypothesized to represent a specific chromatin state that poises developmental genes for either activation or repression. Indeed many lineage-specific bivalent promoters are definitely activated or repressed during differentiation, depending on the cell lineages (Mohn et al., 2008).

## 2.2 – Polycomb repressive complex (PRC1) and H2Aub

PRC1 is responsible for mono-ubiquitylation of lysine 118 or 119 of histone H2A (H2Aub) through its E3 ubiquitin ligase activity (Wang et al., 2004). While canonical PRC1 is composed of four proteins in *Drosophila*, it became clear in recent years that PRC1 is not a single complex in mammals but rather, an ensemble of at least 16 homologs that form multiple different complexes (Piunti & Shilatifard, 2021). However, both canonical and non-canonical PRC1 complexes contain the protein really interesting new gene 1A or 1B (RING1A or RING1B), which is the subunit responsible for the catalytic activity of PRC1 (Wang et al., 2004). RING1B is the most ubiquitous and active of the two enzymes and its knockout results in embryonic lethality, while RING1A-depleted mice survive (del Mar Lorente et al., 2000; Voncken et al., 2003). The second defining feature of PRC1 complexes is the presence of one of the six Polycomb Group Ring Finger proteins (PCGF1 to 6). The association of RING1A/B with a PCGF protein defines the PRC1.1 to PRC1.6 complexes, which have distinct proteins partners and target different genomic regions (Gao et al., 2012). I will not describe here the different PRC1 complexes but their structural and functional divergences have been thoroughly described in this review (Piunti & Shilatifard, 2021).

The targeting of PRC1 to particular chromatin regions is dependent on specific partners of the core RING1A/B-PCGF complex: they associate with Chromobox (CBX) proteins or with RING1 And YY1 Binding Protein (RYBP), which mediate two types of targeting behaviors (**Figure 13**) (Gao et al., 2012). These two proteins compete for the same binding site on the RING1A/B C-terminal domain and are thus mutually exclusive (Wang et al., 2010). First, the CBX proteins contain a chromodomain that recognizes H3K27me3. The binding of CBX

proteins to H3K27me3 allows recruiting CBX-containing PRC1 complexes to PRC2 targets, promoting then H2Aub deposition (**Figure 13A**) (Gao et al., 2012). Depletion of CBX7 leads to reactivation of many PRC2 targets and loss of H3K27me3 decreases the presence of CBX-PRC1 at gene promoters, highlighting the downstream role of CBX-PRC1 at PRC2 targets (Leeb et al., 2010). At the opposite, RYBP-containing PRC1 complexes is recruited to chromatin independently of H3K27me3. RYBP-PRC1 does indeed not possess a chromodomain that could recognize H3K27me3 but seems to be rather recruited at target sequences when H3K27me3 is depleted, either at large promoters or on the inactive X chromosome. In addition to RYBP, these complexes contain indeed binding proteins that trigger their recruitment at specific loci: RUNX1 transcription factors and the H3K36 demethylase KDM2b are known to associate with RYBP-PRC1 complexes (**Figure 13B**) (Yu et al., 2012; Wu et al., 2013). Altogether, PRC1 and PRC2 display complex epistatic relationships involving a lot of developmental stage- or cell type-specific dynamics : both PRC1 and PRC2 are known to be able to recruit or be recruited by the other complex, depending on the cellular context.

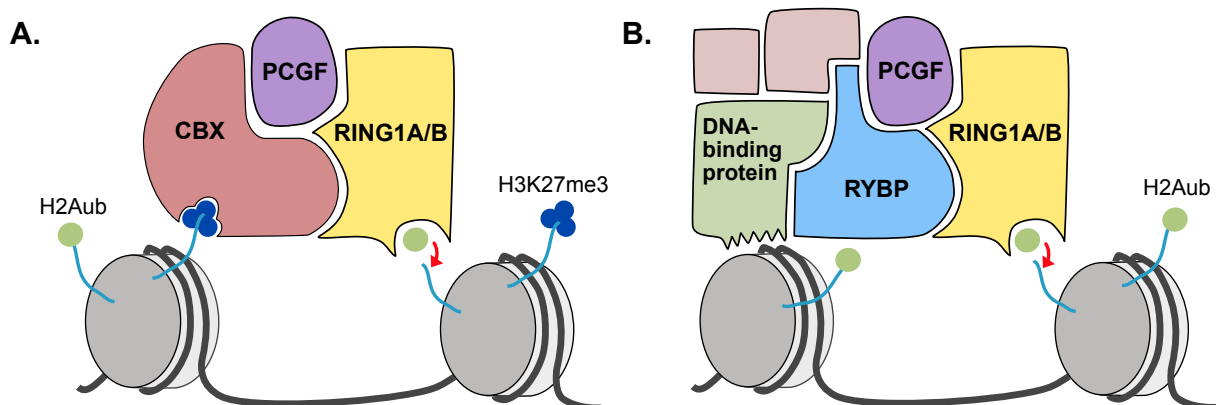


**Figure 13: Alternative modes of PRC1 complexes recruitment to chromatin.** A. CBX-PRC1 complex are recruited at PRC2 targets through CBX chromodomain recognition of H3K27me3. B. RYBP-PRC1 associates with DNA-binding proteins that trigger its recruitment to specific locations. In both cases, RING1A/B enzyme catalyzes mono-ubiquitylation of H2AK119.

### 2.3 – Polycomb-mediated transcriptional silencing

PRC1 and PRC2 complexes seem to be able to regulate chromatin environment and gene expression both through their catalytic activity, by depositing histone modifications, but also independently of their catalytic domains, by inducing chromatin condensation (Aranda et al., 2015).

H3K27me3-enriched domains encompass enhancers, promoters and gene bodies, suggesting that its function might differ depending on its genomic location. In *Drosophila*, H3K27me3 is known to limit RNA polymerase II (RNAPII) recruitment at promoters (Chopra et al., 2011). Similarly, on gene bodies, demethylation of H3K27me3 has been shown to be required for proper RNAPII elongation in differentiating muscle cells (Seenundun et al., 2010; Chen et al., 2012). However, how H3K27me3 or PRC2 binding could result in transcriptional repression is not well understood: they are thought to control transcription mainly by recruiting other factors, principally CBX-containing PRC1.

PRC1 has been more clearly shown to restrain RNAPII elongation by reducing transcriptional burst frequency and transcription initiation (Dobrinić et al., 2021). Different models have tried to explain this transcriptional repression: H2Aub could prevent the recruitment of the FACT (Facilitates Chromatin Transcription) histone chaperone at promoters regions, thus inhibiting H2A-H2B dimer eviction and RNAPII release (Zhou et al., 2008). An alternative model suggested that H2Aub presence leads to a switch of RNAPII to a yet-uncharacterized conformation, which would have less processive activity (Stock et al., 2007). It was recently shown in ES cells that Polycomb target genes become immediately derepressed upon loss of PRC1 and H2Aub, and that this derepression occurs despite the presence of PRC2 (Dobrinić et al., 2021). Moreover, rapid removal of PRC2 has no effect on Polycomb target gene expression (Dobrinić et al., 2021). Altogether, this highlights the predominant role of PRC1 over PRC2 in ensuring repression of polycomb targets.

Beside their potential direct effect on transcription, Polycomb proteins also seem to be playing an important role in inducing chromatin compaction. The mammalian genome is compartmentalized on the basis of preferential interactions between loci, forming multi-looped structures called topologically associated domains (TADs) and flanked by the insulator protein CCCTC-Binding Factor (CTCF). These TADs can correspond to super-enhancer domains of active transcription or at the opposite to transcriptionally repressed chromatin, like Polycomb domains (Downen et al., 2014). Indeed, they are densely marked by H3K27me3 and include most of the PcG-associated genes. These Polycomb domains are highly condensed with poor transcription factor or RNAPII accessibility: the link between Polycomb proteins and chromatin condensation remains, however, not fully understood. Among the most well-studied PcG domains are the *Hox* gene clusters that form large H3K27me3 TADs. During

embryonic development, *Hox* genes are sequentially activated: they segregate into an active TAD compartment at the same time than they lose H3K27me3 patterning and gain H3K4me3 marks (Noordermeer et al., 2011). TADs changes are therefore associated with chromatin mark dynamics but it is not clear whether PRC1/PRC2 are really required for TAD formation. Chromosome conformation assays in ES cells showed that loss of PRC2 (and thus H3K27me3) minimally disrupts global genome conformation (Denholtz et al., 2013). The link between Polycomb proteins and chromatin conformation thus remains an open field of research.

### 3. Histone H3 Lysine-4 Trimethylation (H3K4me)

#### 3.1 – H3K4me3 distribution and functions

The histone H3 lysine 4 (H3K4me3) can be modified by the addition of one, two or three methyl groups. The levels of methylation are thought to reflect the combined concentration and action of H3K4 methyltransferases and demethylases at a given chromatin locus. Although H3K4me3 is one of the best characterized histone mark, many of its features remain enigmatic, including its precise role in gene expression regulation, its targeting and its role in development.

The H3K4me3 modification is conserved across yeasts, plants and animals and its distribution has been mapped in a range of organisms (Santos-Rosa et al., 2002; Bernstein et al., 2005; Chih et al., 2005). Despite the differences between yeast and mammalian genes in terms of length and structure, the most striking feature of H3K4me3 distribution is that it correlates with the TSS of genes. H3K4me3 is thus predominantly present in sharp peaks (1-2kb) at the promoters of actively transcribed genes and positively correlates with the levels of nascent transcription, active polymerase occupancy and histone acetylation (Santos-Rosa et al., 2002; Schübeler et al., 2004; Bernstein et al., 2005).

But is H3K4me3 a cause or consequence of transcriptional activity? This question remains only partially answered, as evidence of both relationships have been described. H3K4me3 has been shown to be able to directly recruit chromatin modifiers and the transcriptional machinery, thus potentially facilitating transcription initiation. In particular, H3K4me3 recruits TFIID, a key complex of general transcription factors that include the TATA-binding protein and is essential for promoter recognition and pre-initiation complex formation (Vermeulen et al., 2007). Indeed, ectopic deposition of H3K4me3 at new loci in the genome is associated with

increased transcriptional activity (Clouaire et al., 2012). Conversely, the core transcriptional machinery can also recruit H3K4 methyltransferases, suggesting that H3K4me3 could be a by-product of transcription initiation. In agreement with this, H3K4me3 deposition is associated with the basal transcriptional machinery, as some H3K4me3 methyltransferases (MLL1 and MLL2) can bind to phosphorylated RNAPII (Dou et al., 2005; Ruthenburg et al., 2007). Moreover, a recent study showed that the SETD1 H3K4 methyltransferase complex could contribute to promote transcriptional activity independently of its catalytic activity, but through interaction with RNAPII-binding proteins involved in premature transcription termination. SETD1 binding would counteract their terminating activity and enables full-length transcription of genes. Transcriptional downregulation observed in *Setd1* knockout cells would therefore be due to the lack of the protein itself, rather than the loss of the H3K4me3 mark (Hughes et al., 2022).

Despite strong evidence that H3K4me3 is tightly linked to transcription initiation, this correlation may not be universal to all genomic loci. Knockout of core subunits of mammalian H3K4 methyltransferases leads to global loss of H3K4me3, but to mis-regulation of a subset of genes only (Wysocka et al., 2005). H3K4me3 is also found at CpG islands irrespective of gene expression: 99% of CG-rich promoters are associated with H3K4me3 enrichment in ES cells, even if the majority of them are not active (Mikkelsen et al., 2007). Moreover, artificial introduction of a CpG-rich sequence with no promoter activity in the genome results in H3K4me3 acquisition (Wachter et al., 2014). CG density and sequence composition could thus play a role in H3K4 methyltransferase recruitment, independently of transcriptional activity.

H3K4me3 is often associated with H3K27me3 : 22% of the H3K4me3-enriched CpG promoters are bivalent, coincidentally displaying both H3K4me3 and H3K27me3 (see III. 2. for more information on bivalent promoters) (Bernstein et al., 2006; Mikkelsen et al., 2007). These bivalent promoters show low transcriptional activity despite the presence of H3K4me3, suggesting that the repressive effect of Polycomb marks is generally dominant over H3K4me3 enrichment. H3K4me3-monovalent promoters typically correspond to ‘housekeeping genes’ that stay stably and highly expressed because of their implication in key pathways like metabolism, replication or cell architecture (Mikkelsen et al., 2007).

Beyond this correlation with transcription, H3K4me3 is also known for being playing a role in DNA repair and targeting of double strand breaks (DSBs) during meiotic recombination. It

serves as prominent mark of active recombination initiation hotspots where it recruits DSB and recombination effectors (Jiang et al., 2020).

### 3.2 – H3K4 methyltransferases

The enzymes that methylate H3K4 are highly conserved from yeasts, flies to humans. They each contain a SET domain, which catalyzes the addition of methyl groups to specific lysine residues. In mammals, the H3K4 methyltransferase family is complex, with at least ten H3K4 methyl writers have been identified (Ruthenburg et al., 2007). Two main family of enzymes can be distinguished based on the origin of their catalytic SET domains: the SETD1 family resembles the yeast *Set1*, while the Mixed Lineage Leukemia (MLL)-family members are related to *Drosophila Trithorax (Trx)*. The multiplicity of methyltransferases in mammalian genomes must result from their functional specialization in cellular expression patterns or in sequence targets. It is considered that SETD1 complexes (SETD1A and SETD1B) are responsible for most of H3K4me3 deposition, in particular at active promoters: comparative RNAi-mediated knockdown studies demonstrated that their loss has the most pronounced effects on H3K4me3 patterns and transcription reduction (Ardehali et al., 2011). At the opposite, the distinguishable phenotypes for deletions of MLL-family members (*Mll1*, *Mll2*, *Mll3* or *Mll4*) suggest that MLL enzymes are not redundant but specialized for precise functions. MLL1 and MLL2 methylate H3K4 at different subsets of homeotic genes (Glaser et al., 2006; Wang et al., 2009): rearrangements of the *MLL1* gene in humans are associated with aggressive leukemia in children caused by *Hox* genes dysregulation (Hess, 2004). MLL3 and MLL4 are rather linked to H3K4me1 and enhancers (Hu et al., 2013).

In both SETD1 and MLL-families, the methyltransferases exist in multiprotein complexes. In addition to the SET domain-bearing catalytic enzyme (SET1A/B or MLL1-4), they share three common subunits: WRD5, RbPB5 and ASH2 (Dou et al., 2006). The WRD5/RbPB5/ASH2 subcomplex can exist independently of the catalytical subunits as a structural platform and can associate with the SET domains of different enzymes (Dou et al., 2006). All three proteins are required for H3K4 methylation, thus forming the core H3K4 methyltransferase complex (Figure 14).

Several other subunits have also been shown to interact with the four-component core complex. In particular, the CxxC-finger protein 1 (CXXC1 or CFP1) is a key regulatory subunit

of SETD1: the SETD1B core complex cannot bind to genomic DNA in its own, but is targeted to chromatin through CXXC1, which can engage in multiple chromatin binding to recognize both pre-existing H3K4me3 and non-methylated CpG islands (**Figure 14**) (Clouaire et al., 2012; Brown et al., 2017). This positive feedback loop of CXXC1-mediated SETD1 recruitment at pre-marked H3K4me3 loci might be responsible for faithful H3K4me3 pattern propagation throughout cell division. CXXC1 is thus essential for proper establishment of H3K4me3 at active promoters, and to avoid “leakage” activity of SETD1 to inappropriate chromatin compartments (Lee & Skalnik, 2005; Brown et al., 2017). Although MLL complexes do not interact with CXXC1, they also possess a CxxC-zinc finger domain to recognize unmethylated CpG and can include among their accessory subunits a PHD finger for H3K4me3 binding (Birke et al., 2002; Allen et al., 2006). MLL-family chromatin recruitment seems therefore more complex, explaining maybe their increased functional specificity.

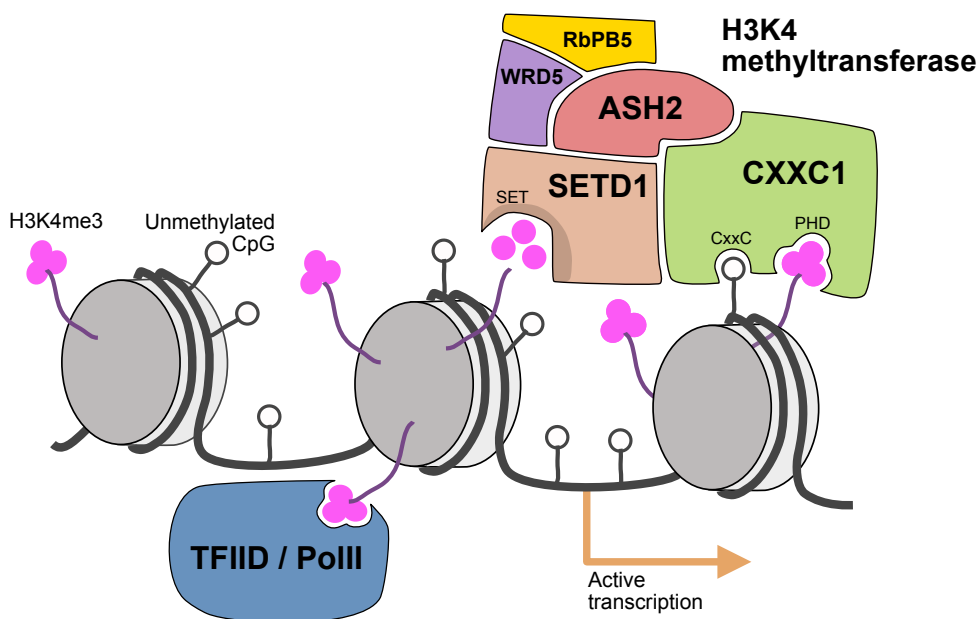


**Figure 14: Recruitment of H3K4 methyltransferases at active CGI promoters: example of the SETD1 complex.** The SETD1-complex is the major writer of H3K4me3 at active promoters in somatic cells. The CXXC1 subunit recognizes pre-existing H3K4me3 and DNA methylation-free CpGs and thus enables recruitment of SETD1B, which catalyzes H3K4 methylation through its SET domain. ASH2, RbPB5 and WRD5 are core components of the H3K4 methyltransferase complex. H3K4me3 is able to recruit or to be recruited by transcription factors (TFIID) or the RNA polymerase II (PolII).

## 4. Other post-translational histone modifications

### 4.1 – Histone H3 Lysine-36 trimethylation (H3K36me3)

Histone H3 can be methylated at lysine 36 with one, two or three methyl groups (H3K36me1, me2 or me3). While several redundant enzymes are able to catalyze mono- or dimethylation of H3K36 (NSD1/2 being the most well-characterized ones), only SETD2 has been found to perform H3K36 trimethylation ([Edmunds et al., 2008](#)).

H3K36me3 is widely recognized to be associated with transcriptional activity ([Wagner & Carpenter, 2012](#)): H3K36me3 distribution tightly correlates with actively transcribed regions ([Bannister et al., 2005](#)). Indeed, several lines of evidence showed that SETD2 is coupled to the process of transcription itself. SETD2 associates with the phosphorylated processive form of RNAPII and catalyzes trimethylation of H3K36 during transcription elongation ([Kizer et al., 2005](#)). This leads to the presence of a shift from mono/dimethylation to trimethylation of H3K36 from the RNAPII initiation site towards the 3' end, covering transcribed gene bodies.

The function of intragenic H3K36me3 is not fully resolved in mammals. In yeasts, SETD2 deposits H3K36me3 co-transcriptionally and recruits the reduced dependency 3 small (Rpd3S) enzymes, whose function is to deacetylate histones ([Li et al., 2009](#)). This enforces repressive chromatin state in transcribed domains, preventing aberrant transcriptional initiation from intragenic cryptic gene promoters. It is not clear whether the deacetylation mechanism is conserved in mammals ; it was rather suggested that a H3K4 demethylase could be coupled to H3K36me3 deposition ([Fang et al., 2010](#)). Whether H3K36me3 role, as a safeguard to prevent cryptic intragenic transcription, is conserved in mammals is however still controversial.

### 4.2- Histone H3 Lysine-9 trimethylation (H3K9me3)

H3K9 methylation is the hallmark of what is considered as heterochromatin, meaning transcriptionally inactive and highly condensed chromosomal regions. It is especially frequent around telomeres and centromeres ([Nicetto & Zaret, 2019](#)). Pericentromeric regions cluster together to form chromocenters during interphase, which can indeed be visualized as bright foci after H3K9me3 staining. H3K9me3 is also present throughout the genome in repressed regions and particularly, at transposable elements.

H3K9 methylation exists at the mono-, di- or tri-methylated states. Eight distinct H3K9 methyltransferases have been described so far: specific enzymes are methylating pericentric H3K9, while G9a/ GLP and ESET/SETDB1 are the primary enzymes responsible respectively for H3K9me2 and H3K9me3 deposition in non-pericentric regions (Schultz et al., 2002; Rice et al., 2003). ESET has been shown to be critical for embryonic development as knockout mouse embryos die around E4.5 (Dodge et al., 2004): it plays a key role in pluripotency maintenance and transposable element repression.

H3K9me2 and H3K9me3 are linked with transcriptional repression and chromatin compaction. H3K9me3 is thought to promote chromatin compaction by recruiting the heterochromatin protein 1 (HP1) architectural protein (Bannister et al., 2001), which is essential for the formation of high-order chromatin structures: it binds nucleosomes as a tetramer, enabling chromatin compaction by through nucleosome bridging (Canzio et al., 2011). HP1 also acts as a shield against transcriptional machinery binding to the underlying chromatin (Smallwood et al., 2008). Apart from its role in HP1-mediated chromatin compaction, H3K9me3 is also linked to transcriptional repression via its association with KRAB-associated protein 1 (KAP1, also known as TRIM28). KAP1 is a multi-domain protein that acts as a binding platform for the establishment of repressive environment around specific DNA sequences (Schultz et al., 2002). It is recruited to chromatin through its binding to KRAB zinc finger protein (KRAB-ZFPs), which recognize specific DNA sequences (Ryan et al., 1999). Once recruited at a specific region, KAP1 will serve as an anchor for the ESET H3K9 methyltransferase, HP1 and the histone remodelers ATRX and DAXX (Schultz et al., 2002; Sadic et al., 2015). These latter mediate the deposition of H3.3 histone variants and therefore increase chromatin condensation and inaccessibility (Elsässer et al., 2015). Altogether, through its interactions with KAP1, DAXX or HP1, the H3K9me2/me3 marks are key mediators of transcriptional repression.

## 5. Interplays between chromatin marks

Although many reports have characterized the functions of chromatin marks in isolation, genome-wide studies have also revealed complex interactions between them. These interplays increasingly appear as essential for locus-specific chromatin modifier recruitment: the sum of attractive and repulsive feedbacks between marks and chromatin proteins seems

to rule the establishment of precise epigenetic patterns (Janssen & Lorincz, 2021). Rather than individual modifications, integration of numerous positive and negative inputs of different marks would also be key for precise and dynamic regulation of transcription. Even if the identities of most chromatin marks are now known, the mechanisms by which their regulatory inputs are integrated remain poorly understood.

The study of these interplays is challenging as the actual techniques of chromatin profiling (CHIP-seq, CUT&RUN) typically enable to focus only on one protein or chromatin mark at a time in a cell population (Park, 2009; Skene & Henikoff, 2017). In order to infer the overall composition of chromatin domains, comparisons of multiple different maps are thus required. However, since different features are mapped in different cells, one cannot distinguish between co-occurrence in the same cell or alternative binding of one or the other at the same sites, but in different cells. Newly developed techniques are trying to overcome these limitations (Weiner et al., 2016; Gopalan et al., 2021). However, no efficient, high-sensitivity and broadly applicable method for simultaneous profiling of chromatin proteins or marks has been described.

As my project aims at understanding the targeting of DNA methylation and H3K27me3 to chromatin in the oocyte and their functional relationship with other chromatin marks, I will here focus on describing the functional relationships involving at least one of these two marks.

### 5.1 – H3K4me3 and DNA methylation antagonism

The strong anti-correlation between DNA methylation and H3K4me3 in mammals represents the first identified crosstalk between DNA methylation and histone methylation. Indeed, as previously described, the ADD domain of DNMT3 proteins interacts specifically with unmodified H3K4 residues (Ooi et al., 2007), relieving the autoinhibitory interaction between this domain and the methyltransferase catalytic domain. In presence of methylated H3K4, the interaction between the histone tail and the ADD domain is abolished, preventing DNMT3-activity on H3K4me3-enriched active promoters (**Figure 15A**). The higher the valency of H3K4 methylation is, the greater the inhibitory effect on DNMT3A. This contributes to prevent DNA methylation-mediated silencing of H3K4me3-marked active promoters (Li et al., 2011). For example, regions enriched in H3K4me3 in the inner cell mass (ICM) remain unmethylated in E7.5 embryos, despite the genome-wide wave of DNA methylation that takes place in this

developmental window (Greenfield et al., 2018). Upon differentiation of ESCs in neuronal progenitor cells, loss of H3K4me3 coincides with subsequential DNA methylation deposition and decreased transcription (Mikkelsen et al., 2007; Meissner et al., 2008). H3K4me3 has clearly an important role in dictating DNA methylation landscape. Further confirming the importance of this ADD domain-mediated antagonism, *Dnmt* triple-knockout ESCs expressing a DNMT3A ADD mutant protein are insensitive to H3K4me3 and show aberrant DNMT3A binding at H3K4me3-marked promoters (Noh et al., 2015). This DNMT3A binding is only observed in high H3K4me3 but low H3K27me3 promoters, reflecting a potential antagonism between H3K27me3 and DNA methylation (discussed further below).

However, the mutual exclusivity between H3K4me3 and DNA methylation patterns is not only due to the inhibiting action of H3K4me3 on DNA methylation deposition, but also to the repulsive action of DNA methylation on H3K4 methyltransferases. Indeed, the main mammalian H3K4 methyltransferase complex, SET1, is selectively recruited to chromatin through binding of its CXXC1 subunit to unmethylated CGIs (Figure 15B) (Clouaire et al., 2012; Brown et al., 2017). In a similar way, the MLL2 protein also possesses a CxxC-zinc finger domain that specifically recognizes unmethylated CpGs. It was also shown that the presence of methylated CpG on one or both DNA strands precludes efficient interaction with MLL proteins (Birke et al., 2002; Allen et al., 2006). The presence of DNA methylation is thus repulsive for H3K4 methyltransferases binding and subsequent H3K4 methylation.

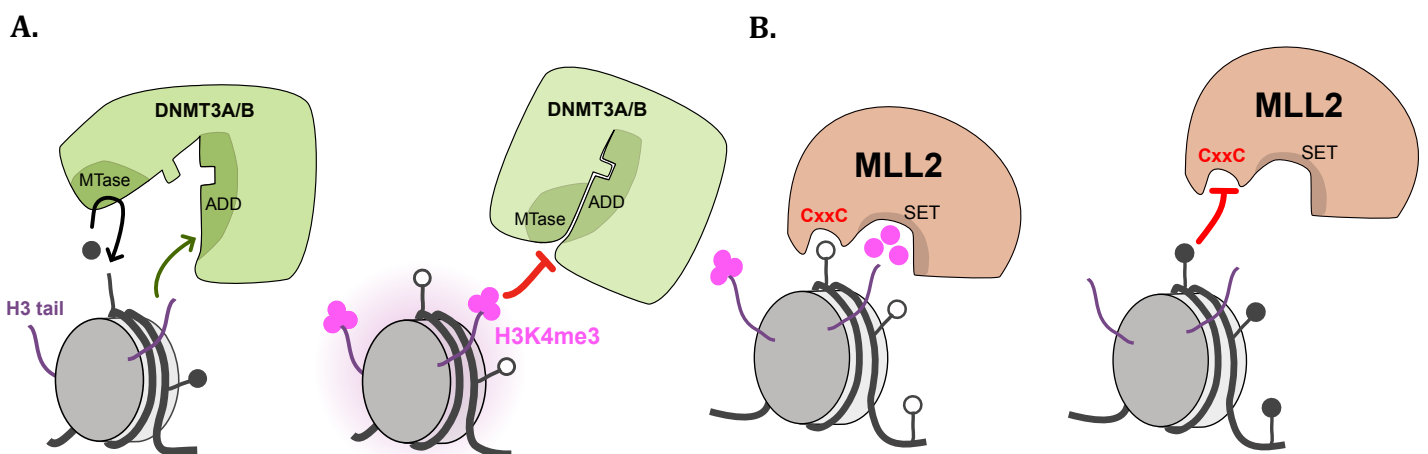


**Figure 15: Molecular basis of H3K4me3 - DNA methylation antagonism.** A. The ADD domain of DNMT3A and DNMT3B interacts with unmethylated H3K4, relieving the autoinhibitory conformation of these proteins. Methylation of H3K4 prevents this interaction and inhibits DNA methylation. B. H3K4me3 methyltransferase complexes, like MLL2, possess a CXXC domain that binds specifically to unmethylated CpGs. DNA methylation thus repulses H3K4methyltransferases and H3K4 methylation.

## 5.2 – H3K36me2/me3 promotes *de novo* DNA methylation

In contrast to the inhibitory role of H3K4me3, genome-wide studies indicate a strong correlation between DNA methylation and H3K36me3 patterns. This correlation can be

explained by the H3K36me2/me3-mediated recruitment of DNA methyltransferases: the PWWP domain of DNMT3A and DNMT3B has been shown to specifically bind to di- or trimethylated H3K36 (Dhayalan et al., 2010). DNMT3A binds preferentially to H3K36me2-marked regions in somatic cells, while DNMT3B appears to favor interactions with H3K36me3 (Baubec et al., 2015; Weinberg et al., 2019). This differential affinity seems nonetheless only preferential and not exclusive, as in absence of H3K36me2, DNMT3A was shown to redistribute to H3K36me3-enriched sequences (Weinberg et al., 2019).

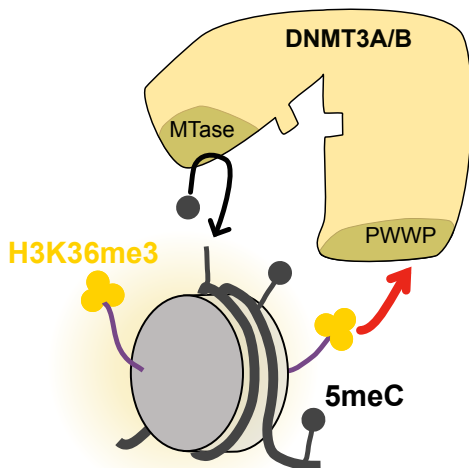


**Figure 11:** H3K36me2/me3 recruits DNMT3A/B through interaction with their PWWP domain.

As H3K36 methylation is deposited co-transcriptionally, it is mainly enriched at actively transcribed regions. H3K36me3-mediated recruitment of the DNA methylation machinery could therefore explain the high enrichment in methylated CpGs at gene bodies. Both DNA methylation and H3K36me3 have been hypothesized to be playing a role in preventing cryptic transcription initiation when located in gene bodies (Fang et al., 2010; Neri et al., 2017). Loss of SETD2 (and the consequent loss of H3K36me3) and intragenic DNA hypomethylation has been shown to be key factors in promoting cancer through abnormal transcript expression (Gaudet et al., 2003; Duns et al., 2010).

In comparison, H3K36me2 is diffusely distributed at both genic and intergenic regions, leading to DNMT3A recruitment and DNA methylation deposition to non-transcribed and intergenic regions. As an example, in *Nsd1* knockout ES cells, H3K36me2 is depleted and intergenic DNA methylation deposition is lost (Weinberg et al., 2019). This phenotype is recapitulated in both Sotos and Tatton-Brown-Rahman overgrowth syndromes characterized respectively by NSD1 haploinsufficiency or by DNMT3A<sub>PWWP</sub> missense mutation, leading to

abrogation of the H3K36me2-specific binding affinity (Kurotaki et al., 2002; Tatton-Brown et al., 2014). In both cases, this results in hypomethylation of intergenic DNA.

Altogether this highlights the critical role of NSD1-deposited H3K36me2 and SETD2-deposited H3K36me3 in orchestrating *de novo* DNA methylation deposition at intergenic and actively transcribed genes.

### 5.3 – Antagonism between H3K27me3 and the DNA methylation - H3K36me3 duo

#### - Negative crosstalks between H3K27me3 and DNA methylation:

DNA methylation and H3K27me3 have been shown to play similar repressive functions when located on gene promoters, but these two marks are generally mutually exclusive in their genomic distribution, in particular at CGIs. Although H3K27me3 and DNA methylation do not usually overlap, their colocalization has been reported outside CGI regions in somatic cells or at CGI promoters in cancer cells (Brinkman et al., 2012; Statham et al., 2012).

Recent studies have begun to unravel the molecular basis of their antagonistic relationships. Indeed, PRC2 recruitment is inhibited by DNA methylation, especially at CGIs. PRC2 is mainly targeted to CGIs via two alternative subunits, PCL proteins (PCL1/PHF1, PCL2/MTF2, PCL3,PHF19) or JARID2, which are both sensitive to DNA methylation. The tight helix structure of PCL proteins enables selective recognition of unmethylated CGIs only (**Figure 16**) (Li et al., 2017; Perino et al., 2018). On another hand, the JARID2 subunit is recruited to CGIs by the H2Aub mark, whose deposition by the PRC1 complex is dependent upon the KDM2B subunit that binds DNA in a DNA methylation-sensitive manner (Farcas et al., 2012; Blackledge et al., 2014). Recruitment of PRC2 is thus sensitive to the DNA methylation state at CGIs. In addition, the TET1 DNA demethylase helps to recruit PRC2 at CGIs and Polycomb targets: TET1-mediated DNA demethylation therefore promotes H3K27me3 deposition (Wu et al., 2011). The negative interplay observed between H3K27me3 and DNA methylation is thus likely to result from crosstalks between the chromatin modifiers that deposit and remove these marks.

In accordance with their mutual exclusivity, deletion of DNMTs has been shown to lead to H3K27me3 gain in regions that have lost DNA methylation, in various cell types (Brinkman et al., 2012; Reddington et al., 2013). In addition, loss of DNA methylation results in widespread redistribution of H3K27me3: while it is gained in regions that lose DNA methylation, the striking H3K27me3 loss at previously-enriched promoters leads to ectopic expression of Polycomb target genes (Reddington et al., 2013). In a comparable manner, when subjecting ES cells to hypomethylating culture conditions (2 inhibitors + vitamin C), H3K27me3 was shown to accumulate at transposable elements and secure transposon repression (Walter et al., 2016), while Polycomb targets underwent decreased chromatin compaction (McLaughlin et al., 2019). Overexpression of DNMT3B in mouse embryonic fibroblasts also leads to ectopic gain of DNA methylation and H3K27me3 decrease (Zhang et al., 2018). Conversely, disruption of H3K27me3 deposition via *Eed* knockout in ESCs is associated with aberrant DNA methylation near developmental genes in DNA methylation valleys, which are usually H3K27me3-enriched (Li et al., 2018). This suggests a bidirectional crosstalk between DNA methylation and H3K27me3.

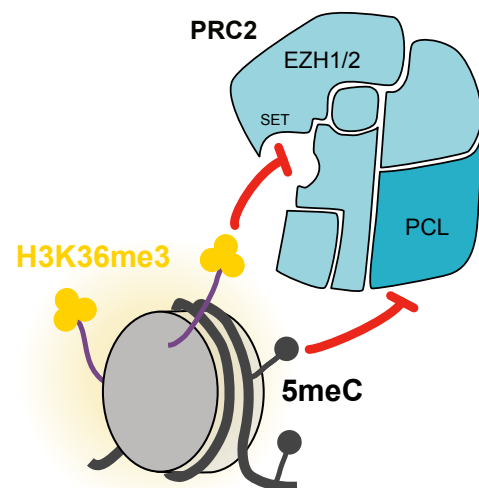


**Figure 16: DNA methylation and H3K36me3 inhibit PRC2 recruitment and activity.** PCL proteins (PRC2 subunits) bind only to unmethylated CpG. Methylated cytosines disrupt EZH2 catalytic activity.

- The complex case of H3K36me3, DNA methylation and H3K27me3 crosstalks:

As H3K36me2/me3 and DNA methylation almost perfectly co-occur genome-wide, it is difficult to deduce the relative importance of H3K36me2/me3 versus DNA methylation in the inhibition of H3K27me3. Both H3K36me3 and H3K36me2 anti-correlate with H3K27me3 (Mikkelsen et al., 2007; Streubel et al., 2018) but this could only be a secondary effect of DNA methylation antagonism with H3K27me3. However, *in vitro* studies demonstrated that H3K27me3 deposition is inhibited by the presence of H3K36me3 on the same nucleosome (Yuan et al., 2011). While EZH2 activity is stimulated by the interaction with unmodified

H3K36, PRC2 catalytic activity is disrupted in the presence of H3K36me<sub>2</sub>/me<sub>3</sub> (**Figure 16**) (Jani et al., 2019). PRC2 can still bind to DNA but the sum of interactions between EZH2, nucleosomal DNA and the H3 tail creates a geometry that permits allosteric inhibition of PRC2 by methylated H3K36 (Finogenova et al., 2020). In the reciprocal experiment, the presence of H3K27me<sub>3</sub> did not impact SETD2 activity (Yuan et al., 2011). These studies support the idea of a direct role for H3K36 methylation in the regulation of PRC2 activity and H3K27me<sub>3</sub> antagonism.

Consistent with an antagonistic role of H3K36me<sub>3</sub> on PRC2 activity, loss of H3K36me<sub>2</sub>/me<sub>3</sub> by depletion of NSD1 or SETD2 results in both DNA methylation decrease and H3K27me<sub>3</sub> spreading (**Figure 17**) (Streubel et al., 2018; Shirane et al., 2020). It is therefore difficult to discriminate which marks between H3K36me<sub>3</sub> and/or DNA methylation are responsible for H3K27me<sub>3</sub> antagonism. In a similar manner, inhibition of transcription leads to decreased co-transcriptional H3K36me<sub>3</sub> establishment, loss of DNA methylation and ectopic gain of H3K27me<sub>3</sub> in gene bodies (Hosogane et al., 2016). Conversely, the observed overexpression of NSD2 in human myeloma cells leads to increased H3K36me<sub>2</sub> and decreased levels (Zheng et al., 2012).

In support of DNA methylation role in mitigating H3K27me<sub>3</sub> antagonism, mutations in the PWWP domain of DNMT3A result in aberrant H3K36me<sub>3</sub>-independent DNA methylation and loss of H3K27me<sub>3</sub> (**Figure 17**) (Heyn et al., 2019; Weinberg et al., 2021). Indeed, in absence of PWWP-mediated targeting of DNMT3A to chromatin, DNMT3A is alternatively recruited at H2Aub-enriched regions through its N-ter domain (see III. 1.4). H3K27me<sub>3</sub> loss from Polycomb promoters would then be a consequence of ectopic DNA methylation deposition, independently of H3K36me<sub>3</sub>. At the opposite, in prospermatogonia, regions showing H3K27me<sub>3</sub> gain in absence of NSD1 do not show increased H3K27me<sub>3</sub> in absence of DNMT3L (**Figure 17**), even though both *Nsd1* and *Dnmt3L* knockout results in DNA methylation loss at H3K36me<sub>2</sub> regions (Shirane et al., 2020). Disruption of DNA methylation was in this context not sufficient for mitigating H3K27me<sub>3</sub> antagonism; loss of H3K36me<sub>2</sub> was necessary to enable H3K27me<sub>3</sub> spreading. Thus, at least in the male germline, H3K36me<sub>2</sub> was shown to be the essential mark for PRC2 inhibition at hypermethylated regions. However, further studies are needed to better understand the complex interactions between H3K36me<sub>2</sub>/me<sub>3</sub>, H3K27me<sub>3</sub> and DNA methylation in other cellular contexts.

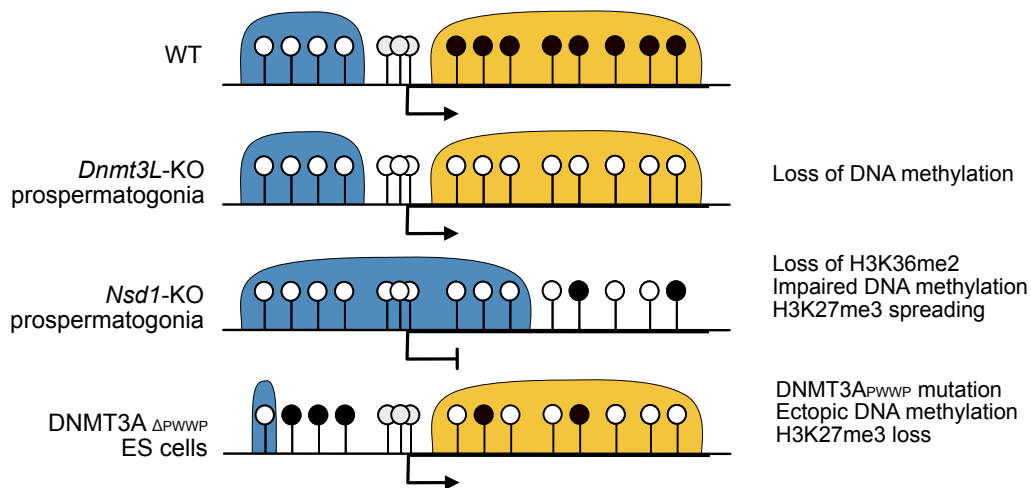


**Figure 17: Complex relationships between DNA methylation, H3K36me3 and H3K27me3.**

#### 5.4 – H3K27me3 and H3K4me3

While PRC2 is able to bind unmodified or H3K4me3-modified nucleosomes with comparable affinity, *in vitro* assays showed that H3K4 methylation specifically inhibits PRC2 activity by allosteric blocking of the PRC2 catalytic domain (Schmitges et al., 2011). However, this PRC2 inhibition is triggered only when H3K4me3 is present on the same histone tail than the H3K27 target lysine. In contrast, the presence of H3K4me3 in the vicinity of PRC2 seems to have little effects on its catalytic activity.

The idea of a restrained biochemical antagonism between these two marks is consistent with the existence of bivalent domains, displaying co-enrichment of both H3K27me3 and H3K4me3 (Bernstein et al., 2006). The two marks have been reported to exist inside these bivalent domains on the same DNA strand by sequential-ChIP, designed to retain only chromatin that concomitantly carries both modifications, and even on the same nucleosome, albeit on opposite H3 tails (Bernstein et al., 2006; Voigt et al., 2012). Given that PRC2 tends to be inhibited by H3K4me3, how could bivalent domains be generated? Their antagonism seems to be limited to an impossible co-enrichment on the same histone tail, so that both mark could co-occur at neighbor nucleosomes or asymmetric histone tails in bivalent domains. Another possibility would be that H3K27me3 is established prior to H3K4 methylation, as SETD1 H3K4 methyltransferase is not inhibited by H3K27me3 (Schmitges et al., 2011). Their antagonism could also be mitigated at bivalent regions specifically by some unknown mechanisms, explaining why their colocalization is restrained to some precise domains.

The co-occurrence of both H3K4me3 and H3K27me3 at bivalent domains is found primarily on CpG-rich promoters of genes implicated in developmental processes and lineage specification (Bernstein et al., 2006; Blanco et al., 2020). They are mainly found in ES cells, where they correspond to around 2700 regions. This bipotential state has been proposed to enable silencing of developmental genes while preserving their potential to become activated upon initiation of differentiation programs. In this model, H3K27me3 helps to repress lineage regulatory genes during the pluripotency phase (Boyer et al., 2006; Chamberlain et al., 2008), while H3K4me3 poises genes for activation upon differentiation (Jiang et al., 2011), potentially by protecting them from permanent silencing by repelling transcriptional repressors or DNA methylation. Indeed, the bivalency state is lost upon ES cell differentiation: active genes lose H3K27me3, and silenced genes lose H3K4me3 depending on their cell lineage commitment (Figure 18). Most bivalent genes are not expressed or expressed at very low levels in ES cells before resolution of the bipotency (Bernstein et al., 2006). How the positioning of H3K4me3 and H3K27me3 at bivalent promoters is directed remains unclear: long non-coding RNAs or DNA binding proteins could recruit both PRC2 and H3K4 methyltransferases to specific sequence elements.

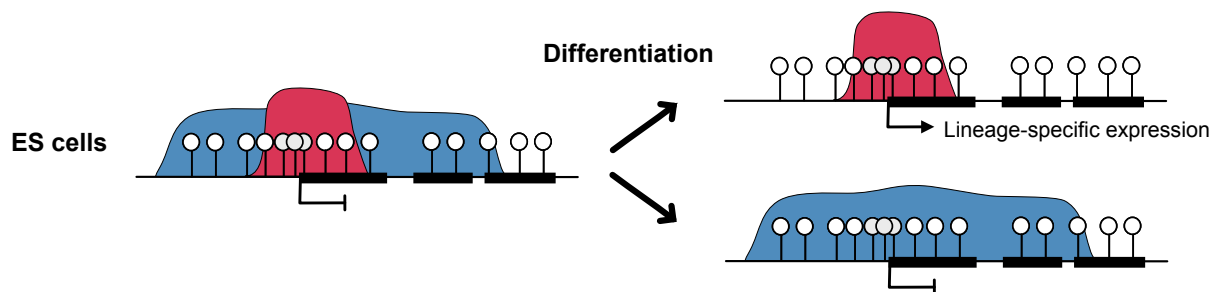


**Figure 18: Bivalent promoter dynamics upon differentiation.** In ES cells, H3K4me3 and H3K27me3 co-occur at developmental genes. They are repressed by H3K27me3 but poised for future activation by H3K4me3. Upon differentiation, this bipotency is resolved: active genes lose H3K27me3 and silenced genes lose H3K4me3 depending on their lineage commitment.

## IV- Epigenetic interplays during oogenesis

### 1 – Epigenetic reprogramming in primordial germ cells

Chromatin marks such as DNA methylation and histone modifications are relatively stable in somatic cells. In contrast, they are reprogrammed on a genome-wide scale in germ cells and in preimplantation embryos in mammals (see III. 1.3 on DNA methylation dynamics in development). In germ cells, it corresponds to the erasure of somatic patterns, inherited from the epiblast, from which primordial germ cells are specified, and to the re-establishment of germline-specific patterns. Reprogramming is required to remove the epigenetic marks acquired during development or imposed by the environment, so that the epigenetic information transmitted to the embryo properly reflects the program characteristic of its species (Heard & Martienssen, 2014). Its biological purposes includes erasure and reestablishment of parental genomic imprinting, reactivation of the silenced X-chromosome in females and erasure of potential epimutations. If germline reprogramming fails, epigenetic marks could be retained and transmitted from one generation to the next. Reprogramming therefore limits transgenerational epigenetic inheritance in mammals, as it resets the chromatin landscape transmitted by the gametes to the next generation.

After specification through BMP signaling, PGCs migrate to the genital ridges between E6.5 and E10.5. At the same time, induction of a small number of transcription factors drive developmental segregation of the germline. This is accompanied by chromatin changes, so that upon arrival in the genital ridges, PGCs are already epigenetically different from their somatic neighbor cells. Upon colonization of the gonads, the process of genome-wide epigenetic reprogramming continues and is completed around E12.5 (Ramakrishna et al., 2021).

Epigenetic changes occurring during PGC migration have been mainly quantified *in vivo* by immunofluorescence staining, as the small number of migratory PGCs is an important limiting factor for more detailed chromatin profiling methods. Instead, the mouse PGC-like cells (mPGCLC) system, which corresponds to *in vitro* model of PGC specification by induction from epiblast-like cells, has been used to generate sufficient cell numbers to perform ChIP-seq (Hayashi et al., 2011; Kurimoto et al., 2015). A lot of information on this developmental window of PGC development is thus coming from *in cellula* experiments. Comparatively,

gonadal PGCs are sufficiently abundant for *in vivo* characterization of their chromatin landscape through low-input chromatin profiling techniques. I will review here the key chromatin changes that occur during germline reprogramming in both migratory and gonadal PGC development.

### 1.1 - DNA methylation erasure

During the course of their proliferation and migration, PGCs undergo DNA methylation reprogramming, leading to erasure of epiblast-transmitted patterns. At E6.5, the level of DNA methylation in PGCs is comparable to adjacent somatic cells (around 70-80% of methylated CpGs), while at E13.5 DNA methylation is almost completely erased (5-7% CpG methylation) (Saitou & Yamaji, 2012). The germline DNA demethylation process occurs in two consecutive steps: passive dilution of methylation from E8.5 to E9.5 followed by TET-dependent active demethylation from E9.5 to E13.5 (**Figure 19**) (Seisenberger et al., 2012; Zeng & Chen, 2019).

The first phase of DNA demethylation is considered to start around E8.5, when the first signs of DNA methylation decrease were observed in PGCs compared to the surrounding somatic cells (Seki et al., 2005). At E9.5, global DNA methylation levels have already dropped to 30%, making it the most intense phase of DNA demethylation (**Figure 19**) (Seisenberger et al., 2012). Passive demethylation is predominantly responsible at this phase: downregulation of maintenance and *de novo* DNA methylation machineries (DNMT3A, DNMT3B and UHRF1) coincides with high proliferation rate of PGCs at these stages, leading to passive dilution of DNA methylation across cell divisions (Kurimoto et al., 2008). In particular, the DNMT1 cofactor UHRF1 is repressed and excluded from the nucleus at E9.0, leading to impaired DNMT1-mediated DNA methylation maintenance (Kagiwada et al., 2013). In agreement with the idea of untargeted passive DNA demethylation, all genomic compartments are affected: promoters, CpG islands, introns, exons and intergenic sequences are all demethylated (Seisenberger et al., 2012). Only some specific regions, including imprinted genes, meiotic gene promoters and endogenous retroviruses of the Intracisternal A particle (IAP) family are resistant to the first phase of DNA demethylation (Seisenberger et al., 2012). These regions seem to be preferentially targeted by DNMT1 and thus protected from passive demethylation. The conditional knock-out of *Dnmt1* in early PGCs (*Prdm1*-CRE driven) results in

hypomethylation of imprinted genes and meiotic gene promoters at E10.5, to decreased PGC numbers and to premature meiosis entry in female PGCs (Hargan-Calvopina et al., 2016).

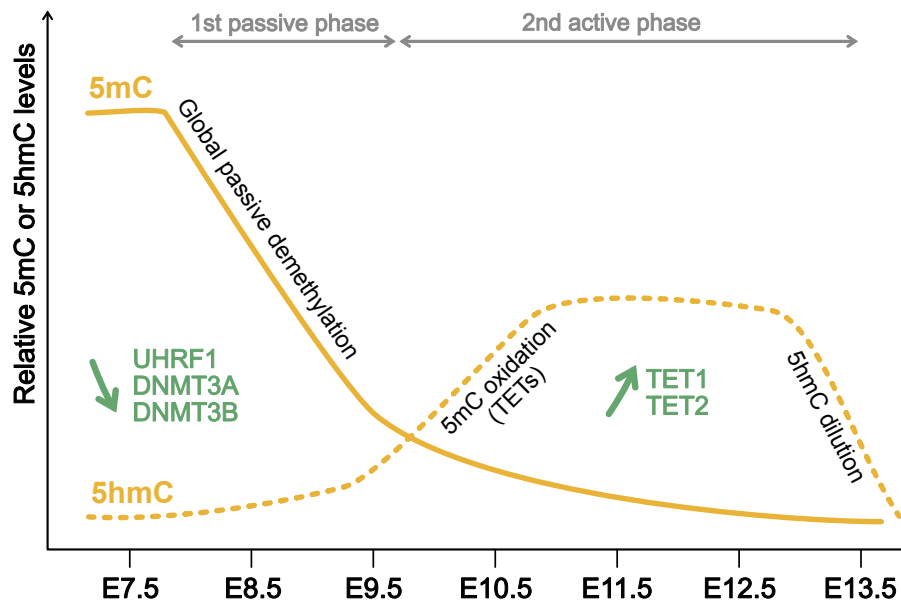


**Figure 19: DNA demethylation dynamics in primordial germ cells (PGCs).** PGCs undergo DNA demethylation in two phases: a first global and passive demethylation wave due to downregulation of DNA methylation machinery proteins (DNMT3A, DNMT3B and UHRF1) and intense cell proliferation. The second phase affects specific loci and correspond to active demethylation through TET1 and TET2-mediated 5mC oxidation into 5hmC. 5hmC is then passively diluted or removed by DNA repair mechanisms.

The second phase of demethylation occurs from E9.5 to E13.5 (**Figure 19**) and leads to demethylation of specific loci that were previously resistant to passive demethylation, including imprinted genes, CGIs of the inactive X chromosome and meiosis/germline-specific promoters (Seisenberger et al., 2012; Hackett et al., 2013; Yamaguchi et al., 2013). This second phase is an active phase that mainly depends on TET1- and TET2-mediated conversion of 5mC to 5hmC (Hackett et al., 2013; Vincent et al., 2013). 5hmC is then passively lost through cell division and progressively transformed back to unmethylated cytosines. TET-mediated active demethylation can thus be monitored by 5hmC level tracking (**Figure 19**): 5hmC level increases at E9.5 and stays globally constant until E13.5. Beyond its demethylase activity, TET1 is also thought to recruit the SET1 H3K4 methyltransferase, which will help initiating transcription of reprogramming-responsive genes (Hill et al., 2018). These reprogramming-responsive genes show progressive transcriptional activation as they become demethylated during the course of germline reprogramming. Even though TETs are only responsible for demethylating a minor portion of the genome, their function is essential. Loss of TET1 leads to hypermethylation and

lack of activation of germline reprogramming-responsive promoters and to germ cell developmental defects: female TET1-deficient PGCs cannot enter meiosis due to meiotic gene hypermethylation (Yamaguchi et al., 2012), while progeny from *Tet1*-mutated spermatozoa present aberrant imprinted gene methylation and associated developmental phenotypes (Yamaguchi et al., 2013). Only one genomic compartment escapes both passive and active DNA demethylation waves: IAPs are indeed still resistant to the second wave of active demethylation and will never show lower than 40% CpG methylation at E13.5 (Seisenberger et al., 2012).

## 1.2 - Remodeling of somatic histone modification patterns

Beside DNA demethylation, the histone landscape also changes during reprogramming of PGCs including alterations in histone modifications, histone exchange and nuclear architecture changes. Different scenarios may explain the extensive loss of histone modifications in PGCs: specific chromatin modifiers, such as histone demethylases, could remove histone tail modifications, or the existing histones could be replaced by new histones carrying different combinations of histone marks. It is difficult to assess whether these histone modification changes are causes, consequences or independent from DNA demethylation. This remains an open question as only few studies have described histone dynamics during epigenetic reprogramming, often through immunostaining without comprehensive genome-wide chromatin profiling.

The first sign of chromatin changes in PGCs is a rapid loss of the linker histone H1 (**Figure 20**), associated with a “loosening” of the chromatin and loss of detectable chromocenters (Hajkova et al., 2008). The nucleus is enlarged and chromatin decondensed, maybe to make the chromatin more permissive for DNA demethylation and histone exchanges. Starting around E8.0, a drop in H3K27me3 and H3K9me2/me3 levels is observed by immunofluorescence (**Figure 20**). This corresponds to the erasure of most H3K9me2 and H3K27me3 somatic patterns (Hajkova et al., 2008).

However, H3K27me3 remodeling seems to involve both erasure of epiblast-inherited domains and redistribution to other regions: while H3K27me3 peak number is greatly reduced from E10.5 to E13.5, some *de novo* H3K27me3 peaks are also simultaneously gained (Huang et al., 2021). Chromatin profiling in mouse PGCLCs showed indeed that H3K27me3 is recruited

at promoters of developmental genes and somatic lineage regulators, perhaps to reinforce their silencing in the germline (Kurimoto et al., 2015). This local H3K27me3 increase could indeed be a transient mechanism that helps protecting certain sequences from aberrant expression during the period of reduced DNA methylation and H3K9me2. A recent study highlighted the importance of this *de novo* H3K27me3 deposition in PGCs in the female germline (Huang et al., 2021). Compared to males, E13.5 female PGCs display more newly acquired peaks of H3K27me3, in particular at transposable elements and meiotic genes (Figure 20). Knockout of *Ezh2* was shown to lead to loss of H3K27me3 deposition and to female-specific widespread transcriptional derepression of both retrotransposons and reprogramming-responsive genes (that lost DNA methylation and became activated in absence of H3K27me3 *de novo* deposition). This transposable element reactivation was associated with DNA damage induction and apoptosis of female germ cells. H3K27me3 seems therefore to be both reprogrammed and *de novo* established at sensitive regions, at least in the female germline, to prevent aberrant transcription triggered by genome-wide hypomethylation. This is also consistent with the notion of DNA methylation–H3K27me3 antagonism and the observation in ES cells that H3K27me3 relocalizes to and silences retrotransposons upon rapid loss of DNA methylation (Walter et al., 2016).

In a similar manner, H3K9me3 is redistributed in PGCs. Its loss is more discrete as its levels remain constant at most constitutive heterochromatin regions, like at pericentromeric regions (Hajkova et al., 2008). At the same time, a process of H3K9me3 deposition can also be seen through *de novo* H3K9me3 peak formation. This gain is particularly important in male PGCs, where the number of peaks is multiplied by three around E13.5 compared to E10.5 PGCs (Figure 20) (Huang et al., 2021). H3K9me3 is highly enriched at transposable elements and seems to play a key role at these stages in protecting them against DNA demethylation: IAPs, the most well characterized DNA demethylation “escapees”, are indeed highly enriched in H3K9me3 at E13.5 (Liu et al., 2014). In *Setdb1* germline conditional mutants, H3K9me3 is drastically reduced in PGCs, in particular at retrotransposons. This H3K9me3 decrease is accompanied by concomitant DNA methylation loss at IAPs that normally escape DNA demethylation (Liu et al., 2014). These data suggests that the resistance to active DNA methylation of IAPs could be due to special retention of H3K9me3. SETD1B-deficient PGCs show derepression of many families of transposable elements, including IAPs, in a male-specific manner (Liu et al., 2014). This is associated with a reduced number of PGCs and

postnatal hypogonadism in the male, suggesting that the male germline rather uses H3K9me3 redistribution to restrain transposable element expression. This divergence in the repressive systems used for transposable element repression between male and female germlines (through H3K9me3 and H3K27me3, respectively) would be particularly interesting to further study.

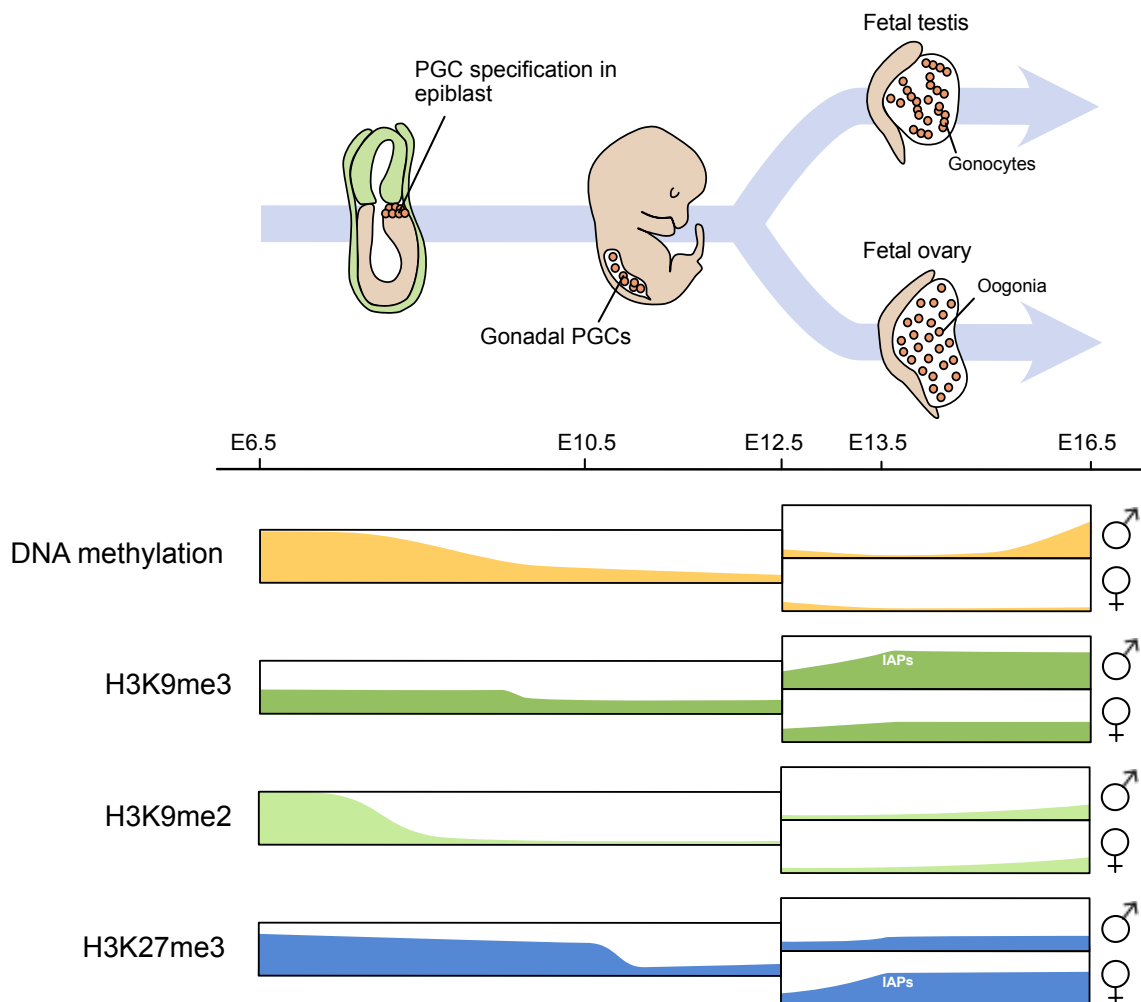


**Figure 20 : Epigenome reprogramming in mouse germline development.** The E6.5-E12.5 developmental window describes PGC development, E13.5-E16.5 describes male gonocytes and female oogonia, respectively. DNA methylation and histone mark dynamics are represented.

### 1.3 – Prolonged phase of female hypomethylation until puberty:

While the male genome is remethylated soon in pre-natal life, the female genome remains unmethylated until puberty. Indeed, following epigenetic reprogramming in PGCs, oogonia directly enter meiosis prophase around E13.5 and reach the diplotene stage of oogenesis while being hypomethylated. Meiosis-arrested oocytes will then enclose in primordial follicles and stay in a quiescent state until puberty, when they will be recruited for maturation. It is

only at this stage, during the growing phase of oogenesis, that oocyte-specific epigenetic patterns will be established: the genome will be remethylated and the peculiar histone mark landscape of oocytes will be shaped.

This delayed re-establishment of oocyte chromatin patterns, in particular of DNA methylation, raises a lot of questions. How is aberrant transcription prevented in hypomethylated conditions? How can the oocyte reach the diplotene stage of prophase of meiosis I in absence of DNA methylation? In the male germline, DNA re-methylation occurs before meiosis. Analysis of spermatogenesis in *Dnmt3A*, *Dnmt3C* and *Dnmt3L* mutants showed that meiosis can also be completed in genome-wide hypomethylated conditions, provided that it does not affect promoters of transposable elements (Dura et al., 2022). The specific loss of DNA methylation from promoters of young transposable elements leads to their reactivation, to pachytene arrest and subsequent sterility (Barau et al., 2016). This raises the question of transposable element regulation in the female germline during meiosis and in primordial follicles. Little information is currently available on the chromatin mark dynamics and transcriptional control during this developmental window.

## 2 – Acquisition of oocyte-specific chromatin patterns with maternal heritable properties

During the growing phase of oogenesis, a distinct transcriptome and epigenome are acquired. Non-canonical patterns of histone modifications and DNA methylation are established progressively as oogenesis proceeds (**Figure 21**). At the final stages, the oocyte undergoes major chromatin organization remodeling and transitions from an open chromatin conformation in non-surrounded nucleoli (NSN) to a tightly condensed and transcriptionally-silenced surrounded nucleoli (SN) stage. The genome will remain silent during fertilization and until zygotic genome activation (ZGA) in two-cell stage embryos: RNAPII is indeed absent from chromatin in MII oocytes and is re-loaded in the zygote at accessible regions and gene targets of ZGA (Liu et al., 2020). The oocyte-specific patterns of epigenetic marks will be transmitted upon fertilization to the progeny. They will be transiently maintained during the first days of embryonic development, before being erased or remodeled to canonical somatic patterns during preimplantation development (**Figure 21**). Some maternally-inherited domains will

escape this genome-wide wave of epigenetic reprogramming, they are called imprinted regions.

The oocyte-specific epigenetic patterns could therefore play different roles in the oocyte and upon transmission to the preimplantation embryo (**Figure 21**). First, they could regulate transcriptional activity in the oocyte itself and ensure complete transcriptional shutdown at the SN stage. Oocyte-specific patterns are still broadly maintained at the two-cell stage and could also control zygotic genome activation. Finally, life-long inheritance of maternal DNA methylation marks at imprinted regions enables mono-allelic expression of genes at later stages of development.

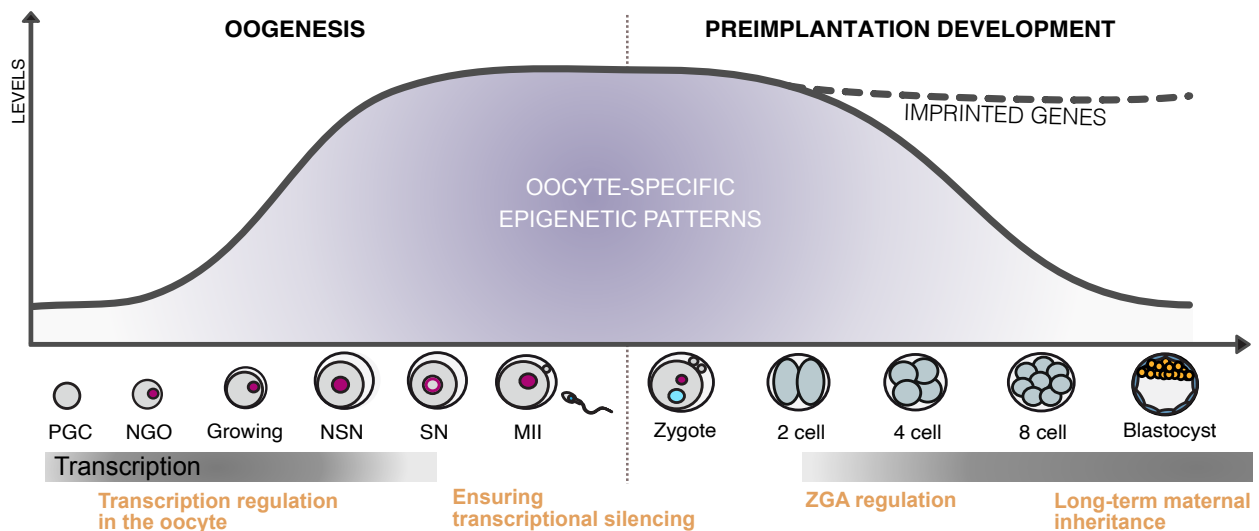


**Figure 21: Oocyte-specific epigenetic patterns dynamics and functions.** Oocyte-specific epigenetic marks are acquired during the growing phase of oogenesis and transmitted upon fertilization to the embryo, before being erased or remodeled during preimplantation development. Only imprinted genes keep their maternally-inherited patterns. Potential roles of these oocyte-specific chromatin marks in transcriptional regulation are listed.

## 2.1 – Maternal DNA methylation establishment and function

The oocyte is a terminally differentiated cell that acquires a unique DNA methylation pattern, distinct from sperm or somatic cells. Acquisition of DNA methylation in the oocyte happens gradually through its growth and development. Non-growing oocytes enclosed in primordial follicles before folliculogenesis are almost completely devoid of DNA methylation. Methylation is acquired during later stages of follicle development as the oocyte increases in size (Veselovska et al., 2015).

While somatic and sperm DNA methylation are evenly dispersed and respectively covering around 80% and 90% of the genome, mature oocytes are globally hypomethylated with only 40% global DNA methylation (Kobayashi et al., 2012). This difference in global methylation levels is linked to the peculiar bimodal and clustered methylation distribution in the oocyte (Figure 23). Unlike somatic cells where most CpGs are methylated, the oocyte methylome is comprised of large genomic domains that are either hyper- (>75%) or hypo- (<25%) methylated (Kobayashi et al., 2012). This bimodal pattern is conserved in all mammalian oocytes so far studied (Brind'Amour et al., 2018; Okae et al., 2014).

The oocyte also has relatively high levels of non-CpG methylation, mainly in the CpA context (Shirane et al., 2013). This is consistent with the previous observation of increased non-CpG methylation in cells with prolonged non-replicative phase and *de novo* DNMT expression. CpA and CpG methylation show positive correlation and are established with similar dynamics (Shirane et al., 2013). The significance of CpA methylation is unclear but a recent hypothesis of a potential role in gene expression regulation through transcription factor interaction has been proposed in human oocytes (Yu et al., 2019).

- DNMT3A-DNMT3L-dependent DNA methylation deposition

What initiates *de novo* methylation is not clear but it could be triggered by the availability of DNMT proteins coupled to a permissive underlying chromatin state. Expression of DNMT3A, DNMT3B and DNMT3L in growing oocytes is coordinated: their expression levels increase as the oocyte enters its growing phase, peaking around the GV stage when *de novo* methylation is complete, and decrease at the MII stage (Lucifero et al., 2007). They are all detectable in the nucleus of GV oocyte (Uysal et al., 2017) and DNMT3A was shown to be dependent on the transcription factor SALL4 to enable its nuclear localization (Xu et al., 2017). DNMT3A is the enzyme responsible for catalyzing DNA methylation but its interaction with its cofactor DNMT3L is essential for *de novo* DNA methylation in the oocyte (Smallwood et al., 2011; Kobayashi et al., 2012). Both *Dnmt3A* and *Dnmt3L* mutant oocytes fail to establish DNA methylation (Shirane et al., 2013), resulting in global lack of DNA methylation, including at maternal imprints, which has an effect in offspring (Bourc'his et al., 2001; Kaneda et al., 2004). DNMT3B, although expressed, seems not to be playing any role in the oocyte, as *Dnmt3B* mutant oocytes display unaffected DNA methylation patterns (Kaneda et al., 2010). The

reason of its presence in oocytes remains unanswered, it could potentially play a role as maternally-inherited protein before zygotic genome activation.

DNMT1 is expressed in an oocyte-specific isoform *Dnmt1o*, which is 118 amino acid shorter due to an alternative splicing of the 5' exon (Mertineit et al., 1998; Howell et al., 2001). DNMT1O accumulates in growing oocytes but mainly in the cytoplasmic compartment. In a similar manner, the DNMT1 cofactor UHRF1 is sequestered in the cytoplasm during oogenesis. Indeed, UHRF1 is known to interact with STELLA in oocytes and a STELLA-dependent nuclear export mechanism controls its subcellular localization outside of the nucleus (Li et al., 2018). Loss of STELLA leads to ectopic nuclear accumulation of both UHRF1 and DNMT1O and acquisition of excessive *de novo* DNA methylation in the oocyte (Li et al., 2018). Such aberrant hypermethylation is inherited by preimplantation embryos and impairs zygotic genome activation. DNMT1O and UHRF1 absence from the nucleus is therefore essential for proper acquisition of the oocyte methylome. This also highlights our lack of understanding of the roles of the DNMT1-UHRF1 complex in *de novo* methylation. Altogether, the relative hypomethylation and bimodal distribution of DNA methylation in the oocyte (40%) could be explained by the activity of the unique *de novo* DNMT3A and the mechanisms of its targeting to permissive chromatin contexts.

- DNA methylation patterns deposition through precise DNMT3 targeting to chromatin

Many studies have tried to understand how the oocyte-specific DNA methylation patterns are established and have shed light onto the mechanisms that allows precise DNMT3A-DNMT3L complex targeting to chromatin. It appeared quite early that the timing and specificity of DNA methylation deposition at specific genomic features was not linked to the underlying DNA sequence but rather to the local chromatin environment and histone post-transcriptional modifications (PTMs). Indeed, deletion of HIRA, a histone chaperone responsible for histone turnover in the oocytes, results in the loss of histone modifications and to genome-wide failure of *de novo* DNA methylation (Nashun et al., 2015). In a similar manner, precocious expression of DNMT3A and DNMT3L accelerates methylation deposition at only a small number of loci, suggesting that the others might be protected by a restrictive chromatin environment (Hara et al., 2014).

The most striking feature of DNA methylation distribution in oocytes is that it strongly correlates with actively transcribed units (**Figure 22**) (Smallwood et al., 2011; Kobayashi et al.,

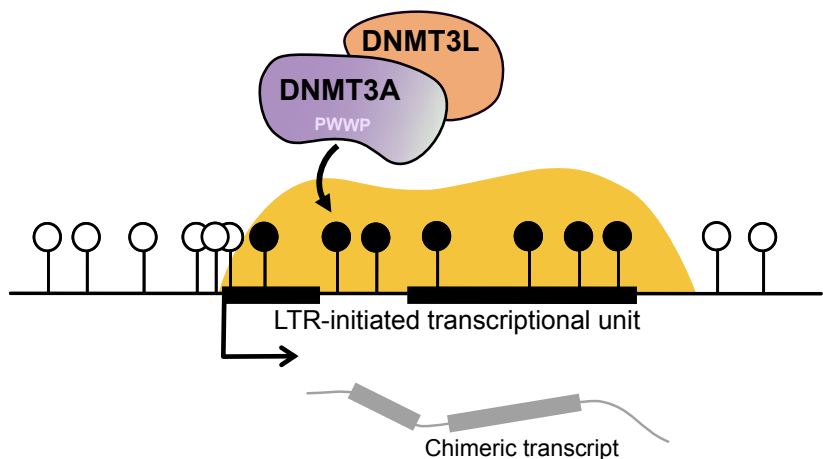
2012; Veselovska et al., 2015; Gahurova et al., 2017). *De novo* DNA methylation has indeed been shown to require active transcription. The generation of a mouse model in which transcription is abrogated across the *Zac1* locus showed that abolishing transcription at individual genes results in failure to establish DNA methylation at all CpG of the loci (Veselovska et al., 2015). This supports the notion that transcription is necessary for *de novo* methylation in the oocyte and associated imprint establishment.

The oocyte also presents a non-canonical transcriptome characterized by the intense expression of a subset of transposable elements of the LTR class, which often act as alternative promoters. This results in production of oocyte-specific transcripts characterized by the use of a LTR-associated upstream promoter: 15% of all oocyte transcripts initiate in an LTR in the mouse (Peaston et al., 2004; Veselovska et al., 2015). These LTR-initiated transcription units contribute to shape the oocyte methylome: DNA methylation is deposited along transcriptional elongation in 3' from oocyte-specific promoters, thus covering the canonical gene promoters and gene bodies (**Figure 22**) (Brind'Amour et al., 2018).

This DNA methylation feature is essential for acquiring maternal genomic imprinting, a process in which parent-of-origin allele-specific DNA methylation evades embryonic reprogramming and results in monoallelic expression in offspring tissues. All the maternal imprinted regions are thus conferred by methylation in the oocyte. Imprinted loci contain genes whose expression patterns are determined by the DNA methylation status of an imprinting control region (ICR). The ICRs have been shown to be methylated in a transcription-dependent manner: ICRs being located downstream from oocyte-specific promoters, disruption of transcription would therefore impair DNA methylation establishment at the ICR. This was for example demonstrated at the imprinted *Gnas* locus that depends on the oocyte-specific promoter from the *Nesp* gene to gain DNA methylation (Chotalia et al., 2009). In humans, chromosome rearrangements can result in transcription interruption across imprinted domains and to imprinted disorders due to lack of methylation at these loci (Valente et al., 2019).

The link between active transcription and DNMT3A-mediated DNA methylation deposition has been resolved by H3K36me3 intermediate function. High levels of transcription correlate with high enrichment in H3K36me3 and DNA hypermethylation in gene bodies (Stewart et al., 2015). H3K36me3 is known to be deposited co-transcriptionally by SETD2 and is indeed acquired during oocyte growth at actively transcribed gene bodies. H3K36me3 then recruits DNMT3A through its PWWP domain that has high affinity for methylated H3K36 nucleosomes (Figure 22) (see III. 5.2). While DNMT3A has been shown to have higher affinity for H3K36me2 than for H3K36me3 in somatic cells and prospermatogonia (Weinberg et al., 2019; Shirane et al., 2020), DNMT3A recruitment in oocytes follows rather H3K36me3 and not H3K36me2 patterns. How this differential recruitment of DNMT3A is achieved remains unknown. Oocyte-specific ablation of SETD2 results in loss of H3K36me3 enrichment and in *de novo* DNA methylation failure (Xu et al., 2019). This demonstrates that H3K36me3 co-transcriptional deposition is responsible for DNMT3A recruitment in oocytes and sets H3K36me3 as master regulator of the oocyte methylome.

**Figure 22: Transcription-dependent *de novo* DNA methylation in the oocyte.** LTR-initiated transcriptional units are marked by H3K36me3. The DNMT3A-DNMT3L complex is recruited at actively transcribed regions through PWWP domain binding to H3K36me3.



Most sequence elements acquire DNA methylation with similar dynamics through H3K36me3-mediated recruitment. However, some loci acquire methylation late in oocyte growth; they correspond to CG-rich regions and include imprinted regions. CGI methylation timing negatively correlates with their enrichment in H3K4me3 (Stewart et al., 2015; Gahurova et al., 2017), suggesting that removal of H3K4me3 is required for DNMT3A-DNMT3L activity. This is in agreement with the known ADD domain-mediated DNMT3 repulsion from H3K4 methylated nucleosomes (see III. 5.1). Supporting the idea that H3K4me2/me3 must be removed from CGIs prior to *de novo* methylation, two H3K4 demethylases, KDM1A and KDM1B, are expressed throughout oocyte growth and actively demethylate H3K4 at these

stages (Ciccone et al., 2009; Ancelin et al., 2016). Oocytes deficient in KDM1B, and to a lower extent in KDM1A, display focal hypomethylation at late methylating CGIs, including over most imprinted genes (Ciccone et al., 2009; Ancelin et al., 2016).

Altogether, CGIs destined for DNA methylation show loss of protective H3K4me3, while permissive H3K36me3 increases along with transcriptional elongation at these CGIs in growing oocytes.

- The functional role of DNA methylation in the oocyte

DNA methylation appears to be dispensable for oocyte development and competence, as ablation of oocyte methylation through *Dnmt3A* or *Dnmt3L* knockout does not impair fertilization and embryonic development until mid-gestation stage (Bourc'his et al., 2001; Kaneda et al., 2004). Methylation seems indeed to have little influence on gene expression control in the oocyte itself: faithful transcription program is initiated in primary oocytes before DNA methylation is acquired and RNA-seq analysis of *Dnmt3L*-KO oocytes show minor transcriptional changes compared to WT oocytes (Kobayashi et al., 2012). Whether the oocyte transcriptome resilience in front of genome-wide DNA methylation loss is due to secondary chromatin compensation, to the absence of available transcription factors or to DNA methylation peculiar intragenic localization remains an open question that I have tried to further investigate during my PhD.

- Maternal DNA methylation inheritance:

Although maternal DNA methylation is not required for development and maturation of the oocyte and fertilization *per se*, it is instrumental for embryonic development. Oocyte-specific DNA methylation patterns are indeed inherited by the embryo and were shown to play a key role in regulating the embryonic program.

The paternal and maternal genomes are differentially marked by DNA methylation: the paternal genome is heavily methylated (80% CpG methylation) but extensively remodeled through active DNA demethylation in the first hours following fertilization (Oswald et al., 2000; Wang et al., 2014). The maternal pronucleus is moderately methylated (40% of CpG methylation), primarily in intragenic regions, and largely resists the initial wave of active demethylation. At the two-cell stage, maternally-inherited DNA methylation patterns are indeed still well identifiable. They will then progressively disappear from the zygotic to the blastocyst stage (**Figure 23**) (Smith et al., 2012). The maternal genome passively loses

methylation during the successive cell divisions of preimplantation development through replication-dependent dilution of DNA methylation in the absence of DNMT1. DNMT1O, transmitted from the oocyte, is the predominant isoform of DNMT1 in preimplantation embryos. It is sequestered outside of the nucleus (Cardoso & Leonhardt, 1999) and is therefore not able to play its role of maintenance methyltransferase. However, the N-terminal truncation of DNMT1O does not fully explain its cytoplasmic localization in the embryo, as ectopically expressed DNMT1O localizes to the nucleus in somatic cells (Cardoso & Leonhardt, 1999). The mechanism behind DNMT1O localization in embryos remains to be determined. At the blastocyst stage, the embryonic genome is hypomethylated (with less than 20% remaining DNA methylation) (Smith et al., 2012). Somatic patterns will be established after implantation from E4.5 and will be associated with cell lineage differentiation.

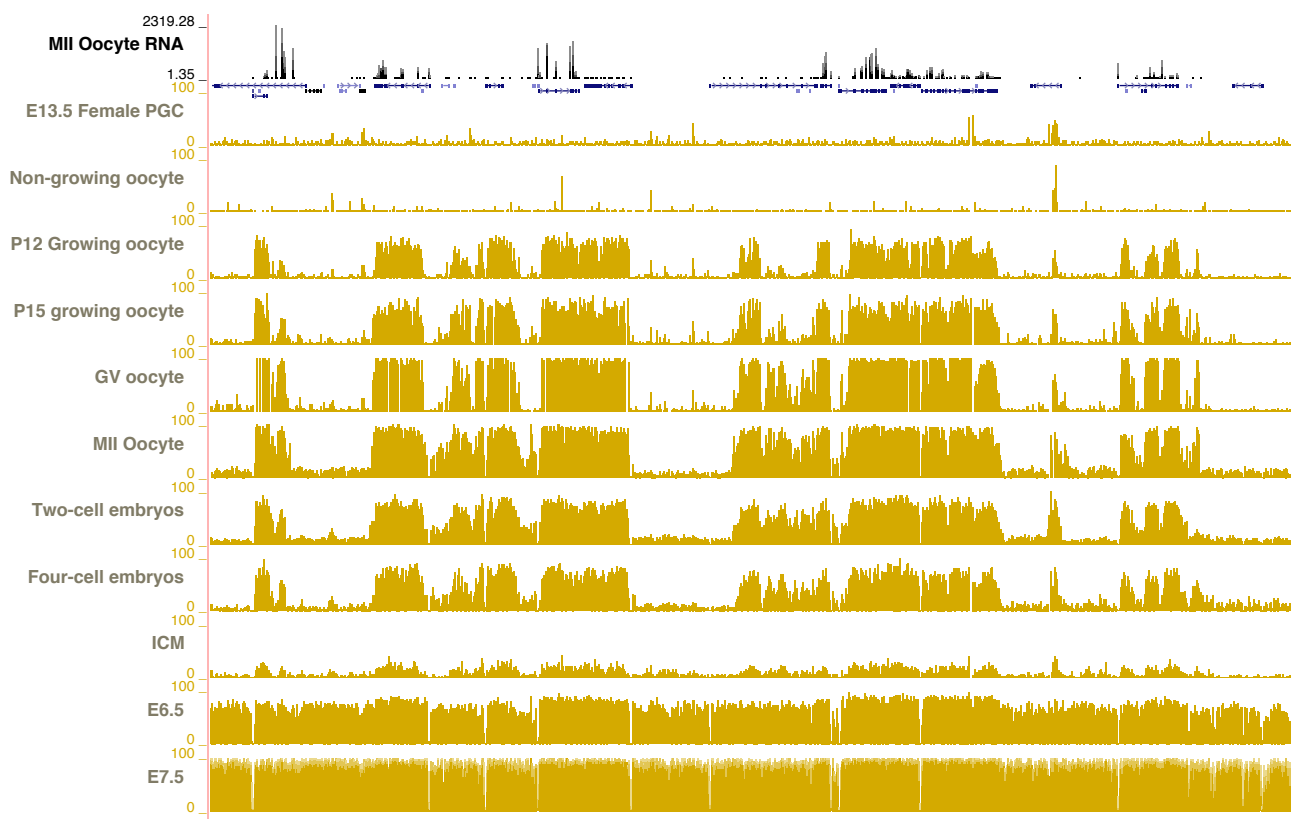


**Figure 23: Oocyte-specific DNA methylation establishment and inheritance in preimplantation embryos.** UCSC genome browser view of DNA methylation and transcription in oocytes and preimplantation embryos. Maternal DNA methylation domains are acquired during the growing phase of oogenesis at actively transcribed gene bodies. They are transmitted to preimplantation embryos and progressively erased until the blastocyst stage. Somatic patterns are established after implantation. Data from Dahl et al., 2016 and Wang et al., 2014.

Few genomic regions escape the genome-wide wave of maternal DNA demethylation during preimplantation development: only methylated CpGs at imprinted loci and IAP

elements are spared. The ICRs are protected from DNA demethylation through specific binding of the ZFP proteins (ZFP57 and ZFP445) and KAP1 complex (Li et al., 2008; Takahashi et al., 2019). ZFP57 is a Kruppel-like zinc finger protein that binds to a consensus hexanucleotide (TGCCGC) present in ICRs, but only when the internal CpG site is methylated (Li et al., 2008; Quenneville et al., 2011). The scaffold protein KAP1 then recruits heterochromatin-inducing complexes and the DNA methylation machinery, DNMT1 and UHRF1, that will ensure maintenance of CpG methylation at ICRs (Messerschmidt et al., 2012). This targeted DNMT1 recruitment explains the resistance of ICRs to the genome-wide wave of DNA demethylation. Impairment of maternal DNA methylation establishment at ICR in oocytes (through *Dnmt3A* or *Dnmt3L* knockout) or failure in the maintenance of maternal ICR methylation in embryos (*Zfp57* or *Kap1* knockouts) both result in embryonic lethality (Bourc'his et al., 2001; Li et al., 2008; Messerschmidt et al., 2012). In absence of DNMT3L, the whole oocyte genome is hypomethylated, including at ICRs. The maternal *Dnmt3L*<sup>KO</sup> embryos die around E9.5-E10.5 in association to misregulation of maternally imprinted genes and their downstream targets, which results in placental abnormalities (Bourc'his et al., 2001).

While only imprint-related maternal DNA methylation has been demonstrated to be essential for embryonic development, more recent evidence suggest that disruption of the oocyte methylome could lead to developmental defects unrelated to imprinted genes. Some oocyte differentially methylated regions (DMRs) show transient or tissue-specific inheritance post-fertilization, where they can play a role in developmental regulation (Branco et al., 2016; Sanchez-Delgado et al., 2016). The majority of those DMRs lose maternal methylation upon implantation but it is not well understood how they could affect preimplantation development. The biological significance of maternal DNA methylation on ZGA or other preimplantation processes also remains to be further studied.

## 2.2 – Oocyte-specific H3K4me3 non-canonical landscape and functions

Similar to DNA methylation patterns, histone modifications also display peculiar patterns in the oocyte epigenome. Recent development of low-input chromatin profiling has allowed defining their precise location and dynamics in oocytes. While H3K4me3 is enriched in canonical sharp peaks at promoters of actively transcribed genes at the early stages of oogenesis, it accumulates in broad non-canonical domains as oogenesis proceeds.

- Canonical promoter H3K4me3 enrichment in oocytes

Before the onset of the growing phase of oogenesis, in non-growing oocytes, H3K4me3 display canonical patterns similar to the ones present in somatic cells—narrow peaks centered on the promoters of actively transcribed genes (**Figure 24**)—(Stewart et al., 2015; Zhang et al., 2016) and clear positive correlation exist between the transcriptome and promoter H3K4me3. Recent studies suggested that SETD1B is the H3K4 methyltransferase responsible for the deposition of promoter-associated H3K4me3 peaks in early oocytes, in association with its CXXC1 cofactor, responsible for CGI targeting (Sha et al., 2020; Hanna et al., 2021). In contrast, SETD1A seems to have no role in oogenesis (Bledau et al., 2014). Both *Setd1b* and *Cxxc1* knockout oocytes display decreased H3K4me3 at promoter regions from pachytene to MII stage (Jiang et al., 2020; Hanna et al., 2021). The loss of SETD1B-mediated H3K4me3 is furthermore associated with impaired recombination during prophase I (Jiang et al., 2020).

Loss of promoter H3K4me3 has also been associated with decreased gene transcription, suggesting a role of SETD1B-deposited H3K4me3 in promoting transcriptional activity (Brici et al., 2017; Hanna et al., 2021). This is consistent with the known ability of H3K4me3 to recruit RNAPII. Importantly, H3K4me3-targeted gene promoters are enriched for oocyte transcriptional regulators, like *Obox1*, *Meis2* or *Sall4* that are upregulated during oogenesis (Brici et al., 2017). The oocyte-specific gene expression program consequently fails to be upregulated in *Gdf9*-CRE mediated *Setd1b* knockout, leading to follicular loss, zona pellucida impairment and developmental arrest at the zygote stage (Brici et al., 2017).

- Non-canonical broad H3K4me3 domains acquisition

As oogenesis proceeds, broad H3K4me3 domains appear in non-canonical patterns (ncH3K4me3) in addition to the pre-established promoter-associated H3K4me3 (**Figures 24, 26, 27**) (Dahl et al., 2016; Zhang et al., 2016). They are gradually established from post-natal day 12 during the growing phase of oogenesis and become widespread in fully-grown and MII oocytes, in which the genome transits to a silenced state. They end up covering 22% of the genome at the end of oogenesis and almost exclusively overlap with DNA hypomethylated domains (Dahl et al., 2016). Indeed, 60% of hypomethylated regions, which mainly correspond to intergenic and non-transcribed loci, are enriched in ncH3K4me3 (Zhang et al., 2016).

The broad ncH3K4me3 domains appear to be catalyzed by the MLL2 H3K4 methyltransferase in a transcription-independent manner (**Figure 24**). Oocyte-specific loss of

MLL2 results in a 80% decrease in H3K4me3 in mature oocytes, principally at untranscribed regions, while active promoter enrichment is unaffected (Hanna et al., 2018). Correspondingly, *MLL2*<sup>ckO</sup> fully-grown oocytes display a similar H3K4me3 pattern than WT non-growing oocytes.

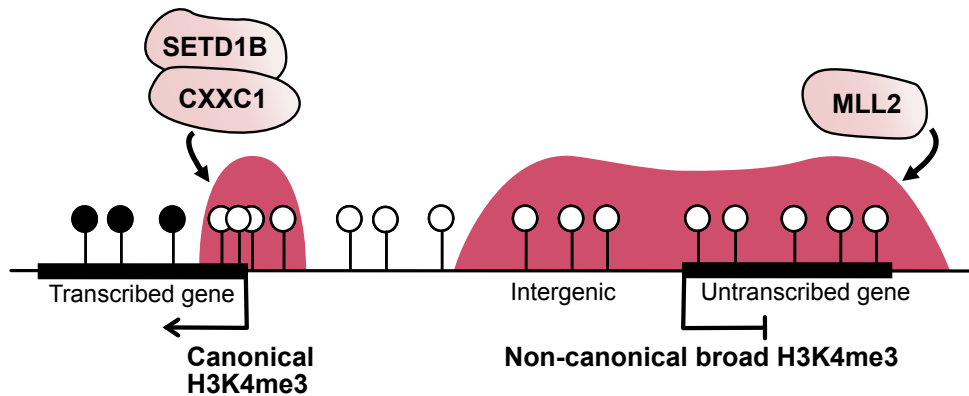


**Figure 24: H3K4me3 patterns in the oocyte epigenome.** Active promoter-associated H3K4me3 depend upon SETD1B/CXXC1 complex. Broad domains of ncH3K4me3 at intergenic and untranscribed region depend upon MLL2 s.

- Repressive function of broad ncH3K4me3 domains in the oocyte

While SETD1B-associated promoter H3K4me3 is linked to active transcription of key oogenesis regulators, the role of MLL2-deposited H3K4me3 is still not fully understood. Nevertheless, MLL2 was shown to be required for global transcriptional silencing at the surrounded nucleolus (SN) stage. *MLL2*<sup>ckO</sup> oocytes can transition to the SN chromatin configuration but fail to undergo complete transcriptional shutdown, as demonstrated by nascent RNA labelling through ethynyl-uridine incorporation (Andreu-Vieyra et al., 2010). Similarly, ablation of ncH3K4me3 in transcriptionally quiescent oocytes through overexpression of the KDM5B demethylase aberrantly reactivates transcription (Figure 25) (Zhang et al., 2016), including at IAP elements and apoptotic genes (Andreu-Vieyra et al., 2010). This aberrant transcription was associated with follicle loss and anovulation. The acquisition of H3K4me3 throughout much of the genome would thus facilitate transcriptional silencing. A theory proposes that acquisition of ‘promoter-like’ signatures, through H3K4me3 enrichment at distal regions, may allow sequestering transcription factors away from TSSs, facilitating oocyte transcriptional arrest (Hanna et al., 2018).

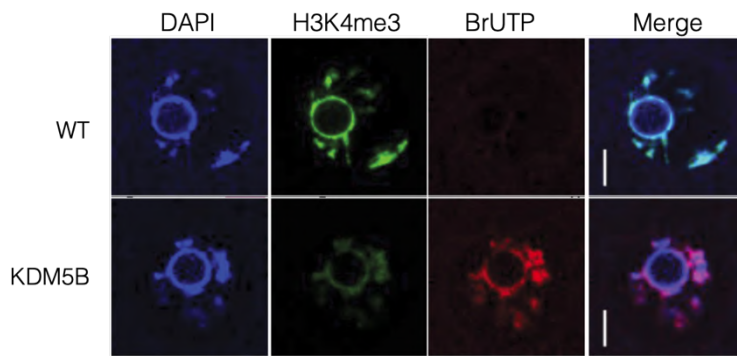


**Figure 25: Overexpression of the H3K4me3 demethylase KDM5B in SN oocytes results in reduced H3K4me3 and incomplete transcriptional silencing.** Extracted from Zhang et al., 2016. Immunostaining of H3K4me3 (green) and BrUTP (red) in SN oocytes. Overexpression of KDM5B by mRNA microinjection.

However, recent analyses reported that the global transcriptome is minimally disrupted upon loss of nH3K4me3. RNA-seq analyses reported that only 793 genes are differentially expressed between *Mll2*<sup>ckO</sup> and WT GV oocytes, while 5,893 genes showed a loss of H3K4me3 peaks (Hanna et al., 2018). As nH3K4me3 is present at non-transcribed genes in WT conditions, it is possible that these genes cannot be overexpressed, even in absence of nH3K4me3, due to absence of their transcription factors in the oocyte. Surprisingly, both up- and down-regulated genes (respectively 344 and 449 genes) in *Mll2*<sup>ckO</sup> were associated with a loss of nH3K4me3 at promoters, calling into question the idea of a direct effect of H3K4me3 depletion. Transposable element expression was not analyzed in this study and could potentially be, rather than genes, targets of nH3K4me3 repression, causing the aberrant nascent-RNA production seen by ethynyl-uridine in *Mll2*<sup>ckO</sup> oocytes at the SN stage.

- Maternal nH3K4me3 inheritance

Genome-wide mapping of H3K4me3 in mouse gametes and preimplantation embryos has revealed that maternal H3K4me3 domains are transiently transmitted upon fertilization to the preimplantation embryo. In late zygotes (PN5) and early 2-cell embryos, H3K4me3 distribution highly correlates with MII oocyte patterns (Liu et al., 2016; Zhang et al., 2016). While the paternal genome appears to be depleted of H3K4me3 in zygotes, the maternal genome exhibits broad non-canonical H3K4me3 domains that resemble the ones present in oocytes (Figure 26). An hypomorph *Mll2* mutant oocyte model also showed decreased H3K4me3 levels in female pronuclei (Andreu-Vieyra et al., 2010), reinforcing the idea of a maternal transmission of oocyte-acquired H3K4me3 domains in the preimplantation embryo.

However, oocyte H3K4me3 patterns seem to be rapidly reprogrammed: distal ncH3K4me3 is significantly reduced in late two-cell stage embryos, and fully erased by the four-cell stage (Liu et al., 2016; Zhang et al., 2016). In parallel, H3K4me3 starts to adopt a canonical form from the two-cell stage onwards (Figure 26). Accordingly, the transcription of *Kdm5b* and *Kdm5a* H3K4 demethylases peaks in 2-cell embryos, and embryos depleted for both demethylases retain high levels of H3K4me3 at the late 2-cell stage (Zhang et al., 2016), indicating that KDM5A and KDM5B are responsible for actively removing broad H3K4me3 domains (Figure 27).

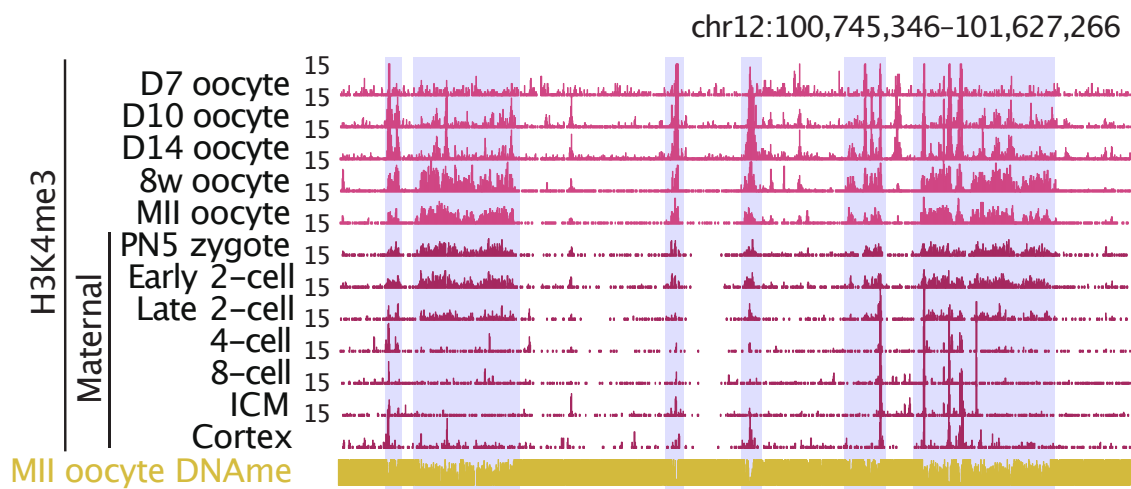


**Figure 26: Oocyte-specific ncH3K4me3 domain establishment and inheritance in preimplantation embryos.** UCSC genome browser view of H3K4me3 enrichment in oocytes and maternal alleles of preimplantation embryos. Maternal ncH3K4me3 domains are acquired during in growing oocytes and maintained until the late 2-cell stage in preimplantation embryos. Shaded scares highlight broad ncH3K4me3 domains. Adapted from Zhang et al., 2016.

As the transition from oocyte ncH3K4me3 to zygotic canonical H3K4me3 patterns happens around the time of zygotic genome activation (ZGA), recent studies also investigated the link between ZGA and H3K4me3 reprogramming. Blockage of ZGA (through transcription inhibition by alpha-amanitin treatment in 2-cell stage embryos) prevents switching from ncH3K4me3 to zygotic H3K4me3 (Zhang et al., 2016), therefore suggesting that H3K4me3 reprogramming requires zygotic transcription.

Conversely, H3K4me3 reprogramming also seems to play a role in ZGA. First, 86% of ZGA genes are found within maternal ncH3K4me3 domains (Dahl et al., 2016). These genes maintain H3K4me3 at their promoter during ZGA, while gaining activating H3K27ac (Dahl et al., 2016). Moreover, the loss of ncH3K4me3 in the *Mll2* hypomorph model was associated with decreased ZGA (Andreu-Vieyra et al., 2010), supporting the influence of ncH3K4me3

domains on ZGA. Deletion of KDM5A and KDM5B, which are responsible for H3K4me3 remodeling from broad to canonical patterns, was also associated with ZGA gene down-regulation (Zhang et al., 2016). Both transmission of maternal broad nH3K4me3 domains and its proper remodeling at the time of ZGA are therefore essential for the control of ZGA gene expression.

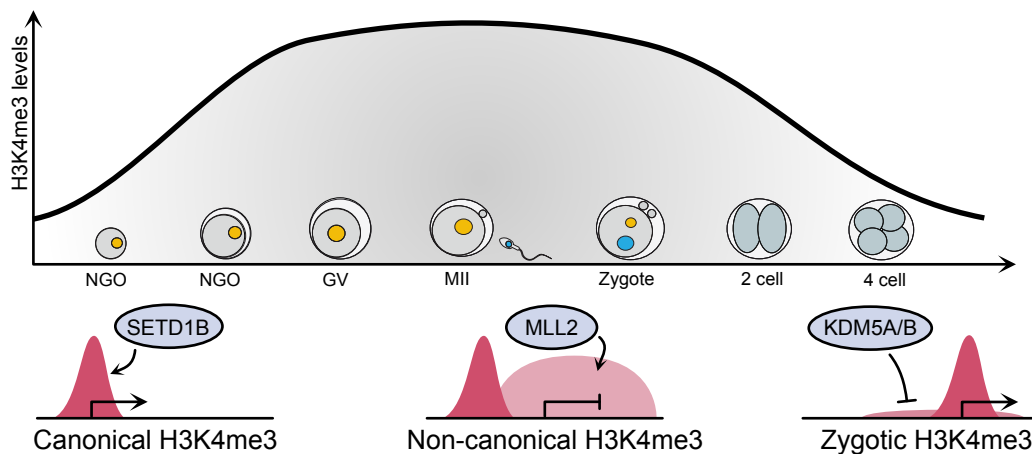


**Figure 27: Dynamic changes of H3K4me3 levels during oocyte-to-embryo transition.** In growing oocytes, H3K4me3 is present in canonical patterns of narrow peaks at active promoters. Deposition of non-canonical broad H3K4me3 domains by MLL2 coincides with genome-wide transcriptional shutdown in mature oocytes and early embryos. Maternal H3K4me3 patterns are transiently transmitted to preimplantation embryos before being remodeled to canonical patterns by KDM5A/B demethylases at the time of ZGA.

### 2.3 - Polycomb marks in maternal epigenetic inheritance

In the last years, the role of Polycomb marks in the oocyte-to-embryo transition has become an intense area of research. Although oocyte-specific H3K27me3 patterns were described some years ago, it is only recently that they were revealed as key players of maternal epigenetic inheritance, acting as fundamental cornerstones of the 3D genome organization in oocytes and embryos and mediating DNA methylation-independent gene imprinting. Additionally, the biological significance and relationships between H2Aub and H3K27me3 during this key phase of development are only starting to be unveiled.

#### - Broad H3K27me3 domains in the oocyte epigenome:

The H3K27me3 mark is typically placed at promoters of developmental genes by PRC2. In contrast, mouse oocytes show relative low to no enrichment in H3K27me3 at classical Polycomb targets, on the promoters of developmental genes (Zheng et al., 2016). However,

large H3K27me3 domains are established in intergenic regions, gene deserts and non-transcribed regions, therefore forming broad nH3K27me3 patterns (**Figure 28**) (Zheng et al., 2016; Lu et al., 2021).

In non-growing oocytes, promoter H3K27me3 at developmental genes is very weak (Zheng et al., 2016). In the early stages of oocyte growth, H3K27me3 is seen at low levels in most regions without transcription, covering up to 94% of the genome (**Figure 28**), and being interrupted by H3K27me3-free actively transcribed regions (Zheng et al., 2016). This indicates a widespread and promiscuous deposition of H3K27me3 prior to DNA methylation establishment. The determinants and timing of establishment of such broad and smeared H3K27me3 domains have not been described yet.

Towards the later stages of oogenesis, nH3K27me3 domains become gradually restricted to a portion of inactive regions (**Figure 28**) (Zheng et al., 2016). Distal nH3K27me3 overlap with hypomethylated regions that correspond to the untranscribed ones.

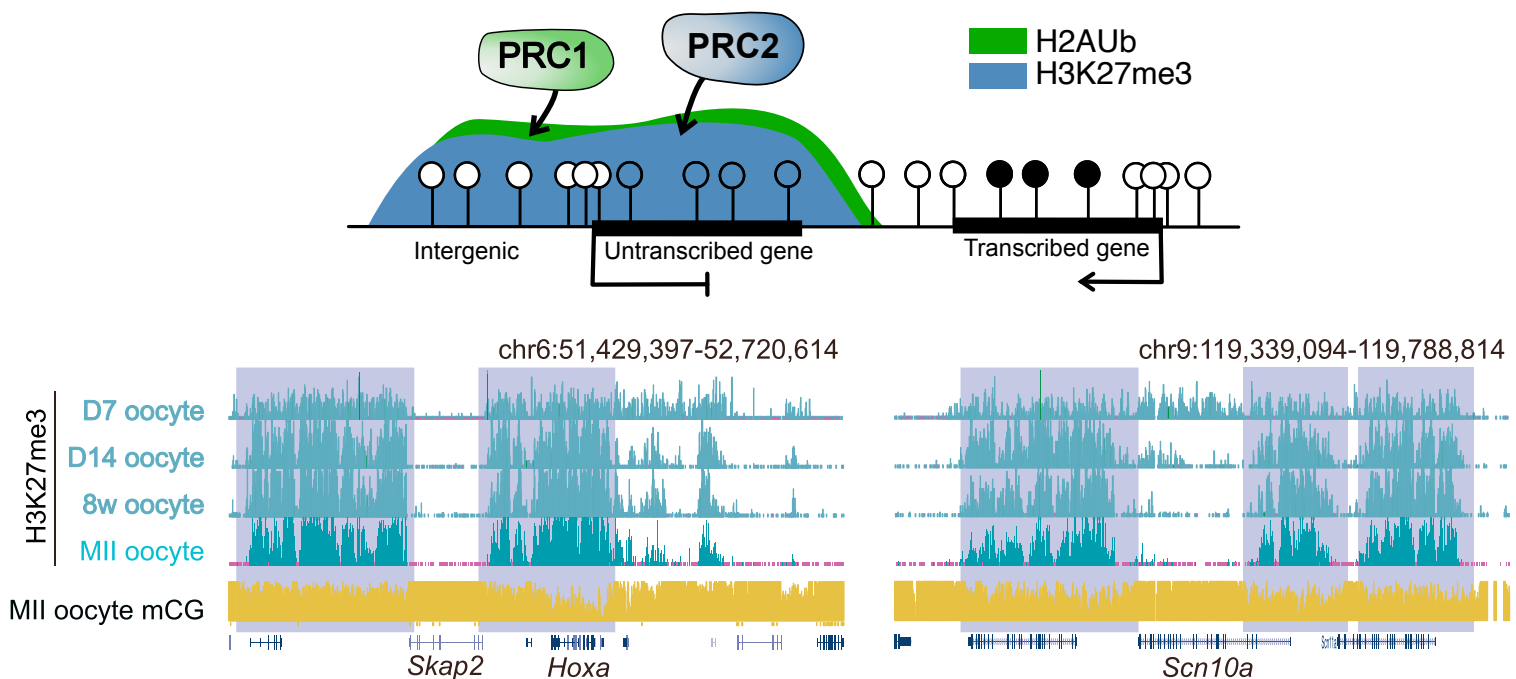


**Figure 28: Non-canonical patterns of Polycomb marks during oogenesis.** Upper panel. Scheme representing Polycomb patterns in mature oocytes. H3K27me3 and H2Aub are co-enriched in broad domains covering hypomethylated intergenic and untranscribed regions. Lower panel. UCSC genome browser view of H3K27me3 and DNA methylation enrichment in developing oocytes. H3K27me3 is restricted to hypomethylated transcriptionally-inactive regions. Shaded scares highlight broad nH3K27me3 domains. Adapted from Zheng et al., 2016.

- The actors of ncH3K27me3 domain establishment:

Oocyte-specific H3K27me3 is deposited by the PRC2 complex and likely involves the EZH1 rather than the EZH2 enzyme: retention of H3K27me3 is observed in the maternal pronuclei of embryos derived from *Zp3-CRE*-driven *Ezh2* knockout oocytes (Erhardt et al., 2003; Puschendorf et al., 2008). This is in agreement with EZH1 expression being linked to non-proliferative cell states, which characterize postnatal oogenesis. In contrast, *Gdf9*-CRE-specific deletion of *Eed*, an essential subunit of both EZH1- or EZH2-containing PRC2 complexes, results in undetectable levels of H3K27me3 by immunofluorescence in mature oocytes (Inoue et al., 2018), and almost complete loss of H3K27me3 patterning by CHIP-seq profiling in *Eed*<sup>CKO</sup> GV oocytes, although with little residual H3K27me3 (Du et al., 2020). It is possible that residual H3K27me3 is established prior to the expression of *Gdf9*-CRE (expressed from the beginning of the growing phase, around P3), in agreement with the observation of low H3K27me3 levels observed in non-growing oocytes.

The restriction of H3K27me3 to specific regions during oocyte growth could be mediated by the activity of the H3K27 demethylases KDM6A or KDM6B. In absence of the SALL4 transcription factor, both KDM6A and KDM6B are downregulated, which results in increased H3K27me3 levels in GV oocytes (Xu et al., 2017). This reinforces the idea of simultaneous H3K27me3 deposition by PRC2 and removal by KDM6A/B during the growing phase of oogenesis.

- H3K27me3 and H2Aub co-enrichment in the oocyte epigenome

Recent analysis of H2Aub distribution in oogenesis confirmed that ncH2Aub is co-established with ncH3K27me3 during oocyte growth (**Figure 28**) (Chen et al., 2021; Mei et al., 2021). H2Aub is shaped by the PRC1 complex in broad domains that overlap with ncH3K27me3 patterns at distal regions. In double mutant oocytes for *Ring1* and *Rnf2*, two PRC1 components, H2Aub patterns are lost (Mei et al., 2021).

Moreover, H2Aub depletion was associated with H3K27me3 decrease at genic regions and modest derepression of H2Aub/H3K27me3-enriched genes in GV oocytes, including both classical Polycomb targets and non-Polycomb targets (Mei et al., 2021). Conversely, PRC2 depletion and H3K27me3 loss minimally affect H2Aub domains. This suggests that H2Aub might be responsible for PRC2 recruitment or H3K27me3 domain maintenance in the oocyte

epigenome. A possible explanation for how H2Aub reduction would lead to H3K27me3 loss and associated derepression is that in absence of H2Aub, genes become transcriptionally derepressed and this in turn causes H3K27me3 loss. This scenario is consistent with the knowledge that H2Aub rather than H3K27me3 mediates silencing and the observation that H3K27me3 is excluded from actively transcribed regions during oocyte growth (Zheng et al., 2016).

However, no study has been properly investigating the role of Polycomb marks in ensuring transcriptional silencing at the SN stage and the existence of chromatin changes that could explain transcriptome resilience in front of genome-wide loss of H3K27me3.

- Maternal inheritance of H3K27me3:

Genome-wide mapping of H3K27me3 in mouse preimplantation embryos have revealed that maternal H3K27me3 is transiently transmitted upon fertilization to the progeny. Maternal H3K27me3 in distal regions is inherited by the zygote and persists until the blastocyst stage, where global H3K27me3 levels decrease (Figure 29) (Zheng et al., 2016). Distal H3K27me3 is no longer detected in E6.5 epiblast and more generally, in post-implantation embryos. This H3K27me3 reprogramming might be due to passive dilution caused by the rapid cell divisions during peri-implantation development or to unidentified action of chromatin modifiers.

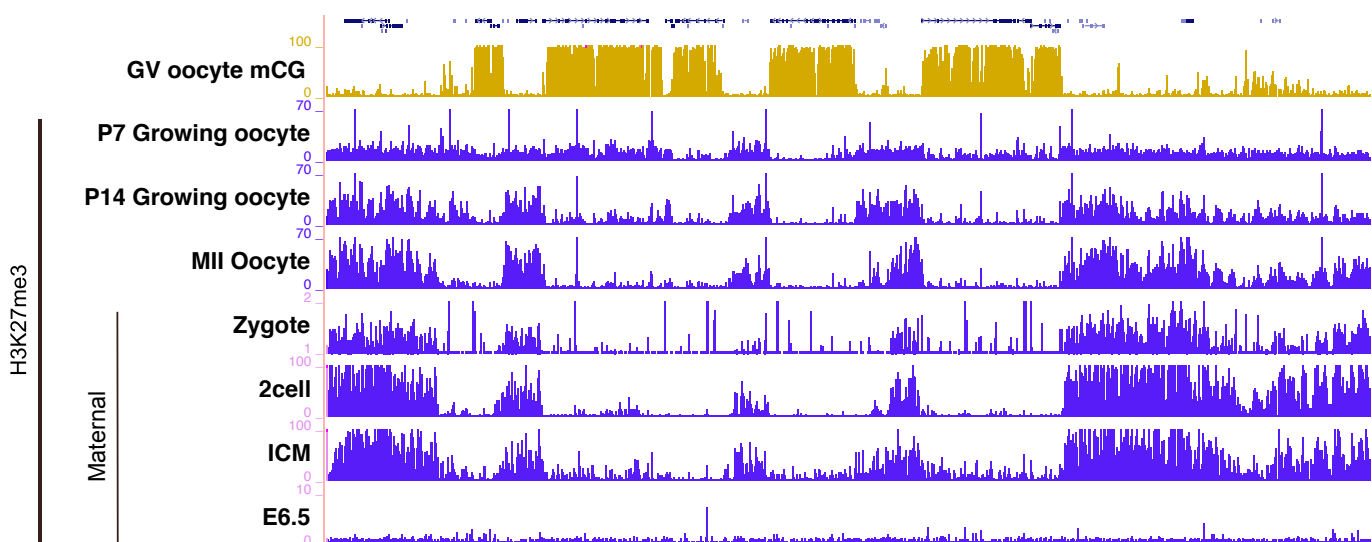


**Figure 29: Maternal H3K27me3 inheritance in preimplantation embryos.** UCSC genome browser view of H3K27me3 enrichment in oocytes and maternal alleles of preimplantation embryos. Maternally-inherited distal domains are kept until blastocyst stage, when promoter H3K27me3 starts to be re-established. Extracted from Zheng et al., 2016.

While the broad H3K27me3 domains are globally maintained during preimplantation development, maternal H3K27me3 is specifically removed from the promoters of developmental genes after fertilization. Around 36% of promoter H3K27me3 sites in MII oocytes show reduction in zygotes (Zheng et al., 2016). Decreased promoter H3K27me3 occurs prior to ZGA and persists until formation of the inner cell mass, where weak enrichment begins to emerge. The associated genes remain repressed in preimplantation embryos, suggesting either existence of additional repressive mechanisms or lack of necessary activators.

- H2Aub guides maternal H3K27me3 inheritance

Although genome-wide patterns of H3K27me3 in mouse embryos have been described some years ago, H2Aub maps have just been recently generated (Chen et al., 2021; Mei et al., 2021). They revealed a key role for H2Aub in guiding H3K27me3 dynamics and complex interplays between PRC1 and PRC2 during embryonic development. H2Aub and H3K27me3 were shown to be co-transmitted to zygotes: their distribution being highly correlated in both MII and zygotes. From the two-cell stage, H2Aub patterns, but not H3K27me3, start to be remodeled genome-wide (**Figure 30**) (Chen et al., 2021; Mei et al., 2021). In gene-poor distal regions, H2Aub enrichment is greatly decreased by the morula stage, as is H3K27me3 from the blastocyst stage, suggesting that loss of H2Aub precedes H3K27me3 loss (Mei et al., 2021). At the opposite, H2Aub is progressively enriched at promoters from the two-cell stage, which clearly precedes the emergence of promoter H3K27me3 at the blastocyst stage (**Figure 30**) (Mei et al., 2021). Some maternal domains keep their non-canonical enrichment in both H3K27me3 and H2Aub during the whole preimplantation development. Both loss and gain of H2Aub precede those of H3K27me3, indicating that H2Aub guides H3K27me3 dynamics during maternal-to-zygotic transition. This is consistent with previous findings that PRC1 can act upstream of PRC2 (Almeida et al., 2017). The precise molecular mechanisms behind this PRC1-PRC2 dynamic still remain to be studied.

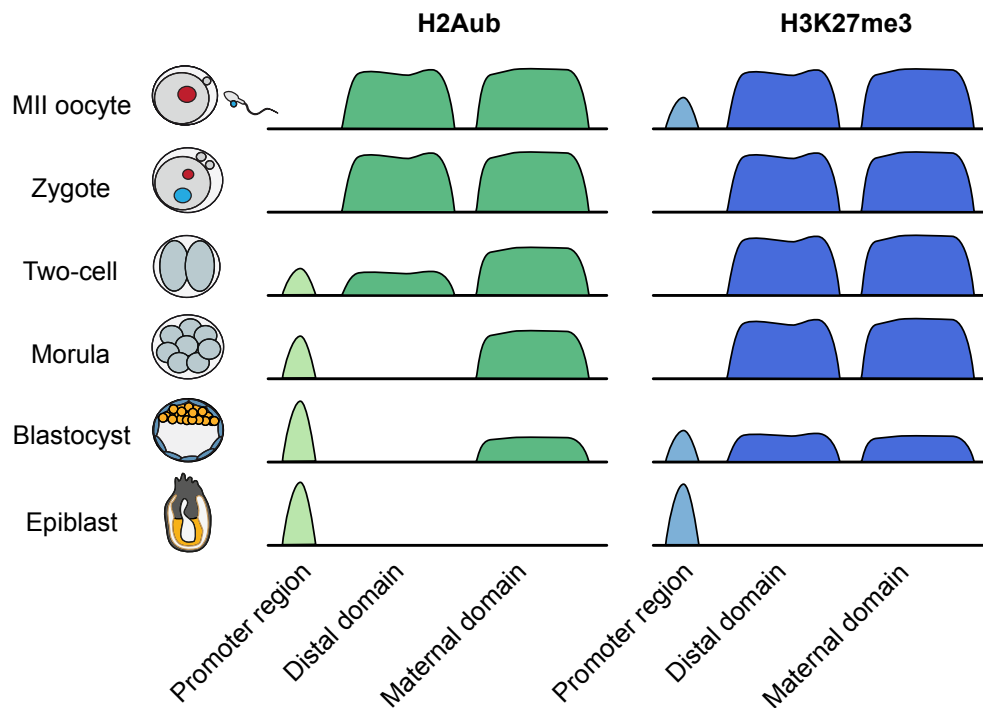


**Figure 30: Schematic of temporal dynamics of H2Aub and H3K27me3 upon maternal transmission.** Promoter regions carry zygotically established Polycomb domains at which deposition of H2Aub precedes H3K27me3. Distal domains correspond to gene-poor regions where H2Aub loss precedes H3K27me3 loss. Some non-canonical broad maternal domains keep both H3K27me3 and H2Aub during preimplantation development.

- Polycomb-mediated non-canonical imprinting

Recent studies showed that the presence of H3K27me3 on the maternal allele regulates allele-specific gene expression during preimplantation development. A substantial number of genes show paternal allele-specific expression independently of oocyte-derived DNA methylation on the maternal allele, suggesting the existence of a DNA methylation-independent imprinting mechanism. These non-canonical imprinted loci harbor high levels of oocyte-specific H3K27me3 (Inoue et al., 2017), whose loss results in imprinting disruption and biallelic expression: this was recapitulated both in *Gdf9*-CRE-driven *Eed* knockout or upon acute depletion of H3K27me3 through H3K27 demethylase KDM6B overexpression (Inoue et al., 2017; Inoue et al., 2018). Twenty-eight non-canonical paternally expressed imprinted genes—whose maternal alleles are repressed by H3K27me3—have been identified in morula embryos. However, this form of imprinting is transient, and no longer present in the epiblast lineages following H3K27me3 reprogramming in the ICM (Inoue et al., 2017). However, 5 of these genes maintain imprinted expression in the extra-embryonic ectoderm (ExE) at E6.5 and the placenta at E9.5. At implantation, a switch from allelic H3K27me3 to allelic DNA methylation enables long-term maintenance of non-canonical imprinting in extra-embryonic tissues (Chen et al., 2019). How oocyte H3K27me3 instructs allele-specific *de novo* DNA

methylation? It seems plausible that while paternally expressed alleles gain H3K4me3 at implantation, H3K4me3-free silent maternal alleles could gain DNA methylation in an allele-biased manner.

Although transient, H3K27me3-mediated imprinting was shown to play a major role in X chromosome inactivation (XCI) in female mice (Inoue et al., 2017). Indeed, one of the H3K27me3-imprinted genes is *Xist*, the lncRNA responsible for initiating XCI by coating the X chromosome and recruiting repressive chromatin modifiers. During preimplantation development, XCI is occurring in an imprinted manner: the paternal X chromosome is inactivated, while *Xist* is silenced on the maternal X chromosome through oocyte-inherited H3K27me3 (Inoue et al., 2017). At implantation, in the ICM, the paternal X chromosome is reactivated and H3K27me3 is lost from the maternal *Xist* allele. This precedes the establishment of paternal or maternal XCI in a random manner in the epiblast, while Imprinted XCI is maintained in the trophectoderm. Loss of oocyte-specific H3K27me3 in the *Eed*<sup>CKO</sup> model leads to loss of maternal H3K27me3 at the *Xist* locus, ectopic maternal *Xist* expression and aberrant XCI in both male and female embryos (Inoue et al., 2018). Aberrant maternal XCI leads to complete silencing of all X-linked genes in male embryos during preimplantation development, resulting in male-biased embryonic lethality at peri- or post-implantation. One reason explaining the female milder phenotype could be that dysregulation of X-linked is buffered by the presence of two X chromosomes.

Regarding H2Aub, maternally inherited patterns are globally lost at imprinted genes from the two-cell stage onwards, following the same dynamics than other distal regions (Chen et al., 2021; Mei et al., 2021). They persist at a few domains only, which may suggest a minor role of H2Aub in the maintenance of non-canonical imprinted patterns.

However, loss of oocyte-specific H2Aub through *Zp3*-CRE-driven *Pcgf1/6* double knockouts leads to partial loss of oocyte-specific H3K27me3 in oocytes, and after fertilization, partial loss of non-canonical imprinting in embryos, including at the *Xist* locus, which results in aberrant maternal XCI (Mei et al., 2021). Placental enlargement was also observed in maternal *Pcgf1/6* double knockout embryos, which could be due to loss of non-canonical imprinting in extra-embryonic tissues (Mei et al., 2021). However, acute H2Aub deletion in zygotes through overexpression of the Polycomb deubiquitinase (PR-DUB) does not affect H3K27me3-imprinted loci (Chen et al., 2021). It seems therefore that complex interplays between PRC1 and PRC2 take place at these imprinted loci: PRC1-mediated H2Aub would be

necessary in the oocyte for maternal Polycomb-dependent imprinting establishment, while H3K27me3 would be responsible for its maintenance during preimplantation development via the self-sustaining PRC2 activity. Interplays between H3K27me3 and H2Aub at imprinted genes still remain to be further explored.

- Maternal H2Aub function in ZGA:

Lack of maternal H3K27me3 through *Gdf9*-CRE-driven *Eed* knockout has a modest effect on the whole transcriptome of morula embryos. Moreover, these embryos develop at a similar developmental rate and reach blastocyst stage at comparable levels to embryos with maternal H3K27me3 (Inoue et al., 2018).

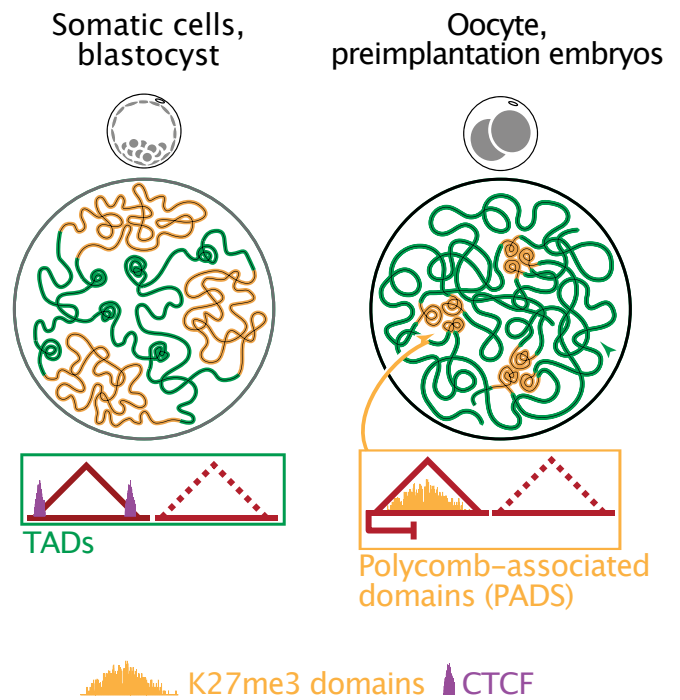
Maternal deficiency in *Ring1/Rnf2*, two components of the PRC1 complex, leads to developmental arrest at the two-cell stage, due to a crucial role of PRC1 proteins in this developmental window (Posfai et al., 2012). The H2Aub mark itself also matters: acute H2Aub depletion in zygotes causes developmental arrest at the four-cell stage, while molecularly, developmental genes are prematurely activated at zygotic genome activation (ZGA) (Chen et al., 2021). The derepressed genes are enriched for polycomb targets and gene ontology terms that do not belong to ZGA but to more advanced differentiation steps. In contrast, the same set of genes remain repressed upon H3K27me3 deletion, consistent with the fact that H3K27me3 is absent from gene promoters at this stage (Chen et al., 2021). Also, ZGA is globally unchanged in embryos derived from *Eed*<sup>CKO</sup> oocytes. These results indicate that H2Aub, but not H3K27me3, safeguards preimplantation development by preventing premature activation of developmental genes during ZGA.

- Polycomb-associated domains (PADs)

Polycomb marks are also associated with 3D organization of the genome in the oocyte (Collombet et al., 2020; Du et al., 2020). Linear DNA in the nucleus is packaged into highly organized chromatin fibers. In interphase, the genome is organized in large self-interacting domains, called topologically associating domains (TADs). These are flanked by convergent CTCF sites and are believed to confine promoter-enhancer interactions within a given domain. Interestingly, recent studies have demonstrated that the three-dimensional genome organization is modified during oogenesis. A transition from the conventional compartments to small CTCF-independent chromatin loops happens in growing oocytes. The self-interacting

oocyte-specific compartments strikingly match H3K27me3 regions in mature oocytes: they were therefore termed Polycomb-associated domains (PADs) (Du et al., 2020). PADs thus correspond to H3K27me3-enriched transcriptionally silent compartments, while the inter-PADs are devoid of H3K27me3 and are enriched in active genes (Figure 31). These PADs disassemble upon meiotic resumption but briefly reappear on the maternal genome from the two-cell stage and progressively disappear until the ICM stage (Du et al., 2020).

**Figure 31 : Model of the Polycomb-associated domains (PADs).** PADs correspond to self-interacting chromatin loops acquired during oocyte growth and reassembled during preimplantation development. They contrast with the usual 3D genome organization in TADs in somatic cells. Adapted from Collombet et al., 2020.



Upon maternal loss of H3K27me3 through *Gdf9*-CRE-driven *Eed* knockout, PADs are largely intact in oocytes but their re-installation after fertilization is compromised. Conversely, depletion of PRC1 proteins attenuates PADs in oocytes, which is associated with derepression of these genes found within PADs (Du et al., 2020). Whether the loss of H2Aub from the genes and/or the disruption of the PADs is responsible for this derepression still needs to be understood.

Whether PADs are functional for oocyte and embryo development is also still an open question: PADs could separate the oocyte genome in defined compartments to ensure proper gene repression. PADs disassembly was shown to correlate with the dynamic of XCI, suggesting that they could play critical roles in regulating allele-specific expression of genes (Collombet et al., 2020).

## 2.4 - H3K36me3 in maternal epigenome and embryonic development

Coherent with the known H3K36me3 distribution in somatic cells, H3K36me3 is also established during the growing phase of oogenesis at actively transcribed gene bodies (Xu et al., 2019). Its distribution perfectly correlates with gene expression in growing oocytes. For example, genes that become transcribed at P7 will subsequently acquire H3K36me3 by P14. Consistent with the non-replicative state of oocytes, pre-established H3K36me3 patterns globally persist in transcriptionally inert MII oocytes. H3K36me3 deposition is mediated by the SETD2 methyltransferase (Xu et al., 2019). Maternal SETD2 deficiency through *Gdf9*-CRE-driven *Setd2* knockout (*Setd2*<sup>CKO</sup>) results in loss of H3K36me3 and surprisingly also, in dramatic decrease in H3K36me2. SETD2 is not required only for deposition of H3K36me3, but also for deposition of the majority of H3K36me2 in oocytes (Shirane et al., 2020). H3K36me2 displays a more diffuse pattern than H3K36me3, covering both intragenic and intergenic regions.

Maternal H3K36me3 profiles are largely reset very early during preimplantation development: oocyte H3K36me3 patterning is globally inherited on maternal chromosomes in zygotes but is already much decreased by the late to-cell stage and completely erased at the eight-cell stage (Xu et al., 2019). For both parental chromosomes, *de novo* zygotic H3K36me3 starts to appear at the late two-cell stage, presumably due to ZGA transcription-dependent deposition.

As previously described, H3K36me3 recruits DNMT3A through its PWWP domain, leading to a strong correlation between DNA methylation and H3K36me3 in mature oocytes. By contrast, H3K4me3 and H3K27me3 reside in hypomethylated regions and anti-correlate with H3K36me3. In maternal SETD2 depletion, regions previously marked by H3K36me3 fail to acquire DNA methylation, while regions outside from former H3K36me3 domains gain ectopic DNA methylation (Xu et al., 2019). This highlights the key role of SETD2-mediated DNA methylation in directing proper DNA methylation establishment in the oocyte. In front of the loss of DNA methylation/H3K36me3-enriched domains in *Setd2*<sup>CKO</sup> oocytes, H3K27me3 and H3K4me3 patterns are remodeled and have been shown to invade these territories, leading to perturbed gene transcription (Lu et al., 2021; Xu et al., 2019). H3K36me3 appears therefore as one of the master regulator of the oocyte epigenome, by ensuring correct methylome establishment and in excluding H3K4me3 and H3K27me3 from transcribed regions.

This key role of H3K36me3 in the oocyte epigenome is also visible through the drastic phenotype of *Setd2*<sup>CKO</sup> oocytes. While transcriptional silencing at the SN stage is properly achieved, *Setd2*<sup>matKO</sup> embryos are arrested at the zygote stage. This developmental arrest is associated with faulty maternal transcript clearance, absence of ZGA and impaired DNA replication of the maternal pronuclei and impaired ZGA (Xu et al., 2019). Spindle transfer experiments have shown that this phenotype can be almost completely rescued in presence of WT cytoplasm, indicating a major role of the cytoplasm and a minor role of chromatin defects in the zygotic arrest of *Setd2*<sup>matKO</sup> embryos. Further development of embryos with WT cytoplasm and a maternal KO genome was analyzed: at E10.5, mutant embryos did not appear to have a placenta (Xu et al., 2019). This phenotype resembles, in a more severe form, the one observed in maternal *Dnmt3L*<sup>KO</sup> embryos, which lose maternal DNA methylation imprints but show placental structures, although apparently non-functional (Bourc'his et al., 2001; Proudhon et al., 2012). The observed phenotype would then probably be due to loss of DNA methylation imprints in absence of H3K36me3-mediated recruitment, while H3K27me3/H3K4me3 mislocalization could worsen the phenotype.

## 2.5 – H3K9 methylation dynamics in oocytes and embryos

The heterochromatin H3K9me3 mark is widely distributed throughout the oocyte genome: it is enriched at endogenous retroviral elements (ERVs), at gene bodies but is excluded from H3K4me3-marked active promoters. This globally follows the same distribution than in somatic cells. The dynamic of H3K9me3 during the growing phase of oogenesis has not been characterized, as H3K9me3 maps have been generated in MII oocytes only (Wang et al., 2018), so it is possible that no oocyte-specific remodeling of the mark is happening. Upon fertilization, most oocyte-inherited H3K9me3 is rapidly lost (Wang et al., 2018). The enzyme(s) responsible for H3K9me3 deposition in the oocyte are also not yet identified, so that no proper model of maternal H3K9me3 deficiency could be developed. SETDB1 seems to be methylating ERVs, given their transcriptional derepression in *Setdb1*-knockout oocytes (Eymerly et al., 2016). *Setdb1*<sup>matKO</sup> embryos stop preimplantation development due to defects in chromosome segregation, in both meiosis resumption and mitotic divisions. H3K9me3 seems to display canonical patterns in the oocyte epigenome and to play a role in transposable element repression.

However, it was shown that H3K9me3 is actively excluded from broad nH3K4me3-enriched regions in oocytes (Sankar et al., 2020). KDM4A, a H3K9 demethylase, was described to be recruited to nH3K4me3 via binding of its Tudor domains and its absence induces H3K9me3 spreading inside broad nH3K4me3 domains, without affecting H3K4me3 levels. This H3K9me3 spreading seems to be maintained in preimplantation embryos, as H3K9me3 levels are increased in the maternal pronuclei of *Kdm4a*<sup>matKO</sup> embryos. Many ZGA genes, which are particularly enriched within broad nH3K4me3 domains, fail to be activated at the two-cell stage (Sankar et al., 2020), likely due to local aberrant H3K9me3 enrichment. Coincidentally, *Kdm4a*<sup>matKO</sup> embryos do not proceed past the 4-6 cell stage. Together, this indicates that KDM4A and nH3K4me3 are responsible for H3K9me3 repulsion and for preventing heterochromatinization of ZGA genes.

Some studies also highlighted the role of the G9a enzyme, responsible for H3K9 dimethylation (H3K9me2), in oocyte and embryo development. Oocyte H3K9me2 patterns are similar to the ones present in somatic cells and correspond, broadly, to heterochromatin regions (Au Yeung et al., 2019). In *Zp3*-CRE-driven *G9a* knockout condition, H3K9me2 signal is decreased and oocytes display impaired chromatin reorganization, notably decreased ability to transition to the SN stage (Au Yeung et al., 2019). This indicates a potential role of H3K9me2 in chromatin compaction at this stage. Maternally-inherited G9a protein was also shown to drive accumulation of H3K9me2 at the four-cell stage (Zylicz et al., 2018). *G9a*<sup>matKO</sup> embryos showed derepression of some transcripts, resulting in developmental delays and some pre-implantation lethality (Zylicz et al., 2018), in parallel with impaired chromosome segregation and mitotic defects (Au Yeung et al., 2019).

### 3 - Interplays between chromatin marks in the oocyte epigenome

The mouse oocyte provides a unique model to investigate the interplay between chromatin-based mechanisms because of its prolonged non-replicative state, in which as previously described, distinctive transcriptome and epigenome are acquired. Because of the simultaneous acquisition of multiple chromatin marks with non-canonical patterns, the oocyte epigenome is shaped by interplays and context-specific recruitment of chromatin modifiers that are unique to this cell type.

#### 3.1 – Active histone marks regulate *de novo* DNA methylation in oocytes

##### - H3K36me3 is essential for DNA methylation patterns establishment

Genetic experiments of locus-specific transcription abrogation have demonstrated that transcription is essential for DNA methylation establishment in the oocyte (Veselovska et al., 2015). Since DNA methylation occurs developmentally after transcription initiation, it was likely that the DNMT3A-DNMT3L complex was not recruited to DNA by the RNAPII machinery itself but rather by a transcription-dependent intermediate. Recent molecular studies revealed that H3K36me3 instructs *de novo* DNA methylation in oocytes (Shirane et al., 2020; Xu et al., 2019). SETD2 catalyzes H3K36me3 deposition along transcriptional elongation, which recruits DNMT3A through its PWWP domain that has high affinity for H3K36me3 (see III. 5.2.). H3K36me3 thus perfectly correlates with DNA methylation domains. SETD2 also deposits intergenic H3K36me2, which is recognized with less affinity by DNMT3A in the oocytes (Shirane et al., 2020).

SETD2 deficiency through *Gdf9*-CRE-driven deletion impairs both H3K36me3, -me2 and DNA methylation deposition (**Table 1**) (Xu et al., 2019). Regions previously marked by H3K36me3 fail to acquire DNA methylation, while regions outside former H3K36me3 territories gain ectopic DNA methylation. This is the confirmation that SETD2 directs proper establishment of DNA methylation. In absence of H3K36me3-mediated targeted recruitment, DNMT3A would then methylate unspecific regions of the genome, including intergenic regions. Consistent with the logical sequence of H3K36me3-mediated DNA methylation recruitment, global H3K36me3 levels are globally unaffected in the absence of DNA methylation through *Dnmt3L* knockout (Xu et al., 2019).

- Promoter H3K4me3 dynamics dictates DNA methylation deposition

Promoter H3K4me3 regulates deposition of DNA methylation in the oocyte through two distinct phenomena. First, in non-growing oocytes, H3K4me3 is present in canonical peaks at CGI promoters of actively transcribed genes and loss of promoter H3K4me3 leads to decreased transcription of associated genes (**Figure 32**). This phenotype was recapitulated in oocytes depleted in either SETD1B, the enzyme responsible for promoter H3K4me3 deposition or CXXC1, its essential cofactor (Sha et al., 2020 ; Hanna et al., 2021). Analysis of both mutants showed that genes usually upregulated during oogenesis significantly fail to activate upon loss of H3K4me3 from their promoters in the mutants. This promoter H3K4me3 loss and transcriptional decrease was associated with impaired intragenic DNA methylation establishment (Sha et al., 2020 ; Hanna et al., 2021) (**Figure 32, Table 1**). Consistent with the known relationship between transcriptional elongation and DNA methylation establishment, a mechanism could explain this DNA methylation loss: the decreased transcription observed in absence of promoter H3K4me3 could lead to impaired H3K36me3 deposition and DNA methylation recruitment (Sha et al., 2020 ; Hanna et al., 2021). Analysis of *Cxxc1* knockout oocytes showed reduced DNA methylation is indeed accompanied by loss of H3K36me3 (Sha et al., 2020). However, the cause-effect relationships between these various changes are difficult to infer without more precise mechanistic studies.

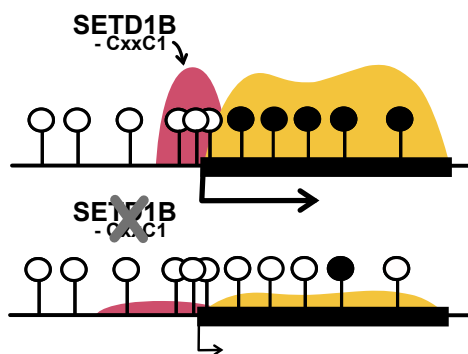


**Figure 32: SETD1B-CXXC1 H3K4 methyltransferase complex is necessary for proper H3K36me3 – DNA methylation domain establishment.** In absence of SETD1B/CXXC1, promoter H3K4me3 is lost and transcription is decreased. This leads to improper H3K36me3 domains establishment and impaired recruitment of DNA methylation machinery at actively transcribed units.

At the same time, CGI methylation timing negatively correlates with H3K4me3 enrichment (Stewart et al., 2015; Gahurova et al., 2017). Active removal of H3K4me3 at certain genomic locations during the growing phase is required for DNMT3A-DNMT3L methylation activity. This is in agreement with the known ADD domain-mediated DNMT3 repulsion from H3K4 methylated nucleosomes (see III. 5.1). Two H3K4 demethylases, KDM1A and KDM1B, are required to overcome the inhibitory effect of H3K4me3 on DNMTs (Stewart

et al., 2015; Gahurova et al., 2017). Oocyte deficient in KDM1B, and in a lower extend KDM1A, display focal hypomethylation at later-methylating CGIs, including over most maternally imprinted loci (Ciccione et al., 2009; Ancelin et al., 2016). The model would be that these KDMs target H3K4me3 erasure from somatic promoters that became intragenic, due to the use of alternative upstream promoters in the oocyte. How this targeting to intragenic H3K4me3-marked CGIs is achieved remains unknown: one possibility is that KDM1B is recruited to H3K36me3 via interaction with N-PAC, a protein also containing a H3K36me3-recognizing PWWP module. KDM1B and N-PAC have already been shown to act together to mediate H3K4 demethylation in cellular assays (Fang et al., 2010, 2013). This would be consistent with H3K36me3 levels increasing at intragenic regions around the time of H3K4me3 removal and DNA methylation acquisition.

### 3.2 – DNA methylation anti-correlates with ncH3K4me3 and H3K27me3

One of the most particular feature of the oocyte epigenome is that DNA methylation has a bimodal distribution. DNA methylation is clustered in broad hypermethylated domains that contrast with hypomethylated stretches. The hypermethylated domains correlate with actively transcribed, H3K36me3-enriched regions. Simultaneously during the growing phase of oogenesis, both ncH3K4me3 and H3K27me3 are acquired at hypomethylated regions. DNA methylation domains are therefore interrupted by broad H3K27me3 or ncH3K4me3 stretches (Figure 33) (Hanna et al., 2018; Zheng et al., 2016).

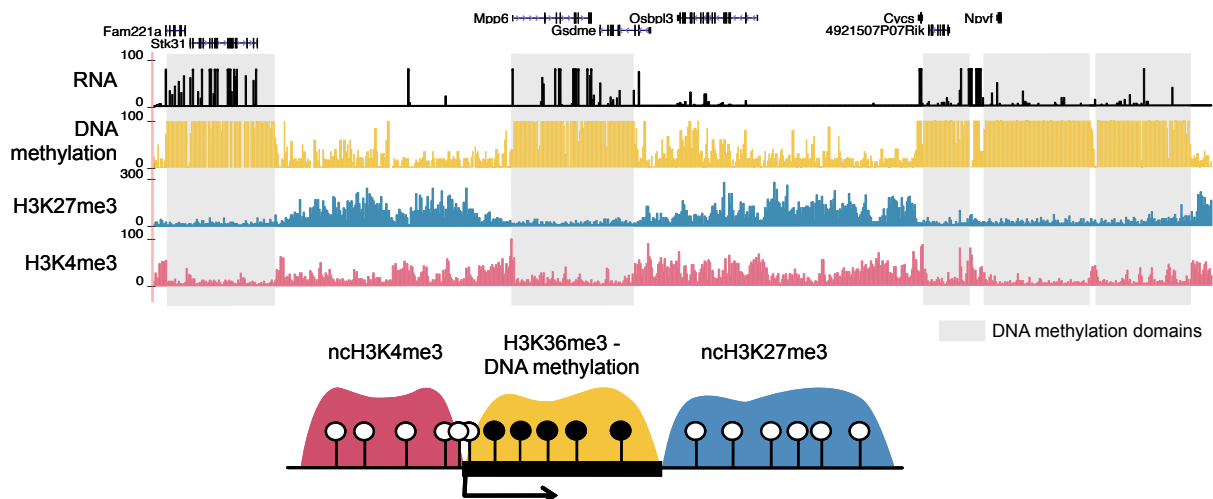


**Figure 33 : DNA methylation anti-correlates with ncH3K4me3 and ncH3K27me3.** UCSC genome browser screenshot and schematics of DNA methylation, H3K4me3 and H3K27me3 distribution in the epigenome of GV oocytes. Gene expression in MII oocytes is also displayed. DNA methylation domains are highlighted in gray.

- ncH3K4me3 and DNA methylation antagonism

The molecular mechanisms behind the antagonism between ncH3K4me3 and DNA methylation have not been formally dissected in the oocyte. However, by analogy with the known mechanisms in somatic cells, their mutual exclusivity could be explained by the repulsion at the molecular levels between H3K4me3 and the ADD domain of DNMT3A (see III. 1.4), through which H3K4me3 inhibits *de novo* DNA methylation (Ooi et al., 2007). Reciprocally, the MLL2 protein, responsible for ncH3K4me3 methylation in the oocyte, only binds unmethylated CpGs through its CxxC domain (Birke et al., 2002; Allen et al., 2006). The presence of DNA methylation would then protect regions from acquiring ncH3K4me3, so that MLL2 is specifically targeted to unmethylated CG-rich regions.

H3K4me3 and DNA methylation antagonism could be further dissected by the use of oocyte mutant models. Oocyte-specific conditional deletion of *Dnmt3A/B* results in accumulation of ncH3K4me3 in previously methylated gene bodies (Table 1) (Hanna et al., 2018). This is presumably due to the targeting of MLL2 to abnormally unmethylated CG-rich regions. This also highlights the role of intragenic DNA methylation in protecting gene bodies against acquisition of H3K4me3, which could in the somatic context of the post-fertilization embryo, participate in setting a chromatin environment favorable for activation of spurious promoters. In the oocyte context, where ncH3K4me3 is associated with transcriptional silencing, loss of DNA methylation and subsequent H3K4me3 spreading were associated with minor changes in gene expression (Hanna et al., 2018). The role of H3K4me3 spreading in ensuring transcriptional resilience in absence of DNA methylation still needs to be further studied. At the opposite, *Mll2* mutant oocytes display no major changes in DNA methylation patterns (Table 1) (Hanna et al., 2018). This indicates that DNA methylation, rather than H3K4me3, guides their antagonism and their reciprocal restriction to certain regions. However, *Mll2*<sup>CKO</sup> oocytes fail to reach complete transcriptional silencing at the end of oogenesis, at the SN stage (Andreu-Vieyra et al., 2010; Zhang et al., 2016), suggesting a more crucial role of H3K4me3 than DNA methylation in oocyte transcriptional shutdown. Alternatively, it might also suggest a key role for the H3K4me3-DNA methylation compensation dynamic observed in absence of DNA methylation in ensuring control of gene expression. *Mll2*<sup>CKO</sup> oocytes display indeed a more pronounced gene misregulation phenotype than *Dnmt3A/B*<sup>DKO</sup> oocytes.

- H3K27me3 and DNA methylation mutual exclusivity:

H3K27me3 and DNA methylation mutual-exclusivity is exacerbated in the oocyte: it is not only restricted to CpG islands, like it was described in ES cells, but it affects all genomic features (Zheng et al., 2016). PCL proteins are known to recruit PRC2 exclusively at unmethylated CGIs and are therefore thought to mediate DNA methylation and H3K27me3 antagonism at CGIs in somatic cells (see III. 5.3). The molecular mechanisms behind their mutual exclusivity outside of CGIs is poorly understood: the PRC2 subunits responsible for catalyzing broad H3K27me3 domains in the oocyte and their interplays with DNA methylation have not yet been identified.

In accordance with their mutual exclusivity, deletion of DNMTs in ES cells was shown to lead to H3K27me3 spreading in regions that have lost DNA methylation (Brinkman et al., 2012). Conversely, disruption of H3K27me3 deposition via *Eed* knockout leads to aberrant DNA methylation accumulation in regions that are usually H3K27me3-enriched (Table 1) (Li et al., 2018). Whether similar spreading dynamics exist in the oocyte remains unknown and left room to investigate the biological significance of potential interplays between DNA methylation and H3K27me3 in the oocyte epigenome.

### 3.3 –Perturbations in absence of DNA methylation-H3K36me3 enriched compartments

As nH3K4me3 and nH3K27me3 have been shown to anti-correlate with methylated regions in the oocyte epigenome, the question of their behavior upon loss of the H3K36me3-DNA methylated regions was raised. The study of the H3K36 methyltransferase SETD2 mutant, in which both H3K36me3 and subsequent DNA methylation deposition were abolished (see 3.1), enabled to better dissect the functional relationships between chromatin marks. H3K27me3 and H3K4me3 show substantial spreading in former H3K36me3-DNA methylated territories, invading therefore actively transcribed units (Xu et al., 2019). This indicates an important role for H3K36me3 in excluding H3K27me3 and H3K4me3 from transcribing regions.

In a similar manner, SETD1B knockout leads to loss of promoter H3K4me3 and to decreased transcription, which induces in turn intragenic hypomethylation (see 3.1). In this context, many regions also gained nH3K4me3, in particular those that have lost DNA methylation and had high CG-content (Figure 34, Table 1) (Hanna et al., 2022). These features are characteristic of MLL2 targets. It was therefore hypothesized that MLL2 is ectopically

targeted to CG-rich loci present in transcribed regions, which were previously protected from MLL2 binding by DNA methylation.

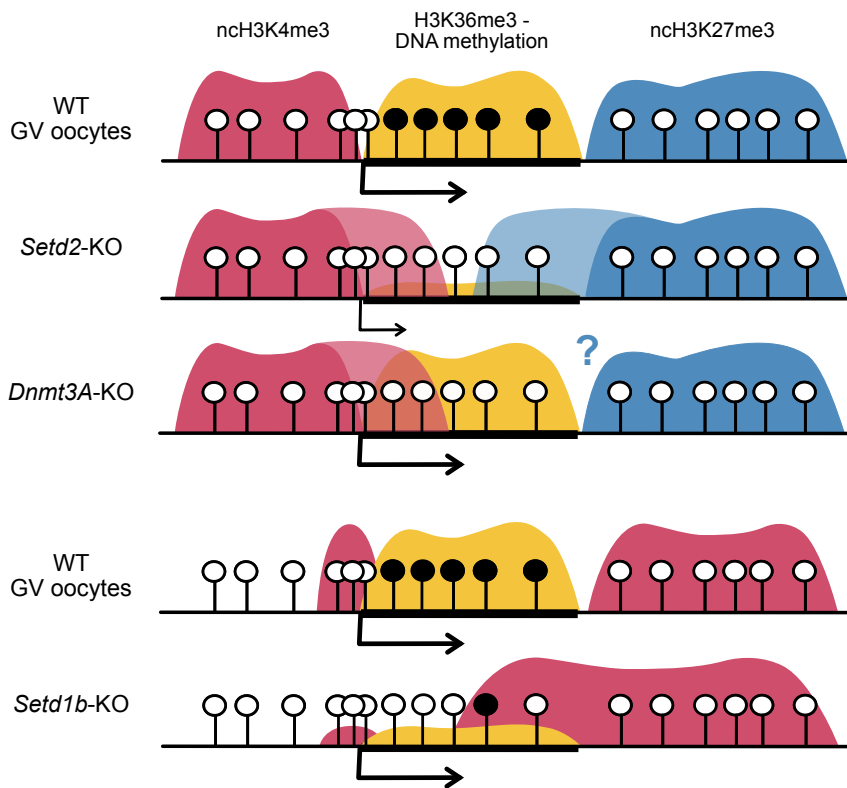


**Figure 34 : ncH3K4me3 and ncH3K27me3 spreading upon perturbations of DNA methylation-H3K36me3 enriched compartments.** The different mutants are described in the text.

Altogether, these studies indicated that H3K36me3-DNA methylation decoration of transcribed regions is essential for restraining H3K27me3 and H3K4me3. The role of DNA methylation versus H3K36me3 in mediating this antagonism remains, however, incompletely understood. In *Dnmt3A/B* double knockout oocytes, H3K36me3 is not affected but H3K4me3 accumulates in intragenic regions (**Figure 34, Table 1**) ([Hanna et al., 2018](#)), indicating that DNA methylation and not H3K36me3 is responsible for H3K4me3 repulsion. This is also coherent with the known DNA methylation-MLL2 antagonism. At the opposite, this relationship is less clear for H3K27me3: while H3K27me3 was shown to spread in absence of both H3K36me3 and DNA methylation (in *Setd2*<sup>CKO</sup> oocytes) (**Figure 34, Table 1**) ([Xu et al., 2019](#)), it is not clear whether the same dynamic is observed in absence of DNA methylation only. Chromatin profiling in *Dnmt3L*<sup>KO</sup> oocytes tended to show that H3K27me3 is largely unaffected in absence of DNA methylation ([Xu et al., 2019](#)). However, this study was performed without appropriate spike-in controls for proper quantitative analysis and could therefore not be fully conclusive. Whether loss of DNA methylation is sufficient for H3K27me3 spreading remains an open

question. The interest of this question was reinforced by the recent notion of H3K36me3-mediated PRC2 inhibition (Finogenova et al., 2020) and the observation in prospermatogonia of H3K27me3 spreading in absence of H3K36me2, but not upon loss of DNA methylation (see III. 5.3) (Shirane et al., 2020).

### 3.4 – ncH3K27me3 and ncH3K4me3 equilibrium

Both broad ncH3K27me3 and ncH3K4me3 domains preferentially overlap with oocyte hypomethylated domains, which are untranscribed regions. However, ncH3K4me3 and ncH3K27me3 tend to reside in different subregions (Zheng et al., 2016). DNA methylation-free regions can be divided in three categories in the oocyte: 15% of them are mainly enriched in H3K27me3, 35% are primarily covered by H3K4me3, while the rest are covered by both H3K4me3 and H3K27me3, but preferentially in non-overlapping subregions of the hypomethylated domain, forming “tandem” rather than “bivalent” patterns. Bivalent regions—with co-occurrence of both H3K4me3 and H3K27me3—correspond to only 18% of the hypomethylated regions in GV oocytes and become restricted to 2% in MII oocytes (Zheng et al., 2016). It is not clear what determines the deposition of H3K4me3 versus H3K27me3 and what drives the progressive reduction in the number of bivalent domains. It also remains to be determined whether the two marks really co-exist in the same cells or the observed bivalency is just the reflect of the alternative presence of these two marks in different cells. This cannot be distinguished by bulk chromatin profiling technics and would require single-cell simultaneous profiling of both marks.

Recent study confirmed the existence of a functional equilibrium between the two marks. Loss of H3K27me3 in MII oocytes, through *Gdf9*-CRE-driven *Eed* knockout, increases H3K4me3 in both formerly bivalent and H3K27me3-only enriched territories (**Figure 35, Table 1**) (Lu et al., 2021). H3K27me3 seems therefore to play a role in restraining H3K4me3 patterns to sub-compartments of the hypomethylated regions. This H3K4me3 spreading has little functional consequences, with observed derepression of H3K27me3-dependent imprinted genes (such as *Xist*) (Inoue et al., 2017) but this seems to be caused by H3K27me3 loss rather than H3K4me3 gain. This derepression can indeed be similarly achieved upon acute H3K27me3 depletion through KDM6B H3K27 demethylase injection after fertilization in early embryos, in which it was assumed that H3K4me3 spreading could not take place (Inoue et al., 2017).

Conversely, the potential remodeling of H3K27me3 patterns in absence of ncH3K4me3 domains in *Mll2*<sup>ckO</sup> oocytes have not been studied yet. However, in *Setd2*<sup>ckO</sup> oocytes, H3K27me3 shows substantial spreading both at previously methylated regions but also in H3K4me3 territories (**Figure 35, Table 1**) (Xu et al., 2019). H3K27me3 forms larger and strengthened domains, therefore tipping the balance towards H3K27me3 against H3K4me3 in hypomethylated regions. Some bivalent regions that preferentially resolve to H3K4me3-only state in MII WT oocytes, become H3K27me3-only domains in *Setd2*<sup>ckO</sup> conditions (Lu et al., 2021). Genes in these H3K4me3-to-H3K27me3 flipped regions show lower maternal expression in preimplantation embryos, suggesting that the spreading of H3K27me3 to H3K4me3 regions in oocytes leads to aberrant repression in embryos (Xu et al., 2019; Lu et al., 2021). This indicates that the separation between ncH3K4me3 and ncH3K27me3 has functional consequences in terms of gene expression regulation. ncH3K4me3 regions, that contain most ZGA genes, need to be protected from ncH3K27me3 to avoid ectopic repression of key genes in early embryos.

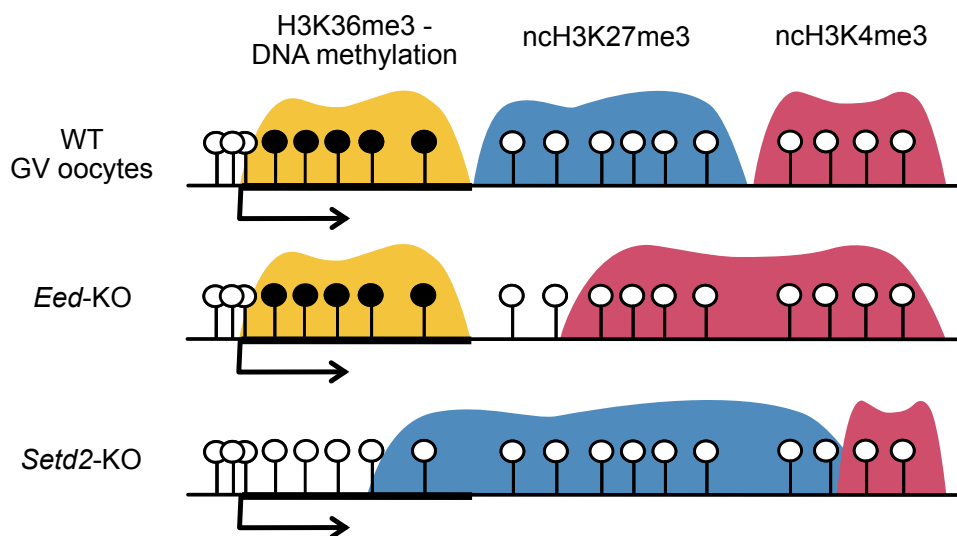


**Figure 35: ncH3K27me3 and ncH3K4me3 equilibrium.** In *Eed*<sup>ckO</sup> oocytes, ncH3K4me3 accumulates at regions that have lost H3K27me3. In *Setd2*<sup>ckO</sup>, ncH3K27me3 shows substantial spreading both in previously methylated or H3K4me3-enriched regions. ncH3K4me3 domains are therefore reduced in MII oocytes.

**Table 1 : Description of the chromatin and developmental outcomes of different oocyte chromatin modifiers**

Factor	Function	Impact on DNA methylation / H3K36me3	Impact on H3K4me3	Impact on H3K27me3	Impact on oocyte development	Impact on preimplantation embryonic development	Impact on post-fertilization development
<b>DNA METHYLATION</b>							
<b>DNMT3A</b>	<i>de novo</i> DNA methylation	Global loss of DNA methylation	<i>In Dnmt3a/b</i> dKO, H3K4me3 accumulation in regions that have lost DNAm	?	?	?	Incorrect imprint establishment, E10.5 lethality
<b>DNMT3L</b>	<i>de novo</i> DNA methylation targeting, DNMT3A cofactor	Global loss of DNA methylation, H3K36me3 patterns unaffected	?	?	Minor transcriptional misregulation, ?	?	Incorrect imprint establishment, E10.5 lethality
<b>H3K4me3</b>							
<b>SETD1B</b>	H3K4 methyltransferase, deposition of canonical H3K4me3 patterns	Intragenic hypomethylation	H3K4me3 decrease at promoter regions, increase in CG-rich intragenic regions	?	Impaired upregulation of oocyte genes, Follicular loss, ZP impairment	/	/
<b>CXXC1</b>	Cofactor of SETD1B, targeting of SETD1B to unmethylated CGIs	Intragenic hypomethylation, H3K36me3 decrease	H3K4me3 decrease at promoter regions	H3K27me3 and H2Aub increase at hypomethylated regions	Impaired upregulation of oocyte genes	/	/
<b>MLL2</b>	H3K4 methyltransferase, deposition of broad nchH3K4me3	Not affected	Loss of nchH3K4me3 broad domains	?	Uncomplete transcriptional silencing in SN, IAP upregulation, Anovulation	In MLL2 hypomorph model, decreased ZGA	/
<b>H3K27me3</b>							
<b>EED</b>	Essential subunit of the PRC2 complex, H3K27me3 deposition	?	H3K4me3 spreading in previously H3K27me3-enriched domains	Global loss of H3K27me3, some residual H3K27me3	?	Improper H3K27me3-dependent maternal Xist imprinting, XCI impairment	Male biased lethality due to improper XCI
<b>H3K36me3</b>							
<b>SETD2</b>	H3K36 methyltransferase, H3K36me2/me3 deposition	Loss of H3K36me3, intragenic hypomethylation, ectopic DNAm	H3K4me3 spreading in previously methylated regions, local H3K4me3 loss	H3K27me3 spreading in previously methylated or H3K4me3-enriched regions	Aberrant transcriptome mainly due to H3K27me3 spreading	One-cell arrest, impaired DNA replication and ZGA (cytosolic defects).	<sup>In cytosol rescue exp.</sup> lower maternal expression of H3K27me3-to-H3K4me3 flipped genes. No placental development (due to imprinted genes ?)

? Unknown

? Questions that I investigated during my PhD

/ Not concerned

## 4 – Relevance for the field of reproductive medicine

Infertility is a disease of the male or female reproductive system defined by a failure to achieve pregnancy after at least 12 months of regular sexual intercourse. One out of six reproductive-aged couples are affected by infertility worldwide, making it a global health issue affecting millions of people. It may be caused by a number of different factors in either the male or female reproductive system but for the majority of patients, the cause of their reproductive dysfunctions remains unknown.

Epigenetic mechanisms are critical for facilitating normal development and cellular differentiation in mammals. For example, unexplained miscarriages have been associated with defects in imprinted DNA methylation in fetal or placental samples ([Pliushch et al., 2010](#); [Hanna et al., 2013](#)). Studies performed in various animal models have further allowed to functionally show that perturbations of epigenetic patterns can result in impaired gamete production or embryonic lethality ([Bourc'his et al., 2001](#); [Andreu-Vieyra et al., 2010](#); [Xu et al., 2019](#); [Dura et al., 2022](#)). Epigenetic anomalies during gametogenesis or early embryonic development could therefore be at the origin of some sterility phenotypes. This highlights the importance of studying chromatin dynamics around the time of fertilization to understand further causes of human infertility.

Nowadays, the mean maternal age at first birth is approaching 30 years in several European countries and the proportion of women who deliver their first child beyond the age of 35 years has greatly increased in recent decades. However, delaying childbearing time is associated with increased risk of infertility. Oocytes accumulate damage in an age-related manner and deteriorate to the point where they are non-functional for fertilization. A well-studied example is the rise with age of aneuploid oocytes, due to a decrease in REC8-mediated sister chromatid cohesion leading to meiotic errors ([Nagaoka et al., 2012](#); [Burkhardt et al., 2016](#)). It is clear that additional factors contribute to oocyte aging: it was shown that epigenetic changes occur in oocytes of advanced maternal age ([Marshall et al., 2018](#); [Wasserzug-Pash et al., 2022](#)). In particular, histone marks associated with heterochromatin were shown to be lost upon aging in human and mouse oocytes. This heterochromatin loss was associated with retrotransposon derepression, DNA damage increase and impair oocyte maturation ([Wasserzug-Pash et al., 2022](#)). In our era of increased rate of delayed childbearing, it is becoming crucial to understand the mechanisms underlying the compromised quality of

oocytes with age and these recent discoveries suggest the importance of chromatin-related dynamics in oocyte aging.

Incidentally, oogenesis and early embryonic development correspond to a highly sensitive developmental window for the epigenome, as it simultaneously undergoes profound genome-wide reprogramming. With the increase in assisted reproductive technologies (ART) use—3.1% of children are born thanks to ART in France—there has been an extensive effort to evaluate whether procedures, such as superovulation, *in vitro* fertilization, embryo culture may increase the risk of developmental epigenetic defects. Indeed, ART procedures have been associated with adverse health outcomes for mothers and babies, including placenta abruption, preterm birth, low-birth weight and perinatal morbidity (Wisborg et al., 2010; Chang et al., 2020). In particular, ART procedures and embryo culture, have been reproducibly associated with increased risk of rare imprinting syndromes like Beckwith-Wiedemann (DeBaun et al., 2003) or Angelman syndrome (Cox et al., 2002), suggesting the existence of ART-related epigenetic disorders. However, contradictory reports exist, suggesting that the association between ART and a higher incidence of imprinting disorders may be due to recruitment and/or statistical biases (Rancourt et al., 2012).

Epigenetic programming of the oocyte occurs during the growing phase that is sensitive at least in its post-antral stages to gonadotropin hormones, so that ovarian stimulation protocols that administer exogenous hormones, as part of the first step for all ART procedures, may interfere with the establishment of appropriate epigenetic states. Moreover, in *in-vitro* fertilization (IVF) or intra-cytoplasmic sperm injection (ICSI) treatments, the dosage of ovarian stimulation is higher to produce an increased number of ovulated oocytes when compared with spontaneous ovulation. This forced oocyte maturation may lead to development of epigenetic anomalies through selection of normally non-ovulated oocytes. For example, Khoureiry et al. observed that the *KCNQ1OT1* imprinted region is more methylated in oocytes of natural cycles than in those from stimulated cycles (Khoureiry et al., 2008), suggesting that hormonal stimulation may recruit too young follicles or modify the dynamics of *de novo* methylation establishment during oogenesis. Similarly, Fauque et al. found abnormal methylation of the *H19* gene in superovulated mouse blastocysts, reinforcing the idea that superovulation could lead to impairment in the methylation status of maternal and paternal imprinted genes (Fauque et al., 2007).

Another study showed methylation abnormalities at the *H19/Igf2*, *Peg3* and *Kcnq1ot1* imprinted loci in mid-gestation IVF mouse placentae (de Waal et al., 2015). However, these methylation defects were only described in the case of superovulation associated with embryo culture and not found for *in vivo* conception with superovulation (de Waal et al., 2015). This suggests that embryo culture and manipulation (culture media, light, thawing...) could have cumulative deleterious consequences on the maintenance of imprinted DNA methylation, additionally to the superovulation process. Maternal imprinting is known to be particularly important in extraembryonic tissues, as loss of maternal DNA methylation imprints in *Dnmt3L*<sup>KO</sup> oocytes results in embryonic lethality due to placental abnormalities (Bourc'his et al., 2001). The imprinting interferences observed in ART conditions may therefore have human clinical implications in assisted reproduction, such as a lack of embryo implantation, spontaneous abortion, or fetal growth retardation by dysfunctional placentas.

However until now, the study of epigenetic anomalies associated with infertility or ART procedures has been mainly focused on maternal imprinting and DNA methylation. Histone marks have been poorly studied in the context of human reproduction, notably low-input chromatin profiling techniques were only recently implemented. It would be very interesting to gain insights into the role of histone modifications patterns in ART-related epigenetic anomalies and in oocyte ageing or further causes of infertility. Multiple chromatin marks (H3K27me3, H3K9me3...) have been shown to be implicated in non-canonical imprinting with significance for embryonic development, raising the question of the intergenerational impact of impaired maternal epigenetic heritage (Inoue et al., 2017). Moreover, recent studies have highlighted in mice the existence of complex and very dynamic interplays between chromatin marks in the oocyte epigenome (Xu et al., 2019; Hanna et al., 2022). As DNA methylation patterns were subject to modifications in ART procedures, we can wonder whether this would coincide with other chromatin mark reorganization.

The role of epigenetics in female sterility has rarely been directly evaluated in humans due to the invasive procedures required to obtain human oocytes. The study of epigenetic marks in oocytes and embryos from other mammalian models is therefore crucial to gain fundamental knowledges, then applicable in reproductive medicine. A long-standing question in the field is to what extent the modes of epigenetic reprogramming in early embryos are conserved between model organisms and humans. Oocyte DNA methylation and its

reprogramming in the early embryo are highly similar between mouse and human (Smith et al., 2012; Guo et al., 2014). The bimodal distribution of DNA methylation is conserved in human oocytes with a strong correlation between active transcription and hypermethylated domains. A moderate gain of DNA methylation at some untranscribed regions can be observed compared to mice. At the opposite, non-canonical H3K4me3 broad domains do not exist in mouse oocytes, where H3K4me3 shows a primarily canonical pattern with enrichment at actively transcribed promoters (Xia et al., 2019). ncH3K4me3 was proved to be involved in transcriptional silencing in mouse oocyte, and the deficiency of its methyltransferase MLL2 leads to severe oocyte defects in mouse and embryonic lethality (Andreu-Vieyra et al., 2010). Other mechanisms may compensate these functions in human. H3K27me3 in human oocytes also largely resembles somatic patterns, with low levels of distal H3K27me3 (Lu et al., 2021; Xia et al., 2019). These distal domains are globally reprogrammed much earlier than in mice, around ZGA. The global depletion of H3K27me3 by ZGA suggests that oocyte-derived H3K27me3 unlikely acts as an imprinting mark in human. This is also consistent with the lack of imprinted XCI in humans, that is mediated by H3K27me3 maternal inheritance in mice. These data call for cautions when extrapolating knowledge learned from animal models to human. Fundamental research works studying the significance of peri-conceptual chromatin dynamics for embryonic development in mammalian models and human are therefore needed to gain insights into epigenetic-related fertility issues.



# **MATERIAL & METHODS**



**Mice.** Mice were hosted on a 12h light/12h dark cycle with free access to food and water in the pathogen-free Animal Care Facility of the Institut Curie (agreement C75-05-18). All experimentations were approved by the Institut Curie Animal Care and Use Committee and adhered to European and national regulation for the protection of vertebrate animals used for experimental and other scientific purposes (directives 86/609 and 2010/63). For oocyte and embryo collection, mice were euthanized by cervical dislocation and either the oviduct or the ovary were placed with M2 media (Sigma-Aldrich, M7167).

Mouse strains, all bred onto C57Bl6/J background, were previously described : *Dnmt3L<sup>KO</sup>* (Bourc'his et al., 2001), *H2B-mCherry* (Abe et al., 2011, gift of J-L. Maitre, Institut Curie, Paris), *Oct4-eGFP* (Lengner et al., 2007, Jackson laboratories, stock #003394, gift of A. Clark, UCLA) and *Eed<sup>2lox/2lox</sup>* (Xie et al., 2014, Jackson laboratories, stock #022727, gift of S. Orkin, Dana Farber Institute). The *Eed<sup>KO/WT</sup>* strain was obtained by constitutive defloxing of the *Eed<sup>2lox/WT</sup>* strain using the *Gdf9-iCre* (Lan et al., 2004, Jackson laboratories, stock #011062, gift of P. Hajkova, Imperial College, London). Oocyte-conditional *Eed* mutants were obtained by crossing *Eed<sup>KO/WT</sup>* ; *Gdf9-Cre<sup>Tg/0</sup>* males with *Eed<sup>2lox/2lox</sup>* females. The mutant genotype of interest was *Eed<sup>2lox/KO</sup>* ; *Gdf9-Cre<sup>Tg/0</sup>* (referred to as *Eed<sup>cKO</sup>* in figures and text); control genotypes were *Eed<sup>2lox/WT</sup>* ; *Gdf9-Cre<sup>Tg/0</sup>* (referred to as *Eed<sup>WT</sup>*). Genotyping primers are available in **Supplementary Table 2**.

Prenatal timepoints were obtained by following timed pregnancies where the day following post-coitum was considered as embryonic day E0.5. Postnatal time points were measured starting from birth, considering the first postnatal day as day 1 post-partum (1dpp).

**PGC collection.** For sorting E12.5 PGCs, *Oct4-eGFP* transgenic mice were used. Pregnant females were euthanized at day E12.5 of their pregnancy (pregnancy was monitored through vaginal plug checking and weight measures). The uteri were opened and E12.5 embryos were released in cold PBS. Embryos were dissected to collect their genital ridges. Embryo's tails were collected to enable sex genotyping of the embryos. Only genital ridges from female embryos with good morphology and at the proper developmental stage were further processed. Genital ridges were dissociated into single cells using the following protocol : genital ridges were transferred to low-binding tubes containing 100  $\mu$ l of collagenase solution in HBSS (collagenase type IV (Gibco), 2X AAs (Gibco), 2X Na-pyruvate (Gibco), 25mM HEPES-KOH pH7.5). Genital ridges were incubated at 37°C for 5-7 min while gently flicking the tube.

400µl of TrypLE Express (Gibco) was added to the cell suspension and incubated for 5min at 37°C. Single-cell suspension was obtained by strong up-and-down pipetting. TrypLE Express was quenched with 140µl of fetal bovine serum (FBS) and the cell suspension was centrifugated at 600g/4min/4°C, washed with FACS buffer (1XPBS, 2mM EDTA, 1% BSA) and filtered through a 35 µm strainer. Washed single-cell suspension was centrifugated and resuspended in FACS buffer supplemented with DAPI (2ng/ml), in order to discriminate dead cells. Cell sorting was performed on Sony SH800 sorter. PGCs were isolated by gating DAPI-negative, OCT4-GFP-positive cells. Further analyses were performed on FlowJo software.

**GV oocyte collection.** Fully-grown oocytes at the germinal vesicle stage were collected from ovaries of 10-12 week-old females. Ovaries were minced mechanically using sterile scalpels to open all ovarian follicles. Oocytes that displayed all characteristics of fully grown GV oocytes were selected: centered germinal vesicle, translucent ooplasm, large diameter and thick zona pellucida. Collected oocytes were placed in M2 medium with 0.4% BSA and 1µmol milrinone (Sigma). Cumulus cells were removed by strong pipetting of the oocytes in a pre-warmed solution of M2-BSA-milrinone with 0.4% pronase (Sigma) on a hot plate at 37°C. Denuded oocytes were then washed 3 times in M2 medium (0.4% BSA;1µmol milrinone) before further experiments. For immunofluorescence experiments, oocytes were used without removal of cumulus cells.

**Non-growing oocyte collection.** Non-growing (NGO) oocytes were collected from ovaries at 5dpp using the same protocol. An eyepiece reticle was used to measure sizes of the oocytes : only non-growing oocytes of 10-30 µm diameter were selected.

**NSN-SN sorting.** *H2B-mCherry*<sup>Tg/0 or Tg/Tg</sup> mice were used to distinguish non-surrounded from surrounded nucleolus GV oocytes. The *Dnmt3L*<sup>KO</sup> strain was crossed with the *H2B-mCherry* strain to enable NSN-SN sorting in *Dnmt3L*<sup>KO/KO</sup>; *H2B-mCherry*<sup>Tg/0 or Tg/Tg</sup> or *Dnmt3L*<sup>WT/WT</sup>; *H2B-mCherry*<sup>Tg/0 or Tg/Tg</sup> oocytes. GV oocytes were collected as previously mentioned and individual oocytes were placed in single M2-BSA-milrinone drops. The H2B-mCherry transgene enabled visualization of their chromatin conformation by 25X observation of the red fluorescent chromatin shape with Leica DMi8 microscope. NSN and SN were then manually sorted and pooled apart.

**Mouse MII oocyte and embryo collection after hormonal superovulation.** Females were superovulated by intraperitoneal injection of pregnant mare serum gonadotropin (PMSG, 5IU) followed by human chorionic gonadotropin (hCG, 5IU) 47h later (3pm, 2pm).

**MI I oocyte collection.** MII oocytes were collected from oviducts of superovulated unmated females 19h post-hCG injection. Oocytes were released from the ampulla in a clean dish with M2 medium containing hyaluronidase (Merck-Millipore MR-051-F) to remove cumulus cells. Good quality oocytes were only kept.

**Embryo collection.** Zygotes (PN4-5) were collected at 23h or 28h post HCG (1pm or 6pm E0.5), 2cell-stage embryos were collected at different timepoints indicated on the figures. They were collected by flushing the infundibulum with M2 medium using a syringe with a blunt needle (30G). Cumulus cells were removed M2 media containing hyaluronidase (Merck-Millipore MR-051-F). Only embryos at the proper developmental stage and with good morphology were kept for further analysis.

**Embryo culture and time-lapse imaging.** Superovulated *Dnmt3L*<sup>WT</sup> and *Dnmt3L*<sup>KO</sup> females were crossed with WT males. After mating, fertilized eggs were harvested at 20h post-hCG in M2 medium. Fertilized eggs (1-cell embryos) were washed twice and cultured in KSOM (Embryomax®, Millipore, MR-020P) at 37°C, 5% CO<sub>2</sub> for 84h. Morphological evaluation was performed every 8h (8am, 4pm, 12am).

For time-lapse experiments, embryo collection and culture was performed as described above. Live imaging was carried out in an inverted Zeiss Observer Z1 microscope with a CSU-X1 spinning disc unit (Yokogawa) with an incubation chamber at 37°C and 5% CO<sub>2</sub> supplied conditions. Brightfield acquisitions were performed using a 40x dry objective. Images were taken every 1h, for a total of 94h.

**Re-implantation experiments.** *Dnmt3L*<sup>WT</sup> and *Dnmt3L*<sup>matKO</sup> zygotes from superovulated females were collected and cultured as described above. Embryo developmental progression was evaluated at E2.5 and the same number of *Dnmt3L*<sup>WT</sup> and *Dnmt3L*<sup>matKO</sup> embryos was mixed and implanted into NMRI pseudo-pregnant females at E0.5. Twenty embryos were transferred per female (10 *Dnmt3L*<sup>WT</sup> and 10 *Dnmt3L*<sup>matKO</sup> embryos). Embryos were then recovered at day E7.5 after hCG injection. All embryos per foster female were collected as described (Nagy et al., 2003) in DMEM/10%FBS/25 mM Hepes pH 7.5, washed three times in

PBS and picked into low-binding microtubes. Genomic DNA was obtained after overnight lysis at 50°C (50 mM Tris, pH 8.0, 5 mM EDTA, 200 mM NaCl, 1% Triton X-100 and 200 µg/ml proteinase K) and isopropanol extraction. *Dnmt3L* genotyping PCR primers are listed in **Supplementary Table 2**.

## **CUT&RUN.**

**Cell preparation.** The CUT&RUN protocol was modified from [Skene & Henikoff, 2017](#). In brief, 20µL of Concanavalin A beads (Polysciences) per sample were resuspended in 1ml of Binding Buffer (20mM HEPES-KOH, 10mM KCl, 1mM CaCl<sub>2</sub>, 1mM MnCl<sub>2</sub>). Beads were washed twice in 1ml Binding Buffer and resuspended in 150µl of Binding Buffer per sample.

Either 1000 E12.5 PGCs or 60 GV /NGO oocytes were used per CUT&RUN experiment. Mouse ES cells were counted using a cell counter and diluted to respective cell amounts in cold PBS. GV and NGO oocytes were counted manually and placed in PBS. E12.5 PGCs were counted and sorted by Sony SH800 sorter and placed in PBS. A volume of 300µl of cold nuclear extraction (NE) buffer (20mM HEPES-KOH, 10mM KCl, 0.5mM Spermidine, 0.1% TritonX-100, 20% glycerol, 1X protease inhibitors) was added to the cell solution. Cells were incubated on ice for 5 minutes in NE buffer. Beads were then added to the cell solution and incubated at rotating at room temperature for 10 minutes.

**Antibody binding.** Cells were then collected on magnetic beads, the supernatant was discarded, the bead-bound cells were resuspended with 1ml Blocking Buffer (20mM HEPES, 150mM NaCl, 0.5mM Spermidine, 0.1% BSA, 2mM EDTA, 1X protease inhibitors) and incubated for 5 min at room temperature. Supernatant was discarded and cells were resuspended in 400µL Wash Buffer (20mM HEPES, 150mM NaCl, 0.5mM Spermidine, 0.1% BSA, 1X protease inhibitors) and 1:200 antibody (**Supplementary Table 1**). For negative controls, rabbit IgG was used. Samples were incubated with rotation at 4°C for 2h30. Supernatant was discarded and samples were washed twice in 1ml Wash Buffer.

**Protein A-micrococcal nuclease (pA-MN) binding and cleavage.** Samples were then incubated with 1:400 of pA-MNase (produced by the Recombination Protein Platform of the Institut Curie, 0.785 mg/ml) in Wash buffer at 4°C for 1 hour. Supernatant was discarded and samples were washed twice in 1ml Wash Buffer. Cells were resuspended in 150ml Wash Buffer and equilibrated to 0° C for 5 minutes. To initiate DNA cleavage, 3µL of 100mM CaCl<sub>2</sub> was added. After 30 min of digestion, reactions were stopped by addition of 150ml 2X STOP buffer

(200mM NaCl, 20mM EDTA, 4mM EGTA, 50µg/ml RNaseA, 40µg/ml glycogen, 0.1% NP40). At this step, 2pg of *Drosophila* spike-in DNA was added for normalization in some CUT&RUN experiments. Samples were then incubated at 37° C for 20 minutes to release DNA fragments into the supernatant. After centrifugation at 12,000 rpm for 5 minutes, supernatants were transferred to new low-binding tubes while pellets and beads were discarded.

**DNA extraction.** Following addition of 0.1% SDS and 0.17mg/ml Proteinase K, samples were incubated at 70° C for 30 min. DNA was purified using phenol/chloroform extraction followed by chloroform extraction and precipitated with 10µg of glycogen and 3 volumes of 100% ethanol for 20 minutes on ice. DNA was pelleted at 12,000 rpm at 4° C for 20 minutes. The DNA pellet was washed in 85% ethanol and resuspended in 40µl low Tris-EDTA (10mM Tris base, 0.1mM EDTA) after complete evaporation of the ethanol.

**Library preparation and sequencing.** Library preparation was performed according to manufacturer's instructions (Accel-NGS 2S PLUS DNA library kit, Swift biosciences). Using four incubations, this protocol repairs both 5' and 3' termini and sequentially attaches Illumina adapter sequences to the ends of fragmented dsDNA. A modified library amplification program was used : cycles of 98°C for 10sec; 60°C for 15 sec followed by a final elongation step of 68°C for 1 min. 21 cycles of PCR were used for low-cell input samples (less than 100 cells), 19 cycles for 1,000-10,000 cells and 17 cycles for more than 10,000 cells. Average library size was tested on Agilent 4200 Tapestation using a DNA5000 screentape and quantification was performed on Invitrogen QUBIT4 using high-sensitivity DNA kit. CUT&RUN libraries were sequenced on a NovaSeq (Illumina) using PE 100bp run, in the Next Generation Sequencing core facility of Institut Curie.

**DNA methylation analysis.** A number of 120 GV oocytes were pulled together in one sample for WGBS protocol. The EZ DNA Methylation-Direct kit (Zymo Research D5020) was used according to the manufacturer's instructions for sample digestion and bisulfite conversion. Together with addition of the CT conversion reagent, 2pg of unmethylated lambda DNA was added to the conversion reaction. Bisulfite-treated DNA was then processed for library preparation with the Accel-NGS Methyl-Seq DNA library kit (Swift Biosciences 30096 and 38096). DNA was amplified with the following PCR program : 21 cycles of 98°C for 10 sec; 60°C for 15 sec followed by a final elongation step of 68°C for 1 min. WGBS libraries were sequenced

with 20% of PhiX DNA on a NovaSeq (Illumina) using PE 100bp run, in the Next Generation Sequencing core facility of Institut Curie.

**Immunofluorescence staining.** Oocytes and zygotes were fixed in PBS containing 2.5% paraformaldehyde (PFA) at room temperature for 20 min and permeabilized in 1% BSA/PBS 0.5% TritonX-100 for 30 min at room temperature. Three washes in 1% BSA/PBS 0.1% TritonX-100 were performed before addition of 1:200 primary antibodies (in **Supplementary Table 1**) for an overnight incubation at 4°C. Oocytes were washed three times in 1% BSA/PBS 0.1% TritonX-100 and incubated for 1 hour in the dark with Alexa Fluor-conjugated IgG secondary antibody (dilution 1:250) in the same buffer. DNA was stained by two sequential incubations in 4,6-diamidino-2-phenylindole (DAPI) (1:50 dilution) in PBS for 15 min at room temperature. Cells were then passed through increasing glycerol concentration to enable a proper embedding of the oocytes without any collapse or morphological changes (2.5% (5'), 5% (5'), 10% (10'), 20% (15'), 50% (15')). Oocytes were mounted in glycerol/DABCO 2.5%/50 mM Tris pH 8.6 (DTG) for sequential Z-stack imaging.

**Confocal imaging and image analysis.** Oocytes and zygotes were imaged with CLSM - LSM 700 UV or LSM 900 UV confocal microscopes (Zeiss). Images were sampled at a resolution of 1024 by 1024 pixels, using a 63x (NA 1.4) objective, and a z-step size of 1µm. Quantification was performed using Imaris 9.0.2 (Bitplane, South Windsor, CT, USA) after 3D reconstruction of the nuclei based on the DAPI signal, with 1µm smoothing surface details and 10µm background subtraction. Statistical analyses of fluorescence intensity were performed with Prism, applying a non-parametrical Mann-Whitney test using GraphPad Prism 8 software.

**Ethynyl-uridine staining.** GV oocytes were collected as previously described and incubated for 4 hours in 0.5mM ethynyl-uridine (EU) in M2 medium supplemented with 1 µM milrinone. Embryos from superovulated females were cultured for 2 hours with 1mM ethynyl-uridine (EU) in KSOM. Oocytes and embryos were fixed immediately after in 4% PFA. EU incorporation was visualized using the Click-it RNA Alexa fluor 488 imaging kit (Invitrogen C10329), as described in the manufacturer's instructions. Fluorescence intensity quantification was performed using Imaris 9.0.2 (Bitplane, South Windsor, CT, USA) after 3D reconstruction of the nuclei based on the DAPI signal, with 1µm smoothing surface details and 10µm

background subtraction. Statistical analyses of fluorescence intensity were performed with Prism, applying a non-parametrical Mann-Whitney test using GraphPad Prism 8 software.

**DNase I TUNEL assay.** Embryos from superovulated females were collected at 20h (early zygote or 28h (late zygote) post-hCG and washed twice with PBS. *In vivo* permeabilization was performed with 0.5% Triton X-100 in pre-extraction buffer (300mM sucrose, 1M CaCl<sub>2</sub>, 50mM NaCl, 3mM MgCl<sub>2</sub>, in 25mM HEPES, pH 7.4) for 5 min on ice, and washed twice in the same buffer without Triton X-100. Embryos were incubated with pre-warmed 0.1U/μl of DNase I in pre-extraction buffer for 5 min at 37 °C. DNase I titration in late zygotes was previously performed to determine the optimal working concentration for that embryonic stage. Embryos were fixed in 2.5% PFA in PBS immediately after and TUNEL assay (Click-iT TUNEL Alexa Fluor 488 Imaging Assay Kit, Invitrogen, C10245) was followed according to the manufacturer's instructions. Fluorescence intensity quantifications were performed with Imaris software (v64.9.0.2) after pronuclei or nuclei 3D reconstruction as described above. Statistical analyses were performed applying Mann-Whitney test using GraphPad Prism 8 software.

**Single-cell RNA-sequencing.** Oocytes from unmated superovulated *Dnmt3L*<sup>WT</sup> or *Dnmt3L*<sup>KO</sup> females, and embryos (zygote and 2-cell stage) from *Dnmt3L*<sup>WT</sup> or *Dnmt3L*<sup>KO</sup> x CAST/Eij natural matings were collected as described above. Cells from 2-cell stage embryos were dissociated by thorough pipetting with a thin capillary (Origio, MXL3-75) in pre-warmed Ca<sup>2+</sup>- and Mg<sup>2+</sup>-free media in consecutive drops covered by mineral oil (Sigma-Aldrich, M5310). Oocytes, zygotes and 2-cell stage single-cells were washed 3 times in PBS-Acetylated BSA (1mg/ml) and manually picked into independent PCR tubes containing lysis buffer. Single-cell cDNA retrotranscription from the 3'UTR and cDNA preamplification were performed using a previously described method (F. Tang et al., 2010). cDNAs were amplified for a total of 20 cycles for oocyte, zygote and 2-cell stage blastomeres.

Extrinsic "ERCC" RNA Spike-In molecules (Invitrogen, 4456740) were added to each lysate (1:1,000,000) to address technical noise, further normalization and the relative quantification of the ratio of endogenous RNA to ERCC molecules. Only cells with the highest quality, based on morphology and amplification yield of housekeeping genes and ERCC Spike-Ins, were sequenced. Single-cell libraries were prepared from 140 samples according to the

manufacturer's protocol (Nextera XT, Illumina). 100bp paired-end sequencing was performed on an Illumina HiSeq instrument.

**Publicly available datasets.** Publicly available datasets were downloaded from multiple resources including: bisulfite-seq from NGO oocytes from 1-3dpp *Dnmt3L*<sup>WT</sup> females, and GV oocytes from 8 week-old *Dnmt3L*<sup>KO</sup> and *Dnmt3L*<sup>WT</sup> females (DRA000570) (Shirane et al., 2013); H3K27me3 CUT&RUN from *Eed*<sup>CKO</sup> and *Eed*<sup>WT</sup> GV oocytes (GSE118263) (Du et al., 2020), H3K4me3 CUT&RUN from *Eed*<sup>CKO</sup> and *Eed*<sup>WT</sup> MII oocytes (GSE163620) (Lu et al., 2021); RNA-seq from *Eed*<sup>CKO</sup> and *Eed*<sup>WT</sup> GV oocytes (GSE118263) (Du et al., 2020).

All raw data files were mapped and trimmed using the pipelines described below.

**RNA-seq analysis.** Single-end reads were trimmed with trim Galore (v0.4.4) in order to remove adapter sequences and Ns nucleotides from both side of the read. Cleaned reads were aligned onto the Mouse reference genome mm10 with STAR (v2.5.0a) in end-to-end mode, reporting random alignment with at most 4 % of mismatches. Genes and TE family-based quantification was performed with featureCounts (v1.5.1) using a concatenated file with repeatMasker and Gencode vM18 annotations. Differential expression analysis was performed using normalization with edgeR (v3.32.1) combined with voom transformation from limma package (v3.46.0). *P* values were computed using limma and adjusted with the Benjamini–Hochberg correction. Genes and transposon families were declared as differentially expressed if  $FDR < 5\%$  and  $\log_2 FC > 1$ . Gene-ontology analysis was performed using the enrichGO function from the clusterProfiler package (v3.18.1).

**Single cell RNA-seq analysis.** Paired-end reads were trimmed with fastx toolkit v0.0.13 with these parameters : -f 11 -Q 33. In order to assess parental origin of the reads, SNPs between C57BL/6 and CAST/EiJ strains were N-masked. Cleaned reads were aligned onto a concatenated genome (the N-masked Mouse reference genome mm10 + fasta file with the ERCC spike-in sequences) with STAR v2.5.0a in end-to-end mode, reporting random alignment with at most 4 % of mismatches. Maternal and paternal reads were split in two files using SNPsplit. Genes and TE family-based quantification was performed with featureCounts v1.5.1 using a concatenated file with repeatMasker and Gencode vM18 annotations. Differential expression and Gene-ontology analyses were performed as previously described. In order to

correlate RNA expression and DNA methylation/histone modifications, -2kb to +100bp regions around the TSS were used.

**CUT&RUN analysis.** Paired-end reads were trimmed with trim Galore (v0.4.4) in order to remove adapter sequences and Ns nucleotides from both side of the read. Cleaned reads were aligned onto the Mouse reference genome mm10 with bowtie2 (v2.2.9) in end-to-end and very sensitive mode. For SN and NSN H3K27me3 samples, a concatenated genome (mm10 Mouse reference and dm6 *Drosophila* reference genomes) was used for the mapping. Duplicated reads were removed using Picard (v2.6.0). Bigwig files for UCSC genome browser and heatmaps were created with deepTools (v2.5.3). Sliding windows approach was used to define enriched regions with csaw R package (v1.24.3). Window size of 2kb and 5 kb was used for H3K4me3 and H3K27me3 samples with a spacing interval of 500bp and 1250bp, respectively. Window-level counts were quantified using the *windowCounts* function, discarding blacklisted regions (ENCODE, accession ENCF547MET), with mapping quality threshold of 20. Non-interesting windows were filtered out using a global background enrichment (*filterWindowsGlobal* function) with large bins (10kb and 25kb for H3K4me3 and H3K27me3 samples, respectively). Normalization and differential binding analysis were performed with csaw. For SN and NSN H3K27me3 samples, total number of *Drosophila* reads  $N$  was used to calculate normalization factor  $\mu$  :  $\mu = N / 10000$ . The normalization factor  $\mu$  was used directly in csaw for normalization. For Bigwig files, the `--scaleFactor 1/ $\mu$`  option was used for deepTools. Windows that are less than 1kb apart were merged into regions. Regions with a FDR<5 % were declared as differentially bound.

For global dynamics of H3K4me3 and H3K27me3 during oogenesis, non-overlapping 5kb-long bins were used. Non-enriched bins were flagged as unmarked using a global background enrichment as before. Enriched H3K4me3 and H3K27me3 bins were flagged as bivalent. The R *ggalluvial* package was used to create alluvial plot.

Genomic annotation was designed as followed : oocyte transcriptome was downloaded from previous data ([Veselovska et al., 2015](#)). Promoters (+/-100bp around the TSS) and gene bodies from this published transcriptome were referred to as active promoters and transcribed gene bodies. Promoters and gene bodies not present in this transcriptome but annotated in Gencode vM18 were referred to as inactive promoters and untranscribed gene bodies. The rest of the genome was annotated as intergenic regions.

CG content was evaluated across gaining and non-differentially bound SN H3K4me3 regions and 5 kb-long random regions (n= 10 000) by determining relative enrichment (log2 observed/genome background) for all dinucleotides with Compter (v0.3) with the precalculated mouse background (<http://www.bioinformatics.babraham.ac.uk/projects/compter/>).

**WGBS analysis.** Paired-end reads were trimmed with fastx toolkit v0.0.13 with these parameters : -f 10 -Q 33. Adapters were removed using Cutadapt v1.3. Cleaned reads were aligned with bismark v0.12.5 onto the Mouse reference Genome mm10 with the option --pbat. Only reads mapping uniquely on the genome were conserved. Methylation calls were extracted after duplicate removal. Only CG dinucleotides covered by a minimum of 5 reads were conserved for the rest of the analysis. The genome was partitioned in 5kb-long windows. DNA methylation level was calculated for *Dnmt3L*<sup>KO</sup> and *Dnmt3L*<sup>WT</sup> GV oocytes. Windows with methylation level > 25 % in WT and <25 % in *Dnmt3L*<sup>KO</sup> were merged if the gap between them was lower than 10kb to call DNA methylation domains.

DMR calling was performed using the bioconductor package DSS with the following parameters: CpG methylation level difference of at least 25%, at least five CpGs called, minimum length of 200 bp and at least 500 bp between two DMRs.

**Supplementary Table 1 : primary antibody list**

Target	Isotype	Source	Use
H3K27me3	Rabbit	Cell signalling technology ref. 9733 (clone C36B11)	IF (1:200) CUT&RUN (1:200)
H3K4me3	Rabbit	Sigma Aldrich 07-473	IF (1:200) CUT&RUN (1:200)
IgG	Rabbit	Sigma 15006	CUT&RUN (1:100)
H2Aub	Rabbit	Cell signaling technology ref. 8240 (clone D27C4)	IF (1:200)
H3K27me2	Mouse	Active motif 61435	IF (1:200)

**Supplementary Table 2 : primers list**

Target	Sequence	Use
<i>Dnmt3L</i>	GGTCCTAGGGGTTCTGGAC TAGCTACCCGTGGCCAATAC GTTGGAGGATTGGGAAGACA CCATGGCATTGATCCTCTCT	<i>Dnmt3L</i> <sup>WT</sup> Forward <i>Dnmt3L</i> <sup>WT</sup> Reverse <i>Dnmt3L</i> <sup>KO</sup> Forward <i>Dnmt3L</i> <sup>KO</sup> Reverse
<i>Eed</i>	GGGACGTGCTGACATTTTCT CTTGGGTGGTTTGGCTAAGA CTGTGCCACCTCATCAGTCT	<i>Eed</i> <sup>2lox</sup> Forward <i>Eed</i> <sup>2lox</sup> Reverse <i>Eed</i> <sup>KO</sup> Reverse
<i>Gdf9-CRE</i>	CCTTCTCTGAACACACCTGGAAGA CTGACTTGGTCAAAGTCAGTGCCT	<i>iCRE</i> Forward <i>iCRE</i> Reverse
<i>H2B-mCherry</i>	TCCCTCGTGATCTGCAACTCCAGTC AACCCAGATGACTACCTATCCTCC GCTGCAGGTCGAGGGACC	<i>H2B-mCherry</i> Forward <i>H2B-mCherry</i> <sup>+</sup> Reverse <i>H2B-mCherry</i> <sup>-</sup> Reverse



# RESULTS



The oocyte epigenome is the theater of intense chromatin interplays: the sum of attractive and repulsive feedbacks between chromatin marks seems to rule their precise targeting, their role in regulating gene expression and the establishment of maternal epigenetic heritage. As in somatic cells, maternal DNA methylation, H3K27me3 and H3K4me3 display complex relationships in the oocyte, involving mutual exclusivity and dependency. However, oocyte distribution of these three marks do not resemble any other cell type. Moreover, all exert repressive functions, including H3K4me3. Finally, this repressive trio displays maternal heritable properties, and each of these marks play important roles in regulating the embryonic program upon transmission to the progeny. Studying the functional relationship between DNA methylation, H3K27me3 and H3K4me3 in the oocyte epigenome is therefore key to better understand the determinants of the maternal epigenetic heritage.

In my PhD work, I investigated the role of the repressive DNA methylation and H3K27me3 marks on the chromatin organisation and transcriptional program of the oocyte. By analysing wild-type and mutant oocytes for either DNA methylation (using the *Dnmt3L*<sup>KO</sup> mutant model) or H3K27me3 (using the oocyte conditional *Gdf9*-CRE driven *Eed*<sup>ckO</sup> model), I found that, surprisingly, neither of these two chromatin marks are essential for transcriptional regulation in the oocyte. I demonstrated that the oocyte epigenome undergoes major chromatin remodelling upon genome-wide loss of DNA methylation and hence discovered new interplays between DNA methylation, H3K27me3 and also H3K4me3 in the oocyte epigenome. The inheritance of a remodelled maternal epigenetic landscape in *Dnmt3L*<sup>matKO</sup> embryos was furthermore associated with an increase in minor ZGA and the concomitant appearance of a developmental delay.

The presented data on chromatin interplays in developing oocytes and zygotes were generated and compiled mostly by myself. Germaine Karam, a Master 2 student that I supervised during six months, helped me generating some microscopy experiments in MII oocytes. I oriented and supervised all the related bioinformatic analyses that were carried out by Aurélie Teissandier, our bioinformatician. Raquel Perez-Palacios (ex-postdoctoral fellow in the lab) performed the single-cell RNA-seq experiments and the developmental characterization of *Dnmt3L*<sup>matKO</sup> embryos, presented at the end of these result section.

## Dynamics of oocyte epigenome establishment

In order to investigate the interplays between chromatin marks and DNA methylation during the establishment of the oocyte epigenome, we first went on generating genome-wide maps of H3K4me3 and H3K27me3 at different timepoints of oogenesis. Profiling of these marks had already been done at some stages of oogenesis but through different chromatin profiling techniques (Zhang et al., 2016; Zheng et al., 2016) that did not really allow integration of the different data for comparison. We optimized cleavage under targets and release using nuclease (CUT&RUN, Skene & Henikoff, 2017) for E12.5 FACS-sorted female PGCs, non-growing oocytes (NGOs) and germinal vesicle oocytes (GV, also called fully grown oocytes FGO). The term “germinal vesicle oocyte” defines a heterogeneous population of mature oocytes, composed of two distinct cell subtypes : non-surrounded nucleoli oocytes (NSN) and surrounded nucleoli oocytes (SN). The NSN-to-SN stage transition corresponds to a key step of complete transcriptional silencing and chromatin reorganization, with SN oocytes displaying a very condensed ring-shaped transcriptionally-quiescent chromatin. To gain for the first time insights into the chromatin remodeling happening during the NSN-to-SN transition, I performed CUT&RUN on the NSN and SN populations distinctively, rather than in a mixed GV population, as usually done in mature oocyte chromatin profiling. The sorting was allowed by the use of a mouse line bearing the *H2B-mCherry* transgene, therefore enabling *in-situ* visualization of the chromatin shape of each GV oocyte, prior to pooling NSN and SN oocytes separately, in distinct CUT&RUN samples. We therefore obtained a timeline of H3K27me3 and H3K4me3 profiles in PGCs, NGO, NSN and SN oocytes (**Figure 1A**). Biological replicates were pooled together for downstream analysis after confirming their reproducibility. To enable correlation of chromatin data with transcriptional information, we also performed single-cell RNA sequencing in MII oocytes (**Figure 1A**). scRNA-seq was performed in MII oocytes, even though they are transcriptionally silent at this stage, so that sequenced mRNAs can be considered as read-outs of the former transcriptional activity during the growing phase of oogenesis. DNA methylation data generated by Shirane et al., 2013 were also incorporated in our analysis.

Focusing on the early stages, we observed a clear decrease in the number of H3K27me3 and H3K4me3 enriched-regions between the PGC and the NGO stages (**Figure 1B**). Conversely, relatively few regions gained *de novo* H3K4me3 or H3K27me3 (**Figure 1B**). NGO patterns were

therefore still resembling PGC patterns, with global or focal decreased in H3K27me3 and H3K4me3 enrichment. In both cell types, H3K4me3 was present in sharp peaks, characteristic of canonical H3K4me3 enrichment at promoters. H3K4me3 was confirmed to be enriched at active promoters in NGOs (**Figure 1C**). H3K27me3 seemed to be decreased at enriched targets between PGC and NGO stages, while low enrichment throughout most untranscribed regions was observed at the NGO stage (**Figure 1A**).

Upon the following phase of oocyte growth, a clear chromatin remodeling was visible between NGO and NSN stages, during which broad nH3K27me3 and nH3K4me3 domains appeared (**Figure 1A**). An important number of regions transitioned from an unmarked- to a H3K27me3 or H3K4me3-enriched state between the NGO and the NSN stage (**Figure 1B**), clearly suggesting *de novo* deposition of the marks. Although, the total number of H3K27me3- or H3K4me3-enriched regions globally increased during the growing phase, chromatin changes also included loss of previously H3K27me3- or H3K4me3-marked regions: respectively 50.8% and 39.7% of NGO-marked regions lost H3K27me3 or H3K4me3 in NSN oocytes (**Figure 1B**). At the NSN stage, 63% of the genome was covered by H3K27me3 and/or H3K4me3 (23.1% by H3K4me3 only and 34% by H3K27me3-only), indicating the presence of broad domains covering large portions of the genome. This remodeling was associated with profound redistribution of the histone marks: H3K27me3 and H3K4me3 were increasingly enriched at intergenic and untranscribed regions, while their enrichment decreased at active promoters and transcribed gene bodies in NSN oocytes (**Figure 1C**). This redistribution and remodeling of H3K27me3 and H3K4me3 patterns signed the switch from canonical patterns to oocyte-specific patterns during the growing phase of oogenesis. Oocyte non-canonical (nc) patterns of H3K27me3 and H3K4me3 are characterized by low enrichment at promoters and the presence of broad domains covering large untranscribed portions of the genome. H3K4me3 and H3K27me3 patterns were then mostly conserved between the NSN and SN stages (**Figure 1A and B**).

This establishment of oocyte-specific nH3K4me3 and nH3K27me3 patterns during the growing phase of oogenesis shows temporal convergence with *de novo* DNA methylation. DNA methylation patterns were indeed gained in the same developmental window, between NGO and GV stages (**Figure 1A**). Consistently with previously published descriptions ([Kobayashi et al., 2012](#)), we observed a strong correlation between DNA methylation distribution and active

transcription: actively transcribed gene bodies were specifically enriched in methylated cytosines, while all other genomic compartments remained hypomethylated (**Figure 1E**).

H3K4me3- and H3K27me3-enriched regions in SN oocytes showed striking DNA hypomethylation, while hypermethylated bins were found only in unmarked regions for these histone marks (**Figure 1D**). This indicates a strong mutual exclusivity between DNA methylated and H3K4me3/H3K27me3-enriched domains. This was also consistent with contrasted genomic distribution: while H3K4me3 and H3K27me3 were enriched at intergenic and untranscribed regions, DNA hypermethylated regions coincided with actively transcribed gene bodies (**Figure 1C and E**). While both enriched in hypomethylated regions, H3K27me3 and H3K4me3 seemed to occupy non-overlapping regions, as only 6% of regions were considered as bivalent (concomitantly H3K27me3- and H3K4me3-enriched) at the NSN stage (**Figure 1B**). H3K27me3 and H3K4me3 are rather present “in tandem” in smaller alternate domains, suggesting a certain antagonism between the two histone marks.

At the NSN-to-SN transition, we observed an important decrease in the number of H3K27me3-enriched regions. Around 32% of H3K27me3-enriched regions in NSN oocytes became unmarked at the SN stage (**Figure 1B**). As oocytes are non-dividing cells, passive dilution of H3K27me3 through cell divisions can be excluded, suggesting the presence of an active mechanism of H3K27me3 removal from these regions. In a similar manner, the number of bivalent regions was decreased between the NSN and SN stage (**Figure 1B**). Half of the NSN stage-bivalent regions resolved in H3K4me3- or H3K27me3-only regions at the SN stage. Only 3% of the genome remained bivalent at the SN stage. The biological significance of this H3K27me3 decrease and bivalent regions resolution at the NSN-to-SN transition remains to be explored.

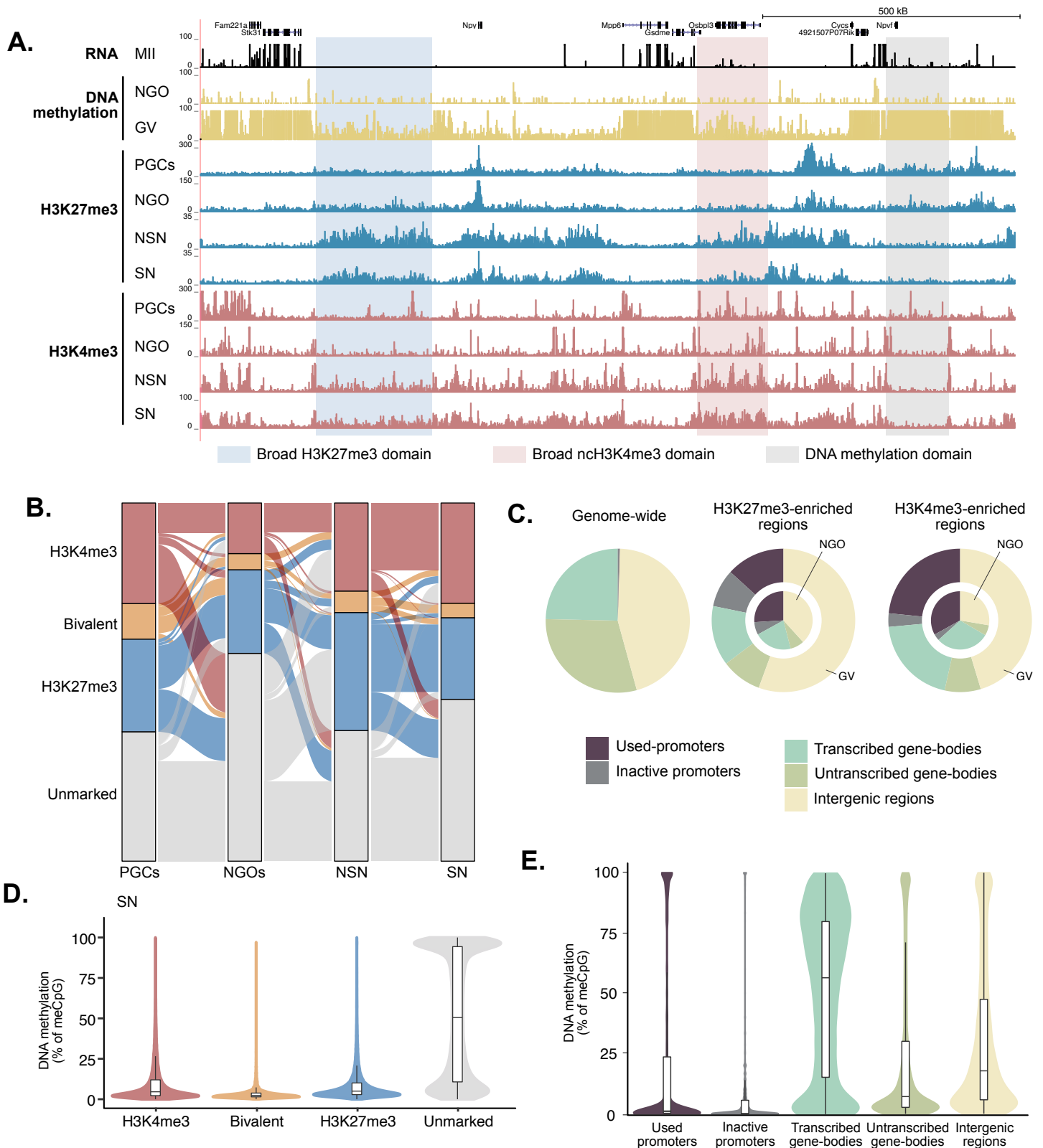
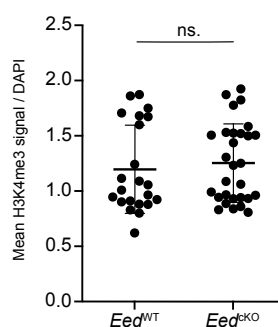
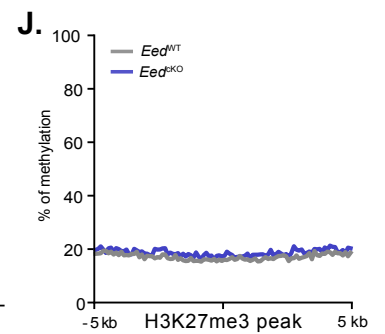
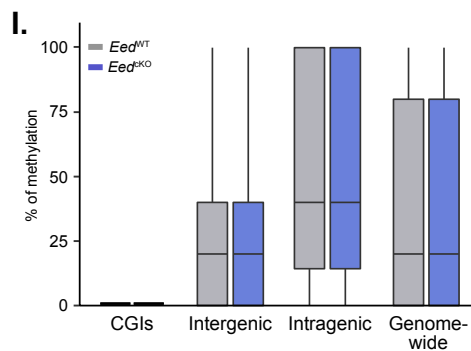
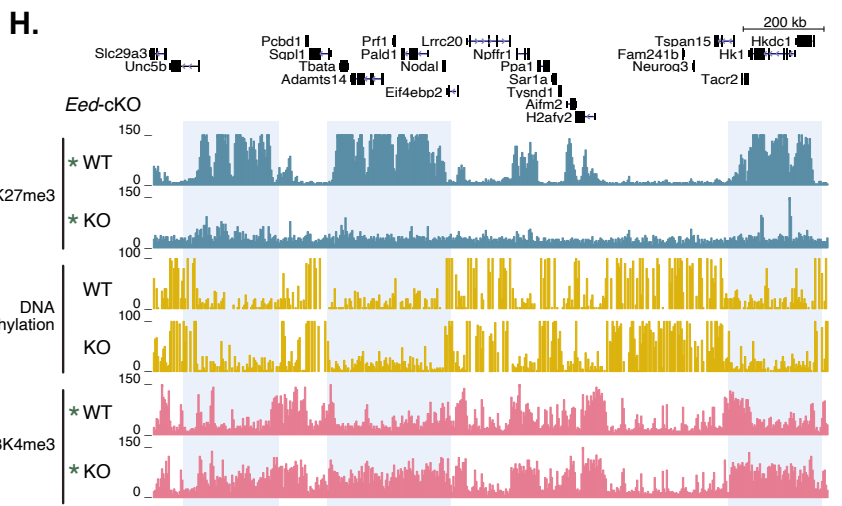
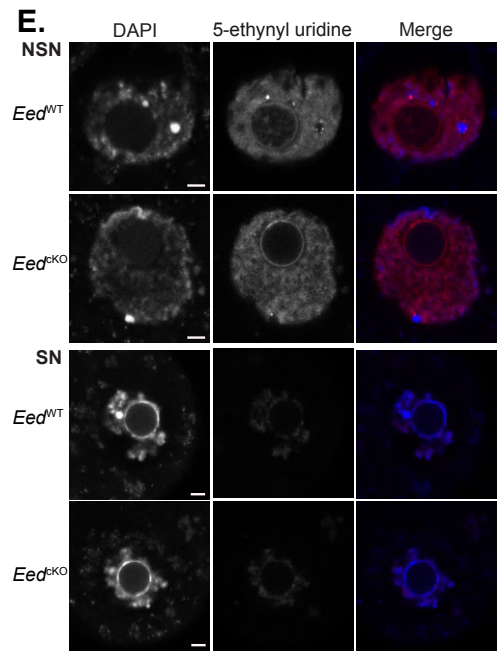
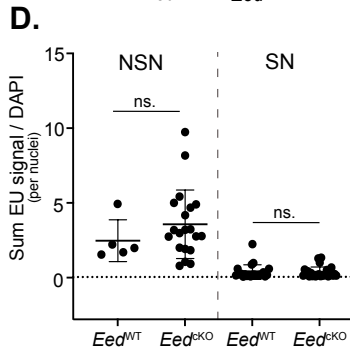
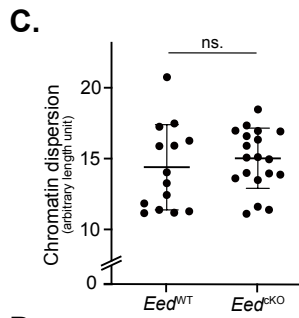
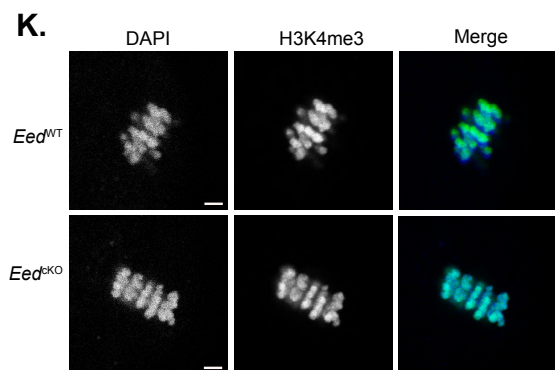
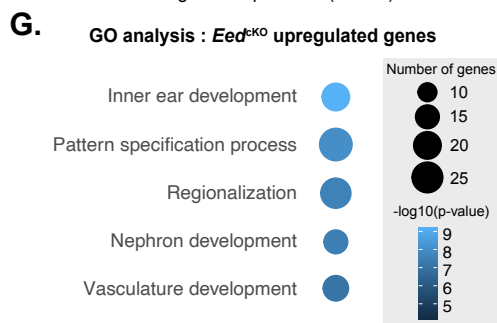
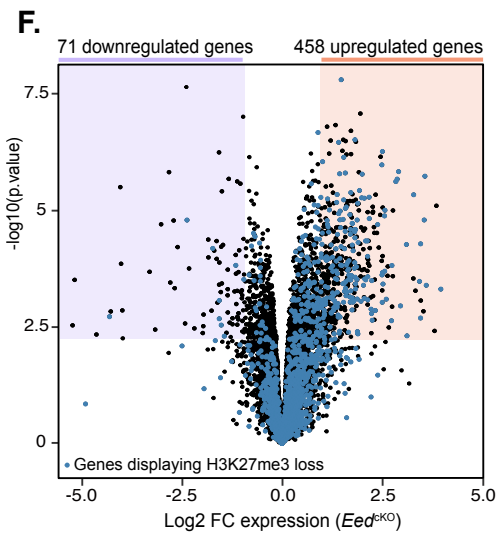
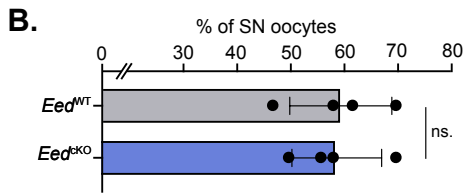
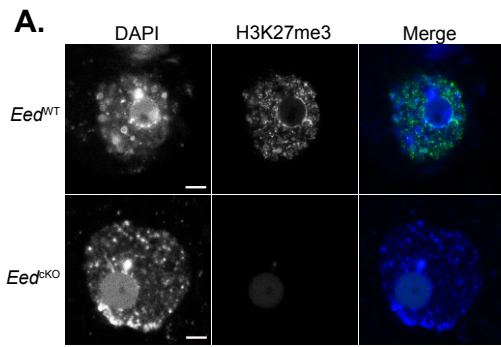


**Figure 1: Dynamics of oocyte epigenome establishment.** **A.** UCSC browser screenshot of DNA methylation, H3K4me3 and H3K27me3 patterns at different stages of oogenesis. E12.5 female PGCs, P5 NGOs and GV oocytes (NSN or SN) are represented. RNA-seq track from scRNA-seq of MII oocytes is also displayed. DNA methylation data were extracted from [Shirane, et al. 2013](#). **B.** Alluvial plot showing the global dynamics of H3K4me3-only, H3K27me3-only and bivalent regions during oogenesis. **C.** Pie chart showing the distribution of H3K27me3- or H3K4me3-enriched domains in the different genomic compartments. The inner circle corresponds to the NGO state, the outer circle represents the GV state (mean NSN-SN states). Genome-wide distribution of the different compartments is displayed on the left panel. **D.** Violin plot showing the distribution of GV oocyte DNA methylation in each of the H3K4me3 and H3K27me3 chromatin states defined in SN oocytes. **E.** Violin plot showing DNA methylation distribution in the different genomic compartments.

## Oocyte development and transcriptome are minimally disrupted in absence of H3K27me3

We next went on analyzing the roles and interplays of H3K27me3 and DNA methylation in the oocyte epigenome. Maternal transmission of oocyte H3K27me3 patterns to the embryo is known to be instrumental for the regulation of H3K27me3-mediated imprinted genes and X chromosome inactivation. But the role of H3K27me3 in the oocyte itself had not been studied yet. To understand H3K27me3 function during oocyte development, we used a mouse model that harbors oocyte-conditional exons deletion (exon 3-6) in the *Eed* gene (Inoue et al., 2018), which codes for a catalytically inactive but essential cofactor of the PRC2 complex. This deletion was under the control of the *Gdf9*-CRE recombinase that is expressed in non-growing oocytes from P3 onwards (Lan et al., 2004). In absence of functional PRC2 complex, H3K27me3 patterns cannot be established during the growing phase of oogenesis in *Gdf9*-CRE; *Eed*<sup>2lox/KO</sup> (*Eed*<sup>ckO</sup>) females. We verified H3K27me3 depletion in *Eed*<sup>ckO</sup> oocytes by H3K27me3 immunofluorescence at the GV stage (Figure 2A). No H3K27me3 was detected in *Eed*<sup>ckO</sup> females compared to *Eed*<sup>WT</sup> females. Because of the known function of Polycomb marks in chromatin compaction, we further analyzed whether H3K27me3 loss had an impact on the global chromatin reorganization that normally happens at the NSN-to-SN transition. First, we found that *Eed*<sup>ckO</sup> oocytes reached the SN stage, characterized by a ring-shaped chromatin structure around the nucleolus, at comparable rates than their WT counterparts (Figure 2B). By measuring the maximum radius of chromatin in *Eed*<sup>ckO</sup> and *Eed*<sup>WT</sup> SN oocytes as an indicator of chromatin dispersion, we further found that *Eed*<sup>ckO</sup> oocytes displayed normal chromatin compaction at the SN stage (Figure 2C). NSN-to-SN transition was therefore not impacted at the chromatin organization level in *Eed*<sup>ckO</sup> oocytes.

**Figure 2: Chromatin remodelling and resilience of the oocyte program in absence of H3K27me3 deposition.** **A.** H3K27me3 immunofluorescence in *Eed*<sup>ckO</sup> and *Eed*<sup>WT</sup> NSN oocytes. Scale bars : 5um. **B.** Proportion of SN stages per collection of *Eed*<sup>ckO</sup> or *Eed*<sup>WT</sup> GV oocytes in 10-12 week-old females ( $n=4$  females per genotype). Mann-Whitney statistical test (ns.  $p>0.05$ ). **C.** Chromatin dispersion analysis in *Eed*<sup>WT</sup> and *Eed*<sup>ckO</sup> surrounded-nucleoli (SN) oocytes. Maximum distance of chromatin from the center of the SN was calculated on DAPI-stained images. Mann-whitney statistical test (ns.  $p>0.05$ ). **D. E.** Ethynyl-uridine (EU) staining of nascent RNAs in NSN and SN oocytes of *Eed*<sup>WT</sup> and *Eed*<sup>ckO</sup> genotypes. **D.** Quantification of EU incorporation in 3D reconstructed nuclei by measure of the EU signal sum normalised to DAPI signal. Mann-Whitney statistical test over WT (ns.  $p>0.05$ ). **E.** Representative images with EU (red) and DAPI (blue) staining. Scale bars : 5um. **F.** Volcano plots showing differential RNA levels between *Eed*<sup>ckO</sup> and *Eed*<sup>WT</sup> GV oocytes in log2 fold-change versus  $-\log_{10}$  p-value. Upregulated genes (458) and downregulated genes (71) are in the red and purple shades, respectively (FDR<5% and FC >2). Genes that display a loss of H3K27me3 in the -10kb/+200bp region around their TSSs are highlighted in blue. RNA-seq datas extracted from Du et al. 2020. **G.** Gene ontology analysis of upregulated genes in *Eed*<sup>ckO</sup> GV oocytes compared to *Eed*<sup>WT</sup>. Number of genes concerned in each categories and mean  $-\log_{10}$  p-value of their misregulation is represented. **H.** UCSC browser screenshot of H3K27me3, H3K4me3 and DNA methylation patterns in *Eed*<sup>WT</sup> and *Eed*<sup>ckO</sup> GV oocytes. DNA methylation tracks were generated by WGBS. \*Previously published data : H3K27me3 in *Eed*<sup>WT</sup> and *Eed*<sup>ckO</sup> GV oocytes by Du et al, 2020 and H3K4me3 in *Eed*<sup>WT</sup> and *Eed*<sup>ckO</sup> GV oocytes by Lu et al., 2021. **I.** DNA methylation enrichment levels in the different genomic compartments in *Eed*<sup>WT</sup> and *Eed*<sup>ckO</sup> GV oocytes. **J.** Metaplot showing DNA methylation levels at H3K27me3-enriched regions in *Eed*<sup>WT</sup> and *Eed*<sup>ckO</sup> GV oocytes. **K.** H3K4me3 immunofluorescence in *Eed*<sup>WT</sup> and *Eed*<sup>ckO</sup> MII oocytes. Left panel : Representative images of H3K4me3 (green) and DAPI (blue) immunostaining. Scale bars : 5um. Right panel : Quantification of H3K4me3 levels in 3D reconstructed chromatin by calculation of the mean H3K4me3 intensity normalised to DAPI. Mann-Whitney statistical test over WT (ns.  $p>0.05$ ).



As H3K27me3 is known to be associated with gene repression, we questioned its role for transcriptional regulation in the oocyte. We assessed the ability of *Eed*<sup>CKO</sup> oocyte to reach complete transcriptional silencing at the SN stage. To evaluate the transcriptional status of *Eed*<sup>CKO</sup> oocytes, we performed nascent RNA labelling by ethynyl-uridin (EU) incorporation in GV oocytes (**Figure 2D and E**). NSN oocytes were transcriptionally active in both mutant and control oocytes. At the SN stage, no EU signal was detected in either *Eed*<sup>CKO</sup> or WT oocytes, indicating that complete transcriptional silencing was achieved at the NSN-to-SN transition in *Eed*<sup>CKO</sup> oocytes. These results indicate that H3K27me3 seems dispensable for transcriptional shutdown of mature oocytes.

To assess how H3K27me3 loss affects transcription in prior growing phase of oogenesis, we analyzed public total RNA-sequencing (RNA-seq) data from *Eed*<sup>CKO</sup> GV oocytes (Du et al., 2020). When comparing *Eed*<sup>CKO</sup> and *Eed*<sup>WT</sup> transcriptomes, we found that most mis-regulated genes were upregulated (458 upregulated versus 71 downregulated genes) in *Eed*<sup>CKO</sup> oocytes (**Figure 2F**). This trend was consistent with the known association of H3K27me3 with transcriptional repression of genes. Gene ontology analysis of upregulated genes in *Eed*<sup>CKO</sup> oocytes indicated, among the main affected pathways, many developmental and morphogenesis processes, characteristic of Polycomb targets (**Figure 2G**). This tends to indicate a direct effect of H3K27me3 loss in gene derepression. However, most of the genes that displayed H3K27me3 loss were not significantly mis-regulated in *Eed*<sup>CKO</sup> oocytes (**Figure 2F**). This transcriptional resilience could be due to the absence of functional role of H3K27me3 at these locations or to compensation of the loss of H3K27me3 due to chromatin remodeling.

### Chromatin remodeling in *Eed*<sup>CKO</sup> oocytes: lack of DNA methylation remodeling

Because of the simultaneous establishment of non-canonical histone mark patterns and a prolonged non-replicative state, the oocyte epigenome is known to be the scene of major chromatin mark interplays. We therefore wanted to assess whether chromatin mark patterns are remodeled in *Eed*<sup>CKO</sup> oocytes. Disruption of H3K27me3 deposition in ESCs had already been shown to lead to aberrant hypermethylation near developmental genes that are usually H3K27me3-enriched (Li et al., 2018), we questioned whether similar dynamics could exist in oocytes. We generated single-base resolution genome-wide DNA methylation maps by Post-Bisulfite Adaptor Tagging (PBAT) in *Eed*<sup>CKO</sup> and *Eed*<sup>WT</sup> GV oocytes. The distribution we observed

in *Eed*<sup>WT</sup> GV oocytes correlated well with previously published oocyte-DNA methylation data, with enrichment over gene bodies (Shirane et al., 2013) (Figure 2H). Upon comparison, we could not find any difference in DNA methylation content and distribution in the different genomic compartments between *Eed*<sup>CKO</sup> and *Eed*<sup>WT</sup> oocytes (Figure 2I). In particular, no ectopic DNA methylation was found to accumulate in previously H3K27me3-enriched regions, with DNA methylation levels remaining low and unchanged at previously H3K27me3-enriched regions (Figure 2J). Despite their mutual exclusivity, H3K27me3 therefore seems to be dispensable for confining DNA methylation to precise genomic regions.

We then decided to analyze H3K4me3 dynamics in absence of H3K27me3. To assess whether global levels of H3K4me3 were affected, we performed H3K4me3 immunofluorescence in *Eed*<sup>CKO</sup> and *Eed*<sup>WT</sup> MII oocytes (Figure 2I and J). We could not detect any change in H3K4me3 global levels upon loss of H3K27me3 in the oocyte. However, recently published CUT&RUN data showed H3K4me3 spreading at regions that have lost H3K27me3 in *Eed*<sup>CKO</sup> oocytes (Lu et al., 2021) (Figure 2H). As this H3K4me3 invasion of H3K27me3 territories was not detected by immunofluorescence, we hypothesized that it does not correspond to an increase in the total amount of H3K4me3-marked nucleosomes, but to a redistribution of H3K4me3 towards previously H3K27me3-enriched regions. However, in absence of normalization strategies with spike-in DNA in this H3K4me3 profiling analysis, it is difficult to demonstrate.

### Oocyte development and transcriptome are minimally disrupted upon genome-wide loss of DNA methylation

The role of maternal DNA methylation has been widely studied during post-implantation development in the context of imprinted genes. Disruption of maternal DNA methylation in the oocyte was indeed shown to lead to embryonic lethality around E9.5 in association with major dysregulation of imprinted genes and placental malformation (Bourc'his et al., 2001). However, the role of maternal DNA methylation in the oocyte itself and upon immediate transmission to the embryo has never been properly studied.

To address the role of DNA methylation during oocyte development, we used the *Dnmt3L*<sup>CKO</sup> mouse model that harbors constitutive deletion (exons 2-5) in the *Dnmt3L* gene (Bourc'his et al., 2001). *Dnmt3L* codes for a catalytically inactive cofactor of DNMT3A, which

is essential for *de novo* DNA methylation in the germline only, both in females and males. Homozygous *Dnmt3L*<sup>KO</sup> females display therefore normal DNA methylation patterns in all tissues, except in oocytes, where *de novo* DNA methylation establishment is abolished. At the end of the growing phase, mature *Dnmt3L*<sup>KO</sup> oocytes show less than 5% remaining DNA methylation compared to WT counterparts (Shirane et al., 2013).

We first evaluated the impact of DNA methylation loss on oogenesis by assessing whether the ovulation rate of *Dnmt3L*<sup>KO</sup> females was affected. By stimulation of pre-pubertal mice with gonadotropin hormones to induce ovulation, we found that *Dnmt3L*<sup>KO</sup> and *Dnmt3L*<sup>WT</sup> females produced similar numbers of ovulated MII oocyte (**Figure 3A**). Global loss of DNA methylation in *Dnmt3L*<sup>KO</sup> oocytes has therefore no impact on ovulation rates.

To enable proper embryonic development, oocytes need to transition through the SN stage, characterized by chromatin compaction and transcriptional silencing, prior to ovulation and meiotic resumption. Ovulation is still possible in absence of SN-conformation acquisition but resultant embryos die around the two-cell stage (Zuccotti et al., 1998). We thus analyzed whether the NSN-to-SN transition was impacted at the 3D nuclear organization level in *Dnmt3L*<sup>KO</sup> oocytes. GV oocytes collected from 10-12 weeks-old females revealed similar proportions of SN oocytes in both mutant and control females, suggesting that *Dnmt3L*<sup>KO</sup> oocytes reached the SN stage with unaffected rates (**Figure 3B**). We additionally measured the maximum radius of chromatin in *Dnmt3L*<sup>KO</sup> and *Dnmt3L*<sup>WT</sup> SN oocytes and found that *Dnmt3L*<sup>KO</sup> oocytes had proper chromatin compaction at the SN stage (**Figure 3C**). DNA methylation loss in *Dnmt3L*<sup>KO</sup> oocytes therefore undergo globally normal NSN-to-SN transition.

As DNA methylation is known to be associated with gene repression, we questioned its role for transcriptional regulation in the oocyte. We assessed the ability of *Dnmt3L*<sup>KO</sup> oocytes to reach complete transcriptional silencing at the SN stage. EU staining of nascent RNA in GV oocytes (**Figure 3D and E**) did not detect significant differences between in *Dnmt3L*<sup>KO</sup> and *Dnmt3L*<sup>WT</sup> oocytes, both at the NSN stage that showed similar EU incorporation, and the SN stage, with lack of labelled EU indicating complete transcriptional silencing. These results indicate that DNA methylation is dispensable for transcriptional shutdown at the NSN-to-SN transition prior to fertilization.

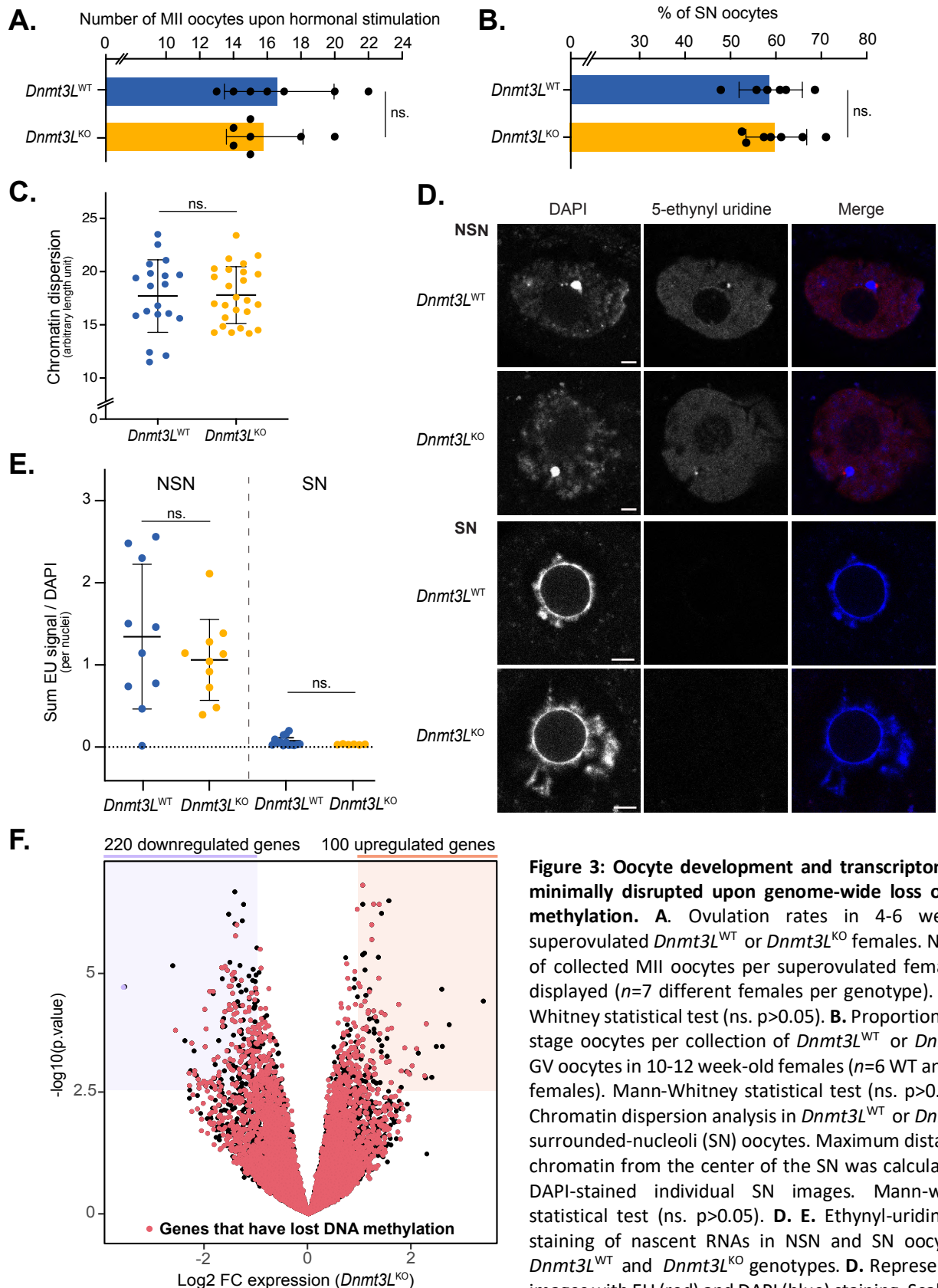


**Figure 3: Oocyte development and transcriptome are minimally disrupted upon genome-wide loss of DNA methylation.** **A.** Ovulation rates in 4-6 week-old superovulated *Dnmt3L*<sup>WT</sup> or *Dnmt3L*<sup>KO</sup> females. Number of collected MII oocytes per superovulated female are displayed ( $n=7$  different females per genotype). Mann-Whitney statistical test (ns.  $p>0.05$ ). **B.** Proportion of SN-stage oocytes per collection of *Dnmt3L*<sup>WT</sup> or *Dnmt3L*<sup>KO</sup> GV oocytes in 10-12 week-old females ( $n=6$  WT and 7 KO females). Mann-Whitney statistical test (ns.  $p>0.05$ ). **C.** Chromatin dispersion analysis in *Dnmt3L*<sup>WT</sup> or *Dnmt3L*<sup>KO</sup> surrounded-nucleoli (SN) oocytes. Maximum distance of chromatin from the center of the SN was calculated on DAPI-stained individual SN images. Mann-Whitney statistical test (ns.  $p>0.05$ ). **D. E.** Ethynyl-uridine (EU) staining of nascent RNAs in NSN and SN oocytes of *Dnmt3L*<sup>WT</sup> and *Dnmt3L*<sup>KO</sup> genotypes. **D.** Representative images with EU (red) and DAPI (blue) staining. Scale bars:

Sum. **E.** Quantification of EU incorporation in 3D reconstructed nuclei by measure of the EU signal sum normalised to DAPI signal. Mann-Whitney statistical test over WT (ns.  $p>0.05$ ). **F.** Volcano plots showing differential RNA levels between single-cell *Dnmt3L*<sup>WT</sup> and *Dnmt3L*<sup>KO</sup> MII oocytes in log<sub>2</sub> fold-change versus  $-\log_{10}$  p-value ( $n=6$  single-cell replicates per genotype). Upregulated genes (100) and downregulated genes (220) are in the red and purple shades, respectively (FDR<5% and FC >2). Genes with significant DNA methylation loss in the -2kb/+100bp region around their TSSs are highlighted in red.

To gain insights into the effects of DNA methylation on transcription in the growing oocyte, we performed single-cell RNA-sequencing (scRNA-seq) in MII oocytes collected from *Dnmt3L*<sup>KO</sup> and *Dnmt3L*<sup>WT</sup> females (**Figure 3F**). *Dnmt3L*<sup>KO</sup> oocytes exhibited mild transcriptomic changes with misregulation of 320 genes (220 downregulated, 100 upregulated). As DNA methylation generally acts as a repressive mark, one could expect upregulation of genes upon loss of the mark. However, the proportion of downregulated genes was unexpectedly greater in *Dnmt3L*<sup>KO</sup> oocytes. A proportion of upregulated genes ( $n= 52$ ) correlated with DNA methylation loss in the region surrounding their transcription start site (TSS) in *Dnmt3L*<sup>KO</sup> oocytes and could therefore still result from a DNA methylation defect. But the remainder of gene misregulation is more likely due to secondary effects or chromatin remodeling in absence of DNA methylation. Moreover, most of the genes that displayed DNA methylation loss around their TSS were not significantly misregulated in *Dnmt3L*<sup>KO</sup> oocytes (**Figure 3F**). This unexpected transcriptional signature and relative resilience in front of genome-wide DNA methylation loss in *Dnmt3L*<sup>KO</sup> oocytes could be due to a limited role of DNA methylation in regulating transcriptional activity in the oocyte epigenome. This would be coherent with the previously described enrichment of DNA methylation in gene bodies in the oocyte (**Figure 1E**), where it could act more as readout of transcriptional activity than as regulator. Moreover, the mild transcriptomic changes observed in *Dnmt3L*<sup>KO</sup> oocytes may actually result from secondary histone mark changes occurring in the absence of DNA methylation.

### Global H3K27me3 decrease in *Dnmt3L*<sup>KO</sup> oocytes

DNA methylation and H3K27me3 are known to display complex relationships involving mutual exclusivity at CGIs in somatic cells and compensatory dynamics (Brinkman et al., 2012; Walter et al., 2016). In oocytes, this anti-correlation is exacerbated, occurring over larger genomic domains (**Figure 1D**, Zheng et al., 2016). We therefore decided to investigate oocyte H3K27me3 patterning in absence of DNA methylation, in *Dnmt3L*<sup>KO</sup> oocytes. We performed H3K27me3 immunofluorescence in *Dnmt3L*<sup>KO</sup> and *Dnmt3L*<sup>WT</sup> oocytes to first visualize potential changes in H3K27me3 global levels. Unexpectedly, H3K27me3 appeared to be dramatically decreased in SN and MII *Dnmt3L*<sup>KO</sup> oocytes (**Figure 4A and C**). This H3K27me3 decrease seemed to be happening from the SN stage on, as *Dnmt3L*<sup>KO</sup> NSN oocytes displayed WT levels of H3K27me3 (**Figure 4A**). H3K27me3 reduction was not associated with

modifications of chromatin compaction in *Dnmt3L*<sup>KO</sup> SN oocytes (**Figure 4B**), indicating that the observed H3K27me3 loss was not biased by chromatin organization differences between *Dnmt3L*<sup>KO</sup> and *Dnmt3L*<sup>WT</sup> oocytes. Altogether, H3K27me3 seemed to be decreased from the SN stage in absence of DNMT3L.

We decided to confirm and precise this finding by performing H3K27me3 genome-wide profiling in *Dnmt3L*<sup>KO</sup> and *Dnmt3L*<sup>WT</sup> oocytes. As NSN and SN oocytes appeared in immunofluorescence to mark the stage just prior and after H3K27me3 decrease appearance, we performed low-input CUT&RUN in sorted populations of NSN and SN oocytes using the H2B-mCherry<sup>+/-</sup> transgene onto *Dnmt3L*<sup>KO</sup> or *Dnmt3L*<sup>WT</sup> background (**Figure 4E**). To avoid normalization of the total number of read counts between samples, which would obscure any change in global H3K27me3 enrichment, we added *Drosophila* spike-in DNA normalizer to our CUT&RUN samples. This enabled us to normalize the number of H3K27me3-enriched mouse reads coming from each samples (**Figure 4D**). Upon spike-in normalization, we observed a decrease in the number of H3K27me3 CUT&RUN mouse reads in *Dnmt3L*<sup>KO</sup> NSN oocytes compared to WT, although the difference was not significant. Interestingly, the number of H3K27me3-reads dropped by roughly half in WT oocytes upon the NSN-to-SN transition. This trend was clearly exacerbated in *Dnmt3L*<sup>KO</sup> oocytes, which had around 1/5 of WT reads at the SN stage, in agreement with our observation by immunofluorescence.

This trend was also reflected on H3K27me3 CUT&RUN tracks (**Figure 4E**). At the NSN stage, a number of 33,820 H3K27me3 peaks were identified in *Dnmt3L*<sup>WT</sup> oocytes, with only very few quantitative changes in *Dnmt3L*<sup>KO</sup> oocytes, with 2.1% being down or up-enriched ( $n=729$  and  $29$ ) (**Figure 4F**). The transition to the SN stage was accompanied by a reduction by half of the number of H3K27me3 peaks in *Dnmt3L*<sup>WT</sup> oocytes, from 33,286 to 17,866. In contrast, almost all peaks lost H3K27me3 in *Dnmt3L*<sup>KO</sup> SN oocytes (96.6% ,  $n=17,330$ ), while only 535 peaks displayed no change and 1 region gained H3K27me3 (**Figure 4F**). In terms of genomic distribution, the lost H3K27me3 regions were mostly found in intergenic and untranscribed gene-body compartments, being not different from the genomic distribution of H3K27me3 (**Figure 1C**). This reinforces the idea of an homogeneous genome-wide loss of H3K27me3 at previously enriched regions in *Dnmt3L*<sup>KO</sup> SN oocytes. Accordingly, in absence of spike-in normalization, H3K27me3 SN *Dnmt3L*<sup>KO</sup> tracks displayed high background (**Figure 4E**), which appeared to be due to the artificial normalization of read counts between samples.

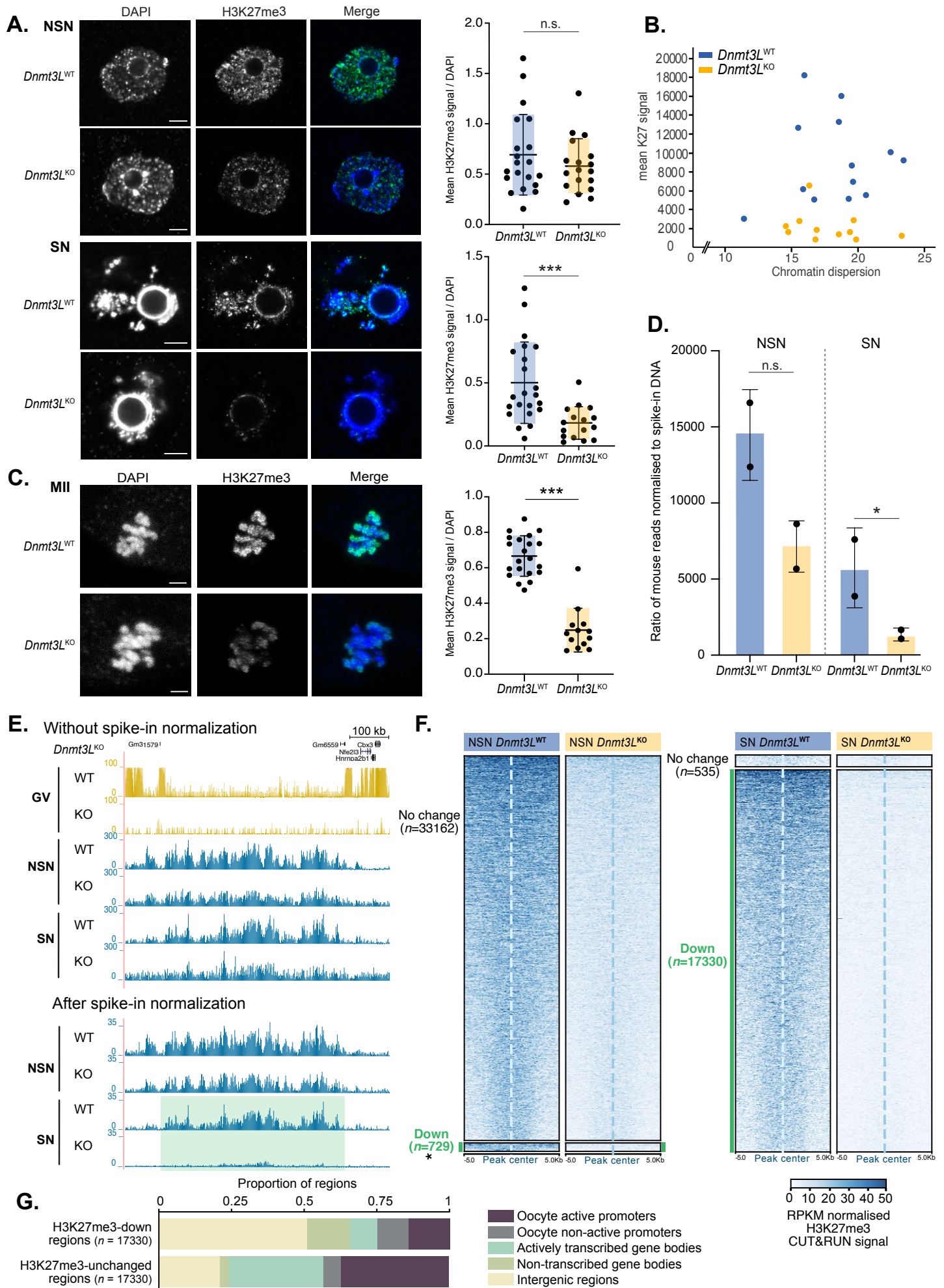


**Figure 4: Global H3K27me3 decrease in *Dnmt3L*<sup>KO</sup> oocytes.** **A.** H3K27me3 immunofluorescence in *Dnmt3L*<sup>WT</sup> and *Dnmt3L*<sup>KO</sup> SN and NSN oocytes. Left panel: Representative images of H3K27me3 (green) and DAPI (blue) immunostaining. Scale bars: 10um. Right panel: Quantification of H3K27me3 levels in 3D reconstructed chromatin by calculation of the mean H3K27me3 intensity normalised to DAPI. Mann-Whitney statistical test over WT (ns  $p > 0.05$ , \*\*\*  $p < 0.001$ ). **B.** Dotplot showing the relationship between mean H3K27me3 fluorescence intensity and chromatin dispersion in *Dnmt3L*<sup>WT</sup> and *Dnmt3L*<sup>KO</sup> SN oocytes. **C.** H3K27me3 immunofluorescence in *Dnmt3L*<sup>WT</sup> and *Dnmt3L*<sup>KO</sup> MII oocytes. Left panel: Representative images of H3K27me3 (green) and DAPI (blue) immunostaining. Scale bars: 10um. Right panel: Quantification of H3K27me3 levels in 3D reconstructed chromatin by calculation of the mean H3K27me3 intensity normalised to DAPI. Mann-Whitney statistical test over WT (\*\*\*  $p < 0.001$ ). **D.** Quantification of the ratio of mouse reads normalised to *Drosophila* DNA spike-in DNA for each H3K27me3 CUT&RUN sample in *Dnmt3L*<sup>WT</sup> and *Dnmt3L*<sup>KO</sup> NSN and SN oocytes ( $n = 2$  biological replicates per condition). Mann-Whitney statistical test (ns.  $p > 0.05$ ; \*  $p < 0.05$ ). **E.** UCSC browser screenshot of DNA methylation and H3K27me3 patterns in *Dnmt3L*<sup>WT</sup> and *Dnmt3L*<sup>KO</sup> NSN and SN oocytes. Tracks obtained with normalisation to the total number of mouse reads or with *Drosophila* spike-in normalisation are displayed. Regions that lose H3K27me3 in *Dnmt3L*<sup>KO</sup> conditions are highlighted. H3K27me3 tracks were generated by CUT&RUN and DNA methylation data were extracted from Shirane, et al. 2013. **F.** Heatmaps showing H3K27me3 levels in RPKM-normalised CUT&RUN data from *Dnmt3L*<sup>WT</sup> and *Dnmt3L*<sup>KO</sup> NSN and SN oocytes. Enrichment is assessed in +/- 5kb from H3K27me3 peaks in WT. Regions are divided in three categories: not differentially enriched (*Dnmt3L*<sup>KO</sup>=WT), up-enriched (*Dnmt3L*<sup>KO</sup>>WT) or down-enriched (*Dnmt3L*<sup>KO</sup><WT). \*Up ( $n=29$ ). **G.** Barplot showing the genomic distribution of H3K27me3-down and -unaffected regions in *Dnmt3L*<sup>KO</sup> SN oocytes.

### H3K4me3 accumulates at regions that have lost DNA methylation in *Dnmt3L*<sup>KO</sup> oocytes

The observed H3K27me3 decrease in the DNA methylation-free *Dnmt3L*-KO oocyte background is in striking contrast with known interplays between H3K27me3 and DNA methylation: multiple studies have described H3K27me3 spreading when DNA methylation is lost in somatic cells (Brinkman et al., 2012; Walter et al., 2016), while here, H3K27me3 seemed to be decreased conjointly with DNA methylation loss in oocytes. We thought that H3K27me3 reduction might be caused by a more complex reorganization of the oocyte epigenome in absence of DNA methylation, involving other histone marks. DNA methylation and H3K4me3 are largely found at non-overlapping regions (Figure 1D) and are both acquired during the growing phase of oogenesis, suggesting the existence of a mutual exclusivity between the two marks in the oocyte epigenome context. H3K4me3 patterns could therefore also be modified by the loss of DNA methylation.

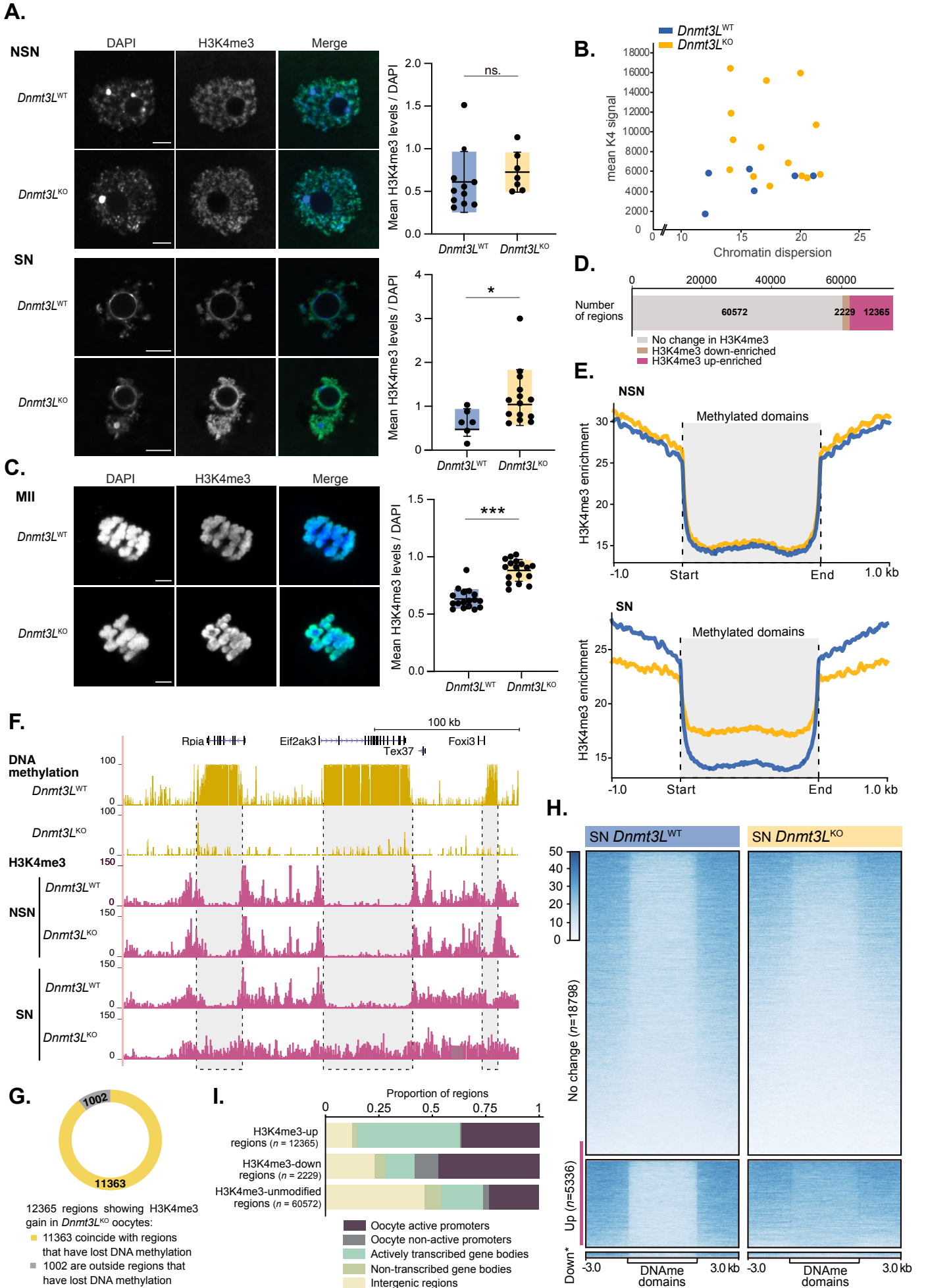
To identify potential chromatin remodeling in absence of DNA methylation, we investigated H3K4me3 dynamics in *Dnmt3L*<sup>KO</sup> oocytes. We first performed H3K4me3 immunofluorescence in *Dnmt3L*<sup>KO</sup> and *Dnmt3L*<sup>WT</sup> oocytes, which enabled us to observe a clear increase in H3K4me3 signal intensity in *Dnmt3L*<sup>KO</sup> oocytes at both SN and MII stages, compared to WT (Figure 5A and C). *Dnmt3L*<sup>KO</sup> NSN oocytes displayed proper levels of H3K4me3, indicating that H3K4me3 increase and H3K27me3 decrease simultaneously occur from the SN stage on (Figure 5A). H3K4me3 increase was not associated with modifications of chromatin compaction in *Dnmt3L*<sup>KO</sup> SN oocytes (Figure 5B), indicating that the observed

H3K4me3 gain was not biased by potential chromatin organization differences between *Dnmt3L*<sup>KO</sup> and *Dnmt3L*<sup>WT</sup> oocytes.

Accumulation of H3K4me3 could be due either to increased H3K4me3 deposition at pre-existing nH3K4me3 broad domains, or to an aberrant gain of H3K4me3 in ectopic regions. To gain insights into H3K4me3 redistribution in absence of DNA methylation and identify the affected genomic regions, we generated genome-wide maps of H3K4me3 in *Dnmt3L*<sup>KO</sup> and *Dnmt3L*<sup>WT</sup> NSN and SN oocytes by CUT&RUN. Among the 75,166 H3K4me3 peaks identified *Dnmt3L*<sup>KO</sup> SN oocytes, we observed 12,365 regions with increased H3K4me3 enrichment, while only 2,229 regions with reduced H3K4me3 levels, confirming a global trend toward H3K4me3 gain in absence of DNA methylation (**Figure 5D**).

We first focused our analysis on *Dnmt3L*<sup>KO</sup> differentially methylated regions (DMRs), which are methylated in WT conditions but lack DNA methylation in *Dnmt3L*<sup>KO</sup> oocytes. A clear increase in H3K4me3 levels was visible in *Dnmt3L*<sup>KO</sup> SN oocytes at these DMRs (**Figure 5E and F**). This increase was not present at earlier stage, in *Dnmt3L*<sup>KO</sup> NSN oocytes, where H3K4me3 did not overlap with DMRs. SN-specific accumulation of H3K4me3 was consistent with the immunofluorescence results, in which H3K4me3 increase was visible only at this stage. Coincidentally with H3K4me3 increase at DMRs, we observed a H3K4me3 decrease on regions flanking the DMRs in *Dnmt3L*<sup>KO</sup> SN oocytes (**Figure 5E**): it could be the sign of a H3K4me3-spreading from neighboring regions to the DMRs, an hypothesis reinforced by the observation of 2,229 H3K4me3 down-enriched regions. However, as the total number of reads is normalized between samples for analysis, this H3K4me3 decrease could also just be an artefact of H3K4me3 gain.

**Figure 5: H3K4me3 accumulates at regions that lack DNA methylation in *Dnmt3L*<sup>KO</sup> oocytes.** **A.** H3K4me3 immunofluorescence in *Dnmt3L*<sup>WT</sup> or *Dnmt3L*<sup>KO</sup> NSN and SN oocytes. Left panel: Representative images of H3K4me3 (green) and DAPI (blue) immunostaining. Scale bars : 10um. Right panel: Quantification of H3K4me3 levels in 3D reconstructed chromatin by calculation of the mean H3K4me3 intensity normalised to DAPI. Mann-Whitney statistical test over WT (ns.  $p>0,05$ , \*  $p<0.05$ ). **B.** Dotplot showing the relationship between mean H3K4me3 fluorescence intensity and chromatin dispersion in *Dnmt3L*<sup>WT</sup> and *Dnmt3L*<sup>KO</sup> SN oocytes. **C.** H3K4me3 immunofluorescence in *Dnmt3L*<sup>WT</sup> and *Dnmt3L*<sup>KO</sup> MII oocytes. Left panel : Representative images of H3K4me3 (green) and DAPI (blue) immunostaining. Scale bars : 10um. Right panel : Quantification of H3K4me3 levels in 3D reconstructed chromatin by calculation of the mean H3K4me3 intensity normalised to DAPI. Mann-Whitney statistical test over WT (\*\*\*)  $p<0.001$ . **D.** Barplot showing H3K4me3 dynamics in *Dnmt3L*<sup>WT</sup> SN oocytes : the number of bins with up-, down- and no-differential H3K4me3 enrichment are shown. **E.** Metaplots showing H3K4me3 enrichment at usually hypermethylated regions in *Dnmt3L*<sup>WT</sup> and *Dnmt3L*<sup>KO</sup> NSN (top) or SN (bottom) oocytes. All regions displaying over 25% DNA methylation in WT were merged and scaled to the same size for analysis. Metaplots were generated from H3K4me3 CUT&RUN data. **F.** UCSC browser screenshot of DNA methylation and H3K4me3 patterns in *Dnmt3L*<sup>WT</sup> and *Dnmt3L*<sup>KO</sup> NSN and SN oocytes. Regions that lack DNA methylation in *Dnmt3L*<sup>KO</sup> conditions are highlighted. H3K4me3 tracks were generated by CUT&RUN and DNA methylation data were extracted from Shirane, et al. 2013. **G.** Pie-chart of regions showing H3K4me3 gain in *Dnmt3L*<sup>KO</sup> SN oocytes and their overlap with regions that lack DNA methylation in the mutant. **H.** Heatmaps showing H3K4me3 levels in RPKM-normalised CUT&RUN data from *Dnmt3L*<sup>WT</sup> and *Dnmt3L*<sup>KO</sup> SN oocytes. Enrichment is assessed in +/- 3kb from regions that lack DNA methylation in the mutant. Regions are divided in three categories: not differentially enriched (*Dnmt3L*<sup>KO</sup>=WT), up-enriched (*Dnmt3L*<sup>KO</sup>>WT) or down-enriched (*Dnmt3L*<sup>KO</sup><WT) \* $n=307$ . **I.** Barplot showing the genomic distribution of H3K4me3-up, -down or -unmodified regions in *Dnmt3L*<sup>KO</sup> SN oocytes.



We found that the vast majority (91.8%) of the 12,365 regions that gained H3K4me3 mapped to *Dnmt3L*<sup>KO</sup> DMRs (**Figure 5G**). Coincidentally, *Dnmt3L*<sup>KO</sup> DMRs that gained H3K4me3 were a minority (21.8%,  $n=5,336$  DMRs). Most of them did not experience H3K4me3 changes (76.9%,  $n=18,798$  DMRs), and very few showed H3K4me3 loss (1.2%,  $n=307$  DMRs) (**Figure 5H**).

While H3K4me3 is mostly found at intergenic regions in the oocyte, regions that gained H3K4me3 enrichment in *Dnmt3L*<sup>KO</sup> SN oocytes ( $n=12,335$ ) mainly coincided with actively transcribed gene bodies or oocyte active promoters (**Figure 5I**). This was consistent with the fact that H3K4me3 accumulates specifically in usually DNA methylated regions, which correlate with active transcriptional units. Conversely, regions that lost H3K4me3 ( $n=2,229$ ) mainly mapped to active oocyte promoters and at a lower extent, to intergenic regions (**Figure 5I**), indicating that both canonical H3K4me3 (promoter-associated) and ncH3K4me3 broad domains displayed a mild decrease in *Dnmt3L*<sup>KO</sup> SN oocytes. Altogether we observed that the lack of DNA methylation in *Dnmt3L*<sup>KO</sup> oocytes is accompanied by a strong dynamic of H3K4me3 accumulation in previously methylated regions, occurring at the SN stage specifically. This finding is in agreement with recently published data that showed H3K4me3 accumulation at DMRs in *Dnmt3A/Dnmt3B*<sup>dKO</sup> GV oocytes (Hanna et al., 2018). We could however not precisely its dynamic by identifying the SN-specific behavior of this H3K4me3 spreading in absence of DNA methylation.

### Towards the mechanisms behind H3K4me3 and H3K27me3 remodeling in absence of DNMT3L

In *Dnmt3L*<sup>KO</sup> SN oocytes, we observed simultaneous H3K27me3 decrease across the genome, and H3K4me3 accumulation in previously methylated regions. As *Dnmt3L* is expressed from the beginning of the growing phase around P7 (Lucifero et al., 2007), we verified that H3K4me3 and H3K27me3 chromatin remodeling specifically occurred during this developmental window. We profiled H3K4me3 and H3K27me3 at the non-growing oocyte stage (NGO) and observed unaffected patterns of H3K4me3 and H3K27me3 in *Dnmt3L*<sup>KO</sup> compared to *Dnmt3L*<sup>WT</sup> NGOs (**Figure 6A**). In particular, while a non-significant decrease in H3K27me3 was already visible at the NSN stage in *Dnmt3L*<sup>KO</sup> oocytes (**Figure 4E and F**), it was absent at the NGO stage. We could conclude that both H3K27me3 decrease and H3K4me3

accumulation happened during the growing phase of oogenesis in *Dnmt3L*<sup>KO</sup> and in particular, at the NSN-SN transition. This could be due to the absence of the DNMT3L protein or to the absence of DNA methylation marks.

The MLL2 protein, responsible for ncH3K4me3 deposition in the oocyte, is known to be targeted to CG rich-regions, through the high affinity of its CxxC domain for unmethylated CpGs (Allen et al., 2006; Hanna et al., 2018). However, in presence of DNA methylation, MLL2 is unable to bind and is repulsed from chromatin. We therefore hypothesized that in absence of DNA methylation in *Dnmt3L*<sup>KO</sup>, MLL2 could catalyze ectopic H3K4me3 at abnormally hypomethylated CG-rich regions that are usually protected against its activity. Because MLL2 activity is dependent on the underlying CpG content, we examined the sequence composition of the regions that lose DNA methylation and gain H3K4me3 in *Dnmt3L*<sup>KO</sup> SN oocytes (**Figure 6B**). CG content was higher in these H3K4me3 up-enriched regions compared to a random set of regions. We also found that among the normally methylated regions, the ones that showed H3K4me3 up-enrichment were significantly more CG-rich than the ones that did not gain H3K4me3 (**Figure 6B**). This observation tends to confirm that H3K4me3 gain in *Dnmt3L*<sup>KO</sup> oocytes could be due to misdirected MLL2 activity at abnormally unmethylated CG-rich regions (**Figure 6I**).

We also tried to understand the mechanisms behind H3K27me3 decrease in absence of DNMT3L. Because of the simultaneous spreading of H3K4me3 and decrease of H3K27me3, we first questioned a potential link between these two phenomena. Indeed, we observed that H3K4me3 and H3K27me3 are rather enriched at non-overlapping regions in the oocyte epigenome, with only rare and unstable bivalent regions (**Figure 1B**), indicating a potential form of mutual exclusivity between the two marks. However, only 2.8% (495) of the “H3K27me3-loss” regions coincided with regions displaying H3K4me3 gain (**Figure 6C**), suggesting a minimal – if any – role of H3K4me3 spreading in triggering H3K27me3 loss.

To gain insights into the nature of the H3K27me3 decrease, we performed immunofluorescence against other histone modifications known to be linked to H3K27me3 states. As H3K27me2 is the first intermediate in the demethylation process of H3K27me3, one could expect to see H3K27me2 accumulation upon reduction of H3K27me3 levels. However, H3K27me2 levels were not affected in *Dnmt3L*<sup>KO</sup> oocytes (**Figure 6D**), indicating that only the me3 to me2 conversion is impaired in *Dnmt3L*<sup>KO</sup> oocytes.

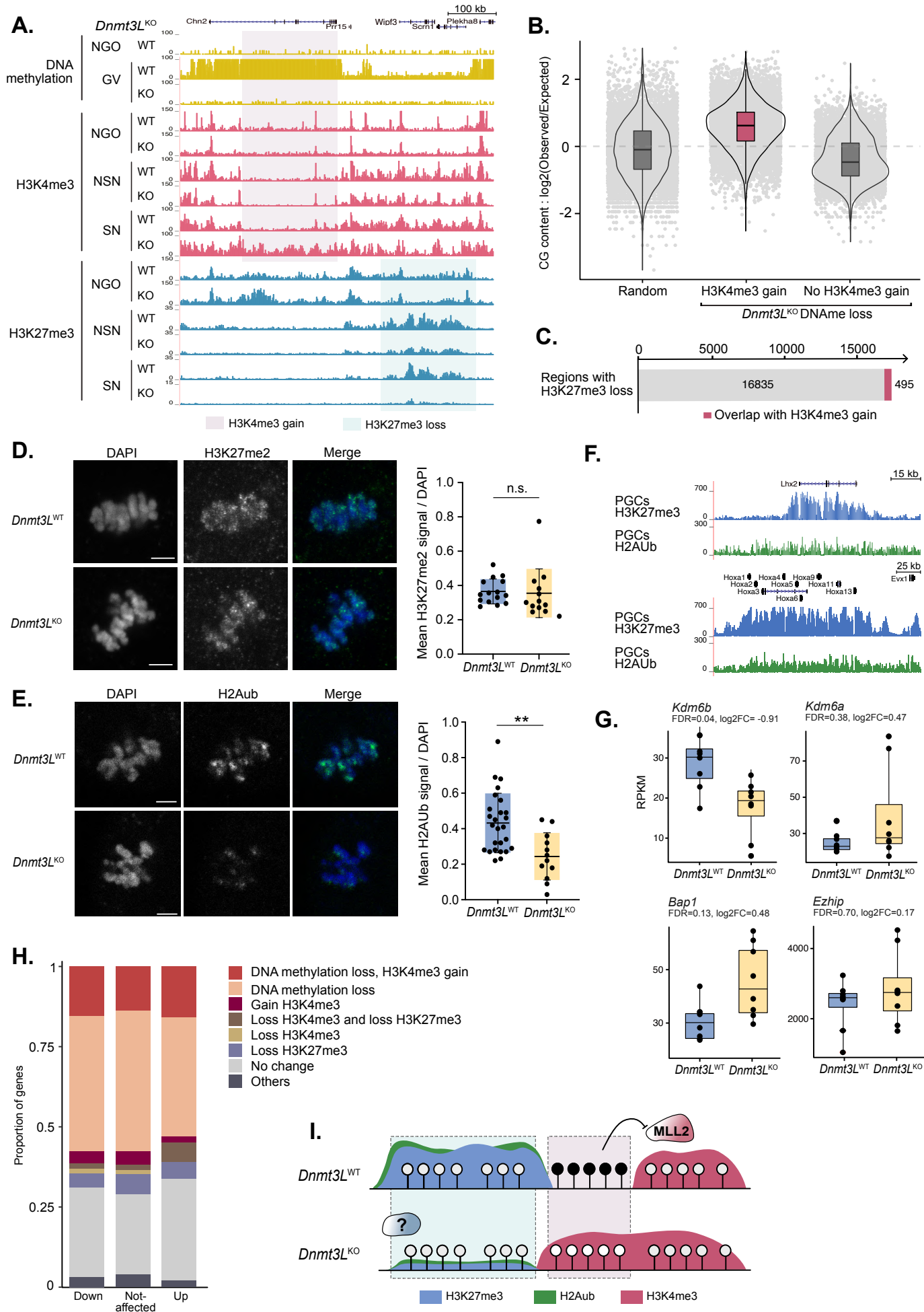


**Figure 6: Analysis of the mechanisms and significance of H3K4me3 and H3K27me3 chromatin remodelling in *Dnmt3L*<sup>KO</sup> oocytes.**

**A.** UCSC browser screenshot of DNA methylation, H3K4me3 and H3K27me3 patterns in NGO, NSN and SN stages of *Dnmt3L*<sup>WT</sup> and *Dnmt3L*<sup>KO</sup> oocytes. Regions that gain H3K4me3 or loose H3K27me3 are highlighted in red and blue, respectively. **B.** Violin plot showing the enrichment for CG content among the regions that loose DNA methylation and gain/do not gain H3K4me3 in *Dnmt3L*<sup>KO</sup> SN oocytes compared to a random set of 5 kb windows. **C.** Boxplot of regions with H3K27me3 loss and their overlap with domains that gain H3K4me3 in *Dnmt3L*<sup>KO</sup> oocytes. **D.** H3K27me2 immunofluorescence in *Dnmt3L*<sup>WT</sup> and *Dnmt3L*<sup>KO</sup> MII oocytes. Left panel: Representative images of H3K27me2 (green) and DAPI (blue) immunostaining. Scale bars: 10um. Right panel: Quantification of H3K27me2 levels in 3D reconstructed chromatin by calculation of the mean H3K27me2 intensity normalised to DAPI. Mann-whitney statistical test over WT (ns.  $p > 0.05$ ). **E.** H2Aub immunofluorescence in *Dnmt3L*<sup>WT</sup> and *Dnmt3L*<sup>KO</sup> MII oocytes. Left panel: Representative images of H2Aub (green) and DAPI (blue) immunostaining. Scale bars: 10um. Right panel: Quantification of H2Aub levels in 3D reconstructed chromatin by calculation of the mean H2Aub intensity normalised to DAPI. Mann-whitney statistical test over WT (\*\*  $p < 0.005$ ). **F.** UCSC genome browser screenshots of H2Aub and H3K27me3 CUT&RUN in 1000 E12.5 female PGCs. *Lhx2* gene and *Hox* cluster are representative of classical Polycomb targets. **G.** Quantification of the RPKM normalised RNA levels of the two H3K27 demethylases (*Kdm6b*, *6a*), the core component of Polycomb deubiquitinylase complex (*Bap1*) and the PRC2 cofactor (*Ezh1*). Data generated by single-cell RNA-seq in MII oocytes. **H.** Barplot showing correlation between gene misregulation and their chromatin state in *Dnmt3L*<sup>KO</sup> vs. WT oocytes. **I.** Scheme representing the chromatin marks remodelling in the epigenome of *Dnmt3L*<sup>KO</sup> oocytes. H3K4me3 accumulation at regions that have lost DNA methylation is highlighted in red. H3K27me3 decrease is highlighted in blue.

H3K27 methylation is also known to be tightly linked to PRC1-deposited H2Aub in the oocyte, whereby H3K27me3 and H2Aub patterns largely overlap (Mei et al., 2021). By immunofluorescence signal quantification, we could see a clear reduction in global H2Aub levels in *Dnmt3L*<sup>KO</sup> MII oocytes (Figure 6E), indicating that the characterized H3K27me3 decrease is accompanied by H2Aub reduction. To gain insights into H2Aub decrease in *Dnmt3L*<sup>KO</sup> oocytes, we tried to optimize H2Aub CUT&RUN for low-input. We thus performed H2Aub CUT&RUN in approximately 1000 FACS sorted-PGCs and somatic cells but could not obtain satisfying maps of H2Aub enrichment even at known Polycomb targets (Figure 6F).

Even if H3K27me3 decrease is already visible at the NSN stage, a clear drop in H3K27me3 enrichment becomes significant between the NSN and SN stages in *Dnmt3L*<sup>KO</sup> oocytes. Because oocytes are non-dividing cells, passive dilution of the mark by PRC2 and/or PRC1 impairment is excluded, rather suggesting an active removal of H3K27me3/H2Aub at the final stages of oogenesis in *Dnmt3L*<sup>KO</sup> oocytes. We therefore analyzed in our RNA-seq data the levels of expression of relevant genes in *Dnmt3L*<sup>KO</sup> versus WT MII oocytes: the two known H3K27 demethylases, *Kdm6a* and *Kdm6b*, as well as *Bap1*, the core component of the recently identified Polycomb deubiquitinylase complex (PR-DUB), (Campagne et al., 2019; Kolovos et al., 2020) and *Ezh1*, a PRC2 cofactor known to constrain PRC2 activity (Ragazzini et al., 2019). We could only detect a slight but clear upregulation of *Bap1*, while H3K27 demethylase expression were unchanged (Figure 6G). This *Bap1* increase may indicate the existence of an active mechanism of H2Aub removal, which would be further enhanced in *Dnmt3L*<sup>KO</sup> MII oocytes. The link between DNMT3L deletion/DNA methylation loss and H2Aub decrease is an ongoing axis of our research (Figure 6I).

## Significance of the observed chromatin remodeling for transcriptional control in *Dnmt3L*<sup>KO</sup> oocytes

Having identified major chromatin remodeling in *Dnmt3L*<sup>KO</sup> oocytes, we questioned whether they impact transcriptional regulation. The observed H3K4me3 and H3K27me3 dynamics could lead to gene expression misregulation or explain the global transcriptome resilience observed in front of genome-wide DNA methylation loss. To know whether some chromatin changes were associated with gene misregulation, we looked at chromatin states around the promoter of genes that were up-, down- or not misregulated in *Dnmt3L*<sup>KO</sup> MII oocytes (single-cell RNA-seq data, **Figure 6H and 3F**). However, we did not detect clear association between H3K4me3 accumulation, H3K4me3 or H3K27me3 decrease and transcriptional patterns. Notably, genes that showed loss of DNA methylation and gain of H3K4me3 at their promoter were equally distributed among up-, down- or not misregulated genes, suggesting no functional role in H3K4me3 spreading in the oocyte. H3K27me3 loss, in association with H3K4me3 loss or not, tended to be slightly more associated with up-regulation of genes. But altogether, H3K27me3 and H3K4me3 chromatin states seemed to play minor roles in the (minor) transcriptome fluctuations observed in *Dnmt3L*<sup>KO</sup> oocytes.

## The remodeled chromatin mark patterns observed in the oocyte are transmitted to the *Dnmt3L*<sup>matKO</sup> preimplantation embryos

DNA methylation, ncH3K4me3 and ncH3K27me3 maternal patterns are transmitted to the preimplantation embryo upon fertilization and persist on the maternal allele at least until the late two-cell stage, before being progressively erased with different dynamics (Zhang et al., 2016; Zheng et al., 2016). Loss of DNA methylation in *Dnmt3L*<sup>KO</sup> oocytes was previously described to result in a lack of maternal DNA methylation in the progeny (Bourc'his et al., 2001; Smallwood et al., 2011). We therefore wondered whether the newly-identified chromatin mark remodeling observed in *Dnmt3L*<sup>KO</sup> oocytes were also transmitted to the preimplantation embryo. We generated *Dnmt3L*<sup>matKO</sup> embryos by natural mating of *Dnmt3L*<sup>KO</sup> females with WT males: the obtained *Dnmt3L*<sup>matKO</sup> embryos are maternal DNA methylation-free and potentially inherit the modified histone mark patterns from *Dnmt3L*<sup>KO</sup> oocytes. To verify whether H3K4me3 accumulation was transmitted to *Dnmt3L*<sup>matKO</sup> embryos, we compared H3K4me3 levels detected by immunofluorescence in *Dnmt3L*<sup>matKO</sup> and *Dnmt3L*<sup>WT</sup>

zygotes. *Dnmt3L<sup>matKO</sup>* zygotes exhibited a significant increase in H3K4me3 levels in maternal pronuclei, while H3K4me3 levels were unaffected in paternal pronuclei (**Figure 7A**). The maternal pronucleus-specific H3K4me3 increase suggested that the accumulation of H3K4me3 at abnormally hypomethylated regions in *Dnmt3L<sup>KO</sup>* oocytes was transmitted to the preimplantation embryo. The same experiment is ongoing for H3K27me3 to define whether H3K27me3 decrease, observed in *Dnmt3L<sup>KO</sup>* oocytes, is also maintained in zygotes. We are also conducting CUT&RUN against H3K27me3 and H3K4me3 in *Dnmt3L<sup>matKO</sup>* zygotes to obtain accurate profiling of their patterns upon transmission to the preimplantation embryos.

### ***Dnmt3L<sup>matKO</sup>* embryos exhibit enhanced zygotic genome activation**

We then questioned whether the presence of remodeled maternal epigenetic heritage could impact zygotic genome activation and subsequent embryonic development. Loss of DNA methylation and associated chromatin marks remodeling seemed to have overall little impact on the transcriptional and developmental program in the *Dnmt3L<sup>KO</sup>* oocyte, but we wanted to investigate their significance upon transmission to the preimplantation embryo.

Considering the role of DNA methylation, H3K27me3 and H3K4me3 in transcriptional regulation, we wondered whether nascent transcription could be altered in *Dnmt3L<sup>matKO</sup>* embryos. To do so, we performed ethynyl-uridin (EU) incorporation at the late zygotic stage (minor ZGA) and at different time-points of two-cell stage development (major ZGA). *Dnmt3L<sup>matKO</sup>* zygotes showed increased levels of EU incorporation at the late zygotic stage (**Figure 7B-D**), supporting the idea of an heightened minor ZGA in *Dnmt3L<sup>matKO</sup>* embryos. The increased levels of nascent transcription occurred similarly in both maternal and paternal pronuclei in *Dnmt3L<sup>matKO</sup>* zygotes (**Figure 7C and D**), indicating that increased nascent transcription is likely due to transactivation, as opposed to a direct effect of the remodeling of chromatin patterns on the maternal allele.

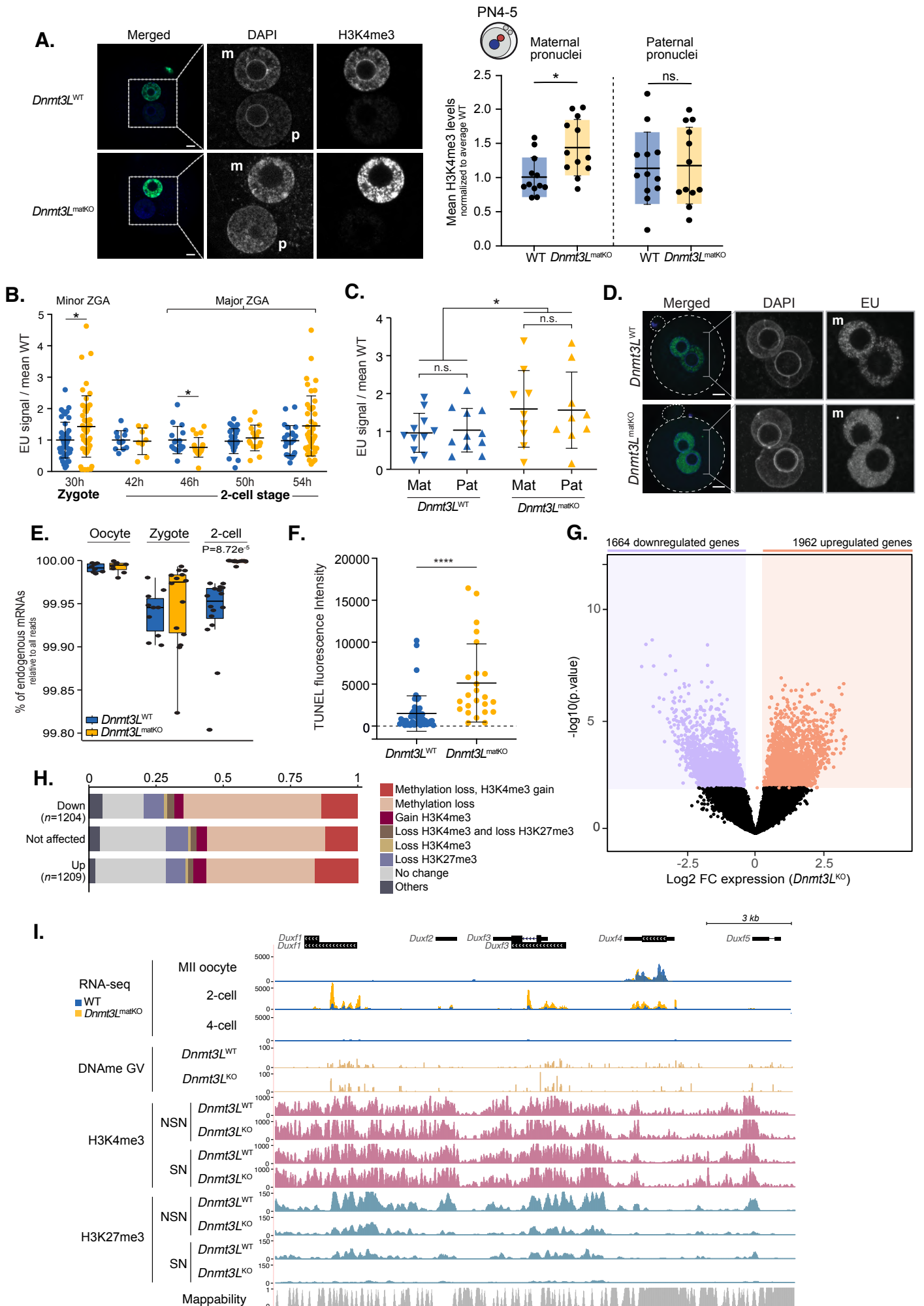
At the two-cell stage, around the time of major ZGA, the levels of nascent transcription in *Dnmt3L<sup>matKO</sup>* embryos were comparable to the ones observed in their WT counterparts (**Figure 7B**). While we did not detect differences at the late two-cell stages time-points, we observed a significant but small down-regulation of transcription in samples fixed 46 hours post phCG injection, which could be due to a potential delay in the entrance to the G2 phase (see **Figure 8C**). Minor ZGA seemed therefore to be specifically impacted in *Dnmt3L<sup>matKO</sup>* embryos.

Higher rates of nascent transcription in the *Dnmt3L*<sup>matKO</sup> zygote could affect the global levels of total RNA in the preimplantation embryo. By using ERCC spike-in RNAs added in scRNA-seq samples, we calculated the percentage of endogenous total mRNA relative to the quantity of spike-in molecules detected in *Dnmt3L*<sup>matKO</sup> or *Dnmt3L*<sup>WT</sup> embryos (**Figure 7E**). We observed no significant difference in mRNA amount in WT and *Dnmt3L*<sup>KO</sup> oocytes but we could observe increased quantity of endogenous mRNAs in *Dnmt3L*<sup>matKO</sup> zygotes compared to WT conditions. The differences were further increased in two-cell *Dnmt3L*<sup>matKO</sup> embryos. Zygotes and two-cell stage *Dnmt3L*<sup>matKO</sup> embryos therefore showed increased global levels of RNA, likely consequence of the increased levels of nascent transcription at minor ZGA.

As nascent transcription and RNA levels were elevated, we wondered if chromatin accessibility was also impacted in the *Dnmt3L*<sup>matKO</sup> embryos. To address this question, we performed DNase I-based TUNEL assays, in which the fluorescence intensity is a readout of the capacity of the DNase I to access DNA and perform double-strand breaks. The levels of TUNEL fluorescence were significantly higher in *Dnmt3L*<sup>matKO</sup> zygotes (**Figure 7F**), again both in maternal and paternal pronuclei, indicating that *Dnmt3L*<sup>matKO</sup> zygotes had significantly enhanced chromatin accessibility at the time of minor ZGA.

---

**Figure 7: Inheritance of altered chromatin patterns in *Dnmt3L*<sup>matKO</sup> embryos associated with impaired ZGA.** **A.** H3K4me3 immunofluorescence in *Dnmt3L*<sup>WT</sup> and *Dnmt3L*<sup>matKO</sup> zygotes (23h post-hCG, here PN4-5 stage). Left panel: Representative images of H3K4me3 (green) and DAPI (blue) immunostaining. Scale bars: 10um. Maternal (m) and paternal (p) pronuclei are indicated. Right panel: H3K4me3 quantification in 3D reconstructed maternal or paternal pronuclei shown as fold intensity relative to the average signal of WT nuclei per experiment. Only PN4-5 zygotes were selected for analysis (distance inter-pronuclei < 25um). Mann-Whitney statistical analysis (ns. p>0.05; \*p<0.05) **B. C. D.** Nascent RNA labeling through EU incorporation in *Dnmt3L*<sup>WT</sup> and *Dnmt3L*<sup>matKO</sup> zygotes and 2-cell embryos at different timepoints. **B.** Quantification of EU incorporation shown as fold intensity relative to the average signal of WT nuclei per experiment. Time points correspond to hours post-hCG injection. Each dot represents either a single pronucleus (zygotic stage) or a single nucleus (2-cell stage). Mann-Whitney statistical test (\* p<0.05). **C.** Quantification of EU fluorescence intensity of *Dnmt3L*<sup>WT</sup> and *Dnmt3L*<sup>matKO</sup> zygotes (30h post-hCG), identifying parental pronuclei. EU fluorescence intensity is shown as fold intensity relative to the average signal of WT nuclei per experiment. Mann-Whitney statistical test (\* p<0.05). **D.** Representative image of EU (green) and DAPI (blue) staining in PN4-5 *Dnmt3L*<sup>WT</sup> and *Dnmt3L*<sup>matKO</sup> zygotes. Scale bars: 10um. Maternal (m) and paternal (p) pronuclei are indicated. **E.** RNA quantity measured as percentage of the total of endogenous RNA reads relative to the total sequenced material (sum of endogenous RNA and ERCC spike-in reads) in RNA-seq of single *Dnmt3L*<sup>WT</sup> and *Dnmt3L*<sup>matKO</sup> embryos. P-values were calculated with Student t-test. **F.** Quantification of TUNEL fluorescence intensity (total intensity in a.u.) in zygotes (28h phCG). Each dot represents a single pronucleus. Mann-Whitney statistical test (\*\*\*\* p < 0.0001). **G.** Volcano plots showing differential RNA levels between *Dnmt3L*<sup>WT</sup> and *Dnmt3L*<sup>matKO</sup> 2-cell embryos in log2 fold-change versus -log10 p-value. Upregulated genes (1962) are highlighted in red, downregulated genes (1664) in purple (FDR<5%). Data generated by single-cell RNAseq (n=10 WT and 14 *Dnmt3L*<sup>matKO</sup> biological replicates). **H.** Barplot showing the chromatin state in the promoter region of genes misregulated from the maternal allele specifically in *Dnmt3L*<sup>matKO</sup> vs. *Dnmt3L*<sup>WT</sup> 2-cell embryos. Correlation between SN oocyte CUT&RUN data and maternal allele analysis of 2-cell embryo scRNA-seq. **I.** UCSC genome browser screenshot of the *Dux* locus. Bulk RNA-seq data in MII oocytes, 2-cell and 4-cell embryos are displayed together with the associated maternal chromatin patterns of DNA methylation, H3K4me3 and H3K27me3 in *Dnmt3L*<sup>KO</sup> oocytes. Unique mapping was used to generate the RNA-seq tracks. Mappability represents the probability that a randomly selected 50 nucleotides-read is uniquely mappable.



We next questioned whether the increase in gene transcription at minor ZGA could be linked to the transmitted maternal chromatin alterations. Loss of maternal DNA methylation and the associated H3K4me3 and H3K27me3 reorganization could have an impact on ZGA regulation, although the multiple nature of these chromatin alterations may make it difficult to pinpoint specific effects. We identified 1,962 up-regulated genes and 1,664 down-regulated genes in scRNA-seq from *Dnmt3L*<sup>matKO</sup> versus WT two-cell embryos (**Figure 7G**). The ratio of significantly up-regulated/down-regulated genes was surprisingly low, when considering that the total mRNA levels and nascent transcription rates were increased at this stage. To know whether chromatin changes were associated with gene misregulation at ZGA, we looked at the chromatin state around the promoter of genes that were up-, down- or not misregulated from the maternal allele in *Dnmt3L*<sup>matKO</sup> embryos (**Figure 7G and H**). However, we could not find clear association between H3K4me3 accumulation, H3K4me3 or H3K27me3 decrease and transcriptional patterns. Altogether, H3K27me3 and H3K4me3 chromatin states seemed to play minor direct roles in explaining the transcriptome fluctuations in *Dnmt3L*<sup>matKO</sup> zygotes.

The fact that increased nascent transcription affected the two parental pronuclei at similar levels suggested an alternative hypothesis regarding the mechanism behind ZGA enhancement in *Dnmt3L*<sup>matKO</sup> embryos. An excess of a minor ZGA transactivator could provoke an exacerbated transcriptional response by opening the chromatin and leading to a more active transcriptional status. The *Dux* transcription factor family is known as a key activator of ZGA in mice (De Iaco et al., 2017, 2020; Hendrickson et al., 2017). Although its absence does not totally impair ZGA *in vivo*, induction of *Dux* expression in ESCs provokes transcriptional activation of genes and transposable elements normally expressed at ZGA (De Iaco et al., 2017, 2020; Bosnakovski et al., 2021).

The *Dux* region exhibits extremely low mappability due to the inherent complexity and repeatability of the *Dux* locus, comprising 28 units in two tandem repeats (Grow et al., 2021), so it is hard to draw definite conclusions. Nonetheless, focusing on uniquely mappable reads in WT and *Dnmt3L*<sup>matKO</sup> bulk RNA-seq datasets, we found that while the oocyte-specific *Duxf4* transcript was unchanged in the oocyte or in two-cell embryos in *Dnmt3L*<sup>matKO</sup> compared to WT conditions, the embryonic *Dux* genes (*Duxf1*, *Duxf2*, *Duxf3* and *Duxf5*) were all overexpressed relative to WT at the two-cell stage (**Figure 7I**). *Dux* copies ceased expression in both WT or *Dnmt3L*<sup>matKO</sup> four-cell stage embryos, indicating proper transcriptional

repression of *Dux* at the end of ZGA. When looking at the chromatin patterns present in *Dnmt3L*<sup>KO</sup> oocytes at the *Dux* locus, we clearly observed H3K27me3 decrease at the SN stage, while DNA methylation and H3K4me3 were unaffected (**Figure 7I**). Decreased H3K27me3 on the maternal allele of the *Dux* locus could be responsible for *Dux* overexpression in the zygote and subsequent excessive ZGA. In turn, *Dux* overexpression could explain the observed genome-wide increase in chromatin accessibility and in transcriptional activity at minor ZGA in *Dnmt3L*<sup>matKO</sup> conditions.

### Developmental delay and fitness decrease in *Dnmt3L*<sup>matKO</sup> preimplantation embryos

We finally wanted to assess the impact of altered maternal chromatin patterns and associated minor ZGA anomaly on the preimplantation development of *Dnmt3L*<sup>matKO</sup> embryos. We performed *in vitro* culture experiments coupled with systematic morphological assessment of the developmental progression of *Dnmt3L*<sup>WT</sup> and *Dnmt3L*<sup>matKO</sup> embryos, from the zygote to the blastocyst stage (**Figure 8A**). *Dnmt3L*<sup>WT</sup> and *Dnmt3L*<sup>matKO</sup> embryos reached the two-cell stage with similar efficiency (**Figure 8B**). However, *Dnmt3L*<sup>matKO</sup> embryos progressed to the three and four-cell stages at a reduced rate compared to their WT counterparts, indicating a developmental delay (**Figure 8B**). *Dnmt3L*<sup>matKO</sup> embryos exhibited a stage-specific developmental delay at the 2- to 4-cell cleavage division, shifted by approximately six hours, after which they appeared to resume normal developmental progression with conserved developmental delay (**Figure 8C**). Importantly, the two- to four-cell cleavage division coincides with the timing when an increase in total RNA levels was observed in *Dnmt3L*<sup>matKO</sup> embryos, suggesting a potential link between RNA excess and cell-cycle slowdown.

Even if normal development could proceed after the two- to four-cell cleavage division delay, *Dnmt3L*<sup>matKO</sup> blastocysts exhibited significantly less cells per embryo than their WT counterparts (30.7% fewer cells) (**Figure 8D**). We therefore decided to test whether the reduced number of cells in *Dnmt3L*<sup>matKO</sup> embryos was associated with a fitness cost. To address this question, we re-implanted the same number of E2.5 *Dnmt3L*<sup>WT</sup> and *Dnmt3L*<sup>matKO</sup> *in vitro* cultured embryos in mixed pools into WT foster females, and assessed the genotype of embryos per uterus at 7.5 days of development. We chose E7.5 as a dissection time-point prior to fetus-maternal contact, to avoid a confounding effect from the previously described

imprinting placental phenotype in *Dnmt3L*<sup>matKO</sup> post-implantation embryos (Bourc'his et al., 2001). The percentage of implanted *Dnmt3L*<sup>matKO</sup> embryos per female was significantly lower compared to WT (Figure 8E), with an average implantation rate/uterus of 68% for *Dnmt3L*<sup>WT</sup> embryos versus 31% of *Dnmt3L*<sup>matKO</sup> embryos.

Altogether we showed that *Dnmt3L*<sup>matKO</sup> embryos exhibit delayed developmental progression specific to the 2-4 cell cleavage division, associated with reduced implantation fitness.

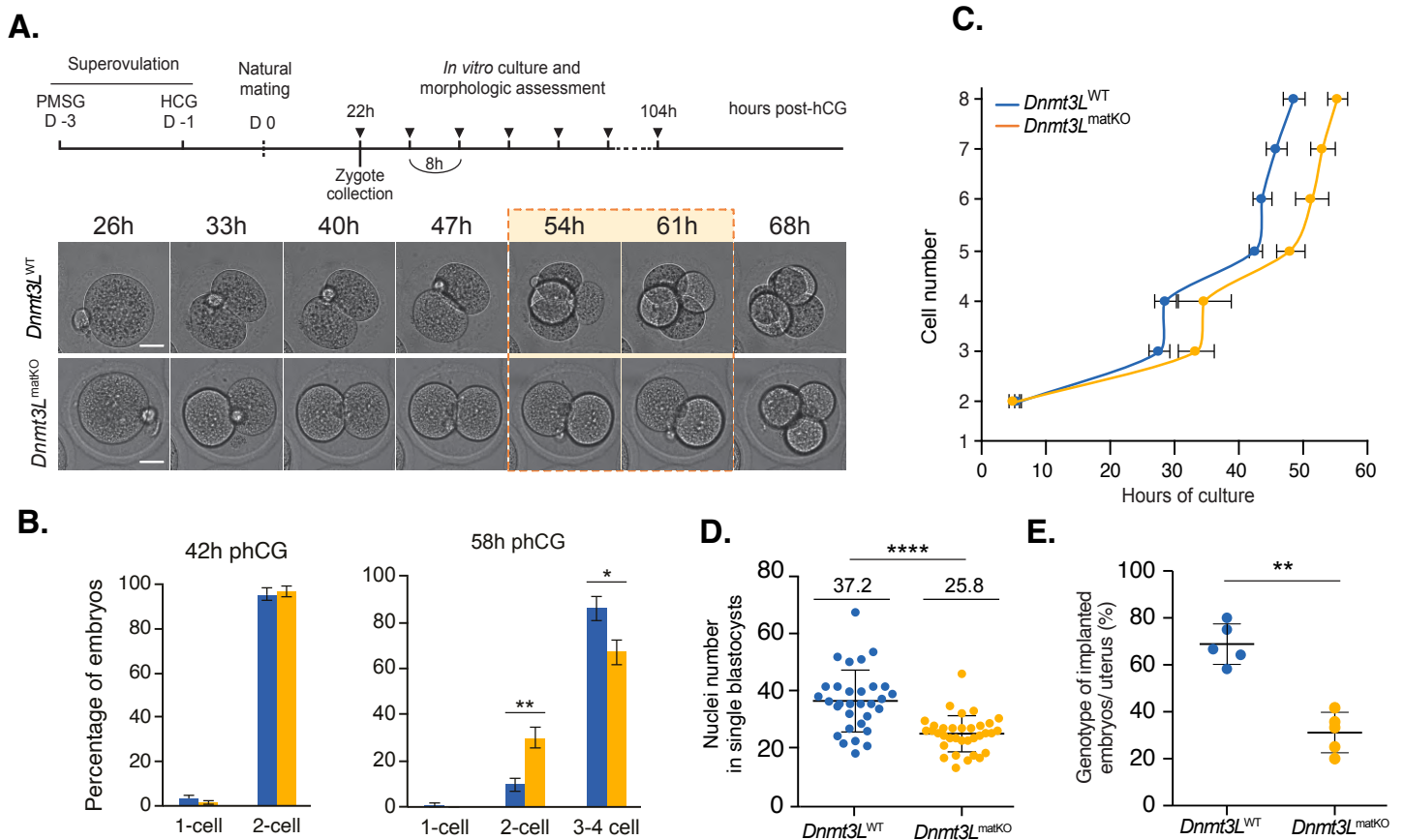


**Figure 8: Developmental delay and fitness decrease in *Dnmt3L*<sup>matKO</sup> embryos.** **A.** Timelapse imaging of *Dnmt3L*<sup>WT</sup> and *Dnmt3L*<sup>matKO</sup> embryos. Schematic of the experimental design and images of one representative embryo per genotype are shown. Scale bars: 25µm. The stage-specific developmental delay at the 2- to 4-cell cleavage division is highlighted. **B.** Bar graph showing the percentage of embryos per developmental stage for each genotype at different hours post-hCG injection (phCG) of *in vitro* culture. ( $n= 570$  WT and  $505$  *Dnmt3L*<sup>matKO</sup> embryos). Mann-Whitney statistical test (\*\*  $p < 0.01$ , \*  $p < 0.05$ ). **C.** Developmental progression of *in vitro* cultured *Dnmt3L*<sup>WT</sup> and *Dnmt3L*<sup>matKO</sup> embryos. Quantification of the number of hours to reach a given developmental stage ( $n=5$  *Dnmt3L*<sup>WT</sup> and  $3$  *Dnmt3L*<sup>matKO</sup> embryos). Only embryos performing all cleavage divisions and developing until the blastocyst stage were included in the analysis. Y axis is set at the beginning of the time course acquisition (26h post-hCG). **D.** Scatterplot comparing the nuclei number of *Dnmt3L*<sup>WT</sup> and *Dnmt3L*<sup>matKO</sup> blastocysts collected at E4.25. The number above the graph represents the mean number. Mann Whitney statistical test ( $n=31$  WT,  $n=34$  matKO, \*\*\*\*  $p < 0.0001$ ). **E.** Dotplot comparing the percentage of *Dnmt3L*<sup>WT</sup> or *Dnmt3L*<sup>matKO</sup> embryos implanted per uterus of a surrogate mother and recovered at E7.5 post-fertilization ( $n=5$  biological replicates, two independent experiments were performed). In total, 54 re-implanted embryos were genotyped and validated, from which 37 and 17 were *Dnmt3L*<sup>WT</sup> and *Dnmt3L*<sup>matKO</sup>, respectively. Mann Whitney statistical test (\*\*  $p < 0.001$ ).

# DISCUSSION



## 1- General conclusion and personal impression

When I started my PhD, the exact function of DNA methylation in oogenesis and preimplantation development was unclear. Even if maternal DNA methylation had been widely studied in the frame of imprinted gene regulation and post-implantation placental formation (Bourc'his et al., 2001), the role of maternally-inherited DNA methylation at earlier stages of development had been poorly studied. The recent discoveries that transient maternal inheritance of histone marks in the preimplantation embryo could play a role in ZGA (Dahl et al., 2018) or in regulating mono-allelic expression of key genes (Inoue et al., 2017), prompted us to investigate the role of maternal DNA methylation heritage for oocyte and preimplantation embryonic development. Furthermore, the oocyte epigenome was shown in recent years to host major interplays between chromatin marks (Hanna et al., 2018; Xu et al., 2019). The concomitant establishment of non-canonical chromatin mark patterns in a non-dividing cells may exacerbate chromatin remodeling upon perturbation of the epigenome. My main work therefore focused on understanding the chromatin reorganization occurring in absence of oocyte DNA methylation and its consequences on oocyte and preimplantation embryo development. Using CUT&RUN (Skene & Henikoff, 2017), which I adapted for chromatin profiling in oocytes, I revealed major changes in H3K4me3 and Polycomb mark patterning in *Dnmt3L*<sup>KO</sup> oocytes, revealing DNA methylation and/or DNMT3L itself as major regulator of the oocyte epigenome. Using RNA-sequencing and developmental analyses, we further studied the impact of maternal DNA methylation loss and of the associated remodeled histone mark patterns on oocyte and preimplantation embryo development. We found that loss of maternal DNA methylation minimally affects oocyte development and transcriptional regulation during oogenesis but induces a developmental delay coupled to enhanced ZGA in the preimplantation embryo, demonstrating for the first time a role of maternal DNA methylation in ZGA and preimplantation development.

I also investigated the impact of H3K27me3 loss on chromatin reorganization and oocyte development. This enabled me to gain insights into the relationships between DNA methylation, H3K4me3 and H3K27me3 in the oocyte epigenome.

Working on these subjects was a rich experience, as they allowed me to discover many aspects of biological research: developmental biology, epigenetics, mouse work, molecular

biology and genomics. Characterizing the remodeling of the *Dnmt3L*<sup>KO</sup> oocyte epigenome was certainly the most exciting part of my PhD, because I enjoyed the technical challenge of having to optimize CUT&RUN for low-input samples and oocytes. Studying the chromatin interplays between DNA methylation, H3K4me3 and Polycomb marks also resonated with a current active area of research on the oocyte epigenome, so that I enjoyed being able to propose ideas and adapt my project along with the new discoveries and publications in the field. Because oocyte development was not a previous field of expertise in the laboratory, I underwent both the challenges and the eagerness of discovering this area of research. This project also required an important number of different mutant mouse lines that were quite challenging to manage, especially in the time of lock-downs and COVID-19 pandemics.

Of course, as such is the way with research in biology, many questions stay unresolved. In the following parts of this discussion, I would like to develop some of them and discuss a number of intriguing observations that I made. I also want to enlighten the perspectives that this study opens for future research directions.

## 2- Transcriptional regulation in the oocyte

### 2.1 – The role of DNA methylation and H3K27me3 in oocyte transcriptional regulation

In this study, we assessed the role of H3K27me3 and DNA methylation in regulating transcriptional activity in the oocyte. We observed a global transcriptome resilience in front of genome-wide loss of DNA methylation or H3K27me3 in the oocyte. Even if DNA methylation and H3K27me3 are usually associated with gene repression, we did not see the overt transcriptional misregulation of genes one could expect upon genome-wide loss of a repressive mark. The resilience of the oocyte transcriptome to the lack of DNA methylation or H3K27me3 could be due to multiple factors :

- 1) Specific transcriptional factors for genes that are normally non-expressed in the first place may be missing in *Dnmt3L*<sup>KO</sup> or *Eed*<sup>CKO</sup> oocytes.

- 2) H3K27me3 and DNA methylation could be non-essential for regulating oocyte transcription but rather be by-products of transcriptional activity. Accordingly, an increasing number of studies tend to indicate that chromatin marks would have only little if any instructive function on transcription but rather serve as readouts of a certain transcriptional status (Hughes et al., 2022; Wang et al., 2022). In particular in the oocyte context, DNA

methylation is known to be secondary to transcriptional elongation through H3K36me3-dependent recruitment and to be globally depleted from promoters (Stewart et al., 2016). Comparatively, mechanisms of H3K27me3 patterning in the oocyte are less well studied but its distribution, away from promoters and widespread in large intergenic domains, suggests little role in transcriptional regulation. Moreover, the notion that H2Aub, and not H3K27me3, would be responsible for initiating gene silencing in the oocyte has been recently advanced through comparative analyses of transcriptome changes in PRC1 and PRC2 mutant oocytes (Du et al., 2020; Chen et al., 2021).

3) Finally, compensatory mechanisms of transcriptional control may exist upon loss of DNA methylation or H3K27me3 in the oocyte. Here we described the highly dynamic redistribution of chromatin marks occurring in DNA methylation-free or H3K27me3-free oocytes. H3K4me3 was shown to invade H3K27me3 territories when the latter is lost (Lu et al., 2021), while we and others demonstrated that DNA methylation-free oocytes display H3K4me3 spreading inside lost DNA methylation domains (Hanna et al., 2018). As ncH3K4me3 was previously shown to be associated with transcriptional silencing in the oocyte epigenome (Andreu-Vieyra et al., 2010), accumulation of H3K4me3 could compensate for the loss of DNA methylation or H3K27me3 and explain the transcriptional resilience of the oocyte epigenome. However, we could not find any correlation between the described chromatin remodeling and the transcriptional status of the genes in the oocyte.

The presence of alternative promoters and non-canonical transcripts also complicates the analysis of gene expression in oocytes. As some genes are expressed in different isoforms spanning common exons, it is sometimes difficult to assess the expression levels of one isoform *versus* the others. It should therefore be pointed that other transcriptional alterations, such as alternative or cryptic promoter usage and alternative splicing, have not been investigated in our analyses and cannot be excluded.

## 2.2 – Oocyte transcriptional shutdown is not affected by the loss of H3K27me3 or DNA methylation

We decided to study the impact of H3K27me3 or DNA methylation loss on the transcriptional status of SN oocytes, because previous studies had shown that in absence of ncH3K4me3, *Mll2*<sup>CKO</sup> oocytes fail to undergo complete transcriptional silencing (Andreu-Vieyra et al., 2010; Zhang et al., 2016). ncH3K4me3 therefore seems essential for transcriptional

shutdown at the end of oogenesis, raising the question of the role of other repressive histone marks for the NSN-to-SN silencing. Surprisingly, we showed that both DNA methylation and H3K27me3 seemed dispensable for complete transcriptional silencing in the SN oocytes: neither *Dnmt3L*<sup>KO</sup>, nor *Eed*<sup>CKO</sup> SN oocytes displayed nascent transcription. This finding is reinforced by the concordant observation that in absence of H3K36me3 and subsequent failure of DNA methylation deposition, silencing in the SN *Setd2*<sup>CKO</sup> oocytes is not affected (Xu et al., 2019). One could therefore conclude that ncH3K4me3 is the only studied chromatin marks that plays a role in the developmentally programmed transcriptional shutdown of the late oocyte. The function of other marks, like H3K9me3, remains to be studied.

Chromatin remodeling have been described by we or others in *Dnmt3L*<sup>KO</sup> (H3K4me3 spreading), *Eed*<sup>CKO</sup> (H3K4me3 spreading) and *Setd2*<sup>CKO</sup> (both H3K4me3 and H3K27me3 spreading) mutants (Xu et al., 2019; Lu et al., 2021; Hanna et al., 2022). These three mutants also seem to exhibit unaffected SN transcriptional silencing. At the opposite, no chromatin remodeling has been described yet in *Mll2*<sup>CKO</sup>, which is the only mutant displaying incomplete transcriptional silencing: DNA methylation was minimally impacted in absence of ncH3K4me3 but H3K27me3 has not been profiled yet (Hanna et al., 2018). This raises the question of the role of chromatin remodeling in compensating the loss of one single mark and ensuring transcriptional shutdown. To answer that question, reorganization of H3K27me3 patterns should be investigated in absence of ncH3K4me3 in *Mll2*<sup>CKO</sup> oocytes. The study of double mutant oocytes, lacking both DNA methylation and H3K4me3 for example, would also be interesting to understand the cumulative and relative role of both marks.

### 2.3 – The puzzling case of transposable element regulation in the oocyte epigenome

While transposable elements (TE) regulation has been widely studied in the male germline, the mechanisms behind their repression and control in the oocytes have always remained unclear. For example, our lab recently demonstrated that male meiosis can proceed in presence of a globally hypomethylated genome but fails during prophase I upon TE loss of DNA methylation and derepression (Barau et al., 2016; Dura et al., 2022). As the first female meiosis prophase occurs before DNA methylation re-establishment, some alternative mechanisms must be controlling TE repression at these stages but the nature of this regulation remains unknown. Huang et al. recently showed that loss of H3K27me3 in pre-natal female germ cells leads to TE derepression and drastic decrease of the pool of oocytes at birth (Huang

et al., 2021). H3K27me3 would then contribute to TE control in the pre-natal stages of oogenesis.

How TE transcriptional control of TE is ensured in the post-natal growing phase of oogenesis, upon establishment of the oocyte epigenome, remains unknown. We analyzed TE expression in *Dnmt3L*<sup>KO</sup> and *Eed*<sup>CKO</sup> RNA-seq datasets but found that only few TEs were marginally misregulated in both conditions (**Figure 1**). Conversely, RT-qPCR analysis showed that IAP elements were abnormally transcribed in *Mll2*<sup>CKO</sup> GV oocytes, in absence of nH3K4me3 (Andreu-Vieyra et al., 2010). RNA-seq analysis would be needed to confirm this observation but this suggests that nH3K4me3, and not DNA methylation or H3K27me3, is playing a role in TE transcriptional regulation in mature oocytes. This assumption is again to consider in the context of chromatin reorganization and potential compensation between chromatin marks.

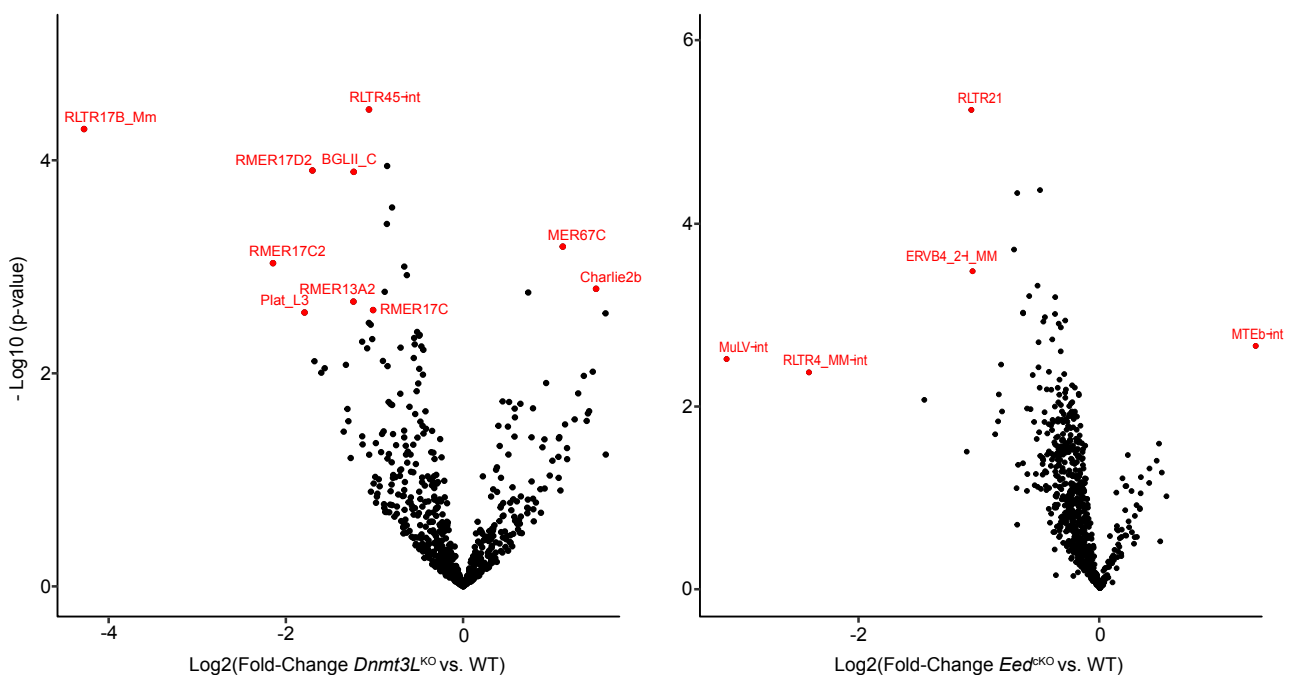


**Figure 1: Minimal transposable element misregulation in *Dnmt3L*<sup>KO</sup> and *Eed*<sup>CKO</sup> oocytes.** Volcano plots showing differential TE RNA levels between single-cell *Dnmt3L*<sup>KO</sup> MII oocytes or bulk *Eed*<sup>CKO</sup> GV oocytes and their respective WT counterparts in log<sub>2</sub> fold-change versus -log<sub>10</sub> p-value. Misregulated TE families are highlighted in red (FDR<5% and FC >2).

## 2.4 – The challenges of studying transcription in the context of oocytes and early embryos

One of the major issue for studying transcriptional regulation in oocytes resides in the fact that oocytes produce a very abundant mRNA pool during the growing phase of oogenesis. The total amount of mRNA present in a GV or MII oocyte is approximately 200 times more important than in an average somatic cell. The half-life of RNAs is also increased in the oocyte due to the action of protective factors, so that discrimination of the gene expression timings becomes more difficult. For a similar RNA sequencing depth, subtle differences in gene expression changes will then be less visible because diluted in the important RNA quantity. In particular, incomplete transcriptional silencing of the oocyte genome at the SN stage or subtle changes in gene expression at ZGA would be hardly visualizable by total RNA sequencing due to the low RNA quantity it would represent compared to the whole pool of maternal mRNAs.

To overcome these limitations, nascent RNA-sequencing would be instrumental to obtain information on the current transcriptional status of oocytes and early embryos. However none of the actual method of nascent RNA-sequencing is optimized for low cell number samples. PRO-seq (precise run-on and sequencing) consists in incorporating biotin-tagged NTPs that halt RNA polymerases and allows, after pull-down of these labeled RNAs, genome-wide profiling of transcriptionally engaged polymerases. It has recently been optimized for down to 250 000 cells but still remains not adapted to the order of magnitude of oocyte input quantities (couple hundreds of cells at most) (Judd et al., 2020). The development of low-input strategies for nascent RNA sequencing would be highly beneficial for the study of oocyte transcriptional status and to enable more precise correlation between chromatin marks modifications and transcriptional changes.

## 3- New insights into DNA methylation, H3K27me3 and H3K4me3 functional relationships

### 3.1 – The overlooked fact: the importance of *spike-in* in chromatin profiling techniques

Chromatin profiling techniques allow to generate genome-wide landscape of histone marks or DNA-binding proteins through selective sequencing of underlying DNA fragments. CUT&RUN indeed relies on antibody-targeted DNA fragmentation and release to specifically sequence DNA fragments bearing a certain feature (Skene & Henikoff, 2017).

The analysis of chromatin sequencing data is typically based on conventional assumptions (Chen et al., 2016). Notably, samples are usually normalized one to another, so that the total amounts of reads from each experimental conditions are identical. This leads to the assumption that the overall yields of DNA to be analyzed are identical between samples (and per cell if the samples contain identical cell number). This assumption is actually already present prior to bioinformatic analyses: when pooling samples together for sequencing, an equimolar mix of samples is performed, which artificially bias the yields of DNA recovery obtained for each sample. However, the assumption that the yields of DNA per cell is identical between compared conditions is far from being always correct. For example, global levels of histone marks can be increased or decreased in WT versus mutant contexts, leading to changes in the amount of DNA per cell recovered by CUT&RUN. One should therefore verify beforehand by quantitative techniques (Immunofluorescence, Western-blot) that the total amount of the profiled chromatin mark is similar in the different experimental conditions. This is actually what we observed in our study: by immunofluorescence, we could see that global H3K4me3 and H3K27me3 levels were increased and decreased in *Dnmt3L*<sup>KO</sup> compared to WT oocytes, respectively.

To avoid normalizing the total number of reads between samples, spike-in DNA normalization strategies can be used (Chen et al., 2016). It consists in the incorporation of a precise quantity of exogenous DNA of known sequence (DNA from another species, artificial DNA...) to each sample. This allows normalizing samples based of the pre-determined quantity of spike-in DNA in the sequencing data. Spike-in DNA normalization therefore allows, beside qualitative assessments of changes in the distribution of a chromatin mark, a quantitative analysis of the enrichment of this mark. This is exactly what we saw in H3K27me3 CUT&RUN in *Dnmt3L*<sup>KO</sup> oocytes: upon normalization to the total amount of reads between samples, H3K27me3 seemed not to be affected, but the use of *Drosophila* spike-in DNA as normalizer revealed consistent genome-wide H3K27me3 decrease in *Dnmt3L*<sup>KO</sup> compared to WT (**Figure 2**), which we also observed by immunofluorescence. A previously published study had profiled H3K27me3 by ChIP-seq and reported that H3K27me3 was globally unaltered in *Dnmt3L*<sup>KO</sup> oocytes (Q. Xu et al., 2019). In absence of spike-in strategy, they indeed failed to identify the genome-wide decrease in H3K27me3 levels (**Figure 2**). This highlights the importance of the use of spike-in normalization strategies.

Conversely, we did not add external spike-in in our H3K4me3 CUT&RUN and were therefore not able to discriminate whether global levels of H3K4me3 were increased in *Dnmt3L*<sup>KO</sup>. We could see aberrant presence of H3K4me3 in ectopic regions but whether it was due to a real accumulation of H3K4me3 or to a spreading of H3K4me3 from other genomic locations could not be defined by CUT&RUN. Only immunofluorescence analysis indicated a real increase in the total levels of H3K4me3.

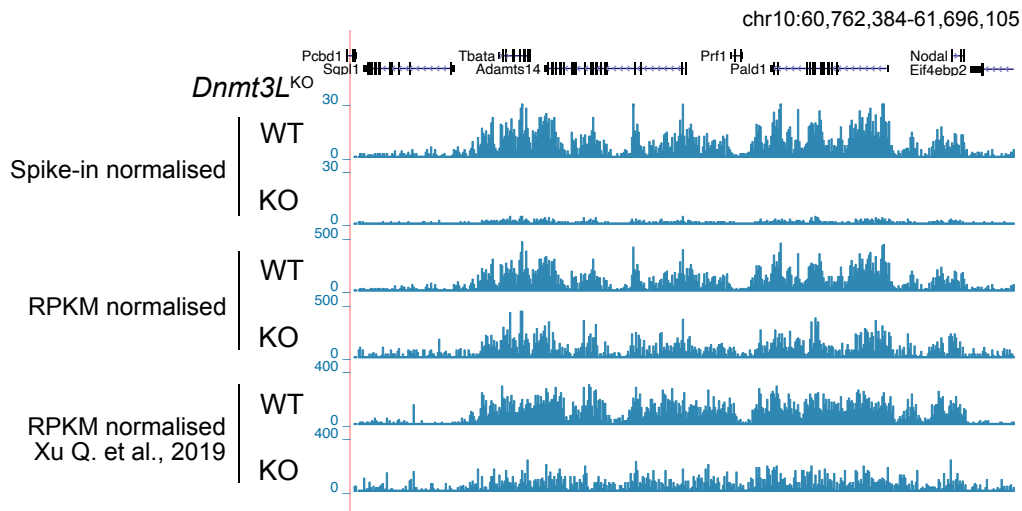


**Figure 2 : H3K27me3 decrease in *Dnmt3L*<sup>KO</sup> oocytes is visible only with spike-in normalization.** UCSC browser screenshot of our H3K27me3 CUT&RUN in WT and *Dnmt3L*<sup>KO</sup> oocytes normalized with spike-in strategy or by RPKM. UCSC screenshot of published H3K27me3 STAR-ChIP-seq normalized by RPKM (Xu Q. et al., 2019)

### 3.2 – H3K4me3 accumulation in absence of DNA methylation at the NSN-to-SN transition

Our study revealed genome-wide accumulation of H3K4me3 in *Dnmt3L*<sup>KO</sup> oocytes at regions usually enriched in DNA methylation, when this mark is absent. This observation is concordant with a recently published paper that showed H3K4me3 spreading in *Dnmt3A/B* double-knockout GV oocytes (Hanna et al., 2018).

We noticed that only 20% of *Dnmt3L*<sup>KO</sup> DMRs showed ectopic H3K4me3 gain, and these were characterized by a higher CG content than non-invaded DMRs. This is consistent with the known targeting of MLL2 enzyme—responsible for nH3K4me3 deposition in the oocyte—to unmethylated CpG-rich regions (Birke et al., 2002). DNA methylation would then protect regions from ectopic MLL2 activity to methylated CpG-rich regions.

The dynamics of H3K4me3 spreading to intragenic hypomethylated regions is also very relevant to the context of cancer cells. Intragenic DNA hypomethylation has been shown to be a hallmark of cancer cells and potentially a key factor in promoting carcinogenesis through abnormal transcript expression (Gaudet et al., 2003; Duns et al., 2010). The notion that DNA methylation loss could also be associated with ectopic H3K4me3 accumulation H3K4me3 would be interesting to study. Loss of DNA methylation could allow binding of DNA methylation-sensitive transcription factors, while H3K4me3 or SETD2 H3K4 methyltransferase could contribute to recruit RNAPII for initiating transcription at aberrant cryptic promoters. The respective and cumulative role of DNA methylation loss or potential H3K4me3 gain in promoting spurious transcription of oncogenes would need to be investigated.

Our study also revealed that H3K4me3 invasion of abnormally hypomethylated regions specifically occurs at the NSN-to-SN transition. Significant accumulation of H3K4me3 was present in *Dnmt3L*<sup>KO</sup> oocytes at the SN stage only. As DNA methylation is considered to be established prior to the NSN stage in WT conditions, it is surprising that its loss impacts H3K4me3 deposition only later during oogenesis. DNA methylation and ncH3K4me3 being deposited concomitantly during the growing phase of oogenesis, we could have expected to see ectopic H3K4me3 progressively spreading while DNA methylation fails to be established. This means that chromatin changes that are specific to the NSN-to-SN transition might be required for ectopic MLL2 recruitment. The genome-wide transcriptional silencing that occurs at this stage could provide favorable chromatin environment and players. To test this, inhibition of RNA polymerase II, through alpha-amanitin treatment in NSN *Dnmt3L*<sup>KO</sup> oocytes, would enable us to test whether transcriptional silencing is required for H3K4me3 ectopic spreading in GC-rich domains that fail to be DNA methylated.

In a more general manner, the generation of CUT&RUN in sorted NSN and SN oocytes separately enabled us to gain unsuspected insights into the chromatin changes associated with the NSN-to-SN transition. We were able to identify changes that the chromatin landscape specifically undergoes between the NSN and SN stages during WT oogenesis: the number of H3K27me3-enriched and bivalent H3K27me3-H3K4me3 domains naturally decrease at the SN stage, while H3K4me3 seems to be gained at a limited set of regions. In particular, bivalent domains tend to resolve in H3K27me3- or H3K4me3-only regions. This dynamics is consistent with previously described reduction in the number of bivalent domains observed at the MII

stage (Lu et al., 2021), indicating that it actually appears earlier in oogenesis, at the time of transcriptional shutdown. Understanding the molecular mechanisms behind these chromatin remodeling at the NSN-to-SN transition could also allow defining why H3K4me3 accumulation in *Dnmt3L*<sup>KO</sup> oocytes appears at this stage specifically.

### 3.3 – DNA methylation – Polycomb marks : unusual relationships in the oocyte context

H3K27me3 and DNA methylation have been shown to have compensatory dynamics in different types of somatic cells. In ES cells for example, H3K27me3 spreads upon loss of DNA methylation, while aberrant DNA methylation is conversely observed in absence of H3K27me3 (Brinkman et al., 2012; Walter et al., 2016; Li et al., 2018). We hypothesized that similar dynamics may occur in the oocyte context and therefore reciprocally profiled H3K27me3 in *Dnmt3L*<sup>KO</sup> oocytes and DNA methylation in H3K27me3-free oocyte (*Eed*<sup>CKO</sup>). We could not detect ectopic gain of H3K27me3 or DNA methylation in *Dnmt3L*<sup>KO</sup> or *Eed*<sup>CKO</sup> oocytes respectively, suggesting that different interplays apply between the two marks in the oocyte context.

Interestingly, H3K27me3 was previously shown to spread in absence of both H3K36me3 and DNA methylation in *Setd2*<sup>CKO</sup> oocytes, where both marks severely altered (Q. Xu et al., 2019). Comparatively, we did not detect H3K27me3 increase in *Dnmt3L*<sup>KO</sup> oocytes, where although DNA methylation is deficient, H3K36me3 was shown to be unaltered (**Figure 3**) (Q. Xu et al., 2019). This strongly suggests that H3K36me3, and not DNA methylation, plays a role in excluding H3K27me3. As H3K36me2/me3 and DNA methylation almost perfectly co-occur genome-wide, it has always been difficult to deduce the relative importance of H3K36me2/me3 versus DNA methylation in the inhibition of H3K27me3. We provide here the demonstration that H3K36 methylation, but not DNA methylation, is the master regulator of for confining Polycomb marks to specific territories. Conversely, DNA methylation loss is sufficient to trigger H3K4me3 accumulation in previously hypermethylated regions in oocytes, independently of the H3K36me3 status. DNA methylation seems therefore to restrain H3K4me3 deposition, while H3K36me3 mediates H3K27me3 antagonism.

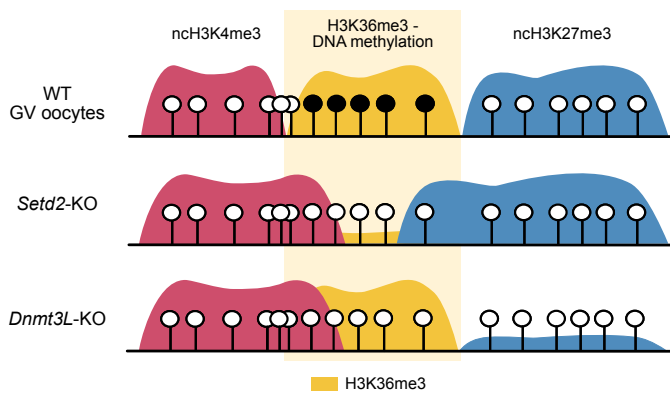


**Figure 3 : H3K27me3 deposition is restricted by H3K36me3, and not DNA methylation, in the oocyte.** H3K27me3 is spreading in absence of both H3K36me3 and DNA methylation in *Setd2*<sup>CKO</sup> oocytes but not in *Dnmt3L*<sup>KO</sup> oocytes. H3K4me3 accumulates in previously hypermethylated regions in both conditions.

H3K36me3 was also shown to play a predominant role in excluding H3K27me3 from actively transcribed units in prospermatogonia (Shirane et al., 2020). This raises some questions regarding the supposed DNA methylation–H3K27me3 antagonism in somatic cells: could it also be mediated by H3K36me3 ?

At the opposite of the expected H3K27me3 spreading, we observed a decrease in H3K27me3 at previously enriched regions in *Dnmt3L*<sup>KO</sup> oocytes (Figure 3). This was accompanied by a genome-wide H2Aub loss, observed by immunofluorescence. The presence of an H3K27me3 decrease upon loss of DNA methylation was really surprising and opens new questions on their functional relationships in the oocyte context. I will try here to explain our current hypothesis regarding the potential molecular mechanisms linking DNMT3L depletion and Polycomb mark reduction.

- Molecular mechanisms behind Polycomb mark reduction observed in *Dnmt3L*<sup>KO</sup> oocytes

PRC2-deposited H3K27 methylation and PRC1-deposited H2Aub are known to be tightly linked: H3K27me3 and H2Aub patterns are largely overlapping in the oocyte and H2Aub was recently shown to act upstream of H3K27me3 during preimplantation development (Mei et al., 2021; Chen et al., 2021). Most importantly, H2Aub loss was previously shown to lead to H3K27me3 decrease in *Pcgf1/6*<sup>dKO</sup> oocytes (Mei et al., 2021). In contrast, H3K27me3 depletion in *Eed*<sup>CKO</sup> oocytes minimally disrupts H2Aub patterns (Chen et al., 2021). We now aim at confirming that H2Aub levels are unaffected in absence of H3K27me3 in *Eed*<sup>CKO</sup> oocytes by immunofluorescence. In this case, we could consider the observed H2Aub decrease in *Dnmt3L*<sup>KO</sup> oocytes as a cause rather than a consequence of H3K27me3 decrease.

According to our CUT&RUN data, the strong decline in H3K27me3 becomes significant in *Dnmt3L*<sup>KO</sup> oocytes at the NSN-to-SN transition. This implies that H3K27me3 may be properly catalyzed by PRC2 in *Dnmt3L*<sup>KO</sup> oocytes, but then lost. Moreover, as oocytes are non-dividing cells (meiotically arrested), it suggests the existence of an active mechanism of H3K27me3-H2Aub removal in SN oocytes. It is noteworthy that we also observed a physiological decrease in the number of H3K27me3 enriched-regions at the NSN-to-SN transition in WT conditions. Whether H2Aub is also remodeled at the NSN-to-SN in WT conditions is unknown. This dynamics of Polycomb reduction could be strengthened in absence of DNMT3L and/or DNA methylation.

As an attempt to understand the origin of Polycomb reduction in *Dnmt3L*<sup>KO</sup> oocytes, we investigated expression levels of known Polycomb modifying actors in our RNA-seq data from MII oocytes. We did not detect transcriptional mis-regulation of the genes encoding the complexes that establish Polycomb marks (PRC1 and PRC2 components) or H3K27me3 demethylases of *Dnmt3L*<sup>KO</sup> MII oocytes. We could only detect an up-regulation of *Bap1*, the core component of the recently described H2Aub deubiquitinylase (PR-DUB) complex (Campagne et al., 2019; Kolovos et al., 2020). This may suggest the existence of an active mechanism of H2Aub removal, which may be enhanced in *Dnmt3L*<sup>KO</sup> MII oocytes and cause the observed decrease in Polycomb marks. To test this hypothesis, we will try to further optimize H2Aub CUT&RUN in GV oocytes, to verify its decrease and profile its distribution in *Dnmt3L*<sup>KO</sup> oocytes. We will also try to gain insights into the temporal dynamic of H2Aub decrease to see whether it precedes H3K27me3 loss. Finally, we are planning to generate BAP1 immunofluorescence in *Dnmt3L*<sup>KO</sup> oocytes to see whether the observed decrease at the RNA level coincides with a reduction at the protein level.

We would then need to investigate whether the absence of DNMT3L protein itself or the loss of DNA methylation mark is responsible for Polycomb mark reduction. In *Dnmt3L*<sup>KO</sup> oocytes, H3K27me3 decrease does not occur at domains that normally carry DNA methylation, so if H3K27me3/H2Aub loss is linked to the loss of the DNA methylation mark, this likely occurs in an indirect manner. For example, it could be that the lack of DNA methylation induces the overexpression of an H2Aub or H3K27me3 demethylase, or the overexpression of a protein that may normally sequester these demethylases. Indeed, increasing numbers of studies have shown that the subcellular localization of chromatin modifiers is tightly controlled in the

oocyte context. For example, DNMT3A was shown to be dependent on the transcription factor SALL4 to enable its nuclear localization and a Stella-dependent nuclear export mechanism controls DNMT1 subcellular localization outside of the nucleus (Xu et al., 2017; Li et al., 2018). It would therefore be important to study if the subcellular localization of polycomb-related proteins is affected. Concerning a role of the DNMT3L protein itself, previous studies have proposed a role of DNMT proteins independently of their catalytic activity, as mediators of transcriptional silencing complex recruitment (Geiman et al., 2004; Nowialis et al., 2019). Immunoprecipitation experiments showed for example that DNMT3B is able to interact with histone deacetylase complexes, HP1 proteins and H3K9 methylase (SUV39H1) (Geiman et al., 2004). The long isoform of DNMT3A, not expressed in the oocyte, was also recently shown to bind to H2Aub through its N-terminal domain (Gu et al., 2022). DNMT3L could therefore also interact with some histone PR-DUB components, acting on their stability or their cellular trafficking. To distinguish between DNA methylation and the DNMT3L protein, we want to assess whether H3K27me3 and H2Aub reduction is recapitulated in *Dnmt3A*<sup>CKO</sup> oocytes, which harbor the same hypomethylation phenotype, but with intact DNMT3L protein. In theory, this could discriminate whether the absence of the DNMT3L protein itself plays a role in H3K27me3/H2Aub decrease. One caveat is that DNMT3A and DNMT3L may both interact with the same chromatin modifier as part of the same complex, therefore the observation of potential H2Aub/H3K27me3 reduction in *Dnmt3A*<sup>CKO</sup> oocytes may be difficult to interpret.

## 4- Maternal epigenetic heritage and zygotic genome activation

### 4.1 – Developmental role for maternal DNA methylation in preimplantation embryos

The role of maternal DNA methylation has been widely studied during post-implantation development in the context of imprinted genes. Proper maternal DNA methylation patterns at imprinted regions are essential for placental and embryonic development beyond E10.5. Impairment of maternal DNA methylation establishment at ICRs in oocytes (through *Dnmt3A* or *Dnmt3L* knockouts) or failure in the maintenance of maternal ICRs methylation in embryos (*Zfp57* or *Kap1* knockouts) both result in embryonic lethality due to major dysregulation of imprinted genes and placental malformation (Bourc'his et al., 2001; Li et al., 2008; Messerschmidt et al., 2012).

However, the role of maternal DNA methylation upon transmission to the preimplantation embryo before genome-wide reprogramming had never been properly

studied. Indeed, DNA maternal DNA methylation patterns are transmitted to the embryo upon fertilization before being progressively erased during the cleavage divisions (Proudhon et al., 2012). The majority of those germline DMRs lose maternal methylation before implantation but it is not well understood how they could affect preimplantation development: they could play a role in transiently regulating mono-allelic expression of genes or by guiding the establishment of zygotic epigenetic patterns.

Here we showed for the first time that disruption of maternal DNA methylation and its associated chromatin remodeling could affect preimplantation development and implantation, independently of long-lasting maternal DNA methylation inheritance. Indeed, *Dnmt3L*<sup>matKO</sup> embryos display enhanced transcription at ZGA and a concomitant developmental delay, associated with decreased implantation success. This observation is coherent with an increasing number of recent studies that converged toward demonstrating a role for maternally inherited chromatin marks in preimplantation development. Notably, maternal H2Aub and nH3K4me3 are instrumental for ZGA regulation (Chen et al., 2021; Dahl et al., 2018), while maternal H3K27me3 is essential for controlling mono-allelic *Xist* expression and imprinted XCI (Inoue et al., 2018). Altogether, this highlights the importance and underestimated role of maternal epigenetic heritage before its reprogramming during preimplantation development.

#### 4.2 – What could cause increased transcription at minor ZGA in *Dnmt3L*<sup>matKO</sup> embryos?

In this study, we identified that *Dnmt3L*<sup>matKO</sup> embryos exhibit an heightened minor ZGA at the late zygote stage. Active transcriptional activity was enhanced at this time specifically and resulted in increased levels of total mRNAs at the two-cell stage. Multiple factors could explain this ZGA increase in *Dnmt3L*<sup>matKO</sup> embryos, and I am going to review here our current working hypothesis :

- Remodeling of maternal chromatin patterns could affect ZGA in *Dnmt3L*<sup>matKO</sup> embryos

First, minor ZGA could be influenced by abnormal maternally inherited chromatin patterns. Indeed, we showed that *Dnmt3L*<sup>KO</sup> females transmit upon fertilization a modified epigenome : lack of DNA methylation, H3K4me3 ectopic accumulation and Polycomb mark decrease. In normal conditions, three marks are known to keep their maternally-inherited patterns at least until the late two-cell stage, before being reprogrammed in canonical somatic

patterns with different dynamics (Wang et al., 2014; Zhang et al., 2016; Zheng et al., 2016). Although we need to confirm this, notably for Polycomb marks, altered maternal chromatin patterns inherited from *Dnmt3L*<sup>KO</sup> oocytes are likely to be still present at the time of zygotic genome activation and could influence its execution.

In particular, loss of maternal H2Aub has been previously associated with premature activation of developmental genes at ZGA (Chen et al., 2021). Perturbation of maternal H3K4me3 transmission and reprogramming was also associated with impaired ZGA (Dahl et al., 2016). ZGA genes are indeed known to be enriched in maternal nH3K4me3 domains. It was previously suggested that, while nH3K4me3 is associated with gene repression in the oocyte, it could be poisoning genes for future activation at ZGA (Dahl et al., 2016). Altogether, this indicates that modifications of the maternal chromatin state could impact gene activation in the zygote. Both nH3K4me3 ectopic accumulation and Polycomb mark decrease, present on the *Dnmt3L*<sup>KO</sup> maternal genome, could lead to gene over-activation and explain heightened ZGA.

We analyzed the chromatin state at promoter regions of genes misregulated from the maternal allele in two-cell *Dnmt3L*<sup>KO</sup> embryos but could not detect any clear correlation between H3K4me3, H3K27me3 or DNA methylation changes. However, this analysis presents several caveats. First, correlation was performed with oocyte chromatin patterns by assuming that they are identically maintained in the early embryo. Performing CUT&RUN against H3K4me3 and H3K27me3 directly in the embryo would enable us to have more accurate information on the chromatin state at the time of ZGA. Secondly, the analysis was performed by using scRNA-seq data from two-cell stage embryos. We detected increased transcriptional activity already during the minor ZGA wave in zygotes, meaning that the gene misregulation present at the two-cell stage could be due to secondary effects and not directly linked to maternal chromatin pattern reorganization. We could not use our scRNA-seq data from *Dnmt3L*<sup>KO</sup> zygotes to perform this analysis because of its lower sequencing quality. We are therefore planning to generate a new bulk RNA-seq in *Dnmt3L*<sup>matKO</sup> zygotes.

Finally, we only analyzed here the promoter regions of misregulated genes, while an increasing number of studies are highlighting the role of chromatin marks at enhancer regions. Modification of chromatin patterns at enhancers could influence transcription-factor binding and have an impact of the transcriptional firing of genes. For example, DNA methylation-

sensitive transcription factors are known to gain novel binding sites in DNA methylation deficient ESCs or male germ cells (Domcke et al., 2015; Yin et al., 2017; Dura et al., 2022), which are associated with appearance of *de novo* H3K27ac-enriched enhancers. Profiling H3K27ac, the mark of active regulatory elements, or chromatin accessibility (by ATAC-seq) at the time of minor ZGA in *Dnmt3L*<sup>KO</sup> zygotes could allow identifying active enhancers and to analyze whether their appearance correlates with specific chromatin changes in *Dnmt3L*<sup>matKO</sup> zygotes.

Following that theory, we would expect expression from the maternal genome only to be affected, as it is the parental genome that bears altered chromatin patterns in *Dnmt3L*<sup>matKO</sup> embryos. However, we observed increased EU incorporation and chromatin accessibility (DNase assay) from both the maternal and paternal pronucleus, suggesting that increased nascent transcription is likely due to transactivation, as opposed to a direct effect of the remodeling of chromatin patterns on the maternal allele.

- Transcriptional kindling of ZGA through *Dux* overexpression in *Dnmt3L*<sup>matKO</sup> embryos

The observation that transcriptional changes similarly affect the two parental pronuclei suggests a transactivating mechanism behind ZGA increase in *Dnmt3L*<sup>matKO</sup> embryos. Excessive maternal expression of a minor ZGA transactivator could provoke an exacerbated bi-allelic transcriptional response by opening the chromatin and leading to a more active transcriptional status.

We indeed identified the *Dux* transcription factor family as a good candidate for mediating the ZGA increase in *Dnmt3L*<sup>matKO</sup> embryos. Induced expression of *Dux* in ESCs provokes the transcriptional activation of genes and transposable elements normally expressed at ZGA in the two-cell stage embryo (De Iaco et al., 2017; Hendrickson et al., 2017). *Dux* overexpression further promotes ESCs to enter a the 2-cell-like (2C-like) state, a rare subpopulation that recapitulate characteristics of the 2-cell embryo by mimicking its transcriptional signature. Additionally, in humans, DUX4 has been shown to act as a pioneer factor by recruiting p300/CBP histone acetyltransferases provoking H3K27 acetylation, chromatin opening, and increased H3K4me3 at previously inaccessible target loci in immortalized myoblasts (Choi et al., 2016).

*Duxf1, Duxf2, Duxf3 and Duxf5* are all overexpressed in *Dnmt3L<sup>matKO</sup>* embryos relative to WT specifically at the 2-cell stage. We noticed that this overexpression is associated with a decrease in H3K27me3 at the *Dux* locus in *Dnmt3L<sup>KO</sup>* oocytes. We are currently trying to confirm that this H3K27me3 loss is transmitted to the zygotes by performing CUT&RUN against H3K27me3 in *Dnmt3L<sup>matKO</sup>* zygotes. If it is the case, decreased maternally-inherited H3K27me3 levels could be responsible for increased or premature activation of the *Dux* maternal allele. It would of course be interesting to gain allelic information on *Dux* expression in WT and *Dnmt3L<sup>matKO</sup>* embryos but the poor mappability of the locus will make this kind of SNP-based analysis very challenging. Nonetheless, we plan on performing CUT&RUN in hybrid *Dnmt3L<sup>matKO</sup>* zygotes (resulting from crosses between *Dnmt3L<sup>KO</sup>* C57Bl6/J mothers and castaneus fathers to allow allelic distinction).

Of course, the two proposed theories are not necessarily mutually-exclusive: remodeling of the maternal chromatin patterns in early embryos could impact expression of a certain number genes, including overexpression of *Dux* through H3K27me3 decrease at its locus. The increased *Dux* activity, together with more permissive chromatin environment, could concomitantly contribute to increased ZGA.

#### 4.3 – Increased RNA production and developmental delay

The timing of the developmental delay, observed at the 2- to 4-cell divisions in *Dnmt3L<sup>matKO</sup>* embryos, coincides with major ZGA timing. This temporal coincidence may suggest that the developmental delay is caused by hypertranscription at ZGA. Aberrant rates of nascent transcription or the accumulation of excessive levels of total RNA might result in a lengthening of the cell cycle. In particular, excessive transcription might need to be controlled to avoid transcription-dependent replication stress. This could be mediated by similar mechanisms than the one described at the mid-blastula transition in flies. Indeed, in *Drosophila*, a functional DNA replication checkpoint was shown to coordinate cell cycle remodeling and ZGA by slowing DNA replication machinery at transcriptionally engaged loci (Blythe & Wieschaus, 2015). In mammals, ZGA also coincides with a period of prolonged cell cycle: the blastomeres divide every 24 hours until the four cell-stage, after which the cell cycle accelerates. This potentially suggests the existence of a transcription-dependent negative feedback on cell division at this stage.

Overactivation of the DUX-dependent pathway could also be associated with a developmental delay. Both *Dux* deletion (De Iaco et al., 2020; Bosnakovski et al., 2021) and its uncontrolled expression, either in levels or timing (Guo et al., 2019), affect ZGA occurrence and embryonic progression resulting in developmental impairment and sub-lethality. Specifically, prolonged *Dux* expression after mRNA injection or inhibition of its degradation using proteasome inhibitors result in embryonic developmental delay in culture, with an increased percentage of embryos stuck at the 2-cell and 3-cell stages (Guo et al., 2019). Excessive endogenous dosage of *Dux*, as we here report in *Dnmt3L*<sup>matKO</sup> embryos, could cause the 2-cell stage delay, and further provoke suboptimal implantation rate. However, it is not yet known whether the developmental defects are a direct consequence the excess of *Dux*, or the subsequent global consequences in transcription. An abnormally opened chromatin conformation or the redistribution of chromatin marks in the maternal allele could also influence the developmental progression of the embryo. The dependency of the delay phenotype upon *Dux* overexpression could be tested by *Dux* mRNA injection in WT zygotes.

#### 4.4 – Significance for the field of reproductive medicine

The notion that modified maternal epigenetic heritage can impact the early embryonic program is also interesting for the field of reproductive medicine. Here we showed that the loss of DNMT3L, a key actor of maternal epigenome establishment, results in reorganization of chromatin patterns transmitted from the oocyte, associated with impaired ZGA and delayed developmental rate in the progeny. We showed that this phenotype can also be related to a decrease in the embryo implantation, raising questions about the significance of these observations for subfertility phenotypes in women.

In our study, perturbation of a single chromatin mark, like DNA methylation, induced remodeling of the whole maternal epigenome. Minor perturbation in the dynamics of oocyte epigenome establishment through ART procedures or pathological conditions could therefore have unexpected drastic consequences.

We also demonstrated that the transmission of abnormal maternal heritage can be associated with early developmental defects, which would be considered as cases of in- or sub-fertility in women. Indeed, *Dnmt3L*<sup>matKO</sup> embryos display aberrant ZGA and early developmental delay, leading to decreased embryos fitness for implantation. This observation is coherent with an increasing number of recent studies that started to demonstrate a role for

maternal chromatin marks in preimplantation development ([Chen et al., 2021](#); [Dahl et al., 2018](#); [Inoue et al., 2018](#)). Maternal epigenetic heritage perturbations could therefore be responsible for cases of subfertility due to preimplantation development defects or decreased implantation rates.

In particular, a study showed that superovulation may alter expression and nuclear localization of DNMT3A, 3B and DNMT1 in oocytes and early embryos, in a gonadotropin dosage-dependent manner ([Uysal et al., 2017](#)). As demonstrated in our study, correct expression of DNMTs is critical for establishing not only DNA methylation, but proper chromatin patterns in oocytes. As our study contributes to determine the significance of *Dnmt3L* gene mis-regulation for the developmental potential of oocytes and embryos, it could help to gain insights into the current concern of ART-related epigenetic anomalies. As this field continues to develop, it will become more clear whether epigenetic patterns established during oogenesis may influence preimplantation development and whether early epigenetic reprogramming events are susceptible to perturbation by external factors or ART procedures.



# REFERENCES



- Abe, K. ichiro, Funaya, S., Tsukioka, D., Kawamura, M., Suzuki, Y., Suzuki, M. G., Schultz, R. M., & Aoki, F. (2018). Minor zygotic gene activation is essential for mouse preimplantation development. *Proceedings of the National Academy of Sciences of the United States of America*, *115*(29), E6780–E6788. <https://doi.org/10.1073/pnas.1804309115>
- Abe, T., Kiyonari, H., Shioi, G., Inoue, K. I., Nakao, K., Aizawa, S., & Fujimori, T. (2011). Establishment of conditional reporter mouse lines at ROSA26 locus for live cell imaging. *Genesis*, *49*(7), 579–590. <https://doi.org/10.1002/dvg.20753>
- Adhikari, D., & Liu, K. (2013). *The regulation of maturation promoting factor during prophase I arrest and meiotic entry in mammalian oocytes*. <https://doi.org/10.1016/j.mce.2013.07.027>
- Allen, M. D., Grummitt, C. G., Hilcenko, C., Min, S. Y., Tonkin, L. M., Johnson, C. M., Freund, S. M., Bycroft, M., & Warren, A. J. (2006). Solution structure of the nonmethyl-CpG-binding CXXC domain of the leukaemia-associated MLL histone methyltransferase. *EMBO Journal*, *25*(19), 4503–4512. <https://doi.org/10.1038/SJ.EMBOJ.7601340>
- Almeida, M., Pintacuda, G., Masui, O., Koseki, Y., Gdula, M., Cerase, A., Brown, D., Mould, A., Innocent, C., Nakayama, M., Schermelleh, L., Nesterova, T. B., Koseki, H., & Brockdorff, N. (2017). PCGF3/5-PRC1 initiates Polycomb recruitment in X chromosome inactivation. *Science (New York, N.Y.)*, *356*(6342), 1081–1084. <https://doi.org/10.1126/SCIENCE.AAL2512>
- Ancelin, K., Syx, L., Borensztein, M., Ranisavljevic, N., Vassilev, I., Briseño-Roa, L., Liu, T., Metzger, E., Servant, N., Barillot, E., Chen, C. J., Schüle, R., & Heard, E. (2016). Maternal LSD1/KDM1A is an essential regulator of chromatin and transcription landscapes during zygotic genome activation. *ELife*, *5*(FEBRUARY2016). <https://doi.org/10.7554/ELIFE.08851>
- Andreu-Vieyra, C. V., Chen, R., Agno, J. E., Glaser, S., Anastassiadis, K., Stewart Francis, A., & Matzuk, M. M. (2010). MLL2 is required in oocytes for bulk histone 3 lysine 4 trimethylation and transcriptional silencing. *PLoS Biology*, *8*(8), 53–54. <https://doi.org/10.1371/journal.pbio.1000453>
- Aranda, S., Mas, G., & Di Croce, L. (2015). Regulation of gene transcription by Polycomb proteins. *Science Advances*, *1*(11), 1–16. <https://doi.org/10.1126/sciadv.1500737>
- Ardehali, M. B., Mei, A., Zobeck, K. L., Caron, M., Lis, J. T., & Kusch, T. (2011). Drosophila Set1 is the major histone H3 lysine 4 trimethyltransferase with role in transcription. *EMBO Journal*, *30*(14), 2817–2828. <https://doi.org/10.1038/emboj.2011.194>
- Artus, J., & Cohen-Tannoudji, M. (2008). Cell cycle regulation during early mouse embryogenesis. *Molecular and Cellular Endocrinology*, *282*(1–2), 78–86. <https://doi.org/10.1016/j.mce.2007.11.008>
- Au Yeung, W. K., Brind'Amour, J., Hatano, Y., Yamagata, K., Feil, R., Lorincz, M. C., Tachibana, M., Shinkai, Y., & Sasaki, H. (2019). Histone H3K9 Methyltransferase G9a in Oocytes Is Essential for Preimplantation Development but Dispensable for CG Methylation Protection. *Cell Reports*, *27*(1), 282–293.e4. <https://doi.org/10.1016/j.celrep.2019.03.002>
- Auclair, G., Guibert, S., Bender, A., & Weber, M. (2014). Ontogeny of CpG island methylation and specificity of DNMT3 methyltransferases during embryonic development in the mouse. *Genome Biology*, *15*(12), 545. <https://doi.org/10.1186/S13059-014-0545-5/FIGURES/7>
- Balakier, H., & Pedersen, R. A. (1982). Allocation of cells to inner cell mass and trophectoderm lineages in preimplantation mouse embryos. *Developmental Biology*, *90*(2), 352–362. [https://doi.org/10.1016/0012-1606\(82\)90384-0](https://doi.org/10.1016/0012-1606(82)90384-0)
- Bannister, A. J., Schneider, R., Myers, F. A., Thorne, A. W., Crane-Robinson, C., & Kouzarides, T. (2005). Spatial distribution of di- and tri-methyl lysine 36 of histone H3 at active genes. *Journal of Biological Chemistry*, *280*(18), 17732–17736. <https://doi.org/10.1074/jbc.M500796200>
- Bannister, A. J., Zegerman, P., Partridge, J. F., Miska, E. A., Thomas, J. O., Allshire, R. C., & Kouzarides, T. (2001). Selective recognition of methylated lysine 9 on histone H3 by the HP1 chromo domain. *Nature*, *410*(6824), 120–124. <https://doi.org/10.1038/35065138>
- Barau, J., Teissandier, A., Zamudio, N., Roy, S., Nalesso, V., Héroult, Y., Guillou, F., & Bourc'his, D. (2016). The DNA methyltransferase DNMT3C protects male germ cells from transposon activity. *Science (New York, N.Y.)*, *354*(6314), 909–912. <https://doi.org/10.1126/SCIENCE.AAH5143>

- Barcroft, L. C., Offenberg, H., Thomsen, P., & Watson, A. J. (2003). Aquaporin proteins in murine trophectoderm mediate transepithelial water movements during cavitation. *Developmental Biology*, 256(2), 342–354. [https://doi.org/10.1016/S0012-1606\(02\)00127-6](https://doi.org/10.1016/S0012-1606(02)00127-6)
- Baubec, T., Colombo, D. F., Wirbelauer, C., Schmidt, J., Burger, L., Krebs, A. R., Akalin, A., & Schübeler, D. (2015). Genomic profiling of DNA methyltransferases reveals a role for DNMT3B in genic methylation. *Nature*, 520(7546), 243–247. <https://doi.org/10.1038/nature14176>
- Baudat, F., Manova, K., Yuen, J. P., Jasin, M., & Keeney, S. (2000). Chromosome Synapsis Defects and Sexually Dimorphic Meiotic Progression in Mice Lacking Spo11. *Molecular Cell*, 6(5), 989–998. [https://doi.org/10.1016/S1097-2765\(00\)00098-8](https://doi.org/10.1016/S1097-2765(00)00098-8)
- Bennabi, I., Terret, M. E., & Verlhac, M. H. (2016). Meiotic spindle assembly and chromosome segregation in oocytes. *Journal of Cell Biology*, 215(5), 611–619. <https://doi.org/10.1083/jcb.201607062>
- Bernstein, B. E., Kamal, M., Lindblad-Toh, K., Bekiranov, S., Bailey, D. K., Huebert, D. J., McMahon, S., Karlsson, E. K., Kulbokas, E. J., Gingeras, T. R., Schreiber, S. L., & Lander, E. S. (2005). Genomic maps and comparative analysis of histone modifications in human and mouse. *Cell*, 120(2), 169–181. <https://doi.org/10.1016/j.cell.2005.01.001>
- Bernstein, B. E., Mikkelsen, T. S., Xie, X., Kamal, M., Huebert, D. J., Cuff, J., Fry, B., Meissner, A., Wernig, M., Plath, K., Jaenisch, R., Wagschal, A., Feil, R., Schreiber, S. L., & Lander, E. S. (2006). A Bivalent Chromatin Structure Marks Key Developmental Genes in Embryonic Stem Cells. *Cell*, 125(2), 315–326. <https://doi.org/10.1016/j.cell.2006.02.041>
- Bird, A. P. (1980). DNA methylation and the frequency of CpG in animal DNA. *Nucleic Acids Research*, 8(7), 1499–1504. <https://doi.org/10.1093/NAR/8.7.1499>
- Birke, M., Schreiner, S., García-Cuéllar, M. P., Mahr, K., Titgemeyer, F., & Slany, R. K. (2002). The MT domain of the proto-oncoprotein MLL binds to CpG-containing DNA and discriminates against methylation. *Nucleic Acids Research*, 30(4), 958–965. <https://doi.org/10.1093/NAR/30.4.958>
- Blackledge, N. P., Farcas, A. M., Kondo, T., King, H. W., McGouran, J. F., Hanssen, L. L. P., Ito, S., Cooper, S., Kondo, K., Koseki, Y., Ishikura, T., Long, H. K., Sheahan, T. W., Brockdorff, N., Kessler, B. M., Koseki, H., & Klose, R. J. (2014). Variant PRC1 complex-dependent H2A ubiquitylation drives PRC2 recruitment and polycomb domain formation. *Cell*, 157(6), 1445–1459. <https://doi.org/10.1016/J.CELL.2014.05.004>
- Blanco, E., González-Ramírez, M., Alcaine-Colet, A., Aranda, S., & Di Croce, L. (2020). The Bivalent Genome: Characterization, Structure, and Regulation. *Trends in Genetics*, 36(2), 118–131. <https://doi.org/10.1016/J.TIG.2019.11.004>
- Bledau, A. S., Schmidt, K., Neumann, K., Hill, U., Ciotta, G., Gupta, A., Torres, D. C., Fu, J., Kranz, A., Stewart, A. F., & Anastasiadis, K. (2014). The H3K4 methyltransferase Setd1a is first required at the epiblast stage, whereas Setd1b becomes essential after gastrulation. *Development (Cambridge, England)*, 141(5), 1022–1035. <https://doi.org/10.1242/DEV.098152>
- Blythe, S. A., & Wieschaus, E. F. (2015). Zygotic genome activation triggers the DNA replication checkpoint at the midblastula transition. *Cell*, 160(6), 1169–1181. <https://doi.org/10.1016/j.cell.2015.01.050>
- Bosnakovski, D., Gearhart, M. D., Ho Choi, S., & Kyba, M. (2021). Dux facilitates post-implantation development, but is not essential for zygotic genome activation†. *Biology of Reproduction*, 104(1), 83–93. <https://doi.org/10.1093/BIOLRE/IOAA179>
- Bostick, M., Jong, K. K., Estève, P. O., Clark, A., Pradhan, S., & Jacobsen, S. E. (2007). UHRF1 plays a role in maintaining DNA methylation in mammalian cells. *Science*, 317(5845), 1760–1764. <https://doi.org/10.1126/science.1147939>
- Bouniol-Baly, C., Hamraoui, L., Guibert, J., Beaujean, N., Szöllösi, M. S., & Debey, P. (1999). Differential transcriptional activity associated with chromatin configuration in fully grown mouse germinal vesicle oocytes. *Biology of Reproduction*, 60(3), 580–587. <https://doi.org/10.1095/BIOLREPROD60.3.580>
- Bourc'his, D., & Bestor, T. H. (2004). Meiotic catastrophe and retrotransposon reactivation in male germ cells lacking Dnmt3L. *Nature*, 431(7004), 96–99. <https://doi.org/10.1038/NATURE02886>
- Bourc'his, D., Xu, G. L., Lin, C. S., Bollman, B., & Bestor, T. H. (2001). Dnmt3L and the establishment of maternal

- genomic imprints. *Science*, 294(5551), 2536–2539. <https://doi.org/10.1126/science.1065848>
- Boyer, L. A., Plath, K., Zeitlinger, J., Brambrink, T., Medeiros, L. A., Lee, T. I., Levine, S. S., Wernig, M., Tajonar, A., Ray, M. K., Bell, G. W., Otte, A. P., Vidal, M., Gifford, D. K., Young, R. A., & Jaenisch, R. (2006). Polycomb complexes repress developmental regulators in murine embryonic stem cells. *Nature*, 441(7091), 349–353. <https://doi.org/10.1038/NATURE04733>
- Branco, M. R., King, M., Perez-Garcia, V., Bogutz, A. B., Caley, M., Fineberg, E., Lefebvre, L., Cook, S. J., Dean, W., Hemberger, M., & Reik, W. (2016). Maternal DNA Methylation Regulates Early Trophoblast Development. *Developmental Cell*, 36(2), 152–163. <https://doi.org/10.1016/J.DEVCEL.2015.12.027/ATTACHMENT/A31455B2-04DB-42FC-9109-C1038E560304/MMC2.XLSX>
- Brici, D., Zhang, Q., Reinhardt, S., Dahl, A., Hartmann, H., Schmidt, K., Goveas, N., Huang, J., Gahurova, L., Kelsey, G., Anastassiadis, K., Stewart, A. F., & Kranz, A. (2017). Setd1b, encoding a histone 3 lysine 4 methyltransferase, is a maternal effect gene required for the oogenic gene expression program. *Development (Cambridge)*, 144(14), 2606–2617. <https://doi.org/10.1242/dev.143347>
- Brind'Amour, J., Kobayashi, H., Richard Albert, J., Shirane, K., Sakashita, A., Kamio, A., Bogutz, A., Koike, T., Karimi, M. M., Lefebvre, L., Kono, T., & Lorincz, M. C. (2018). LTR retrotransposons transcribed in oocytes drive species-specific and heritable changes in DNA methylation. *Nature Communications*, 9(1). <https://doi.org/10.1038/s41467-018-05841-x>
- Brinkman, A. B., Gu, H., Bartels, S. J. J., Zhang, Y., Matarese, F., Simmer, F., Marks, H., Bock, C., Gnirke, A., Meissner, A., & Stunnenberg, H. G. (2012). Sequential ChIP-bisulfite sequencing enables direct genome-scale investigation of chromatin and DNA methylation cross-talk. *Genome Research*, 22(6), 1128–1138. <https://doi.org/10.1101/gr.133728.111>
- Brown, D. A., Di Cerbo, V., Feldmann, A., Ahn, J., Ito, S., Blackledge, N. P., Nakayama, M., McClellan, M., Dimitrova, E., Turberfield, A. H., Long, H. K., King, H. W., Kriaucionis, S., Schermelleh, L., Kutateladze, T. G., Koseki, H., & Klose, R. J. (2017). The SET1 Complex Selects Actively Transcribed Target Genes via Multivalent Interaction with CpG Island Chromatin. *Cell Reports*, 20(10), 2313–2327. <https://doi.org/10.1016/j.celrep.2017.08.030>
- Brunet, S., & Verlhac, M. H. (2011). Positioning to get out of meiosis: the asymmetry of division. *Human Reproduction Update*, 17(1), 68–75. <https://doi.org/10.1093/humupd/dmq044>
- Burkhardt, S., Borsos, M., Szydłowska, A., Godwin, J., Williams, S. A., Cohen, P. E., Hirota, T., Saitou, M., & Tachibana-Konwalski, K. (2016). Chromosome Cohesion Established by Rec8-Cohesin in Fetal Oocytes is Maintained without Detectable Turnover in Oocytes Arrested for Months in Mice. *Current Biology*, 26(5), 678–685. <https://doi.org/10.1016/j.cub.2015.12.073>
- Campagne, A., Lee, M. K., Zielinski, D., Michaud, A., Le Corre, S., Dingli, F., Chen, H., Shahidian, L. Z., Vassilev, I., Servant, N., Loew, D., Pasmant, E., Postel-Vinay, S., Wassef, M., & Margueron, R. (2019). BAP1 complex promotes transcription by opposing PRC1-mediated H2A ubiquitylation. *Nature Communications*, 10(1), 1–15. <https://doi.org/10.1038/s41467-018-08255-x>
- Canzio, D., Chang, E. Y., Shankar, S., Kuchenbecker, K. M., Simon, M. D., Madhani, H. D., Narlikar, G. J., & Al-Sady, B. (2011). Chromodomain-mediated oligomerization of HP1 suggests a nucleosome-bridging mechanism for heterochromatin assembly. *Molecular Cell*, 41(1), 67–81. <https://doi.org/10.1016/J.MOLCEL.2010.12.016>
- Cao, R., Wang, L., Wang, H., Xia, L., Erdjument-Bromage, H., Tempst, P., Jones, R. S., & Zhang, Y. (2002). Role of histone H3 lysine 27 methylation in polycomb-group silencing. *Science*, 298(5595), 1039–1043. [https://doi.org/10.1126/SCIENCE.1076997/SUPPL\\_FILE/CAOR1076997.SUP.PDF](https://doi.org/10.1126/SCIENCE.1076997/SUPPL_FILE/CAOR1076997.SUP.PDF)
- Cao, R., & Zhang, Y. (2004). SUZ12 is required for both the histone methyltransferase activity and the silencing function of the EED-EZH2 complex. *Molecular Cell*, 15(1), 57–67. <https://doi.org/10.1016/J.MOLCEL.2004.06.020>
- Cardoso, M. C., & Leonhardt, H. (1999). DNA methyltransferase is actively retained in the cytoplasm during early development. *The Journal of Cell Biology*, 147(1), 25–32. <https://doi.org/10.1083/JCB.147.1.25>
- Chaigne, A., Terret, M. E., & Verlhac, M. H. (2017). Asymmetries and symmetries in the mouse oocyte and zygote.

- In *Results and Problems in Cell Differentiation* (Vol. 61, pp. 285–299). Springer Verlag. [https://doi.org/10.1007/978-3-319-53150-2\\_13](https://doi.org/10.1007/978-3-319-53150-2_13)
- Challen, G. A., Sun, D., Jeong, M., Luo, M., Jelinek, J., Berg, J. S., Bock, C., Vasanthakumar, A., Gu, H., Xi, Y., Liang, S., Lu, Y., Darlington, G. J., Meissner, A., Issa, J. P. J., Godley, L. A., Li, W., & Goodell, M. A. (2011). Dnmt3a is essential for hematopoietic stem cell differentiation. *Nature Genetics*, *44*(1), 23–31. <https://doi.org/10.1038/NG.1009>
- Chamberlain, S. J., Yee, D., & Magnuson, T. (2008). Polycomb repressive complex 2 is dispensable for maintenance of embryonic stem cell pluripotency. *Stem Cells (Dayton, Ohio)*, *26*(6), 1496–1505. <https://doi.org/10.1634/STEMCELLS.2008-0102>
- Chang, H.-Y., Hwu, W.-L., Chen, C.-H., Hou, C.-Y., & Cheng, W. (2020). Children Conceived by Assisted Reproductive Technology Prone to Low Birth Weight, Preterm Birth, and Birth Defects: A Cohort Review of More Than 50,000 Live Births During 2011–2017 in Taiwan. *Frontiers in Pediatrics*, *8*, 87. <https://doi.org/10.3389/fped.2020.00087>
- Chatzidaki, E. E., Powell, S., Dequeker, B. J. H., Gassler, J., Silva, M. C. C., & Tachibana, K. (2021). Ovulation suppression protects against chromosomal abnormalities in mouse eggs at advanced maternal age. *Current Biology : CB*, *31*(18), 4038–4051.e7. <https://doi.org/10.1016/J.CUB.2021.06.076>
- Chen, D., Sun, N., Hou, L., Kim, R., Faith, J., Aslanyan, M., Tao, Y., Zheng, Y., Fu, J., Liu, W., Kellis, M., & Clark, A. (2019). Human Primordial Germ Cells Are Specified from Lineage-Primed Progenitors. *Cell Reports*, *29*(13), 4568–4582.e5. <https://doi.org/10.1016/j.celrep.2019.11.083>
- Chen, K., Hu, Z., Xia, Z., Zhao, D., Li, W., & Tyler, J. K. (2016). The Overlooked Fact: Fundamental Need for Spike-In Control for Virtually All Genome-Wide Analyses. *Molecular and Cellular Biology*, *36*(5), 662–667. <https://doi.org/10.1128/mcb.00970-14>
- Chen, S., Ma, J., Wu, F., Xiong, L. J., Ma, H., Xu, W., Lv, R., Li, X., Villen, J., Gygi, S. P., Liu, X. S., & Shi, Y. (2012). The histone H3 Lys 27 demethylase JMJD3 regulates gene expression by impacting transcriptional elongation. *Genes & Development*, *26*(12), 1364–1375. <https://doi.org/10.1101/GAD.186056.111>
- Chen, Z., Djekidel, M. N., & Zhang, Y. (2021). Distinct dynamics and functions of H2AK119ub1 and H3K27me3 in mouse preimplantation embryos. *Nature Genetics*, 1–13. <https://doi.org/10.1038/s41588-021-00821-2>
- Chen, Z., Yin, Q., Inoue, A., Zhang, C., & Zhang, Y. (2019). Allelic H3K27me3 to allelic DNA methylation switch maintains noncanonical imprinting in extraembryonic cells. *Science Advances*, *5*(12). <https://doi.org/10.1126/sciadv.aay7246>
- Chen, Z., & Zhang, Y. (2020). *Annual Review of Biochemistry Role of Mammalian DNA Methyltransferases in Development*. <https://doi.org/10.1146/annurev-biochem-103019>
- Chiang, T., Duncan, F. E., Schindler, K., Schultz, R. M., & Lampson, M. A. (2010). Evidence that weakened centromere cohesion is a leading cause of age-related aneuploidy in oocytes. *Current Biology*, *20*(17), 1522–1528. <https://doi.org/10.1016/j.cub.2010.06.069>
- Chih, L. L., Kaplan, T., Kim, M., Buratowski, S., Schreiber, S. L., Friedman, N., & Rando, O. J. (2005). Single-nucleosome mapping of histone modifications in *S. cerevisiae*. *PLoS Biology*, *3*(10). <https://doi.org/10.1371/journal.pbio.0030328>
- Chiquoine, A. D. (1954). The identification, origin, and migration of the primordial germ cells in the mouse embryo. *The Anatomical Record*, *118*(2), 135–146. <https://doi.org/10.1002/AR.1091180202>
- Choi, S. H., Gearhart, M. D., Cui, Z., Bosnakovski, D., Kim, M., Schennum, N., & Kyba, M. (2016). DUX4 recruits p300/CBP through its C-terminus and induces global H3K27 acetylation changes. *Nucleic Acids Research*, *44*(11), 5161–5173. <https://doi.org/10.1093/NAR/GKW141>
- Chopra, V. S., Hendrix, D. A., Core, L. J., Tsui, C., Lis, J. T., & Levine, M. (2011). The Polycomb group mutant *esc* leads to augmented levels of paused Pol II in the *Drosophila* embryo. *Molecular Cell*, *42*(6), 837. <https://doi.org/10.1016/J.MOLCEL.2011.05.009>
- Chotalia, M., Smallwood, S. A., Ruf, N., Dawson, C., Lucifero, D., Frontera, M., James, K., Dean, W., & Kelsey, G. (2009). Transcription is required for establishment of germline methylation marks at imprinted genes. *Genes & Development*, *23*(1), 105–117. <https://doi.org/10.1101/GAD.495809>

- Christians, E., Boiani, M., Garagna, S., Dessy, C., Redi, C. A., Renard, J. P., & Zuccotti, M. (1999). Gene expression and chromatin organization during mouse oocyte growth. *Developmental Biology*, *207*(1), 76–85. <https://doi.org/10.1006/dbio.1998.9157>
- Ciccone, D. N., Su, H., Hevi, S., Gay, F., Lei, H., Bajko, J., Xu, G., Li, E., & Chen, T. (2009). KDM1B is a histone H3K4 demethylase required to establish maternal genomic imprints. *Nature* *2009* *461*:7262, *461*(7262), 415–418. <https://doi.org/10.1038/nature08315>
- Ciferri, C., Lander, G. C., Maiolica, A., Herzog, F., Aebersold, R., & Nogales, E. (2012). Molecular architecture of human polycomb repressive complex 2. *ELife*, *1*(1). <https://doi.org/10.7554/ELIFE.00005>
- Clift, D., & Schuh, M. (2013). Restarting life: Fertilization and the transition from meiosis to mitosis. In *Nature Reviews Molecular Cell Biology* (Vol. 14, Issue 9, pp. 549–562). Nat Rev Mol Cell Biol. <https://doi.org/10.1038/nrm3643>
- Clouaire, T., Webb, S., Skene, P., Illingworth, R., Kerr, A., Andrews, R., Lee, J. H., Skalnik, D., & Bird, A. (2012). Cfp1 integrates both CpG content and gene activity for accurate H3K4me3 deposition in embryonic stem cells. *Genes and Development*, *26*(15), 1714–1728. <https://doi.org/10.1101/gad.194209.112>
- Collombet, S., Ranisavljevic, N., Nagano, T., Varnai, C., Shisode, T., Leung, W., Piolot, T., Galupa, R., Borensztein, M., Servant, N., Fraser, P., Ancelin, K., & Heard, E. (2020). Parental-to-embryo switch of chromosome organization in early embryogenesis. *Nature*, *580*(7801), 142–146. <https://doi.org/10.1038/s41586-020-2125-z>
- Cox, G. F., Bürger, J., Lip, V., Mau, U. A., Sperling, K., Wu, B. L., & Horsthemke, B. (2002). Intracytoplasmic sperm injection may increase the risk of imprinting defects. *American Journal of Human Genetics*, *71*(1), 162–164. <https://doi.org/10.1086/341096>
- Czermin, B., Melfi, R., McCabe, D., Seitz, V., Imhof, A., & Pirrotta, V. (2002). Drosophila enhancer of Zeste/ESC complexes have a histone H3 methyltransferase activity that marks chromosomal Polycomb sites. *Cell*, *111*(2), 185–196. [https://doi.org/10.1016/S0092-8674\(02\)00975-3](https://doi.org/10.1016/S0092-8674(02)00975-3)
- da Rocha, S. T., Boeva, V., Escamilla-Del-Arenal, M., Ancelin, K., Granier, C., Matias, N. R., Sanulli, S., Chow, J., Schulz, E., Picard, C., Kaneko, S., Helin, K., Reinberg, D., Stewart, A. F., Wutz, A., Margueron, R., & Heard, E. (2014). Jarid2 Is Implicated in the Initial Xist-Induced Targeting of PRC2 to the Inactive X Chromosome. *Molecular Cell*, *53*(2), 301–316. <https://doi.org/10.1016/J.MOLCEL.2014.01.002>
- Dahl, J. A., Jung, I., Aanes, H., Greggains, G. D., & Manaf, A. (2018). Broad histone H3K4me3 domains in mouse oocytes modulate maternal-to-zygotic transition. *537*(7621), 548–552. <https://doi.org/10.1038/nature19360>
- Dahl, J. A., Jung, I., Aanes, H., Greggains, G. D., Manaf, A., Lerdrup, M., Li, G., Kuan, S., Li, B., Lee, A. Y., Preissl, S., Jermstad, I., Haugen, M. H., Suganthan, R., Bjørås, M., Hansen, K., Dalen, K. T., Fedorcsak, P., Ren, B., & Klungland, A. (2016). Broad histone H3K4me3 domains in mouse oocytes modulate maternal-to-zygotic transition. *Nature*, *537*(7621), 548–552. <https://doi.org/10.1038/NATURE19360>
- De Iaco, A., Planet, E., Coluccio, A., Verp, S., Duc, J., & Trono, D. (2017). DUX-family transcription factors regulate zygotic genome activation in placental mammals. *Nature Genetics*, *49*(6), 941–945. <https://doi.org/10.1038/NG.3858>
- De Iaco, A., Verp, S., Offner, S., Grun, D., & Trono, D. (2020). DUX is a non-essential synchronizer of zygotic genome activation. *Development (Cambridge, England)*, *147*(2). <https://doi.org/10.1242/DEV.177725>
- De Vantéry, C., Stutz, A., Vassalli, J. D., & Schorderet-Slatkine, S. (1997). Acquisition of meiotic competence in growing mouse oocytes is controlled at both translational and posttranslational levels. *Developmental Biology*, *187*(1), 43–54. <https://doi.org/10.1006/dbio.1997.8599>
- de Waal, E., Vrooman, L. A., Fischer, E., Ord, T., Mainigi, M. A., Coutifaris, C., Schultz, R. M., & Bartolomei, M. S. (2015). The cumulative effect of assisted reproduction procedures on placental development and epigenetic perturbations in a mouse model. *Human Molecular Genetics*, *24*(24), 6975–6985. <https://doi.org/10.1093/hmg/ddv400>
- DeBaun, M. R., Niemitz, E. L., & Feinberg, A. P. (2003). Association of in vitro fertilization with Beckwith-Wiedemann syndrome and epigenetic alterations of LIT1 and H19. *American Journal of Human Genetics*, *72*(1), 156–160. <https://doi.org/10.1086/346031>

- Dekel, N. (1988). Regulation of Oocyte Maturation. *Annals of the New York Academy of Sciences*, 541(1), 211–216. <https://doi.org/10.1111/J.1749-6632.1988.TB22258.X>
- del Mar Lorente, M., Marcos-Gutierrez, C., Perez, C., Schoorlemmer, J., Ramirez, A., Magin, T., & Vidal, M. (2000). Loss- and gain-of-function mutations show a polycomb group function for Ring1A in mice. *Development (Cambridge, England)*, 127(23), 5093–5100. <https://doi.org/10.1242/dev.127.23.5093>
- Denholtz, M., Bonora, G., Chronis, C., Splinter, E., de Laat, W., Ernst, J., Pellegrini, M., & Plath, K. (2013). Long-range chromatin contacts in embryonic stem cells reveal a role for pluripotency factors and polycomb proteins in genome organization. *Cell Stem Cell*, 13(5), 602–616. <https://doi.org/10.1016/J.STEM.2013.08.013>
- Deplus, R., Brenner, C., Burgers, W. A., Putmans, P., Kouzarides, T., De Launoit, Y., & Fuks, F. (2002). Dnmt3L is a transcriptional repressor that recruits histone deacetylase. *Nucleic Acids Research*, 30(17), 3831. <https://doi.org/10.1093/NAR/GKF509>
- Dhayalan, A., Rajavelu, A., Rathert, P., Tamas, R., Jurkowska, R. Z., Ragozin, S., & Jeltsch, A. (2010). The Dnmt3a PWWP domain reads histone 3 lysine 36 trimethylation and guides DNA methylation. *Journal of Biological Chemistry*, 285(34), 26114–26120. <https://doi.org/10.1074/jbc.M109.089433>
- Dobrinić, P., Szczurek, A. T., & Klose, R. J. (2021). PRC1 drives Polycomb-mediated gene repression by controlling transcription initiation and burst frequency. *Nature Structural & Molecular Biology* 2021 28:10, 28(10), 811–824. <https://doi.org/10.1038/S41594-021-00661-Y>
- Dodge, J. E., Kang, Y.-K., Beppu, H., Lei, H., & Li, E. (2004). Histone H3-K9 methyltransferase ESET is essential for early development. *Molecular and Cellular Biology*, 24(6), 2478–2486. <https://doi.org/10.1128/MCB.24.6.2478-2486.2004>
- Domcke, S., Bardet, A. F., Adrian Ginno, P., Hartl, D., Burger, L., & Schübeler, D. (2015). Competition between DNA methylation and transcription factors determines binding of NRF1. *Nature* 2015 528:7583, 528(7583), 575–579. <https://doi.org/10.1038/nature16462>
- Dou, Y., Milne, T. A., Ruthenburg, A. J., Lee, S., Lee, J. W., Verdine, G. L., Allis, C. D., & Roeder, R. G. (2006). Regulation of MLL1 H3K4 methyltransferase activity by its core components. *Nature Structural and Molecular Biology*, 13(8), 713–719. <https://doi.org/10.1038/nsmb1128>
- Dou, Y., Milne, T. A., Tackett, A. J., Smith, E. R., Fukuda, A., Wysocka, J., Allis, C. D., Chait, B. T., Hess, J. L., & Roeder, R. G. (2005). Physical association and coordinate function of the H3 K4 methyltransferase MLL1 and the H4 K16 acetyltransferase MOF. *Cell*, 121(6), 873–885. <https://doi.org/10.1016/j.cell.2005.04.031>
- Downen, J. M., Fan, Z. P., Hnisz, D., Ren, G., Abraham, B. J., Zhang, L. N., Weintraub, A. S., Schuijers, J., Lee, T. I., Zhao, K., & Young, R. A. (2014). Control of cell identity genes occurs in insulated neighborhoods in mammalian chromosomes. *Cell*, 159(2), 374–387. <https://doi.org/10.1016/J.CELL.2014.09.030>
- Du, Z., Zheng, H., Kawamura, Y. K., Zhang, K., Gassler, J., Powell, S., Xu, Q., Lin, Z., Xu, K., Zhou, Q., Ozonov, E. A., Véron, N., Huang, B., Li, L., Yu, G., Liu, L., Au Yeung, W. K., Wang, P., Chang, L., ... Xie, W. (2020). Polycomb Group Proteins Regulate Chromatin Architecture in Mouse Oocytes and Early Embryos. *Molecular Cell*, 77(4), 825–839.e7. <https://doi.org/10.1016/j.molcel.2019.11.011>
- Duns, G., Van Berg, E. Den, Van Duivenbode, I., Osinga, J., Hollema, H., Hofstra, R. M. W., & Kok, K. (2010). Histone methyltransferase gene SETD2 is a novel tumor suppressor gene in clear cell renal cell carcinoma. *Cancer Research*, 70(11), 4287–4291. <https://doi.org/10.1158/0008-5472.CAN-10-0120>
- Dura, M., Teissandier, A., Armand, M., Barau, J., Lapoujade, C., Fouchet, P., Bonneville, L., Schulz, M., Weber, M., Baudrin, L. G., Lameiras, S., & Bourc'his, D. (2022). DNMT3A-dependent DNA methylation is required for spermatogonial stem cells to commit to spermatogenesis. *Nature Genetics* 2022 54:4, 54(4), 469–480. <https://doi.org/10.1038/s41588-022-01040-z>
- Eckersley-Maslin, M., Alda-Catalinas, C., Blotenburg, M., Kreibich, E., Krueger, C., & Reik, W. (2019). Dppa2 and Dppa4 directly regulate the Dux-driven zygotic transcriptional program. *Genes & Development*, 33(3–4), 194–208. <https://doi.org/10.1101/GAD.321174.118>
- Edgar, B. A., & Schubiger, G. (1986). Parameters controlling transcriptional activation during early drosophila development. *Cell*, 44(6), 871–877. [https://doi.org/10.1016/0092-8674\(86\)90009-7](https://doi.org/10.1016/0092-8674(86)90009-7)

- Edmunds, J. W., Mahadevan, L. C., & Clayton, A. L. (2008). Dynamic histone H3 methylation during gene induction: HYPB/Setd2 mediates all H3K36 trimethylation. *The EMBO Journal*, *27*(2), 406–420. <https://doi.org/10.1038/SJ.EMBOJ.7601967>
- Edson, M. A., Nagaraja, A. K., & Matzuk, M. M. (2009). The mammalian ovary from genesis to revelation. In *Endocrine Reviews* (Vol. 30, Issue 6, pp. 624–712). Oxford Academic. <https://doi.org/10.1210/er.2009-0012>
- Ehrlich, M., Gama-Sosa, M. A., Huang, L. H., Midgett, R. M., Kuo, K. C., Mccune, R. A., & Gehrke, C. (1982). Amount and distribution of 5-methylcytosine in human DNA from different types of tissues of cells. *Nucleic Acids Research*, *10*(8), 2709–2721. <https://doi.org/10.1093/NAR/10.8.2709>
- Elsässer, S. J., Noh, K. M., Diaz, N., Allis, C. D., & Banaszynski, L. A. (2015). Histone H3.3 is required for endogenous retroviral element silencing in embryonic stem cells. *Nature*, *522*(7555), 240–244. <https://doi.org/10.1038/NATURE14345>
- Elvin, J. A., Yan, C., & Matzuk, M. M. (2000). At the Cutting Edge Oocyte-expressed TGF- $\beta$  superfamily members in female fertility. *Molecular and Cellular Endocrinology*, *159*, 1–5. [www.elsevier.com/locate/mce](http://www.elsevier.com/locate/mce)
- Erhardt, S., Su, I. H., Schneider, R., Barton, S., Bannister, A. J., Perez-Burgos, L., Jenuwein, T., Kouzarides, T., Tarakhovskiy, A., & Azim Surani, M. (2003). Consequences of the depletion of zygotic and embryonic enhancer of zeste 2 during preimplantation mouse development. *Development*, *130*(18), 4235–4248. <https://doi.org/10.1242/DEV.00625>
- Estève, P. O., Hang, G. C., Smallwood, A., Feehery, G. R., Gangisetty, O., Karpf, A. R., Carey, M. F., & Pradhan, S. (2006). Direct interaction between DNMT1 and G9a coordinates DNA and histone methylation during replication. *Genes & Development*, *20*(22), 3089–3103. <https://doi.org/10.1101/GAD.1463706>
- Ewen, K. A., & Koopman, P. (2010). Mouse germ cell development: From specification to sex determination. *Molecular and Cellular Endocrinology*, *323*, 76–93. <https://doi.org/10.1016/j.mce.2009.12.013>
- Eymery, A., Liu, Z., Ozonov, E. A., Stadler, M. B., & Peters, A. H. F. M. (2016). The methyltransferase Setdb1 is essential for meiosis and mitosis in mouse oocytes and early embryos. *Development (Cambridge, England)*, *143*(15), 2767–2779. <https://doi.org/10.1242/DEV.132746>
- Fang, R., Barbera, A. J., Xu, Y., Rutenberg, M., Leonor, T., Bi, Q., Lan, F., Mei, P., Yuan, G. C., Lian, C., Peng, J., Cheng, D., Sui, G., Kaiser, U. B., Shi, Y., & Shi, Y. G. (2010). Human LSD2/KDM1b/AOF1 Regulates Gene Transcription by Modulating Intragenic H3K4me2 Methylation. *Molecular Cell*, *39*(2), 222–233. <https://doi.org/10.1016/J.MOLCEL.2010.07.008>
- Fang, R., Chen, F., Dong, Z., Hu, D., Barbera, A. J., Clark, E. A., Fang, J., Yang, Y., Mei, P., Rutenberg, M., Li, Z., Zhang, Y., Xu, Y., Yang, H., Wang, P., Simon, M. D., Zhou, Q., Li, J., Marynick, M. P., ... Shi, Y. G. (2013). LSD2/KDM1B and Its Cofactor NPAC/GLYR1 Endow a Structural and Molecular Model for Regulation of H3K4 Demethylation. *Molecular Cell*, *49*(3), 558–570. <https://doi.org/10.1016/J.MOLCEL.2012.11.019>
- Farcas, A. M., Blackledge, N. P., Sudbery, I., Long, H. K., McGouran, J. F., Rose, N. R., Lee, S., Sims, D., Cerase, A., Sheahan, T. W., Koseki, H., Brockdorff, N., Ponting, C. P., Kessler, B. M., & Klose, R. J. (2012). KDM2B links the Polycomb Repressive Complex 1 (PRC1) to recognition of CpG islands. *ELife*, *1*(1). <https://doi.org/10.7554/ELIFE.00205>
- Fauque, P., Jouannet, P., Lesaffre, C., Ripoche, M. A., Dandolo, L., Vaiman, D., & Jammes, H. (2007). Assisted reproductive technology affects developmental kinetics, H19 imprinting control region methylation and H19 gene expression in individual mouse embryos. *BMC Developmental Biology*, *7*(1), 116. <https://doi.org/10.1186/1471-213X-7-116>
- Finogenova, K., Bonnet, J., Poepsel, S., Schäfer, I. B., Finkl, K., Schmid, K., Litz, C., Strauss, M., Benda, C., & Müller, J. (2020). Structural basis for PRC2 decoding of active histone methylation marks H3K36me2/3. *ELife*, *9*. <https://doi.org/10.7554/eLife.61964>
- Fleming, T. P. (1987). A quantitative analysis of cell allocation to trophectoderm and inner cell mass in the mouse blastocyst. *Developmental Biology*, *119*(2), 520–531. [https://doi.org/10.1016/0012-1606\(87\)90055-8](https://doi.org/10.1016/0012-1606(87)90055-8)
- Fu, B., Ma, H., & Liu, D. (2019). Endogenous retroviruses function as gene expression regulatory elements during mammalian pre-implantation embryo development. In *International Journal of Molecular Sciences* (Vol. 20, Issue 3, p. 790). MDPI AG. <https://doi.org/10.3390/ijms20030790>

- Gahurova, L., Tomizawa, S. ichi, Smallwood, S. A., Stewart-Morgan, K. R., Saadeh, H., Kim, J., Andrews, S. R., Chen, T., & Kelsey, G. (2017). Transcription and chromatin determinants of de novo DNA methylation timing in oocytes. *Epigenetics and Chromatin*, *10*(1), 1–19. <https://doi.org/10.1186/s13072-017-0133-5>
- Gao, Z., Zhang, J., Bonasio, R., Strino, F., Sawai, A., Parisi, F., Kluger, Y., & Reinberg, D. (2012). PCGF homologs, CBX proteins, and RYBP define functionally distinct PRC1 family complexes. *Molecular Cell*, *45*(3), 344–356. <https://doi.org/10.1016/J.MOLCEL.2012.01.002>
- Gaudet, F., Hodgson, J. G., Eden, A., Jackson-Grusby, L., Dausman, J., Gray, J. W., Leonhardt, H., & Jaenisch, R. (2003). Induction of tumors in mice by genomic hypomethylation. *Science*, *300*(5618), 489–492. <https://doi.org/10.1126/science.1083558>
- Geiman, T. M., Sankpal, U. T., Robertson, A. K., Zhao, Y., Zhao, Y., & Robertson, K. D. (2004). DNMT3B interacts with hSNF2H chromatin remodeling enzyme, HDACs 1 and 2, and components of the histone methylation system. *Biochemical and Biophysical Research Communications*, *318*(2), 544–555. <https://doi.org/10.1016/J.BBRC.2004.04.058>
- Gelfman, S., & Ast, G. (2013). When epigenetics meets alternative splicing: the roles of DNA methylation and GC architecture. *Epigenomics*, *5*(4), 351–353. <https://doi.org/10.2217/EPI.13.32>
- Glaser, S., Schaft, J., Lubitz, S., Vintersten, K., van der Hoeven, F., Tufttland, K. R., Aasland, R., Anastassiadis, K., Ang, S. L., & Stewart, A. F. (2006). Multiple epigenetic maintenance factors implicated by the loss of Mll2 in mouse development. *Development*, *133*(8), 1423–1432. <https://doi.org/10.1242/dev.02302>
- Goll, M. G., & Bestor, T. H. (2005). Eukaryotic cytosine methyltransferases. *Annual Review of Biochemistry*, *74*, 481–514. <https://doi.org/10.1146/ANNUREV.BIOCHEM.74.010904.153721>
- Gopalan, S., Wang, Y., Harper, N. W., Garber, M., & Fazio, T. G. (2021). Simultaneous profiling of multiple chromatin proteins in the same cells. *Molecular Cell*, *81*(22), 4736–4746.e5. <https://doi.org/10.1016/J.MOLCEL.2021.09.019>
- Granot, I., & Dekel, N. (1994). Phosphorylation and expression of connexin-43 ovarian gap junction protein are regulated by luteinizing hormone. *Journal of Biological Chemistry*, *269*(48), 30502–30509. [https://doi.org/10.1016/S0021-9258\(18\)43842-2](https://doi.org/10.1016/S0021-9258(18)43842-2)
- Greenberg, M. V. C., & Bourc'his, D. (2019). The diverse roles of DNA methylation in mammalian development and disease. In *Nature Reviews Molecular Cell Biology* (Vol. 20, Issue 10, pp. 590–607). Nature Publishing Group. <https://doi.org/10.1038/s41580-019-0159-6>
- Greenfield, R., Tabib, A., Keshet, I., Moss, J., Sabag, O., Goren, A., & Cedar, H. (2018). Role of transcription complexes in the formation of the basal methylation pattern in early development. *Proceedings of the National Academy of Sciences of the United States of America*, *115*(41), 10387–10391. <https://doi.org/10.1073/PNAS.1804755115>
- Grow, E. J., Weaver, B. D., Smith, C. M., Guo, J., Stein, P., Shadle, S. C., Hendrickson, P. G., Johnson, N. E., Butterfield, R. J., Menafra, R., Kloet, S. L., van der Maarel, S. M., Williams, C. J., & Cairns, B. R. (2021). p53 convergently activates Dux/DUX4 in embryonic stem cells and in facioscapulohumeral muscular dystrophy cell models. *Nature Genetics*, *53*(8), 1207–1220. <https://doi.org/10.1038/S41588-021-00893-0>
- Gu, T., Hao, D., Woo, J., Huang, T.-W., Guo, L., Lin, X., Guzman, A. G., Tovy, A., Rosas, C., Jeong, M., Zhou, Y., Deneen, B., Huang, Y., Li, W., & Goodell, M. A. (2022). The disordered N-terminal domain of DNMT3A recognizes H2AK119ub and is required for postnatal development. *Nature Genetics*. <https://doi.org/10.1038/S41588-022-01063-6>
- Guo, H., Zhu, P., Yan, L., Li, R., Hu, B., Lian, Y., Yan, J., Ren, X., Lin, S., Li, J., Jin, X., Shi, X., Liu, P., Wang, X., Wang, W., Wei, Y., Li, X., Guo, F., Wu, X., ... Qiao, J. (2014). The DNA methylation landscape of human early embryos. *Nature*, *511*(7511), 606–610. <https://doi.org/10.1038/nature13544>
- Guo, M., Zhang, Y., Zhou, J., Bi, Y., Xu, J., Xu, C., Kou, X., Zhao, Y., Li, Y., Tu, Z., Liu, K., Lin, J., Yang, P., Gao, S., & Wang, Y. (2019). Precise temporal regulation of Dux is important for embryo development. *Cell Research*, *29*(11), 956–959. <https://doi.org/10.1038/S41422-019-0238-4>
- Guo, X., Wang, L., Li, J., Ding, Z., Xiao, J., Yin, X., He, S., Shi, P., Dong, L., Li, G., Tian, C., Wang, J., Cong, Y., & Xu, Y. (2015). Structural insight into autoinhibition and histone H3-induced activation of DNMT3A. *Nature*, *517*(7536), 640–644. <https://doi.org/10.1038/nature13899>

- Hackett, J. A., Sengupta, R., Zyllicz, J. J., Murakami, K., Lee, C., Down, T. A., & Surani, M. A. (2013). Germline DNA demethylation dynamics and imprint erasure through 5-hydroxymethylcytosine. *Science (New York, N.Y.)*, 339(6118), 448–452. <https://doi.org/10.1126/SCIENCE.1229277>
- Hajkova, P., Ancelin, K., Waldmann, T., Lacoste, N., Lange, U. C., Cesari, F., Lee, C., Almouzni, G., Schneider, R., & Surani, M. A. (2008). Chromatin dynamics during epigenetic reprogramming in the mouse germ line. *Nature*, 452(7189), 877–881. <https://doi.org/10.1038/NATURE06714>
- Hanna, C. W., Huang, J., Belton, C., Reinhardt, S., Dahl, A., Andrews, S., Stewart, A. F., Kranz, A., & Kelsey, G. (2021). Loss of histone methyltransferase SETD1B in oogenesis results in the redistribution of genomic histone 3 lysine 4 trimethylation. *BioRxiv*, 2021.03.11.434836. <https://doi.org/10.1101/2021.03.11.434836>
- Hanna, C. W., Huang, J., Belton, C., Reinhardt, S., Dahl, A., Andrews, S., Stewart, A. F., Kranz, A., & Kelsey, G. (2022). Loss of histone methyltransferase SETD1B in oogenesis results in the redistribution of genomic histone 3 lysine 4 trimethylation. *Nucleic Acids Research*, 1. <https://doi.org/10.1093/nar/gkac051>
- Hanna, C. W., McFadden, D. E., & Robinson, W. P. (2013). DNA methylation profiling of placental villi from karyotypically normal miscarriage and recurrent miscarriage. *American Journal of Pathology*, 182(6), 2276–2284. <https://doi.org/10.1016/j.ajpath.2013.02.021>
- Hanna, C. W., Taudt, A., Huang, J., Gahurova, L., Kranz, A., Andrews, S., Dean, W., Stewart, A. F., Colomé-Tatché, M., & Kelsey, G. (2018). MLL2 conveys transcription-independent H3K4 trimethylation in oocytes. *Nature Structural and Molecular Biology*, 25(1), 73–82. <https://doi.org/10.1038/s41594-017-0013-5>
- Hara, S., Takano, T., Fujikawa, T., Yamada, M., Wakai, T., Kono, T., & Obata, Y. (2014). Forced expression of DNA methyltransferases during oocyte growth accelerates the establishment of methylation imprints but not functional genomic imprinting. *Human Molecular Genetics*, 23(14), 3853–3864. <https://doi.org/10.1093/HMG/DDU100>
- Hargan-Calvopina, J., Taylor, S., Cook, H., Hu, Z., Lee, S. A., Yen, M. R., Chiang, Y. S., Chen, P. Y., & Clark, A. T. (2016). Stage-Specific Demethylation in Primordial Germ Cells Safeguards against Precocious Differentiation. *Developmental Cell*, 39(1), 75–86. <https://doi.org/10.1016/J.DEVCEL.2016.07.019>
- Hayashi, K., Ohta, H., Kurimoto, K., Aramaki, S., & Saitou, M. (2011). Reconstitution of the mouse germ cell specification pathway in culture by pluripotent stem cells. *Cell*, 146(4), 519–532. <https://doi.org/10.1016/J.CELL.2011.06.052>
- Heard, E., & Martienssen, R. A. (2014). Transgenerational Epigenetic Inheritance: myths and mechanisms. *Cell*, 157(1), 95. <https://doi.org/10.1016/J.CELL.2014.02.045>
- Hendrickson, P. G., Doráis, J. A., Grow, E. J., Whiddon, J. L., Lim, J. W., Wike, C. L., Weaver, B. D., Pflueger, C., Emery, B. R., Wilcox, A. L., Nix, D. A., Peterson, C. M., Tapscott, S. J., Carrell, D. T., & Cairns, B. R. (2017). Conserved roles of mouse DUX and human DUX4 in activating cleavage-stage genes and MERVL/HERVL retrotransposons. *Nature Genetics*, 49(6), 925–934. <https://doi.org/10.1038/NG.3844>
- Hess, J. L. (2004). Mechanisms of transformation by MLL. In *Critical Reviews in Eukaryotic Gene Expression* (Vol. 14, Issue 4, pp. 235–254). <https://doi.org/10.1615/CritRevEukaryotGeneExpr.v14.i4.10>
- Heyn, P., Logan, C. V., Fluteau, A., Challis, R. C., Auchynnikava, T., Martin, C. A., Marsh, J. A., Taglini, F., Kilanowski, F., Parry, D. A., Cormier-Daire, V., Fong, C. T., Gibson, K., Hwa, V., Ibáñez, L., Robertson, S. P., Sebastiani, G., Rappsilber, J., Allshire, R. C., ... Jackson, A. P. (2019). Gain-of-function DNMT3A mutations cause microcephalic dwarfism and hypermethylation of Polycomb-regulated regions. *Nature Genetics*, 51(1), 96–105. <https://doi.org/10.1038/s41588-018-0274-x>
- Hill, P. W. S., Leitch, H. G., Requena, C. E., Sun, Z., Amouroux, R., Roman-Trufero, M., Borkowska, M., Terragni, J., Vaisvila, R., Linnett, S., Bagci, H., Dharmalingham, G., Haberle, V., Lenhard, B., Zheng, Y., Pradhan, S., & Hajkova, P. (2018). Epigenetic reprogramming enables the transition from primordial germ cell to gonocyte. *Nature*, 555(7696), 392–396. <https://doi.org/10.1038/nature25964>
- Holliday, R., & Pugh, J. E. (1975). DNA modification mechanisms and gene activity during development. *Science (New York, N.Y.)*, 187(4173), 226–232. <https://doi.org/10.1126/science.1111098>
- Hosogane, M., Funayama, R., Shiota, M., & Nakayama, K. (2016). Lack of Transcription Triggers H3K27me3 Accumulation in the Gene Body. *Cell Reports*, 16(3), 696–706. <https://doi.org/10.1016/j.celrep.2016.06.034>

- Howell, C. Y., Bestor, T. H., Ding, F., Latham, K. E., Mertineit, C., Trasler, J. M., & Chaillet, J. R. (2001). Genomic Imprinting Disrupted by a Maternal Effect Mutation in the Dnmt1 Gene. *Cell*, *104*(6), 829–838. [https://doi.org/10.1016/S0092-8674\(01\)00280-X](https://doi.org/10.1016/S0092-8674(01)00280-X)
- Hu, D., Gao, X., Morgan, M. A., Herz, H.-M., Smith, E. R., & Shilatifard, A. (2013). The MLL3/MLL4 Branches of the COMPASS Family Function as Major Histone H3K4 Monomethylases at Enhancers. *Molecular and Cellular Biology*, *33*(23), 4745–4754. <https://doi.org/10.1128/mcb.01181-13>
- Huang, T.-C., Wang, Y.-F., Vazquez-Ferrer, E., Theofel, I., Requena, C. E., Hanna, C. W., Kelsey, G., & Hajkova, P. (2021). Sex-specific chromatin remodelling safeguards transcription in germ cells. *Nature*, 1–6. <https://doi.org/10.1038/s41586-021-04208-5>
- Hughes, A. L., Szczurek, A. T., Kelley, J. R., Lastuvkova, A., Turberfield, A. H., Dimitrova, E., Blackledge, N. P., & Kloise, R. J. (2022). A CpG island-encoded mechanism protects genes from premature transcription termination. *BioRxiv*, 2022.03.24.485638. <https://doi.org/10.1101/2022.03.24.485638>
- Hyafil, F., Morello, D., Babinet, C., & Jacob, F. (1980). A cell surface glycoprotein involved in the compaction of embryonal carcinoma cells and cleavage stage embryos. *Cell*, *21*(3), 927–934. [https://doi.org/10.1016/0092-8674\(80\)90456-0](https://doi.org/10.1016/0092-8674(80)90456-0)
- Inoue, A., Chen, Z., Yin, Q., & Zhang, Y. (2018a). Maternal Eed knockout causes loss of H3K27me3 imprinting and random X inactivation in the extraembryonic cells. *Genes and Development*, *32*(23–24), 1525–1536. <https://doi.org/10.1101/gad.318675.118>
- Inoue, A., Chen, Z., Yin, Q., & Zhang, Y. (2018b). Maternal Eed knockout causes loss of H3K27me3 imprinting and random X inactivation in the extraembryonic cells. *Genes and Development*, *32*(23–24), 1525–1536. <https://doi.org/10.1101/gad.318675.118>
- Inoue, A., Jiang, L., Lu, F., Suzuki, T., & Zhang, Y. (2017). Maternal H3K27me3 controls DNA methylation-independent imprinting. *Nature*, *547*(7664), 419–424. <https://doi.org/10.1038/nature23262>
- Inoue, A., Jiang, L., Lu, F., & Zhang, Y. (2017). Genomic imprinting of Xist by maternal H3K27me3. *Genes and Development*, *31*(19), 1927–1932. <https://doi.org/10.1101/gad.304113.117>
- Inoue, A., Nakajima, R., Nagata, M., & Aoki, F. (2008). Contribution of the oocyte nucleus and cytoplasm to the determination of meiotic and developmental competence in mice. *Human Reproduction (Oxford, England)*, *23*(6), 1377–1384. <https://doi.org/10.1093/HUMREP/DEN096>
- Inoue, N., Satouh, Y., Ikawa, M., Okabe, M., & Yanagimachi, R. (2011). Acrosome-reacted mouse spermatozoa recovered from the perivitelline space can fertilize other eggs. *Proceedings of the National Academy of Sciences of the United States of America*, *108*(50), 20008–20011. <https://doi.org/10.1073/pnas.1116965108>
- Jani, K. S., Jain, S. U., Ge, E. J., Diehl, K. L., Lundgren, S. M., Müller, M. M., Lewis, P. W., & Muir, T. W. (2019). Histone H3 tail binds a unique sensing pocket in EZH2 to activate the PRC2 methyltransferase. *Proceedings of the National Academy of Sciences of the United States of America*, *116*(17), 8295–8300. <https://doi.org/10.1073/pnas.1819029116>
- Janssen, S. M., & Lorincz, M. C. (2021). Interplay between chromatin marks in development and disease. *Nature Reviews Genetics*, 1–17. <https://doi.org/10.1038/s41576-021-00416-x>
- Jermann, P., Hoerner, L., Burger, L., & Schübeler, D. (2014). Short sequences can efficiently recruit histone H3 lysine 27 trimethylation in the absence of enhancer activity and DNA methylation. *Proceedings of the National Academy of Sciences of the United States of America*, *111*(33). <https://doi.org/10.1073/PNAS.1400672111>
- Jia, D., Jurkowska, R. Z., Zhang, X., Jeltsch, A., & Cheng, X. (2007). Structure of Dnmt3a bound to Dnmt3L suggests a model for de novo DNA methylation. *Nature*, *449*(7159), 248–251. <https://doi.org/10.1038/nature06146>
- Jiang, H., Shukla, A., Wang, X., Chen, W. Y., Bernstein, B. E., & Roeder, R. G. (2011). Role for Dpy-30 in ES cell-fate specification by regulation of H3K4 methylation within bivalent domains. *Cell*, *144*(4), 513–525. <https://doi.org/10.1016/J.CELL.2011.01.020>
- Jiang, Y., Zhang, H.-Y., Lin, Z., Zhu, Y.-Z., Yu, C., Sha, Q.-Q., Tong, M.-H., Shen, L., & Fan, H.-Y. (2020). CXXC finger protein 1-mediated histone H3 lysine-4 trimethylation is essential for proper meiotic crossover formation in

mice. <https://doi.org/10.1242/dev.183764>

- Johnson, J., Canning, J., Kaneko, T., Pru, J. K., & Tilly, J. L. (2004). Germline stem cells and follicular renewal in the postnatal mammalian ovary. *Nature*, *428*(6979), 145–150. <https://doi.org/10.1038/nature02316>
- Johnson, M. H., & Ziomek, C. A. (1981). Induction of polarity in mouse 8-cell blastomeres: Specificity, geometry, and stability. *Journal of Cell Biology*, *91*(1), 303–308. <https://doi.org/10.1083/jcb.91.1.303>
- Jones, P. A. (2012). Functions of DNA methylation: islands, start sites, gene bodies and beyond. *Nature Reviews Genetics* *2012* *13*:7, *13*(7), 484–492. <https://doi.org/10.1038/NRG3230>
- Judd, J., Wojenski, L. A., Wainman, L. M., Tippens, N. D., Rice, E. J., Dziubek, A., Villafano, G. J., Wissink, E. M., Versluis, P., Bagepalli, L., Shah, S. R., Mahat, D. B., Tome, J. M., Danko, C. G., Lis, J. T., & Core, L. J. (2020). A rapid, sensitive, scalable method for Precision Run-On sequencing (PRO-seq). *BioRxiv*, 2020.05.18.102277. <https://doi.org/10.1101/2020.05.18.102277>
- Kagiwada, S., Kurimoto, K., Hirota, T., Yamaji, M., & Saitou, M. (2013). Replication-coupled passive DNA demethylation for the erasure of genome imprints in mice. *The EMBO Journal*, *32*(3), 340–353. <https://doi.org/10.1038/EMBOJ.2012.331>
- Kaneda, M., Hirasawa, R., Chiba, H., Okano, M., Li, E., & Sasaki, H. (2010). Genetic evidence for Dnmt3a-dependent imprinting during oocyte growth obtained by conditional knockout with Zp3-Cre and complete exclusion of Dnmt3b by chimera formation. *Genes to Cells*, *15*(3), 169–179. <https://doi.org/10.1111/J.1365-2443.2009.01374.X>
- Kaneda, M., Okano, M., Hata, K., Sado, T., Tsujimoto, H., Li, E., & Sasaki, H. (2004). Essential role for de novo DNA methyltransferase Dnmt3a in paternal and maternal imprinting. *Nature*, *429*(6994), 900–903. <https://doi.org/10.1038/NATURE02633>
- Kar, F. M., & Hochwagen, A. (2021). Phospho-Regulation of Meiotic Prophase. *Frontiers in Cell and Developmental Biology*, *9*, 862. <https://doi.org/10.3389/FCELL.2021.667073/BIBTEX>
- Khoureiry, R., Ibalá-Rhondane, S., Méry, L., Blachère, T., Guérin, J. F., Lornage, J., & Lefèvre, A. (2008). Dynamic CpG methylation of the KCNQ10T1 gene during maturation of human oocytes. *Journal of Medical Genetics*, *45*(9), 583–588. <https://doi.org/10.1136/jmg.2008.057943>
- Kibe, K., Shirane, K., Ohishi, H., Uemura, S., Toh, H., & Sasaki, H. (2021). The DNMT3A PWWP domain is essential for the normal DNA methylation landscape in mouse somatic cells and oocytes. *PLOS Genetics*, *17*(5), e1009570. <https://doi.org/10.1371/journal.pgen.1009570>
- Kizer, K. O., Phatnani, H. P., Shibata, Y., Hall, H., Greenleaf, A. L., & Strahl, B. D. (2005). A novel domain in Set2 mediates RNA polymerase II interaction and couples histone H3 K36 methylation with transcript elongation. *Molecular and Cellular Biology*, *25*(8), 3305–3316. <https://doi.org/10.1128/MCB.25.8.3305-3316.2005>
- Kobayashi, H., Sakurai, T., Imai, M., Takahashi, N., Fukuda, A., Yayoi, O., Sato, S., Nakabayashi, K., Hata, K., Sotomaru, Y., Suzuki, Y., & Kono, T. (2012). Contribution of intragenic DNA methylation in mouse gametic DNA methylomes to establish Oocyte-specific heritable marks. *PLoS Genetics*, *8*(1). <https://doi.org/10.1371/journal.pgen.1002440>
- Kolovos, P., Nishimura, K., Sankar, A., Sidoli, S., Cloos, P. A., Helin, K., & Christensen, J. (2020). PR-DUB maintains the expression of critical genes through FOXK1/2- And ASXL1/2/3-dependent recruitment to chromatin and H2AK119ub1 deubiquitination. *Genome Research*, *30*(8), 1119–1130. <https://doi.org/10.1101/gr.261016.120>
- Koopman, P., Gubbay, J., Vivian, N., Goodfellow, P., & Lovell-Badge, R. (1991). Male development of chromosomally female mice transgenic for Sry. *Nature*, *351*(6322), 117–121. <https://doi.org/10.1038/351117a0>
- Kurimoto, K., Yabuta, Y., Hayashi, K., Ohta, H., Kiyonari, H., Mitani, T., Moritoki, Y., Kohri, K., Kimura, H., Yamamoto, T., Katou, Y., Shirahige, K., & Saitou, M. (2015). Quantitative Dynamics of Chromatin Remodeling during Germ Cell Specification from Mouse Embryonic Stem Cells. *Cell Stem Cell*, *16*(5), 517–532. <https://doi.org/10.1016/J.STEM.2015.03.002>
- Kurimoto, K., Yabuta, Y., Ohinata, Y., Shigeta, M., Yamanaka, K., & Saitou, M. (2008). Complex genome-wide

- transcription dynamics orchestrated by Blimp1 for the specification of the germ cell lineage in mice. *Genes & Development*, 22(12), 1617–1635. <https://doi.org/10.1101/GAD.1649908>
- Kurotaki, N., Imaizumi, K., Harada, N., Masuno, M., Kondoh, T., Nagai, T., Ohashi, H., Naritomi, K., Tsukahara, M., Makita, Y., Sugimoto, T., Sonoda, T., Hasegawa, T., Chinen, Y., Tomita, H. aki, Kinoshita, A., Mizuguchi, T., Yoshiura, K. ichiro, Ohta, T., ... Matsumoto, N. (2002). Haploinsufficiency of NSD1 causes Sotos syndrome. *Nature Genetics*, 30(4), 365–366. <https://doi.org/10.1038/ng863>
- Lan, J., Lepikhov, K., Giehr, P., & Walter, J. (2017). Histone and DNA methylation control by H3 serine 10/threonine 11 phosphorylation in the mouse zygote. *Epigenetics and Chromatin*, 10(1), 1–19. <https://doi.org/10.1186/s13072-017-0112-x>
- Lan, Z.-J., Xu, X., & Cooney, A. J. (2004). Differential Oocyte-Specific Expression of Cre Recombinase Activity in GDF-9-iCre, Zp3cre, and Msx2Cre Transgenic Mice1. *Biology of Reproduction*, 71(5), 1469–1474. <https://doi.org/10.1095/biolreprod.104.031757>
- Lee, J. H., & Skalnik, D. G. (2005). CpG-binding protein (CXXC finger protein 1) is a component of the mammalian Set1 histone H3-Lys4 methyltransferase complex, the analogue of the yeast Set1/COMPASS complex. *Journal of Biological Chemistry*, 280(50), 41725–41731. <https://doi.org/10.1074/jbc.M508312200>
- Leeb, M., Pasini, D., Novatchkova, M., Jaritz, M., Helin, K., & Wutz, A. (2010). Polycomb complexes act redundantly to repress genomic repeats and genes. *Genes & Development*, 24(3), 265–276. <https://doi.org/10.1101/GAD.544410>
- Lengner, C. J., Camargo, F. D., Hochedlinger, K., Welstead, G. G., Zaidi, S., Gokhale, S., Scholer, H. R., Tomilin, A., & Jaenisch, R. (2007). Oct4 Expression Is Not Required for Mouse Somatic Stem Cell Self-Renewal. *Cell Stem Cell*, 1(4), 403–415. <https://doi.org/10.1016/j.stem.2007.07.020>
- Lewis, E. B. (1978). A gene complex controlling segmentation in *Drosophila*. *Nature*, 276(5688), 565–570. <https://doi.org/10.1038/276565A0>
- Li, B., Jackson, J., Simon, M. D., Fleharty, B., Gogol, M., Seidel, C., Workman, J. L., & Shilatifard, A. (2009). Histone H3 lysine 36 dimethylation (H3K36me2) is sufficient to recruit the Rpd3s histone deacetylase complex and to repress spurious transcription. *The Journal of Biological Chemistry*, 284(12), 7970–7976. <https://doi.org/10.1074/JBC.M808220200>
- Li, B. Z., Huang, Z., Cui, Q. Y., Song, X. H., Du, L., Jeltsch, A., Chen, P., Li, G., Li, E., & Xu, G. L. (2011). Histone tails regulate DNA methylation by allosterically activating de novo methyltransferase. *Cell Research*, 21(8), 1172–1181. <https://doi.org/10.1038/CR.2011.92>
- Li, H., Liefke, R., Jiang, J., Kurland, J. V., Tian, W., Deng, P., Zhang, W., He, Q., Patel, D. J., Bulyk, M. L., Shi, Y., & Wang, Z. (2017). Polycomb-like proteins link the PRC2 complex to CpG islands. *Nature*, 549(7671), 287–291. <https://doi.org/10.1038/nature23881>
- Li, X., Ito, M., Zhou, F., Youngson, N., Zuo, X., Leder, P., & Ferguson-Smith, A. C. (2008). A maternal-zygotic effect gene, *Zfp57*, maintains both maternal and paternal imprints. *Developmental Cell*, 15(4), 547–557. <https://doi.org/10.1016/J.DEVCEL.2008.08.014>
- Li, Yingfeng, Zhang, Z., Chen, J., Liu, W., Lai, W., Liu, B., Li, X., Liu, L., Xu, S., Dong, Q., Wang, M., Duan, X., Tan, J., Zheng, Y., Zhang, P., Fan, G., Wong, J., Xu, G. L., Wang, Z., ... Zhu, B. (2018). Stella safeguards the oocyte methylome by preventing de novo methylation mediated by DNMT1. *Nature*, 564(7734), 136–140. <https://doi.org/10.1038/s41586-018-0751-5>
- Li, Yuanyuan, Zheng, H., Wang, Q., Zhou, C., Wei, L., Liu, X., Zhang, W., Zhang, Y., Du, Z., Wang, X., & Xie, W. (2018). Genome-wide analyses reveal a role of Polycomb in promoting hypomethylation of DNA methylation valleys. *Genome Biology*, 19(1), 1–16. <https://doi.org/10.1186/s13059-018-1390-8>
- Lister, R., Pelizzola, M., Dowen, R. H., Hawkins, R. D., Hon, G., Tonti-Filippini, J., Nery, J. R., Lee, L., Ye, Z., Ngo, Q. M., Edsall, L., Antosiewicz-Bourget, J., Stewart, R., Ruotti, V., Millar, A. H., Thomson, J. A., Ren, B., & Ecker, J. R. (2009). Human DNA methylomes at base resolution show widespread epigenomic differences. *Nature*, 462(7271), 315. <https://doi.org/10.1038/NATURE08514>
- Liu, B., Xu, Q., Wang, Q., Feng, S., Lai, F., Wang, P., Zheng, F., Xiang, Y., Wu, J., Nie, J., Qiu, C., Xia, W., Li, L., Yu, G., Lin, Z., Xu, K., Xiong, Z., Kong, F., Liu, L., ... Xie, W. (2020). The landscape of RNA Pol II binding reveals a step-wise transition during ZGA. *Nature*, 3(September 2019), 1–6. <https://doi.org/10.1038/s41586-020->

- Liu, S., Brind'Amour, J., Karimi, M. M., Shirane, K., Bogutz, A., Lefebvre, L., Sasaki, H., Shinkai, Y., & Lorincz, M. C. (2014). Setdb1 is required for germline development and silencing of H3K9me3-marked endogenous retroviruses in primordial germ cells. *Genes & Development*, 28(18), 2041. <https://doi.org/10.1101/GAD.244848.114>
- Liu, X., Wang, C., Liu, W., Li, J., Li, C., Kou, X., Chen, J., Zhao, Y., Gao, H., Wang, H., Zhang, Y., Gao, Y., & Gao, S. (2016). Distinct features of H3K4me3 and H3K27me3 chromatin domains in pre-implantation embryos. *Nature*, 537(7621), 558–562. <https://doi.org/10.1038/nature19362>
- Lu, X., Zhang, Y., Wang, L., Wang, L., Wang, H., Xu, Q., Xiang, Y., Chen, C., Kong, F., Xia, W., Lin, Z., Ma, S., Liu, L., Wang, X., Ni, H., Li, W., Guo, Y., & Xie, W. (2021). Evolutionary epigenomic analyses in mammalian early embryos reveal species-specific innovations and conserved principles of imprinting. *Science Advances*, 7(48), 6178. <https://doi.org/10.1126/SCIADV.ABI6178>
- Lucifero, D., La Salle, S., Bourc'his, D., Martel, J., Bestor, T. H., & Trasler, J. M. (2007). Coordinate regulation of DNA methyltransferase expression during oogenesis. *BMC Developmental Biology*, 7(1), 1–14. <https://doi.org/10.1186/1471-213X-7-36/FIGURES/6>
- Lui, C., Litscher, E. S., Mortillo, S., Sakai, Y., Kinloch, R. A., Stewart, C. L., & Wassarman, P. M. (1996). Targeted disruption of the mZP3 gene results in production of eggs lacking a zona pellucida and infertility in female mice. *Proceedings of the National Academy of Sciences of the United States of America*, 93(11), 5431–5436. <https://doi.org/10.1073/PNAS.93.11.5431>
- Magoffin, D. A. (2005). Ovarian theca cell. In *International Journal of Biochemistry and Cell Biology* (Vol. 37, Issue 7, pp. 1344–1349). Elsevier Ltd. <https://doi.org/10.1016/j.biocel.2005.01.016>
- Manzo, M., Wirz, J., Ambrosi, C., Villaseñor, R., Roschitzki, B., & Baubec, T. (2017). Isoform-specific localization of DNMT3A regulates DNA methylation fidelity at bivalent CpG islands. *The EMBO Journal*, 36(23), 3421–3434. <https://doi.org/10.15252/embj.201797038>
- Margueron, Raphael, Justin, N., Ohno, K., Sharpe, M. L., Son, J., Drury, W. J., Voigt, P., Martin, S. R., Taylor, W. R., De Marco, V., Pirrotta, V., Reinberg, D., & Gamblin, S. J. (2009). Role of the polycomb protein EED in the propagation of repressive histone marks. *Nature*, 461(7265), 762–767. <https://doi.org/10.1038/NATURE08398>
- Margueron, Raphaël, & Reinberg, D. (2010). Chromatin structure and the inheritance of epigenetic information. *Nature Reviews. Genetics*, 11(4), 285–296. <https://doi.org/10.1038/NRG2752>
- Margueron, Raphaël, & Reinberg, D. (2011). The Polycomb complex PRC2 and its mark in life. In *Nature* (Vol. 469, Issue 7330, pp. 343–349). Nature. <https://doi.org/10.1038/nature09784>
- Marshall, K. L., Wang, J., Ji, T., & Rivera, R. M. (2018). The effects of biological aging on global DNA methylation, histone modification, and epigenetic modifiers in the mouse germinal vesicle stage oocyte. *Animal Reproduction*, 15(4), 1253–1267. <https://doi.org/10.21451/1984-3143-AR2018-0087>
- Mattei, A. L., Bailly, N., & Meissner, A. (2022). DNA methylation: a historical perspective. *Trends in Genetics*. <https://doi.org/10.1016/J.TIG.2022.03.010>
- McGhee, J. D., & Ginder, G. D. (1979). Specific DNA methylation sites in the vicinity of the chicken  $\beta$ -globin genes. *Nature* 1979 280:5721, 280(5721), 419–420. <https://doi.org/10.1038/280419a0>
- Mclaren, A., & Mammalian, M. R. C. (1981). The fate of germ cells in the testis of fetal Sex-reversed mice. *Reproduction*, 61(2), 461–467. <https://doi.org/10.1530/JRF.0.0610461>
- McLaughlin, K., Flyamer, I. M., Thomson, J. P., Mjoseng, H. K., Shukla, R., Williamson, I., Grimes, G. R., Illingworth, R. S., Adams, I. R., Pennings, S., Meehan, R. R., & Bickmore, W. A. (2019). DNA Methylation Directs Polycomb-Dependent 3D Genome Re-organization in Naive Pluripotency. *Cell Reports*, 29(7), 1974–1985.e6. <https://doi.org/10.1016/J.CELREP.2019.10.031>
- Mei, H., Kozuka, C., Hayashi, R., Kumon, M., Koseki, H., & Inoue, A. (2021). H2AK119ub1 guides maternal inheritance and zygotic deposition of H3K27me3 in mouse embryos. *Nature Genetics*, 1–12. <https://doi.org/10.1038/s41588-021-00820-3>
- Meissner, A., Mikkelsen, T. S., Gu, H., Wernig, M., Hanna, J., Sivachenko, A., Zhang, X., Bernstein, B. E., Nusbaum,

- C., Jaffe, D. B., Gnirke, A., Jaenisch, R., & Lander, E. S. (2008). Genome-scale DNA methylation maps of pluripotent and differentiated cells. *Nature*, *454*(7205), 766–770. <https://doi.org/10.1038/NATURE07107>
- Menke, D. B., Koubova, J., & Page, D. C. (2003). Sexual differentiation of germ cells in XX mouse gonads occurs in an anterior-to-posterior wave. *Developmental Biology*, *262*(2), 303–312. [https://doi.org/10.1016/S0012-1606\(03\)00391-9](https://doi.org/10.1016/S0012-1606(03)00391-9)
- Mertineit, C., Yoder, J. A., Taketo, T., Laird, D. W., Trasler, J. M., & Bestor, T. H. (1998). Sex-specific exons control DNA methyltransferase in mammalian germ cells. *Development (Cambridge, England)*, *125*(5), 889–897. <https://doi.org/10.1242/DEV.125.5.889>
- Messerschmidt, D. M., De Vries, W., Ito, M., Solter, D., Ferguson-Smith, A., & Knowles, B. B. (2012). Trim28 is required for epigenetic stability during mouse oocyte to embryo transition. *Science*, *335*(6075), 1499–1502. [https://doi.org/10.1126/SCIENCE.1216154/SUPPL\\_FILE/1216154S1.XLS](https://doi.org/10.1126/SCIENCE.1216154/SUPPL_FILE/1216154S1.XLS)
- Mihajlović, A. I., & Bruce, A. W. (2017). The first cell-fate decision of mouse preimplantation embryo development: Integrating cell position and polarity. In *Open Biology* (Vol. 7, Issue 11). Royal Society Publishing. <https://doi.org/10.1098/rsob.170210>
- Mihajlović, A. I., & FitzHarris, G. (2018). Segregating Chromosomes in the Mammalian Oocyte. *Current Biology*, *28*(16), R895–R907. <https://doi.org/10.1016/J.CUB.2018.06.057>
- Mikkelsen, T. S., Ku, M., Jaffe, D. B., Issac, B., Lieberman, E., Giannoukos, G., Alvarez, P., Brockman, W., Kim, T. K., Koche, R. P., Lee, W., Mendenhall, E., O'Donovan, A., Presser, A., Russ, C., Xie, X., Meissner, A., Wernig, M., Jaenisch, R., ... Bernstein, B. E. (2007). Genome-wide maps of chromatin state in pluripotent and lineage-committed cells. *Nature*, *448*(7153), 553–560. <https://doi.org/10.1038/nature06008>
- Mohn, F., Weber, M., Rebhan, M., Roloff, T. C., Richter, J., Stadler, M. B., Bibel, M., & Schübeler, D. (2008). Lineage-specific polycomb targets and de novo DNA methylation define restriction and potential of neuronal progenitors. *Molecular Cell*, *30*(6), 755–766. <https://doi.org/10.1016/J.MOLCEL.2008.05.007>
- Molaro, A., Malik, H. S., & Bourc'his, D. (2020). Dynamic Evolution of De Novo DNA Methyltransferases in Rodent and Primate Genomes. *Molecular Biology and Evolution*, *37*(7), 1882–1892. <https://doi.org/10.1093/molbev/msaa044>
- Nagaoka, S. I., Hassold, T. J., & Hunt, P. A. (2012). Human aneuploidy: Mechanisms and new insights into an age-old problem. In *Nature Reviews Genetics* (Vol. 13, Issue 7, pp. 493–504). Nat Rev Genet. <https://doi.org/10.1038/nrg3245>
- Nagy, A., Gertsenstein, M., Vintersten, K., & Behringer, R. (2003). *Manipulating the Mouse Embryo: A Laboratory Manual, Fourth Edition*. Cold Spring Harbor Laboratory Press, Cold Spring Harbor, NY. [https://www.cshlpress.com/default.tpl?cart=16508213941638805022&fromlink=T&linkaction=full&linksortby=oop\\_title&--eqSKUdataq=982](https://www.cshlpress.com/default.tpl?cart=16508213941638805022&fromlink=T&linkaction=full&linksortby=oop_title&--eqSKUdataq=982)
- Nashun, B., Hill, P. W. S., Smallwood, S. A., Dharmalingam, G., Amouroux, R., Clark, S. J., Sharma, V., Ndjetehe, E., Pelczar, P., Festenstein, R. J., Kelsey, G., & Hajkova, P. (2015). Continuous Histone Replacement by Hira Is Essential for Normal Transcriptional Regulation and De Novo DNA Methylation during Mouse Oogenesis. *Molecular Cell*, *60*(4), 611–625. <https://doi.org/10.1016/J.MOLCEL.2015.10.010/ATTACHMENT/1CDD71A8-25FE-41AC-9AA0-32B958013059/MMC5.XLSX>
- Neri, F., Rapelli, S., Krepelova, A., Incarnato, D., Parlato, C., Basile, G., Maldotti, M., Anselmi, F., & Oliviero, S. (2017). Intragenic DNA methylation prevents spurious transcription initiation. *Nature*, *543*(7643), 72–77. <https://doi.org/10.1038/nature21373>
- Nicetto, D., & Zaret, K. S. (2019). Role of H3K9me3 Heterochromatin in Cell Identity Establishment and Maintenance. *Current Opinion in Genetics & Development*, *55*, 1. <https://doi.org/10.1016/J.GDE.2019.04.013>
- Nikolic, A., Volarevic, V., Armstrong, L., Lako, M., & Stojkovic, M. (2016). Primordial Germ Cells: Current Knowledge and Perspectives. *Stem Cells International*, *2016*. <https://doi.org/10.1155/2016/1741072>
- Noh, K. M., Wang, H., Kim, H. R., Wenderski, W., Fang, F., Li, C. H., Dewell, S., Hughes, S. H., Melnick, A. M., Patel, D. J., Li, H., & Allis, C. D. (2015). Engineering of a Histone-Recognition Domain in Dnmt3a Alters the Epigenetic Landscape and Phenotypic Features of Mouse ESCs. *Molecular Cell*, *59*(1), 89–103.

<https://doi.org/10.1016/J.MOLCEL.2015.05.017>

- Noordermeer, D., Leleu, M., Splinter, E., Rougemont, J., De Laat, W., & Duboule, D. (2011). The dynamic architecture of Hox gene clusters. *Science (New York, N.Y.)*, 334(6053), 222–225. <https://doi.org/10.1126/SCIENCE.1207194>
- Nowialis, P., Lopusna, K., Opavska, J., Haney, S. L., Abraham, A., Sheng, P., Riva, A., Natarajan, A., Guryanova, O., Simpson, M., Hlady, R., Xie, M., & Opavsky, R. (2019). Catalytically inactive Dnmt3b rescues mouse embryonic development by accessory and repressive functions. *Nature Communications* 2019 10:1, 10(1), 1–16. <https://doi.org/10.1038/s41467-019-12355-7>
- O’Carroll, D., Erhardt, S., Pagani, M., Barton, S. C., Surani, M. A., & Jenuwein, T. (2001). The Polycomb-Group Gene Ezh2 Is Required for Early Mouse Development. *Molecular and Cellular Biology*, 21(13), 4330. <https://doi.org/10.1128/MCB.21.13.4330-4336.2001>
- Okae, H., Chiba, H., Hiura, H., Hamada, H., Sato, A., Utsunomiya, T., Kikuchi, H., Yoshida, H., Tanaka, A., Suyama, M., & Arima, T. (2014). Genome-wide analysis of DNA methylation dynamics during early human development. *PLoS Genetics*, 10(12). <https://doi.org/10.1371/JOURNAL.PGEN.1004868>
- Okano, M., Bell, D. W., Haber, D. A., & Li, E. (1999). DNA methyltransferases Dnmt3a and Dnmt3b are essential for de novo methylation and mammalian development. *Cell*, 99(3), 247–257. [https://doi.org/10.1016/S0092-8674\(00\)81656-6](https://doi.org/10.1016/S0092-8674(00)81656-6)
- Ooi, S. K. T., Qiu, C., Bernstein, E., Li, K., Jia, D., Yang, Z., Erdjument-Bromage, H., Tempst, P., Lin, S. P., Allis, C. D., Cheng, X., & Bestor, T. H. (2007). DNMT3L connects unmethylated lysine 4 of histone H3 to de novo methylation of DNA. *Nature*, 448(7154), 714–717. <https://doi.org/10.1038/nature05987>
- Oswald, J., Engemann, S., Lane, N., Mayer, W., Olek, A., Fundele, R., Dean, W., Reik, W., & Walter, J. (2000). Active demethylation of the paternal genome in the mouse zygote. *Current Biology: CB*, 10(8), 475–478. [https://doi.org/10.1016/S0960-9822\(00\)00448-6](https://doi.org/10.1016/S0960-9822(00)00448-6)
- Page, S. L., & Hawley, R. S. (2004). THE GENETICS AND MOLECULAR BIOLOGY OF THE SYNAPTONEMAL COMPLEX. <http://Dx.Doi.Org.Proxy.Insermbiblio.Inist.Fr/10.1146/Annurev.Cellbio.19.111301.155141>, 20, 525–558. <https://doi.org/10.1146/ANNUREV.CELLBIO.19.111301.155141>
- Pan, B., & Li, J. (2019). The art of oocyte meiotic arrest regulation. *Reproductive Biology and Endocrinology* 2019 17:1, 17(1), 1–12. <https://doi.org/10.1186/S12958-018-0445-8>
- Parfenov, V., Potchukalina, G., Dudina, L., Kostyuchek, D., & Gruzova, M. (1989). Human antral follicles: oocyte nucleus and the karyosphere formation (electron microscopic and autoradiographic data). *Gamete Research*, 22(2), 219–231. <https://doi.org/10.1002/MRD.1120220209>
- Park, P. J. (2009). ChIP–seq: advantages and challenges of a maturing technology. *Nature Reviews Genetics* 2009 10:10, 10(10), 669–680. <https://doi.org/10.1038/nrg2641>
- Peaston, A. E., Evsikov, A. V., Graber, J. H., de Vries, W. N., Holbrook, A. E., Solter, D., & Knowles, B. B. (2004). Retrotransposons regulate host genes in mouse oocytes and preimplantation embryos. *Developmental Cell*, 7(4), 597–606. <https://doi.org/10.1016/j.devcel.2004.09.004>
- Pepling, M. E. (2006). From primordial germ cell to primordial follicle: Mammalian female germ cell development. *Genesis*, 44(12), 622–632. <https://doi.org/10.1002/DVG.20258>
- Pepling, M. E. (2012). Follicular assembly: mechanisms of action. *Reproduction*, 143(2), 139–149. <https://doi.org/10.1530/REP-11-0299>
- Perino, M., Van Mierlo, G., Karemaker, I. D., Van Genesen, S., Vermeulen, M., Marks, H., Van Heeringen, S. J., & Veenstra, G. J. C. (2018). MTF2 recruits Polycomb Repressive Complex 2 by helical-shape-selective DNA binding. *Nature Genetics*, 50(7), 1002–1010. <https://doi.org/10.1038/S41588-018-0134-8>
- Peters, A. H. F. M., Kubicek, S., Mechtler, K., O’Sullivan, R. J., Derijck, A. A. H. A., Perez-Burgos, L., Kohlmaier, A., Opravil, S., Tachibana, M., Shinkai, Y., Martens, J. H. A., & Jenuwein, T. (2003). Partitioning and plasticity of repressive histone methylation states in mammalian chromatin. *Molecular Cell*, 12(6), 1577–1589. [https://doi.org/10.1016/S1097-2765\(03\)00477-5](https://doi.org/10.1016/S1097-2765(03)00477-5)
- Piunti, A., & Shilatifard, A. (2021). The roles of Polycomb repressive complexes in mammalian development and cancer. In *Nature Reviews Molecular Cell Biology* (Vol. 22, Issue 5, pp. 326–345). Nature Research.

<https://doi.org/10.1038/s41580-021-00341-1>

- Plath, K., Fang, J., Mlynarczyk-Evans, S. K., Cao, R., Worringer, K. A., Wang, H., De la Cruz, C. C., Otte, A. P., Panning, B., & Zhang, Y. (2003). Role of histone H3 lysine 27 methylation in X inactivation. *Science (New York, N.Y.)*, *300*(5616), 131–135. <https://doi.org/10.1126/SCIENCE.1084274>
- Pliushch, G., Schneider, E., Weise, D., El Hajj, N., Tresch, A., Seidmann, L., Coerdts, W., Müller, A. M., Zechner, U., & Haaf, T. (2010). Extreme methylation values of imprinted genes in human abortions and stillbirths. *American Journal of Pathology*, *176*(3), 1084–1090. <https://doi.org/10.2353/ajpath.2010.090764>
- Portoso, M., Ragazzini, R., Bren Ci C, Z., Moiani, A., Michaud, A., Vassilev, I., Wassef, M., Servant, N., Sargueil, B., & Margueron, R. (2017). PRC2 is dispensable for HOTAIR-mediated transcriptional repression. *The EMBO Journal*, *36*(8), 981–994. <https://doi.org/10.15252/EMBJ.201695335>
- Posfai, E., Kunzmann, R., Brochard, V., Salvaing, J., Cabuy, E., Roloff, T. C., Liu, Z., Tardat, M., van Lohuizen, M., Vidal, M., Beaujean, N., & Peters, A. H. F. M. (2012). Polycomb function during oogenesis is required for mouse embryonic development. *Genes & Development*, *26*(9), 920–932. <https://doi.org/10.1101/GAD.188094.112>
- Proudhon, C., Duffié, R., Ajjan, S., Cowley, M., Iranzo, J., Carbajosa, G., Saadeh, H., Holland, M. L., Oakey, R. J., Rakyán, V. K., Schulz, R., & Bourc'his, D. (2012). Protection against De Novo Methylation Is Instrumental in Maintaining Parent-of-Origin Methylation Inherited from the Gametes. *Molecular Cell*, *47*(6), 909–920. <https://doi.org/10.1016/j.molcel.2012.07.010>
- Puschendorf, M., Terranova, R., Boutsma, E., Mao, X., Isono, K. I., Brykczynska, U., Kolb, C., Otte, A. P., Koseki, H., Orkin, S. H., Van Lohuizen, M., & Peters, A. H. F. M. (2008). PRC1 and Suv39h specify parental asymmetry at constitutive heterochromatin in early mouse embryos. *Nature Genetics* *2008* *40*:4, *40*(4), 411–420. <https://doi.org/10.1038/ng.99>
- Quenneville, S., Verde, G., Corsinotti, A., Kapopoulou, A., Jakobsson, J., Offner, S., Baglivo, I., Pedone, P. V., Grimaldi, G., Riccio, A., & Trono, D. (2011). In embryonic stem cells, ZFP57/KAP1 recognize a methylated hexanucleotide to affect chromatin and DNA methylation of imprinting control regions. *Molecular Cell*, *44*(3), 361–372. <https://doi.org/10.1016/J.MOLCEL.2011.08.032/ATTACHMENT/8A3DBDD5-8D71-4738-A2B9-CD15C11B1C37/MMC2.ZIP>
- Ragazzini, R., Pérez-Palacios, R., Baymaz, I. H., Diop, S., Ancelin, K., Zielinski, D., Michaud, A., Givélet, M., Borsos, M., Aflaki, S., Legoix, P., Jansen, P. W. T. C., Servant, N., Torres-Padilla, M. E., Bourc'his, D., Fouchet, P., Vermeulen, M., & Margueron, R. (2019). EZHIP constrains Polycomb Repressive Complex 2 activity in germ cells. *Nature Communications* *2019* *10*:1, *10*(1), 1–18. <https://doi.org/10.1038/s41467-019-11800-x>
- Ramakrishna, N. B., Murison, K., Miska, E. A., & Leitch, H. G. (2021). Epigenetic Regulation during Primordial Germ Cell Development and Differentiation. *Sexual Development*, *15*(5–6), 1–21. <https://doi.org/10.1159/000520412>
- Rancourt, R. C., Harris, H. R., & Michels, K. B. (2012). Methylation levels at imprinting control regions are not altered with ovulation induction or in vitro fertilization in a birth cohort. *Human Reproduction*, *27*(7), 2208–2216. <https://doi.org/10.1093/humrep/des151>
- Rasmussen, K. D., & Helin, K. (2016). Role of TET enzymes in DNA methylation, development, and cancer. *Genes & Development*, *30*(7), 733. <https://doi.org/10.1101/GAD.276568.115>
- Reddington, J. P., Perricone, S. M., Nestor, C. E., Reichmann, J., Youngson, N. A., Suzuki, M., Reinhardt, D., Dunican, D. S., Prendergast, J. G., Mjoseng, H., Ramsahoye, B. H., Whitelaw, E., Grealley, J. M., Adams, I. R., Bickmore, W. A., & Meehan, R. R. (2013). Redistribution of H3K27me3 upon DNA hypomethylation results in de-repression of Polycomb target genes. *Genome Biology*, *14*(3). <https://doi.org/10.1186/GB-2013-14-3-R25>
- Rice, J. C., Briggs, S. D., Ueberheide, B., Barber, C. M., Shabanowitz, J., Hunt, D. F., Shinkai, Y., & Allis, C. D. (2003). Histone methyltransferases direct different degrees of methylation to define distinct chromatin domains. *Molecular Cell*, *12*(6), 1591–1598. [https://doi.org/10.1016/S1097-2765\(03\)00479-9](https://doi.org/10.1016/S1097-2765(03)00479-9)
- Riggs, A. D. (1975). X inactivation, differentiation, and DNA methylation. *Cytogenetics and Cell Genetics*, *14*(1), 9–25. <https://doi.org/10.1159/000130315>
- Rimon-Dahari, N., Yerushalmi-Heinemann, L., Alyagor, L., & Dekel, N. (2016). Ovarian folliculogenesis. *Results*

- and *Problems in Cell Differentiation*, 58, 167–190. [https://doi.org/10.1007/978-3-319-31973-5\\_7](https://doi.org/10.1007/978-3-319-31973-5_7)
- Rinn, J. L., Kertesz, M., Wang, J. K., Squazzo, S. L., Xu, X., Bruggmann, S. A., Goodnough, L. H., Helms, J. A., Farnham, P. J., Segal, E., & Chang, H. Y. (2007). Functional demarcation of active and silent chromatin domains in human HOX loci by noncoding RNAs. *Cell*, 129(7), 1311–1323. <https://doi.org/10.1016/J.CELL.2007.05.022>
- Rossant, J., & Tam, P. P. L. (2009). Blastocyst lineage formation, early embryonic asymmetries and axis patterning in the mouse. In *Development* (Vol. 136, Issue 5, pp. 701–713). Development. <https://doi.org/10.1242/dev.017178>
- Ruthenburg, A. J., Allis, C. D., & Wysocka, J. (2007). Methylation of Lysine 4 on Histone H3: Intricacy of Writing and Reading a Single Epigenetic Mark. In *Molecular Cell* (Vol. 25, Issue 1, pp. 15–30). Cell Press. <https://doi.org/10.1016/j.molcel.2006.12.014>
- Ryan, R. F., Schultz, D. C., Ayyanathan, K., Singh, P. B., Friedman, J. R., Fredericks, W. J., & Rauscher, F. J. (1999). KAP-1 corepressor protein interacts and colocalizes with heterochromatic and euchromatic HP1 proteins: a potential role for Krüppel-associated box-zinc finger proteins in heterochromatin-mediated gene silencing. *Molecular and Cellular Biology*, 19(6), 4366–4378. <https://doi.org/10.1128/MCB.19.6.4366>
- Sadic, D., Schmidt, K., Groh, S., Kondofersky, I., Ellwart, J., Fuchs, C., Theis, F. J., & Schotta, G. (2015). Atrx promotes heterochromatin formation at retrotransposons. *EMBO Reports*, 16(7), 836–850. <https://doi.org/10.15252/EMBR.201439937>
- Sager, R., & Kitchin, R. (1975). Selective Silencing of Eukaryotic DNA. *Science*, 189(4201), 426–433. <https://doi.org/10.1126/SCIENCE.189.4201.426>
- Saitou, M., & Yamaji, M. (2012). Primordial germ cells in mice. *Cold Spring Harbor Perspectives in Biology*, 4(11). <https://doi.org/10.1101/CSHPERSPECT.A008375>
- Sanchez-Delgado, M., Court, F., Vidal, E., Medrano, J., Monteagudo-Sánchez, A., Martin-Trujillo, A., Tayama, C., Iglesias-Platas, I., Kondova, I., Bontrop, R., Poo-Llanillo, M. E., Marques-Bonet, T., Nakabayashi, K., Simón, C., & Monk, D. (2016). Human Oocyte-Derived Methylation Differences Persist in the Placenta Revealing Widespread Transient Imprinting. *PLOS Genetics*, 12(11), e1006427. <https://doi.org/10.1371/JOURNAL.PGEN.1006427>
- Sánchez, F., & Smitz, J. (2012). Molecular control of oogenesis. *Biochimica et Biophysica Acta (BBA) - Molecular Basis of Disease*, 1822(12), 1896–1912. <https://doi.org/10.1016/J.BBADIS.2012.05.013>
- Sankar, A., Lerdrup, M., Manaf, A., Johansen, J. V., Gonzalez, J. M., Borup, R., Blanshard, R., Klungland, A., Hansen, K., Andersen, C. Y., Dahl, J. A., Helin, K., & Hoffmann, E. R. (2020). KDM4A regulates the maternal-to-zygotic transition by protecting broad H3K4me3 domains from H3K9me3 invasion in oocytes. *Nature Cell Biology*, 22(4), 380–388. <https://doi.org/10.1038/s41556-020-0494-z>
- Santos-Rosa, H., Schneider, R., Bannister, A. J., Sherriff, J., Bernstein, B. E., Emre, N. C. T., Schreiber, S. L., Mellor, J., & Kouzarides, T. (2002). Active genes are tri-methylated at K4 of histone H3. *Nature*, 419(6905), 407–411. <https://doi.org/10.1038/nature01080>
- Sarma, K., Margueron, R., Ivanov, A., Pirrotta, V., & Reinberg, D. (2008). Ezh2 requires PHF1 to efficiently catalyze H3 lysine 27 trimethylation in vivo. *Molecular and Cellular Biology*, 28(8), 2718–2731. <https://doi.org/10.1128/MCB.02017-07>
- Schmitges, F. W., Prusty, A. B., Faty, M., Stützer, A., Lingaraju, G. M., Aiwazian, J., Sack, R., Hess, D., Li, L., Zhou, S., Bunker, R. D., Wirth, U., Bouwmeester, T., Bauer, A., Ly-Hartig, N., Zhao, K., Chan, H., Gu, J., Gut, H., ... Thomä, N. H. (2011). Histone Methylation by PRC2 Is Inhibited by Active Chromatin Marks. *Molecular Cell*, 42(3), 330–341. <https://doi.org/10.1016/J.MOLCEL.2011.03.025/ATTACHMENT/A7A75332-5ACB-4704-A477-11EB848FFD51/MMC1.PDF>
- Schübeler, D., MacAlpine, D. M., Scalzo, D., Wirbelauer, C., Kooperberg, C., Van Leeuwen, F., Gottschling, D. E., O'Neill, L. P., Turner, B. M., Delrow, J., Bell, S. P., & Groudine, M. (2004). The histone modification pattern of active genes revealed through genome-wide chromatin analysis of a higher eukaryote. *Genes and Development*, 18(11), 1263–1271. <https://doi.org/10.1101/gad.1198204>
- Schultz, D. C., Ayyanathan, K., Negorev, D., Maul, G. G., & Rauscher, F. J. (2002). SETDB1: a novel KAP-1-associated histone H3, lysine 9-specific methyltransferase that contributes to HP1-mediated silencing of euchromatic genes by KRAB zinc-finger proteins. *Genes & Development*, 16(8), 919–932.

<https://doi.org/10.1101/GAD.973302>

- Seenundun, S., Rampalli, S., Liu, Q. C., Aziz, A., Palii, C., Hong, S., Blais, A., Brand, M., Ge, K., & Dilworth, F. J. (2010). UTX mediates demethylation of H3K27me3 at muscle-specific genes during myogenesis. *The EMBO Journal*, 29(8), 1401. <https://doi.org/10.1038/EMBOJ.2010.37>
- Seisenberger, S., Andrews, S., Krueger, F., Arand, J., Walter, J., Santos, F., Popp, C., Thienpont, B., Dean, W., & Reik, W. (2012). The dynamics of genome-wide DNA methylation reprogramming in mouse primordial germ cells. *Molecular Cell*, 48(6), 849–862. <https://doi.org/10.1016/j.MOLCEL.2012.11.001>
- Seki, Y., Hayashi, K., Itoh, K., Mizugaki, M., Saitou, M., & Matsui, Y. (2005). Extensive and orderly reprogramming of genome-wide chromatin modifications associated with specification and early development of germ cells in mice. *Developmental Biology*, 278, 440–458. <https://doi.org/10.1016/j.ydbio.2004.11.025>
- Sha, Q.-Q., Zhang, J., & Fan, H.-Y. (2020). Function and Regulation of Histone H3 Lysine-4 Methylation During Oocyte Meiosis and Maternal-to-Zygotic Transition. *Frontiers in Cell and Developmental Biology*, 8, 1106. <https://doi.org/10.3389/fcell.2020.597498>
- Shao, Z., Raible, F., Mollaaghababa, R., Guyon, J. R., Wu, C. T., Bender, W., & Kingston, R. E. (1999). Stabilization of chromatin structure by PRC1, a Polycomb complex. *Cell*, 98(1), 37–46. [https://doi.org/10.1016/S0092-8674\(00\)80604-2](https://doi.org/10.1016/S0092-8674(00)80604-2)
- Shayevitch, R., Askayo, D., Keydar, I., & Ast, G. (2018). The importance of DNA methylation of exons on alternative splicing. *RNA*, 24(10), 1351–1362. <https://doi.org/10.1261/RNA.064865.117/-/DC1>
- Shirane, K., Miura, F., Ito, T., & Lorincz, M. C. (2020). NSD1-deposited H3K36me2 directs de novo methylation in the mouse male germline and counteracts Polycomb-associated silencing. *Nature Genetics*, 52(10), 1088–1098. <https://doi.org/10.1038/s41588-020-0689-z>
- Shirane, K., Toh, H., Kobayashi, H., Miura, F., Chiba, H., Ito, T., Kono, T., & Sasaki, H. (2013a). Mouse Oocyte Methylomes at Base Resolution Reveal Genome-Wide Accumulation of Non-CpG Methylation and Role of DNA Methyltransferases. *PLoS Genetics*, 9(4). <https://doi.org/10.1371/journal.pgen.1003439>
- Shirane, K., Toh, H., Kobayashi, H., Miura, F., Chiba, H., Ito, T., Kono, T., & Sasaki, H. (2013b). Mouse Oocyte Methylomes at Base Resolution Reveal Genome-Wide Accumulation of Non-CpG Methylation and Role of DNA Methyltransferases. *PLoS Genetics*, 9(4), e1003439. <https://doi.org/10.1371/journal.pgen.1003439>
- Simon, A. M., Goodenough, D. A., Li, E., & Paul, D. L. (1997). Female infertility in mice lacking connexin 37. *Nature*, 385(6616), 525–529. <https://doi.org/10.1038/385525A0>
- Skene, P. J., & Henikoff, S. (2017). An efficient targeted nuclease strategy for high-resolution mapping of DNA binding sites. *ELife*, 6, 1–35. <https://doi.org/10.7554/eLife.21856>
- Smallwood, A., Black, J. C., Tanese, N., Pradhan, S., & Carey, M. (2008). HP1-mediated silencing targets Pol II coactivator complexes. *Nature Structural & Molecular Biology*, 15(3), 318–320. <https://doi.org/10.1038/NSMB.1385>
- Smallwood, S. A., Tomizawa, S. I., Krueger, F., Ruf, N., Carli, N., Segonds-Pichon, A., Sato, S., Hata, K., Andrews, S. R., & Kelsey, G. (2011). Dynamic CpG island methylation landscape in oocytes and preimplantation embryos. *Nature Genetics*, 43(8), 811–814. <https://doi.org/10.1038/ng.864>
- Smith, Z. D., Chan, M. M., Mikkelsen, T. S., Gu, H., Gnirke, A., Regev, A., & Meissner, A. (2012). A unique regulatory phase of DNA methylation in the early mammalian embryo. *Nature*, 484(7394), 339. <https://doi.org/10.1038/NATURE10960>
- Statham, A. L., Robinson, M. D., Song, J. Z., Coolen, M. W., Stirzaker, C., & Clark, S. J. (2012). Bisulfite sequencing of chromatin immunoprecipitated DNA (BisChIP-seq) directly informs methylation status of histone-modified DNA. *Genome Research*, 22(6), 1120–1127. <https://doi.org/10.1101/GR.132076.111>
- Stewart, K. R., Veselovska, L., & Kelsey, G. (2016). Establishment and functions of DNA methylation in the germline. In *Epigenomics* (Vol. 8, Issue 10, pp. 1399–1413). Future Medicine Ltd. <https://doi.org/10.2217/epi-2016-0056>
- Stewart, K. R., Veselovska, L., Kim, J., Huang, J., Saadeh, H., Tomizawa, S. I., Smallwood, S. A., Chen, T., & Kelsey, G. (2015). Dynamic changes in histone modifications precede de novo DNA methylation in oocytes. *Genes and Development*, 29(23), 2449–2462. <https://doi.org/10.1101/gad.271353.115>

- Stock, J. K., Giadrossi, S., Casanova, M., Brookes, E., Vidal, M., Koseki, H., Brockdorff, N., Fisher, A. G., & Pombo, A. (2007). Ring1-mediated ubiquitination of H2A restrains poised RNA polymerase II at bivalent genes in mouse ES cells. *Nature Cell Biology*, *9*(12), 1428–1435. <https://doi.org/10.1038/NCB1663>
- Streubel, G., Watson, A., Jammula, S. G., Scelfo, A., Fitzpatrick, D. J., Oliviero, G., McCole, R., Conway, E., Glancy, E., Negri, G. L., Dillon, E., Wynne, K., Pasini, D., Krogan, N. J., Bracken, A. P., & Cagney, G. (2018). The H3K36me2 Methyltransferase Nsd1 Demarcates PRC2-Mediated H3K27me2 and H3K27me3 Domains in Embryonic Stem Cells. *Molecular Cell*, *70*(2), 371–379.e5. <https://doi.org/10.1016/j.molcel.2018.02.027>
- Suetake, I., Shinozaki, F., Miyagawa, J., Takeshima, H., & Tajima, S. (2004). DNMT3L stimulates the DNA methylation activity of Dnmt3a and Dnmt3b through a direct interaction. *Journal of Biological Chemistry*, *279*(26), 27816–27823. <https://doi.org/10.1074/jbc.M400181200>
- Tachibana-Konwalski, K., Godwin, J., Van Der Weyden, L., Champion, L., Kudo, N. R., Adams, D. J., & Nasmyth, K. (2010). Rec8-containing cohesin maintains bivalents without turnover during the growing phase of mouse oocytes. *Genes & Development*, *24*(22), 2505. <https://doi.org/10.1101/GAD.605910>
- Takahashi, N., Coluccio, A., Thorball, C. W., Planet, E., Shi, H., Offner, S., Turelli, P., Imbeault, M., Ferguson-Smith, A. C., & Trono, D. (2019). ZNF445 is a primary regulator of genomic imprinting. *Genes and Development*, *33*(1–2), 49–54. <https://doi.org/10.1101/GAD.320069.118/-/DC1>
- Tang, F., Barbacioru, C., Nordman, E., Li, B., Xu, N., Bashkirov, V. I., Lao, K., & Surani, M. A. (2010). RNA-Seq analysis to capture the transcriptome landscape of a single cell. *Nature Protocols* *2010* *5*:3, *5*(3), 516–535. <https://doi.org/10.1038/nprot.2009.236>
- Tang, W. W. C., Kobayashi, T., Irie, N., Dietmann, S., & Surani, M. A. (2016). Specification and epigenetic programming of the human germ line. *Nature Reviews Genetics* *2016* *17*:10, *17*(10), 585–600. <https://doi.org/10.1038/NRG.2016.88>
- Tatton-Brown, K., Seal, S., Ruark, E., Harmer, J., Ramsay, E., Del Vecchio Duarte, S., Zachariou, A., Hanks, S., O'Brien, E., Aksglaede, L., Baralle, D., Dabir, T., Gener, B., Goudie, D., Homfray, T., Kumar, A., Pilz, D. T., Selicorni, A., Temple, I. K., ... Rahman, N. (2014). Mutations in the DNA methyltransferase gene DNMT3A cause an overgrowth syndrome with intellectual disability. *Nature Genetics*, *46*(4), 385–388. <https://doi.org/10.1038/ng.2917>
- Uysal, F., Ozturk, S., & Akkoyunlu, G. (2017). DNMT1, DNMT3A and DNMT3B proteins are differently expressed in mouse oocytes and early embryos. *Journal of Molecular Histology* *2017* *48*:5, *48*(5), 417–426. <https://doi.org/10.1007/S10735-017-9739-Y>
- Valente, F. M., Sparago, A., Freschi, A., Hill-Harfe, K., Maas, S. M., Frints, S. G. M., Alders, M., Pignata, L., Franzese, M., Angelini, C., Carli, D., Mussa, A., Gazzin, A., Gabbarini, F., Acurzio, B., Ferrero, G. B., Blied, J., Williams, C. A., Riccio, A., & Cerrato, F. (2019). Transcription alterations of KCNQ1 associated with imprinted methylation defects in the Beckwith-Wiedemann locus. *Genetics in Medicine : Official Journal of the American College of Medical Genetics*, *21*(8), 1808–1820. <https://doi.org/10.1038/S41436-018-0416-7>
- Vermeulen, M., Mulder, K. W., Denissov, S., Pijnappel, W. W. M. P., van Schaik, F. M. A., Varier, R. A., Baltissen, M. P. A., Stunnenberg, H. G., Mann, M., & Timmers, H. T. M. (2007). Selective Anchoring of TFIID to Nucleosomes by Trimethylation of Histone H3 Lysine 4. *Cell*, *131*(1), 58–69. <https://doi.org/10.1016/j.cell.2007.08.016>
- Veselovska, L., Smallwood, S. A., Saadeh, H., Stewart, K. R., Krueger, F., Maupetit Méhouas, S., Arnaud, P., Tomizawa, S. ichi, Andrews, S., & Kelsey, G. (2015). Deep sequencing and de novo assembly of the mouse oocyte transcriptome define the contribution of transcription to the DNA methylation landscape. *Genome Biology*, *16*(1), 1–17. <https://doi.org/10.1186/s13059-015-0769-z>
- Vincent, J. J., Huang, Y., Chen, P. Y., Feng, S., Calvopiña, J. H., Nee, K., Lee, S. A., Le, T., Yoon, A. J., Faull, K., Fan, G., Rao, A., Jacobsen, S. E., Pellegrini, M., & Clark, A. T. (2013). Stage-specific roles for tet1 and tet2 in DNA demethylation in primordial germ cells. *Cell Stem Cell*, *12*(4), 470–478. <https://doi.org/10.1016/J.STEM.2013.01.016>
- Voigt, P., LeRoy, G., Drury, W. J., Zee, B. M., Son, J., Beck, D. B., Young, N. L., Garcia, B. A., & Reinberg, D. (2012). Asymmetrically Modified Nucleosomes. *Cell*, *151*(1), 181–193. <https://doi.org/10.1016/J.CELL.2012.09.002>
- Voncken, J. W., Roelen, B. A. J., Roefs, M., De Vries, S., Verhoeven, E., Marino, S., Deschamps, J., & Van Lohuizen,

- M. (2003). Rnf2 (Ring1b) deficiency causes gastrulation arrest and cell cycle inhibition. *Proceedings of the National Academy of Sciences of the United States of America*, 100(5), 2468–2473. <https://doi.org/10.1073/PNAS.0434312100>
- Wachter, E., Quante, T., Merusi, C., Arczewska, A., Stewart, F., Webb, S., & Bird, A. (2014). Synthetic CpG islands reveal DNA sequence determinants of chromatin structure. *ELife*, 3, e03397. <https://doi.org/10.7554/eLife.03397>
- Wagner, E. J., & Carpenter, P. B. (2012). Understanding the language of Lys36 methylation at histone H3. In *Nature Reviews Molecular Cell Biology* (Vol. 13, Issue 2, pp. 115–126). NIH Public Access. <https://doi.org/10.1038/nrm3274>
- Walsh, C. P., Chaillet, J. R., & Bestor, T. H. (1998). Transcription of IAP endogenous retroviruses is constrained by cytosine methylation [4]. In *Nature Genetics* (Vol. 20, Issue 2, pp. 116–117). Nature Publishing Group. <https://doi.org/10.1038/2413>
- Walter, M., Teissandier, A., Pérez-Palacios, R., & Bourc'his, D. (2016). An epigenetic switch ensures transposon repression upon dynamic loss of DNA methylation in embryonic stem cells. *ELife*, 5, 1–30. <https://doi.org/10.7554/elife.11418>
- Wang, C., Liu, X., Gao, Y., Yang, L., Li, C., Liu, W., Chen, C., Kou, X., Zhao, Y., Chen, J., Wang, Y., Le, R., Wang, H., Duan, T., Zhang, Y., & Gao, S. (2018). Reprogramming of H3K9me3-dependent heterochromatin during mammalian embryo development. *Nature Cell Biology* 2018 20:5, 20(5), 620–631. <https://doi.org/10.1038/S41556-018-0093-4>
- Wang, H., Wang, L., Erdjument-Bromage, H., Vidal, M., Tempst, P., Jones, R. S., & Zhang, Y. (2004). Role of histone H2A ubiquitination in Polycomb silencing. *Nature* 2004 431:7010, 431(7010), 873–878. <https://doi.org/10.1038/NATURE02985>
- Wang, L., Zhang, J., Duan, J., Gao, X., Zhu, W., Lu, X., Yang, L., Zhang, J., Li, G., Ci, W., Li, W., Zhou, Q., Aluru, N., Tang, F., He, C., Huang, X., & Liu, J. (2014). Programming and inheritance of parental DNA methylomes in mammals. *Cell*, 157(4), 979–991. <https://doi.org/10.1016/j.cell.2014.04.017>
- Wang, P., Lin, C., Smith, E. R., Guo, H., Sanderson, B. W., Wu, M., Gogol, M., Alexander, T., Seidel, C., Wiedemann, L. M., Ge, K., Krumlauf, R., & Shilatifard, A. (2009). Global Analysis of H3K4 Methylation Defines MLL Family Member Targets and Points to a Role for MLL1-Mediated H3K4 Methylation in the Regulation of Transcriptional Initiation by RNA Polymerase II. *Molecular and Cellular Biology*, 29(22), 6074–6085. <https://doi.org/10.1128/mcb.00924-09>
- Wang, R., Taylor, A. B., Leal, B. Z., Chadwell, L. V., Ilangovan, U., Robinson, A. K., Schirf, V., Hart, P. J., Lafer, E. M., Demeler, B., Hinck, A. P., McEwen, D. G., & Kim, C. A. (2010). Polycomb group targeting through different binding partners of RING1B C-terminal domain. *Structure (London, England : 1993)*, 18(8), 966–975. <https://doi.org/10.1016/J.STR.2010.04.013>
- Wang, Z., Chivu, A. G., Choate, L. A., Rice, E. J., Miller, D. C., Chu, T., Chou, S. P., Kingsley, N. B., Petersen, J. L., Finno, C. J., Bellone, R. R., Antczak, D. F., Lis, J. T., & Danko, C. G. (2022). Prediction of histone post-translational modification patterns based on nascent transcription data. *Nature Genetics*, 54(3), 295–305. <https://doi.org/10.1038/s41588-022-01026-x>
- Wassarman, P. (2001). *A profile of fertilization in mammals*. [www.ch.embnet.org/](http://www.ch.embnet.org/)
- Wassarman, P. M., Jovine, L., & Litscher, E. S. (2004). Mouse zona pellucida genes and glycoproteins. *Cytogenetic and Genome Research*, 105(2–4), 228–234. <https://doi.org/10.1159/000078193>
- Wasserzug-Pash, P., Rothman, R., Reich, E., Zecharyahu, L., Schonberger, O., Weiss, Y., Srebnik, N., Cohen-Hadad, Y., Weintraub, A., Ben-Ami, I., Holzer, H., & Klutstein, M. (2022). Loss of heterochromatin and retrotransposon silencing as determinants in oocyte aging. *Aging Cell*, 21(3), e13568. <https://doi.org/10.1111/acel.13568>
- Weber, M., Hellmann, I., Stadler, M. B., Ramos, L., Pääbo, S., Rebhan, M., & Schübeler, D. (2007). Distribution, silencing potential and evolutionary impact of promoter DNA methylation in the human genome. *Nature Genetics* 2007 39:4, 39(4), 457–466. <https://doi.org/10.1038/ng1990>
- Weinberg, D. N., Papillon-Cavanagh, S., Chen, H., Yue, Y., Chen, X., Rajagopalan, K. N., Horth, C., McGuire, J. T., Xu, X., Nikbakht, H., Lemiesz, A. E., Marchione, D. M., Marunde, M. R., Meiners, M. J., Cheek, M. A., Keogh,

- M. C., Bareke, E., Djedid, A., Harutyunyan, A. S., ... Lu, C. (2019). The histone mark H3K36me2 recruits DNMT3A and shapes the intergenic DNA methylation landscape. *Nature*, *573*(7773), 281–286. <https://doi.org/10.1038/s41586-019-1534-3>
- Weinberg, D. N., Rosenbaum, P., Chen, X., Barrows, D., Horth, C., Marunde, M. R., Popova, I. K., Gillespie, Z. B., Keogh, M. C., Lu, C., Majewski, J., & Allis, C. D. (2021). Two competing mechanisms of DNMT3A recruitment regulate the dynamics of de novo DNA methylation at PRC1-targeted CpG islands. *Nature Genetics*, 1–7. <https://doi.org/10.1038/s41588-021-00856-5>
- Weiner, A., Lara-Astiaso, D., Krupalnik, V., Gafni, O., David, E., Winter, D. R., Hanna, J. H., & Amit, I. (2016). Co-ChIP enables genome-wide mapping of histone mark co-occurrence at single-molecule resolution. *Nature Biotechnology* *2016* *34*:9, *34*(9), 953–961. <https://doi.org/10.1038/nbt.3652>
- Wiley, L. M. (1984). Cavitation in the mouse preimplantation embryo: Na K-ATPase and the origin of nascent blastocoele fluid. *Developmental Biology*, *105*(2), 330–342. [https://doi.org/10.1016/0012-1606\(84\)90290-2](https://doi.org/10.1016/0012-1606(84)90290-2)
- Wisborg, K., Ingerslev, H. J., & Henriksen, T. B. (2010). In vitro fertilization and preterm delivery, low birth weight, and admission to the neonatal intensive care unit: A prospective follow-up study. *Fertility and Sterility*, *94*(6), 2102–2106. <https://doi.org/10.1016/j.fertnstert.2010.01.014>
- Wu, E., & Vastenhouw, N. L. (2020). From mother to embryo: A molecular perspective on zygotic genome activation. *Current Topics in Developmental Biology*, *140*, 209–254. <https://doi.org/10.1016/BS.CTDB.2020.02.002>
- Wu, H., D'Alessio, A. C., Ito, S., Xia, K., Wang, Z., Cui, K., Zhao, K., Eve Sun, Y., & Zhang, Y. (2011). Dual functions of Tet1 in transcriptional regulation in mouse embryonic stem cells. *Nature*, *473*(7347), 389–394. <https://doi.org/10.1038/NATURE09934>
- Wu, X., Johansen, J. V., & Helin, K. (2013). Fbxl10/Kdm2b recruits polycomb repressive complex 1 to CpG islands and regulates H2A ubiquitylation. *Molecular Cell*, *49*(6), 1134–1146. <https://doi.org/10.1016/J.MOLCEL.2013.01.016>
- Wysocka, J., Swigut, T., Milne, T. A., Dou, Y., Zhang, X., Burlingame, A. L., Roeder, R. G., Brivanlou, A. H., & Allis, C. D. (2005). WDR5 associates with histone H3 methylated at K4 and is essential for H3 K4 methylation and vertebrate development. *Cell*, *121*(6), 859–872. <https://doi.org/10.1016/j.cell.2005.03.036>
- Xia, W., Xu, J., Yu, G., Yao, G., Xu, K., Ma, X., Zhang, N., Liu, B., Li, T., Lin, Z., Chen, X., Li, L., Wang, Q., Shi, D., Shi, S., Zhang, Y., Song, W., Jin, H., Hu, L., ... Sun, Y. P. (2019). Resetting histone modifications during human parental-to-zygotic transition. *Science*, *365*(6451), 353–360. <https://doi.org/10.1126/science.aaw5118>
- Xie, H., Xu, J., Hsu, J. H., Nguyen, M., Fujiwara, Y., Peng, C., & Orkin, S. H. (2014). Polycomb repressive complex 2 regulates normal hematopoietic stem cell function in a developmental-stage-specific manner. *Cell Stem Cell*, *14*(1), 68–80. <https://doi.org/10.1016/j.stem.2013.10.001>
- Xu, K., Chen, X., Yang, H., Xu, Y., He, Y., Wang, C., Huang, H., Liu, B., Liu, W., Li, J., Kou, X., Zhao, Y., Zhao, K., Zhang, L., Hou, Z., Wang, H., Wang, H., Li, J., Fan, H., ... Gao, S. (2017). Maternal Sall4 is indispensable for epigenetic maturation of mouse oocytes. *Journal of Biological Chemistry*, *292*(5), 1798–1807. <https://doi.org/10.1074/JBC.M116.767061/ATTACHMENT/42A87858-F620-4B8B-81FE-363752B9EEDC/MMC1.ZIP>
- Xu, Q., Xiang, Y., Wang, Q., Wang, L., Brind'Amour, J., Bogutz, A. B., Zhang, Y., Zhang, B., Yu, G., Xia, W., Du, Z., Huang, C., Ma, J., Zheng, H., Li, Y., Liu, C., Walker, C. L., Jonasch, E., Lefebvre, L., ... Xie, W. (2019). SETD2 regulates the maternal epigenome, genomic imprinting and embryonic development. *Nature Genetics*, *51*(5), 844–856. <https://doi.org/10.1038/s41588-019-0398-7>
- Yamaguchi, S., Hong, K., Liu, R., Inoue, A., Shen, L., Zhang, K., & Zhang, Y. (2013). Dynamics of 5-methylcytosine and 5-hydroxymethylcytosine during germ cell reprogramming. *Cell Research*, *23*(3), 329. <https://doi.org/10.1038/CR.2013.22>
- Yamaguchi, S., Hong, K., Liu, R., Shen, L., Inoue, A., Diep, D., Zhang, K., & Zhang, Y. (2012). Tet1 controls meiosis by regulating meiotic gene expression. *Nature*, *492*(7429), 443–447. <https://doi.org/10.1038/NATURE11709>
- Yamaguchi, S., Shen, L., Liu, Y., Sandler, D., & Zhang, Y. (2013). Role of Tet1 in erasure of genomic imprinting.

*Nature*, 504(7480), 460–464. <https://doi.org/10.1038/NATURE12805>

- Yin, Y., Morgunova, E., Jolma, A., Kaasinen, E., Sahu, B., Khund-Sayeed, S., Das, P. K., Kivioja, T., Dave, K., Zhong, F., Nitta, K. R., Taipale, M., Popov, A., Ginno, P. A., Domcke, S., Yan, J., Schübeler, D., Vinson, C., & Taipale, J. (2017). Impact of cytosine methylation on DNA binding specificities of human transcription factors. *Science (New York, N.Y.)*, 356(6337). <https://doi.org/10.1126/SCIENCE.AAJ2239>
- Yu, B., Doni Jayavelu, N., Battle, S. L., Smith, T. H., Zimmerman, S. E., Schimmel, T., Cohen, J., Mar, J. C., David Hawkins, R., & David, R. (2019). Single-cell analysis of Non-CG methylation dynamics and gene expression in human oocyte maturation. *BioRxiv*, 651141. <https://doi.org/10.1101/651141>
- Yu, M., Mazor, T., Huang, H., Huang, H. T., Kathrein, K. L., Woo, A. J., Chouinard, C. R., Labadorf, A., Akie, T. E., Moran, T. B., Xie, H., Zacharek, S., Taniuchi, I., Roeder, R. G., Kim, C. F., Zon, L. I., Fraenkel, E., & Cantor, A. B. (2012). Direct recruitment of polycomb repressive complex 1 to chromatin by core binding transcription factors. *Molecular Cell*, 45(3), 330–343. <https://doi.org/10.1016/J.MOLCEL.2011.11.032>
- Yuan, W., Xu, M., Huang, C., Liu, N., Chen, S., & Zhu, B. (2011). H3K36 methylation antagonizes PRC2-mediated H3K27 methylation. *Journal of Biological Chemistry*, 286(10), 7983–7989. <https://doi.org/10.1074/jbc.M110.194027>
- Zeng, Y., & Chen, T. (2019). DNA Methylation Reprogramming during Mammalian Development. *Genes*, 10(4). <https://doi.org/10.3390/GENES10040257>
- Zhang, B., Zheng, H., Huang, B., Li, W., Xiang, Y., Peng, X., Ming, J., Wu, X., Zhang, Y., Xu, Q., Liu, W., Kou, X., Zhao, Y., He, W., Li, C., Chen, B., Li, Y., Wang, Q., Ma, J., ... Xie, W. (2016). Allelic reprogramming of the histone modification H3K4me3 in early mammalian development. *Nature*, 537(7621), 553–557. <https://doi.org/10.1038/nature19361>
- Zhang, Y., Charlton, J., Karnik, R., Beerman, I., Smith, Z. D., Gu, H., Boyle, P., Mi, X., Clement, K., Pop, R., Gnirke, A., Rossi, D. J., & Meissner, A. (2018). Targets and genomic constraints of ectopic Dnmt3b expression. *ELife*, 7. <https://doi.org/10.7554/ELIFE.40757>
- Zheng, H., Huang, B., Zhang, B., Xiang, Y., Du, Z., Xu, Q., Li, Y., Wang, Q., Ma, J., Peng, X., Xu, F., & Xie, W. (2016). Resetting Epigenetic Memory by Reprogramming of Histone Modifications in Mammals. *Molecular Cell*, 63(6), 1066–1079. <https://doi.org/10.1016/j.molcel.2016.08.032>
- Zheng, Y., Sweet, S. M. M., Popovic, R., Martinez-Garcia, E., Tipton, J. D., Thomas, P. M., Licht, J. D., & Kelleher, N. L. (2012). Total kinetic analysis reveals how combinatorial methylation patterns are established on lysines 27 and 36 of histone H3. *Proceedings of the National Academy of Sciences of the United States of America*, 109(34), 13549–13554. <https://doi.org/10.1073/pnas.1205707109>
- Zhou, W., Zhu, P., Wang, J., Pascual, G., Ohgi, K. A., Lozach, J., Glass, C. K., & Rosenfeld, M. G. (2008). Histone H2A Monoubiquitination Represses Transcription by Inhibiting RNA Polymerase II Transcriptional Elongation. *Molecular Cell*, 29(1), 69. <https://doi.org/10.1016/J.MOLCEL.2007.11.002>
- Zuccotti, M., Giorgi Rossi, P., Martinez, A., Garagna, S., Forabosco, A., & Redi, C. A. (1998). Meiotic and developmental competence of mouse antral oocytes. *Biology of Reproduction*, 58(3), 700–704. <https://doi.org/10.1095/BIOLREPROD58.3.700>
- Zuccotti, Maurizio, Piccinelli, A., Rossi, P. G., Garagna, S., & Redi, C. A. (1995). Chromatin organization during mouse oocyte growth. *Molecular Reproduction and Development*, 41(4), 479–485. <https://doi.org/10.1002/mrd.1080410410>
- Zylicz, J. J., Borensztein, M., Wong, F. C. K., Huang, Y., Lee, C., Dietmann, S., & Surani, M. A. (2018). G9a regulates temporal preimplantation developmental program and lineage segregation in blastocyst. *ELife*, 7. <https://doi.org/10.7554/ELIFE.33361>





## ABSTRACT

Germ cells have the unique ability to transmit not only the genetic material but also epigenetic information to the progeny. During oogenesis, the epigenome of future female gametes is extensively reprogrammed: somatic patterns are erased and an oocyte-specific chromatin landscape is acquired. After fertilization, the oocyte epigenetic information can persist at least during the first days of preimplantation development. Whether maternally-inherited chromatin patterns can influence the transcriptional program and the phenotype of the progeny is an intense area of research.

The oocyte is known to be the theater of unusual chromatin interplays: the sum of attractive and repulsive feedbacks between chromatin marks seems to rule their precise targeting, their role in regulating gene expression and their transmission to the embryo. In particular, two repressive chromatin marks –DNA methylation and trimethylation of histone H3 lysine 27 (H3K27me3)– show mirror distribution patterns, which are transmitted to the preimplantation embryo. However, while known for their functional antagonism in somatic cells, the nature of their relationship and their mutual impact on oocyte and preimplantation development remained unknown. In particular, while maternal DNA methylation inheritance has been extensively studied in the context of maternal imprinting and post-implantation development, its role, prior to reprogramming, in zygotic genome activation (ZGA) and pre-implantation development had never been studied. During my PhD, I therefore investigated the determinants and functions of DNA methylation and H3K27me3 in shaping the maternal epigenetic heritage.

First, by analysing the chromatin features of wild-type and mutant oocytes for either DNA methylation (using the *Dnmt3L* mutant model) or H3K27me3 (using the *Eed*-cKO model) by both cytological and molecular means, I discovered novel interplays in the oocyte epigenome. I showed that the classical compensation mechanisms observed in somatic cells between H3K27me3 and DNA methylation do not apply to oocytes. In contrast, DNA methylation-free oocytes displayed genome-wide reduction in Polycomb marks, both H3K27me3 and H2Aub. This unveils an unsuspected positive link between DNMT3L-dependent DNA methylation and Polycomb dynamics, whose origin and significance require further study. In parallel, I found H3K4me3 to accumulate at normally hypermethylated regions in *Dnmt3L*<sup>KO</sup> oocytes, demonstrating a role for DNA methylation in protecting CG-rich regions against ectopic H3K4me3 invasion.

While these multiple chromatin changes seem to have little impact on the oocyte developmental program itself, I showed that it impacts ZGA fine-tuning after fertilization. I observed an excessive transcriptional activity during the minor wave of ZGA in *Dnmt3L*<sup>matKO</sup> zygotes. This increase in RNA production was associated with a developmental delay and a decrease in embryo implantation rate.

As a whole, my work demonstrated a novel function of DNA methylation as a master regulator of the maternal chromatin landscape, with consequences on preimplantation development. It allowed to gain insights into the complexity and importance of maternal epigenetic heritage in the control of zygotic genome activation.